LINEAR AND NONLINEAR STABILITY OF PLANE POISEUILLE–COUETTE FLOW

SUBMITTED IN PART FULFILMENT OF THE
REQUIREMENTS FOR THE DEGREE OF
DOCTOR OF PHILOSOPHY OF IMPERIAL COLLEGE LONDON
AND THE
DIPLOMA OF IMPERIAL COLLEGE LONDON
BY

RISHI KUMAR

DEPARTMENT OF MATHEMATICS
IMPERIAL COLLEGE LONDON

October 2020

Declaration Of Originality

I certify that this thesis, and the research to which it refers, are the product of my own work, and that any ideas or quotations from the work of other people, published or otherwise, are fully acknowledged in accordance with the standard referencing practices of the discipline.

Rishi Kumar

Copyright Declaration

Acknowledgements

Firstly, I would like to express my sincere gratitude to my supervisor Dr. Andrew Walton for his patience, motivation and support throughout the past three years. I gratefully acknowledge the funding received towards my PhD from Imperial College London President's PhD scholarship. Finally, I would like to thank my family: my parents and to my younger sisters for supporting me spiritually and emotionally throughout writing this thesis and my life.

Abstract

The problem of the response of a viscous fluid in a channel to the dual effects of wall sliding and constant streamwise pressure gradient has received considerable attention from researchers over the years, due to its relevance to applications such as micro-electro-mechanical systems, aerodynamics heating, electrostatic precipitation and also of course the fact that the basic undisturbed profile, plane Poiseuille–Couette flow (PPCF), is an exact Navier–Stokes solution. The purpose of the thesis is to investigate the linear and nonlinear stability of this flow at asymptotically large Reynolds numbers and numerically at finite Reynolds numbers. The advantage of using an asymptotic approach is that it provides useful physical insight, theoretical understanding of underlying physical mechanisms, gives an easier access to the non-linear regime and forms the basis for carrying out numerical work at finite Reynolds numbers for the flow.

The linear and nonlinear stability of PPCF to three-dimensional disturbances is investigated asymptotically at large values of the Reynolds numbers R based on channel half-width and the maximum velocity of the Poiseuille component. One of the main achievements of the thesis is demonstrating that three-dimensional nonlinear neutral modes exist in PPCF for disturbances with the magnitude of $O(R^{-4/9})$ when $R \gg 1$. The asymptotic theory, aimed at a detailed understanding of the physical mechanisms governing the amplitude-dependent stability properties of the flow, shows that the phase shifts induced across the critical layer and a near-wall shear layer are comparable when the disturbance size $\Delta = O(R^{-4/9})$. In addition, it emerges that at this crucial size both streamwise and spanwise wavelengths of the travelling wave disturbance are comparable with the channel width, with an associated phase speed of $O(1)$. Neutral solutions are found to exist in the range $0 < V < 2$ with $c_0 = V$ to leading order, where c_0 and V are non-dimensional quantities representing the dominant phasespeed of the nonlinear travelling waves and the wall sliding speed respectively. Moreover, these instability modes exist at sliding speeds well in excess of the linear instability cut-off $V \simeq 0.34$. The amplitude equation governing these modes is derived analytically and we further find that this asymptotic structure breaks down in the limit $V \to 2$ when the disturbance streamwise wavelength decreases to $O(R^{-1/3})$ and the maximum of the basic flow becomes located at the upper wall. The numerical results from this interaction are found to compare well with full solutions of the Navier–Stokes equations.

The second achievement of the thesis is that we demonstrate that three-dimensional nonlinear neutral modes exist in PPCF for disturbances with the magnitude of $O(R^{-1/3})$ when $R \gg 1$. By analysing the nature of the instability for increasing disturbance size Δ, the scaling $\Delta = O(R^{-1/3})$ is identified for which a strongly nonlinear neutral wave structure emerges, involving the interaction of two inviscid critical layers. The striking feature of this structure is that the travelling wave disturbances have both streamwise and spanwise wavelengths comparable to the channel width, with an associated phase speed of $O(1)$. A method involving the classical balancing of the phase shifts enables the amplitude-dependence of the

neutral modes to be determined in terms of the wavenumbers and the properties of the basic flow. Numerical computation of the Rayleigh equation which governs the flow outside of the critical layers shows that neutral solutions exist for non-dimensional wall sliding speeds in the range $0 \leq V < 2$. It transpires that the critical layers merge and the asymptotic structure referred to above breaks down both in the large-amplitude limit and the limit $V \to 2$ when the maximum of the basic flow becomes located at the upper wall. The validity of these asymptotic structures is confirmed by comparison with numerical solutions obtained at finite Reynolds numbers.

Contents

List of Figures

Chapter 1

Introduction

The field of hydrodynamic stability examines the stability and the onset of instability of various fluid flows such as plane Poiseuille–Couette flow (PPCF), Hagen–Poiseuille flow (HPF) through a tube of circular cross-section and Blasius boundary layer flow. The objective of studying hydrodynamic stability is to obtain knowledge of how to determine whether a given flow is stable or unstable. This field also provides essential insights into the contribution of each type of instability to the process of transition to turbulence. The foundations of this field go back to the late 19th century when some eminent mathematicians including Helmholtz, Kelvin, Rayleigh and Reynolds made remarkable contributions both theoretically and experimentally. Because of their astounding work, there are many useful tools with which to study hydrodynamic stability. These involve the concept of the Reynolds number R whose explicit form depends on the flow geometry. Since the 1980s, more powerful computational methods have been developed to obtain numerical solutions of the challenging flow stability problems. In this thesis, we use a mixture of analytical and numerical techniques, exploiting the largeness of the Reynolds number to develop asymptotic theories.

One of the earliest investigations of hydrodynamic stability and the laminar-turbulent transition process was Reynolds' (1883) experiment relating to the stability of the Hagen–Poiseuille flow in a circular pipe. As a result of his observations, he identified the important non-dimensional parameter now called the Reynolds number, which is denoted by R and defined as the ratio of inertial to viscous forces within a fluid. At low Reynolds numbers, the laminar flow is observed, and it is characterized by smooth, steady fluid motion. In contrast, turbulent flow occurs at high Reynolds number and is dominated by inertial forces, which results in the development of chaotic eddies and vortices. Following the Reynolds' (1883) discovery various other flows were studied extensively. Schubauer & Skramstad (1947) not only proved the experimental confirmation of a laminar-instability theory, but they also introduced the vibrating-ribbon technique, which was then used in the experiment in boundary-layer instability. Detailed examination of the transition in the boundary-layer flow on a flat plate was carried out by Dryden (1947) and Klebanoff & Tidstrom (1959). They observed that the flow exhibits the laminar behavior near the leading edge, and may be described by the classical Blasius solution. However, at a certain distance from the leading edge disturbance

in the form of the Tollmien–Schlichting waves were found to occur.

The nonlinear stability theories that have been formulated to gain insight into laminar-turbulent transition processes in boundary and free shear layers (see Wu (2019)). He adopted a high-Reynolds number approach, which gives rise to low-dimensional evolution systems and provides a better description of the observations in spatially developing shear flows. In his work, theories have also been developed for nonlinear intermodal interactions, which forms the basis for many intriguing behaviours in the three-dimensional stages of transition. There has been a lot of interest in tracing the development of an initially linear mode to its nonlinear stage. Maslowe (1986) focussed upon the parallel shear flow as the prototypal example and discussed the issue of the interplay of time-dependence, nonlinearity, and dissipative effects in several examples from geophysical fluid dynamics. He emphasized on nonlinear aspects of critical layer theory. He addressed a point about the question of whether it is essential to compute a steady, nonlinear mode that is unconnected to some linear solution from which it has developed gradually. In his review, it is stressed that there are essential nonlinear phenomena that will be overlooked if one insists on always starting from a linear problem.

Hydrodynamic stability theory is concerned with the response of laminar flow to a disturbance (perturbations). If all disturbances decay and the flow returns to its original state, the flow is defined as stable, whereas if a disturbance grows in amplitude in such a way that the flow leaves the initial state and never returns to it, the flow is defined as unstable. The method of linear stability analysis is often employed to ascertain whether a flow is stable or unstable. In this type of analysis, an infinitesimal disturbance is superimposed upon the basic flow. The governing equations for the disturbance are obtained by substituting the perturbed flow into the dimensionless Navier–Stokes equations, leading to a set of linear equations. As the disturbance amplitude grows, nonlinear effects eventually come into play, and these linearised disturbance equations no longer accurately forecast the growth of the disturbance. This signifies a limited domain of validity for this part of the analysis. However, these equations are useful as a first step in analysing the sensitivity of the neutral modes to finite disturbances.

The quasi-linear partial differential equations governing fluid flows are known as the Navier–Stokes equations (NSE), named after Claude Louis Navier and George Gabriel Stokes. They describe the conservation of mass and momentum. These equations are deduced from applying Newton's second law to a fluid element, together with the assumption that the deviatoric stresses are proportional to the strain rate. NSE are the fundamental building blocks of fluid mechanics as these play a key role in understanding the physics of many phenomena of scientific and engineering interest such as blood flow, weather, water flow in a pipe, air flow around a wing, boundary-layer separation from a rigid body surface, formation of eddy wake, hydrodynamic instability, transition to turbulence and hysteresis of fluid flows. NSE are useful in the designing of aircraft, cars and power stations, the analysis of air and water pollution, modelling the weather, and many other things. Coupled with Maxwell's equations,

they can be used to study the magnetic properties and behaviour of electrically conducting fluids, for example, plasmas, liquid metals, salt water, and electrolytes. Although it is possible to obtain a direct analytical solution of the NSE in a few rather simple situations, the asymptotic analysis and numerical simulations are used mainly to examine a wide range of complicated physical phenomena.

Using an asterisk to denote a dimensional quantity, the Cartesian coordinate system $(x^*, y^*, z^*) = (b^*x, b^*y, b^*z)$ is used throughout this thesis where x, y and z represent the non-dimensional coordinates in the streamwise, wall-normal and spanwise directions, respectively, with b^* the channel half-width. The (x, y, z) velocity components are written as $(u^*, v^*, w^*) = (U_m^*)(u, v, w)$, where U_m^* is the maximum speed of the Poiseuille component of the dimensional basic streamwise flow $U_0^*(y^*)$. The density of the incompressible fluid is ρ^* and its kinematic viscosity is ν^*, where ρ^* and ν^* are constants. The pressure is expressed as $p^* = (\rho^* U_m^{*2})p$ and the time is written in the form $t^* = (b^*/U_m^*)t$. These scalings allow us to write the continuity equation and the governing three-dimensional unsteady Navier–Stokes equations in the non-dimensional form:

$$\frac{\partial u}{\partial x} + \frac{\partial v}{\partial y} + \frac{\partial w}{\partial z} = 0, \tag{1.1a}$$

$$\frac{\partial u}{\partial t} + u\frac{\partial u}{\partial x} + v\frac{\partial u}{\partial y} + w\frac{\partial u}{\partial z} = -\frac{\partial p}{\partial x} + R^{-1}\left(\frac{\partial^2 u}{\partial x^2} + \frac{\partial^2 u}{\partial y^2} + \frac{\partial^2 u}{\partial z^2}\right), \tag{1.1b}$$

$$\frac{\partial v}{\partial t} + u\frac{\partial v}{\partial x} + v\frac{\partial v}{\partial y} + w\frac{\partial v}{\partial z} = -\frac{\partial p}{\partial y} + R^{-1}\left(\frac{\partial^2 v}{\partial x^2} + \frac{\partial^2 v}{\partial y^2} + \frac{\partial^2 v}{\partial z^2}\right), \tag{1.1c}$$

$$\frac{\partial w}{\partial t} + u\frac{\partial w}{\partial x} + v\frac{\partial w}{\partial y} + w\frac{\partial w}{\partial z} = -\frac{\partial p}{\partial z} + R^{-1}\left(\frac{\partial^2 w}{\partial x^2} + \frac{\partial^2 w}{\partial y^2} + \frac{\partial^2 w}{\partial z^2}\right), \tag{1.1d}$$

where the parameter R is the Reynolds number specifically defined as

$$R = b^* U_m^* / \nu^*.$$

These four equations involve four unknown functions: the velocity components u, v, w and the pressure p. The terms on the left-hand side of the momentum equations are called the convection terms, while the terms on the right-hand side that are multiplied by the inverse Reynolds number are called the diffusion terms. Taking the limit $R \to \infty$ these equations become the Euler equations. It is clear that we are dealing here with a singular perturbation problem since the highest order terms multiplied by R^{-1} tends to zero in the aforementioned limit. In consequence, all the boundary conditions cannot be satisfied. It was suggested by Prandtl (1904) that at large values of the Reynolds number, although the majority of the flow field can be treated as inviscid, a thin layer known as the boundary layer, where the viscous forces are important, always exists near a solid surface. The characteristic size of this layer is a function of the Reynolds number. Based on the structure, the boundary layer flows are classified into two types: laminar and turbulent. In the next section, we will provide a brief overview of the linear stability for parallel base flows.

1.1 Linear instability

1.1.1 Inviscid Linear Stability Equations

We shall start by considering the stability equations for the infinitesimal disturbances when the viscous effects are negligible. Suppose that the flow is parallel and let us denote the base pressure by $P = P(x)$ and the base flow by $U = U(y)$, i.e., a steady flow in the streamwise direction that varies with y. Substituting a perturbed state $(U + u, v, w, P + p)$ into (1.1) and neglecting the nonlinear and viscous terms, we find that

$$\frac{\partial u}{\partial t} + U\frac{\partial u}{\partial x} + vU' = -\frac{\partial p}{\partial x}, \tag{1.2a}$$

$$\frac{\partial v}{\partial t} + U\frac{\partial v}{\partial x} = -\frac{\partial p}{\partial y}, \tag{1.2b}$$

$$\frac{\partial w}{\partial t} + U\frac{\partial w}{\partial x} = -\frac{\partial p}{\partial z}, \tag{1.2c}$$

$$\frac{\partial u}{\partial x} + \frac{\partial v}{\partial y} + \frac{\partial w}{\partial z} = 0. \tag{1.2d}$$

A prime ($\prime$) represents a $y-$derivative. If we take the divergence of the linearized momentum equations, and use the continuity equation, the resulting equation for the perturbation pressure can be written as

$$\nabla^2 p = -2U'\frac{\partial v}{\partial x}. \tag{1.3}$$

If we eliminate p by combining (1.3) with equation (1.2b), we obtain an equation for the normal velocity, v:

$$\left[\left(\frac{\partial}{\partial t} + U\frac{\partial}{\partial x}\right)\nabla^2 - U''\frac{\partial}{\partial x}\right]v = 0. \tag{1.4}$$

This equation is subject to the following boundary and initial conditions:

$$v = 0 \quad \text{at a solid wall}, \tag{1.5}$$

$$v(x, y, z, 0) = v_0(x, y, z). \tag{1.6}$$

We are interested in analyzing the stability of the mean flow travelling-wave disturbance, namely

$$v(x, y, z, t) = \tilde{v}(y)e^{i(\alpha x + \beta z - \alpha c t)}, \tag{1.7}$$

with c as the complex phase speed and α, β as the real streamwise and spanwise wavenumbers. By substituting (1.7) into (1.4), we obtain the Rayleigh equation

$$(U - c)(D^2 - k^2)\tilde{v} - U''\tilde{v} = 0, \tag{1.8}$$

with $k^2 = \alpha^2 + \beta^2$ and the boundary conditions

$$\tilde{v} = 0 \quad \text{for} \quad y = \pm 1, \tag{1.9}$$

where we restrict our choice to a bounded domain, $y \in [-1, 1]$. The symbol D represents differentiation with respect to y. The Rayleigh equation with the homogeneous boundary conditions (1.9) poses an eigenvalue problem with c as the complex eigenvalue. It is worth noting that if c is an eigenvalue of the Rayleigh equation, so is the complex conjugate c^*.

1.1.2 Critical layers and Tollmien's inviscid solutions

We observe that the Rayleigh equation (1.8) has a regular singular point where the phase velocity equals the mean velocity, $U(y) = c$. We define the critical layer to be the corresponding real part of this location y_r where $U(y_r) = c_r$. It is interesting to see that the solutions to the Rayleigh equation possess logarithmic singularity around this point, and the solution about this point can be determined by applying the Frobenius method to be discussed in 1.2.5.

Denoting the location of the regular singular point by y_c and expanding $U(y)$ in the Rayleigh equation (1.8) about this critical point in a Taylor series, we find that

$$\begin{aligned}\tilde{v}'' - \tilde{v}\{k^2[U'(y_c)(y-y_c) + \cdots] + U''(y_c) + U'''(y_c)(y-y_c) + \cdots \\ + U'(y_c)(y-y_c) + \frac{U''(y_c)}{2}(y-y_c)^2 + \cdots\} = 0.\end{aligned} \tag{1.10}$$

If we drop $O((y-y_c)^2)$ terms and higher, we obtain the equation

$$(y-y_c)\tilde{v}'' - \tilde{v}\left[\frac{U''(y_c)}{U'(y_c)} + \left(\frac{U'''(y_c)}{U'(y_c)} + k^2 - \frac{(U''(y_c))^2}{2(U'(y_c))^2}\right)(y-y_c)\right] = 0, \tag{1.11}$$

which can be expressed in the form

$$(y-y_c)\tilde{v}'' + q(y-y_c)\tilde{v} = 0, \tag{1.12}$$

with $q(y-y_c)$ as the coefficient in the square brackets in equation (1.12).

A Frobenius series around the regular singular point $y = y_c$ can be written in the form

$$\tilde{v} = \sum_{n=0}^{\infty} a_n (y-y_c)^{n+\mu}. \tag{1.13}$$

Substituting (1.13) into (1.11), expanding $q(y-y_c)$ in a power series $q=\sum_{n=0}^{\infty} q_n(y-y_c)^n$, and collecting terms of equal power in $(y-y_c)^{\mu-1}$ we get the indicial equation,

$$a_0\mu(\mu-1)=0, \tag{1.14}$$

which yields $\mu=0$, $\mu=1$. It is easy to show that the two linearly independent solutions to the Rayleigh equation (1.8) attain the following form

$$\tilde{v}_1(y)=(y-y_c)P_1(y), \tag{1.15}$$

$$\tilde{v}_2(y)=P_2(y)+\left(\frac{U''(y_c)}{U'(y_c)}\right)\tilde{v}_1(y)\ln(y-y_c), \tag{1.16}$$

where $P_1(y)$ and $P_2(y)$ are analytic functions. Equations (1.15) and (1.16) are known as Tollmien's inviscid solutions (see Tollmien, 1929).

It follows that (1.16) is multivalued owing to the appearance of a logarithmic term. It is easy to inspect that the critical layer is on the real axis and $y<y_c$ when the imaginary part of c is zero. The logarithmic term gives

$$\ln(y-y_c)=\ln|y-y_c|\pm i\pi \quad \text{for} \quad \mathrm{Im}(y_c)>0. \tag{1.17}$$

The reader is referred to Schmid & Henningson (2001) for the main details of how to choose the sign of the imaginary part. In sections 4.1.3 and 4.2.3 of chapter 4, we will address the important question of how to take the logarithmic singularity into account when numerically tackling the Rayleigh equation. Next, we present two key results which can be deduced from the Rayleigh equation without indicating a particular mean velocity profile: Rayleigh's inflection point criterion and Fjortoft's criterion.

1.1.3 Rayleigh's inflection point criterion

Rayleigh's inflection point criterion states that if there exist perturbations with $c_i>0$, then $U''(y)=0$ for some $y\in[-1,1]$. The theorem can be proved easily if we multiply the Rayleigh equation by the complex conjugate of the normal velocity $\tilde{v}^*$, and integrate in y from -1 to 1. After integrating by parts we obtain

$$\int_{-1}^{1}|D\tilde{v}|^2+k^2|\tilde{v}|^2dy+\int_{-1}^{1}\frac{U''}{U-c}|\tilde{v}|^2dy=0. \tag{1.18}$$

It remains to note that the first integral is real and positive definite, and the second integral is complex-valued. Taking the imaginary part of (1.18) gives the result

$$\mathrm{Im}\left\{\int_{-1}^{1}\frac{U''}{U-c}|\tilde{v}|^2dy\right\}=\int_{-1}^{1}\frac{U''c_i|\tilde{v}|^2}{|U-c|^2}dy=0. \tag{1.19}$$

We observe that both $|\tilde{v}|^2$ and $|U-c|^2$ are nonnegative, and since c_i has been assumed positive, it follows that U'' in (1.19) has to change sign in order to render the integral zero. We draw the conclusion that Rayleigh's inflection point criterion only gives a necessary condition for instability.

1.1.4 Fjortoft's criterion

Fjortoft's criterion states that a necessary condition for instability is that $U''(U-U_c) < 0$ for $y \in [-1,1]$, with $U_c = U(y_c)$. This criterion can be deduced by considering the real part of equation (1.18). We obtain

$$\int_{-1}^{1} \frac{U''(U-c_r)|\tilde{v}|^2}{|U-c|^2} dy = -\int_{-1}^{1} |D\tilde{v}|^2 + k^2|\tilde{v}|^2 dy. \tag{1.20}$$

If we add the following expression

$$(c_r - U_c) \int_{-1}^{1} \frac{U''|\tilde{v}|^2}{|U-c|^2} dy, \tag{1.21}$$

to the left side of the equation (1.20), and note that (1.21) is identically zero due to (1.19). We then obtain

$$\int_{-1}^{1} \frac{U''(U-U_c)|\tilde{v}|^2}{|U-c|^2} dy = -\int_{-1}^{1} |D\tilde{v}|^2 + k^2|\tilde{v}|^2 dy. \tag{1.22}$$

It remains to observe that the integral on the left side is negative if and only if $U''(U-U_c)$ is negative somewhere in the flow field. This completes the proof of Fjortoft's theorem. In the next section, we shall consider the linear stability equations when the viscous effects become important.

1.2 Viscous linear stability equations

We begin this section by considering the stability equations for infinitesimal disturbances in parallel flows. As in the preceding section, the base flow is steady in the streamwise direction that varies with y. Substituting a perturbed state $(U+u, v, w, P+p)$ into (1.1) and neglecting the nonlinear terms, we obtain the following equations:

$$\frac{\partial u}{\partial t} + U\frac{\partial u}{\partial x} + vU' = -\frac{\partial p}{\partial x} + R^{-1}\left(\frac{\partial^2 u}{\partial x^2} + \frac{\partial^2 u}{\partial y^2} + \frac{\partial^2 u}{\partial z^2}\right), \tag{1.23a}$$

$$\frac{\partial v}{\partial t} + U\frac{\partial v}{\partial x} = -\frac{\partial p}{\partial y} + R^{-1}\left(\frac{\partial^2 v}{\partial x^2} + \frac{\partial^2 v}{\partial y^2} + \frac{\partial^2 v}{\partial z^2}\right), \tag{1.23b}$$

$$\frac{\partial w}{\partial t} + U\frac{\partial w}{\partial x} = -\frac{\partial p}{\partial z} + R^{-1}\left(\frac{\partial^2 w}{\partial x^2} + \frac{\partial^2 w}{\partial y^2} + \frac{\partial^2 w}{\partial z^2}\right), \tag{1.23c}$$

$$\frac{\partial u}{\partial x} + \frac{\partial v}{\partial y} + \frac{\partial w}{\partial z} = 0. \tag{1.23d}$$

As before, we take the divergence of the linearized momentum equations, and use the continuity equation to obtain the perturbation pressure equation:

$$\nabla^2 p = -2U' \frac{\partial v}{\partial x}. \tag{1.24}$$

Eliminating the pressure p yields an equation for the normal velocity v:

$$\left[\left(\frac{\partial}{\partial t} + U\frac{\partial}{\partial x}\right)\nabla^2 - U''\frac{\partial}{\partial x} - \frac{1}{R}\nabla^4\right] v = 0. \tag{1.25}$$

Following the derivation of the Rayleigh equation, we seek the travelling wave solutions of the form

$$v(x, y, z, t) = \tilde{v}(y) e^{i(\alpha x + \beta z - \omega t)}, \tag{1.26}$$

where α and β represent the streamwise and spanwise wavenumbers, respectively, and ω denotes the frequency.

Substituting (1.26) into (1.25) yields the following equation for $\tilde{v}$:

$$\left[(-i\omega + i\alpha U)(D^2 - k^2) - i\alpha U'' - \frac{1}{R}(D^2 - k^2)^2\right]\tilde{v} = 0, \tag{1.27}$$

with the boundary conditions $\tilde{v} = D\tilde{v} = 0$ at solid walls. The homogeneous equation (1.27) for the normal velocity $\tilde{v}$ is known as the classical Orr–Sommerfeld equation. Although there is no restriction to real or complex frequencies or wavenumbers, we will adopt a temporal approach to the stability problem, where the wavenumbers α and β are assumed real. The frequency $\omega = \alpha c$ is the complex eigenvalue in the Orr–Sommerfeld equation with the associated eigenfunctions $\tilde{v}$. It is clear that the Orr–Sommerfeld equation is the viscous extension of the Rayleigh equation (1.8).

1.2.1 Squire's transformation and Squire's theorem

It is convenient to use the complex phase speed c as the eigenvalue instead of the complex frequency ω, where

$$\omega = \alpha c, \tag{1.28}$$

which yields the following slightly different version of (1.27), namely

$$(U - c)(D^2 - k^2)\tilde{v} - U''\tilde{v} - \frac{1}{i\alpha R}(D^2 - k^2)^2\tilde{v} = 0. \tag{1.29}$$

The underlying idea behind the Squire's transformation is to compare (1.29) with the two-dimensional Orr–Sommerfeld equation (set $\beta = 0$), which takes the form

$$(U - c)(D^2 - \alpha_{2D}^2)\tilde{v} - U''\tilde{v} - \frac{1}{i\alpha_{2D} R_{2D}}(D^2 - \alpha_{2D}^2)^2\tilde{v} = 0. \tag{1.30}$$

Comparison of these two equations reveals that they have identical solutions if and only if the following relations hold

$$\alpha_{2D} = k = \sqrt{(\alpha^2 + \beta^2)}, \tag{1.31}$$

$$\alpha_{2D} R_{2D} = \alpha R, \tag{1.32}$$

from which we conclude that

$$R_{2D} = R\frac{\alpha}{k} < R. \tag{1.33}$$

The implication of (1.33) is that to each three-dimensional Orr–Sommerfeld mode corresponds a two-dimensional Orr–Sommerfeld mode at a lower Reynolds number. Next, we state the Squire's theorem. For a given α, β and the Reynolds number R_c below which no instabilities exist for any wavenumbers, we have R_L as the critical Reynolds number for the onset of linear instability which satisfies

$$R_c = \min_{\alpha,\beta} R_L(\alpha, \beta) = \min_{\alpha} R_L(\alpha, 0). \tag{1.34}$$

This result has an interesting implication that parallel shear flows first exhibit instability to two-dimensional wavelike disturbances at a value of the Reynolds number that is smaller than any value for which unstable three-dimensional disturbances exist. It is straightforward to see that the proof of this theorem follows directly from Squire's transformation. In the next section, we will discuss the asymptotic methods in fluid mechanics.

1.3 Asymptotic methods in fluid mechanics

During the last century, remarkable progress in fluid dynamics was achieved due to the development of the classical boundary-layer theory and perturbation methods, which facilitated much of research of high-Reynolds-number flows, such as transonic flows or boundary layers. The parameters used in the asymptotic theory of fluid flows may be subdivided into two classes: dynamics parameters and geometric parameters. Examples of dynamic parameters are Reynolds number and Mach number, while an example of a geometric parameter is the aspect ratio of an aircraft wing, which can be small or large, thus allowing us to apply asymptotic analysis to gain insight into the physical mechanisms of a fluid-dynamic phenomenon considered. We begin by discussing the Laplace method and will provide a brief overview of the asymptotic methods applied throughout this thesis.

1.3.1 Laplace's method and Watson's lemma

Laplace's method, named after Pierre-Simon Laplace, is a technique used to approximate integrals of the form

$$F(x) = \int_a^b f(t) e^{x\phi(t)}\, dt, \tag{1.35}$$

where $f(t)$ and $\phi(t)$ are real continuous functions defined on the interval (a, b) of real variable t with x being the positive parameter in the argument of the exponential function $e^{x\phi(t)}$. The aim is to obtain the leading asymptotic behavior of $F(x)$ as $x \to \infty$. Assume that the real continuous function $\phi(t)$ attains its maximum on the interval (a, b) at $t = t_0$. The Taylor expansion of $\phi(t)$ about $t = t_0$ yields

$$\phi(t) = \phi(t_0) + \phi'(t_0)(t - t_0) + \phi''(t_0)\frac{(t - t_0)^2}{2} + \cdots . \tag{1.36}$$

Noting that at the maximum $\phi'(t_0) = 0$, and assuming $\phi''(t_0) \neq 0$, we can express (1.36) as

$$\phi(t) = \phi(t_0) - \zeta(t - t_0)^2 + \cdots , \tag{1.37}$$

where $\zeta = -\frac{1}{2}\phi''(t_0) > 0$. With the aid of (1.37), the exponential $e^{x\phi(t)}$ may be expressed as

$$e^{x\phi(t)} = e^{x\phi(t_0)}e^{-x\zeta(t-t_0)^2}. \tag{1.38}$$

The idea is to split the interval of integration (a, b) in (1.35) into three parts, namely,

$$F(x) = \int_a^{t_0-\epsilon} f(t)e^{x\phi(t)}\,dt + \int_{t_0-\epsilon}^{t_0+\epsilon} f(t)e^{x\phi(t)}\,dt + \int_{t_0+\epsilon}^{b} f(t)e^{x\phi(t)}\,dt, \tag{1.39}$$

with ϵ chosen to be an arbitrary positive number. Suppose that ϵ satisfies the following constraints (see Bender & Orszag (1999)):

$$1 \gg \epsilon \gg 1/\sqrt{x}. \tag{1.40}$$

The first inequality $1 \gg \epsilon$ ensures that the Taylor expansion (1.37) can be used in the second integral in (1.39), while the second inequality $\epsilon \gg 1/\sqrt{x}$ guarantees that the entire region of dominant contribution is covered in the middle subinterval $(t_0 - \epsilon, t_0 + \epsilon)$. It remains to note that the fact that dominant contribution to $F(x)$ comes from the second integral follows from inspection of the graph of $e^{-x\zeta(t-t_0)^2}$, the function which appears in (1.38). Discarding contributions from the first and third integrals in (1.39) and using (1.37) for the second integral, we find that

$$F(x) = e^{x\phi(t_0)} \int_{t_0-\epsilon}^{t_0+\epsilon} f(t)e^{-x\zeta(t-t_0)^2}\,dt + \cdots .$$

Since $f(t)$ is continuous, it may be approximated to $f(t_0)$ in the vicinity of t_0, to leading order, so that

$$\begin{aligned} F(x) &\sim f(t_0)e^{x\phi(t_0)} \int_{-\infty}^{\infty} e^{-x\zeta(t-t_0)^2}\,dt, \quad x \to \infty, \\ &= \frac{\sqrt{2}f(t_0)e^{x\phi(t_0)}}{\sqrt{-x\phi''(t_0)}} \int_{-\infty}^{\infty} e^{-\tau^2}\,d\tau, \end{aligned}$$

where we have substituted $\tau = \sqrt{x}\zeta^{1/2}(t-t_0)$. It remains to recall that $\int_{-\infty}^{\infty} e^{-\tau^2}\,d\tau = \Gamma(\frac{1}{2}) = \sqrt{\pi}$, which results in

$$F(x) \sim \frac{\sqrt{2\pi} f(t_0) e^{x\phi(t_0)}}{\sqrt{-x\phi''(t_0)}}, \quad x \to \infty. \tag{1.41}$$

This result is valid if and only if t_0 is interior to the interval (a, b). It is easy to see that the integral in (1.35) approximates to

$$F_1(x) = \int_a^{a+\epsilon} f(t) e^{x\phi(t)}\,dt,$$

if the maximum of $\phi(t)$ is at $t = a$, and

$$F_2(x) = \int_{b-\epsilon}^{b} f(t) e^{x\phi(t)}\,dt,$$

if the maximum of $\phi(t)$ is at $t = b$. It is straightforward to show that a similar computation, as presented above, gives the following results:

$$F_1(x) \sim -\frac{f(a)e^{x\phi(a)}}{x\phi'(a)}, \quad x \to \infty, \quad \text{with} \quad \phi'(a) < 0, \tag{1.42}$$

$$F_2(x) \sim \frac{f(b)e^{x\phi(b)}}{x\phi'(b)}, \quad x \to \infty, \quad \text{with} \quad \phi'(b) > 0. \tag{1.43}$$

Watson's lemma is concerned with asymptotic behaviour of integrals of the form

$$F(x) = \int_0^b t^\beta f(t) e^{-xt^\alpha}\,dt, \quad 0 < a \leq \infty,$$

where we require that $\beta > -1$ for the integral to converge at $t = 0$. Suppose that function $f(t)$ has $N + 1$ derivatives bounded on an interval $t \in [0, m]$, where $0 < m < b$, and satisfies

$$\int_0^b t^\beta |f(t)| e^{-x_0 t^\alpha}\,dt \leq N,$$

for some value x_0, with N being a positive constant. Then

$$F(x) = \sum_{n=0}^{N} \frac{c_n}{\alpha} \Gamma\left(\frac{\beta + n + 1}{\alpha}\right) x^{-(\beta+n+1)/\alpha} + \cdots \quad \text{as} \quad x \to \infty, \tag{1.44}$$

where $c_n = \frac{1}{n!} f^{(n)}(0)$, and Γ stands for the gamma function. Using the formulas in (1.41) to (1.43) we have

$$\Gamma(x) = \int_0^\infty \tau^{x-1} e^{-\tau} d\tau \sim \sqrt{2\pi(x-1)} \left(\frac{x-1}{e}\right)^{x-1} \quad \text{as} \quad x \to \infty,$$

where Γ is the Euler's gamma function and K_v is the modified Bessel function of order v.

1.3.2 Method of steepest descents

The method of steepest descents is a technique for finding the asymptotic behaviour of integrals of the form

$$M(x) = \int_C g(t)e^{x\rho(t)}dt, \tag{1.45}$$

as $x \to \infty$, where C is an integration contour in the complex plane t and $g(t)$ and $\rho(t)$ are analytic functions of t in some neighbourhood of C. The idea is to deform the contour C to a new contour C' in such a way that $\rho(t)$ has a constant imaginary part on C' to eliminate rapid oscillations of the integrand in the limit of large x and C' passes through one or more zeros (saddle points) of $\rho(t)$, in roughly the direction of steepest descent. Once this has been achieved, we write $\rho(t) = \phi(t) + i\psi(t)$, where $\psi(t)$ and $\phi(t)$ are real functions. Thus, $M(x)$ in (1.45) assumes the form

$$M(x) = e^{ix\psi} \int_{C'} g(t)e^{x\phi(t)}dt. \tag{1.46}$$

Although t is complex, $M(x)$ in (1.46) can be evaluated asymptotically as $x \to \infty$ using Laplace's method since $\phi(t)$ is real. In the following example we show how the method of steepest descent can be used to examine the asymptotic behavior of the integral $\int_0^1 e^{ixt^2}dt$ as $x \to \infty$.

First we note that here $\rho(t) = it^2$ and $\psi(t) = t^2$, so the saddle point lies at $t = 0$. Our objective is to deform the contour C defined for $0 \le t \le 1$ into new contours along which $\mathrm{Im}(\rho(t))$ is constant. We start by seeking such a new contour which passes through $t = 0$. We write $t = x_1 + ix_2$ with x_1 and x_2 real so that $\mathrm{Im}(\rho(t)) = x_1^2 - x_2^2$. Since $\mathrm{Im}(\rho(t)) = 0$ at $t = 0$, we infer that constant-phase contours passing through $t = 0$ satisfy the relations $x_1 = x_2$ or $x_1 = -x_2$. On the contour $x_1 = -x_2$, $\mathrm{Re}(\rho(t)) = 2x_2^2$, so $|e^{x\rho(t)}| = e^{2xx_2^2}$ increases as $t \to \infty$, while on the contour $x_1 = x_2$, $\mathrm{Re}(\rho(t)) = -2x_2^2$, so $|e^{x\rho(t)}| = e^{-2xx_2^2}$ decreases in the same limit. Therefore, $x_1 = x_2$ is a steepest-descent contour denoted by L_1 parametrised as $t = (1 + i)x_2$ $(0 \le x_2 < \infty)$. It is easy to show that the steepest-descent contour passing through $t = 1$ takes the form $L_3 : t = \sqrt{x_2^2 + 1} + ix_2, 0 \le x_2 < \infty$. We observe that along L_1, $\mathrm{Im}(\rho(t)) = 0$, while along L_3, $\mathrm{Im}(\rho(t)) = 1$, it is clear that a third contour L_2 is required to connect the points $(1+i)X_2$ on L_1 and $\sqrt{X_2^2 + 1}+iX_2$ on L_3 with the portions of L_1 and L_3 satisfying $0 \le x_2 \le X_2$ as shown in figure 1.1. It emerges that the contribution from the contour L_2 approaches zero in the limit $X_2 \to \infty$. Therefore,

$$\int_0^1 e^{ixt^2}dt = \int_{L_1} e^{ixt^2}dt - \int_{L_3} e^{ixt^2}dt. \tag{1.47}$$

The integrals along L_1 and L_3 can be calculated easily. Setting $t = (1 + i)x_2$, we get

$$\int_{L_1} e^{ixt^2}dt = (1 + i)\int_0^\infty e^{-2xx_2^2}dx_2 = \frac{1}{2}\sqrt{\frac{\pi}{x}}e^{i\pi/4}. \tag{1.48}$$

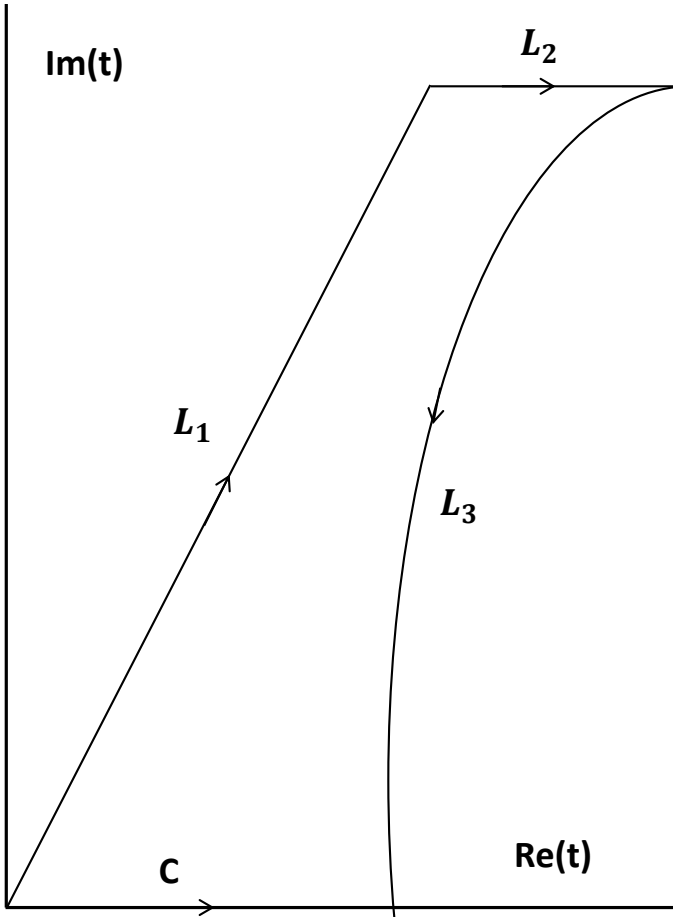

Figure 1.1: Diagram illustrating continuously deformation of the original contour C into new contours $L_1 + L_2 + L_3$.

Setting $t = \sqrt{x_2^2 + 1} + ix_2$ and $p = 2x_2\sqrt{x_2^2 + 1}$, we obtain

$$\int_{L_3} e^{ixt^2} dt = \frac{1}{2} i e^{ix} \int_0^\infty \frac{e^{-xp}}{\sqrt{1 + ip}} \, dp = \frac{1}{2} i e^{ix} \sum_{n=0}^{\infty} (-i)^n \frac{\Gamma(n + \frac{1}{2})}{\Gamma(\frac{1}{2}) x^{n+1}}, \tag{1.49}$$

upon using Watson's lemma. Combining (1.48) and (1.49) yields the asymptotic expansion of the integral as

$$\int_0^1 e^{ixt^2} dt \sim \frac{1}{2}\sqrt{\frac{\pi}{x}} e^{i\pi/4} - \frac{1}{2} i e^{ix} \sum_{n=0}^{\infty} (-i)^n \frac{\Gamma(n + \frac{1}{2})}{\Gamma(\frac{1}{2}) x^{n+1}} \quad \text{as} \quad x \to \infty.$$

1.3.3 Method of matched asymptotic expansions

In this subsection, we consider the method of matched asymptotic expansions useful to determining an approximation to the solution of a differential equation, or a system of differential

equations. We will restrict our attention to the discussion of perturbative methods required for solving a differential equation whose highest derivative is multiplied by the parameter ε. The approximations in the form of an asymptotic series called the inner and outer solutions, respectively, are obtained in a small neighbourhood of the boundary of the domain (inner region) and the main part of the domain (outer region), respectively, and combined through a process called matching, leading to an appropriate solution for the whole domain. This technique is extremely useful because it enables us to determine an approximate solution to a differential equation, even when an exact answer is not achievable. The asymptotic match takes place on the overlap region which is defined by the intermediate limit $x \to 0$, $X = x/\varepsilon^\gamma \to \infty$, $\varepsilon \to 0$, where $\gamma > 0$. To demonstrate how the method works, we shall consider the following problem whose solution exhibits boundary-layer structure.

We wish to obtain an approximate solution to the boundary-value problem

$$\varepsilon \frac{d^2y}{dx^2} + \frac{dy}{dx} + y = 0, \quad y(0) = 0, \quad y(1) = 1, \tag{1.50}$$

where ε is a small positive parameter, such that $0 < \varepsilon \ll 1$. Note that this is a singular perturbation problem since (1.50) has a small parameter multiplying the highest-order derivative.

Outer region. In this region, asymptotic analysis is based on the limit $x = O(1)$, $\varepsilon \to 0$, and we seek the solution in the form of a perturbation series in powers of ε:

$$y = y_0(x) + \varepsilon y_1(x) + \cdots . \tag{1.51}$$

Substituting (1.51) into (1.50) and collecting powers of ε gives a sequence of differential equations:

$$O(1): \quad y_0' + y_0 = 0, \quad y_0(0) = 0, \quad y_0(1) = 1, \tag{1.52}$$

$$O(\varepsilon): \quad y_1' + y_1 = -y_0'', \quad y_1(0) = 0, \quad y_1(1) = 0. \tag{1.53}$$

The general solution to the equation (1.52) has the form

$$y_0(x) = De^{-x}, \tag{1.54}$$

where constant D is to be determined from the boundary conditions in (1.50). It is evident that $y_0(x)$ cannot satisfy the boundary condition $y_0 = 0$ since we obtain a trivial solution with $D = 0$; therefore, a boundary layer at $x = 0$ is necessary. A boundary layer is a narrow region where the solution of a differential equation changes rapidly. Thus, we obtain the leading-order solution as

$$y_0(x) = e^{1-x}. \tag{1.55}$$

This completes the determination of the outer solution to zeroth order in powers of ε. We infer that the outer region occupies the majority of the interval $x \in [0, 1]$, next we consider

the inner region positioned in the vicinity of $x = 0$.

Inner region. Suppose that the thickness of the inner region is $\delta(\varepsilon)$ so that the appropriate scaled independent variable X is given by

$$X = x/\delta(\varepsilon), \tag{1.56}$$

with $X = O(1)$ and $\delta(\varepsilon) \to 0$ as $\varepsilon \to 0$. In terms of the variable X, (1.50) becomes

$$\varepsilon \frac{d^2y}{dX^2} + \delta(\varepsilon)\frac{dy}{dX} + \delta^2(\varepsilon)y = 0, \quad y(0) = 0. \tag{1.57}$$

The inner asymptotic expansion of $y(x, \varepsilon)$ is sought in the form

$$y(x, \varepsilon) = Y_0(X) + \varepsilon Y_1(X) + \cdots . \tag{1.58}$$

Substituting (1.58) into (1.57) and working with the leading-order terms, we find

$$\frac{\varepsilon}{\delta(\varepsilon)}\frac{d^2Y_0}{dX^2} + \frac{dY_0}{dX} = 0, \quad Y_0(0) = 0. \tag{1.59}$$

Next, we explain the procedure for calculating the thickness δ of the boundary layer. With (1.59) we have the following three possibilities:

$$(i). \quad \frac{\varepsilon}{\delta(\varepsilon)} \ll 1, \tag{1.60}$$

$$(ii). \quad \frac{\varepsilon}{\delta(\varepsilon)} = O(1), \tag{1.61}$$

$$(iii). \quad \frac{\varepsilon}{\delta(\varepsilon)} \gg 1. \tag{1.62}$$

It emerges that the first option cannot represent a distinguished limit since then the equation in (1.59) degenerates into

$$\frac{dY_0}{dX} = 0, \tag{1.63}$$

whose solution cannot satisfy simultaneously the boundary condition in (1.59) and the condition of matching with the outer solution (1.55). With the third option (1.62), equation in (1.59) degenerates into

$$\frac{d^2Y_0}{dX^2} = 0, \tag{1.64}$$

with the general solution being

$$Y_0 = C_1 + C_2X. \tag{1.65}$$

Imposing the boundary condition $Y_0(0) = 0$, we find that $C_1 = 0$. However, the matching with the outer solution fails, thus eliminating the choice of the third option. If we choose the second option (1.61) with $\delta(\varepsilon) = \varepsilon$, the problem (1.59) reduces to

$$\frac{d^2Y_0}{dX^2} + \frac{dY_0}{dX} = 0, \quad Y_0(0) = 0. \tag{1.66}$$

The general solution of this equation is written as

$$Y_0 = A_1 + A_2 e^{-X}, \tag{1.67}$$

where A_1 and A_2 are arbitrary constants. Applying the boundary condition $Y_0(0) = 0$ yields the relation $A_1 + A_2 = 0$, while asymptotically matching the outer and inner solutions gives $A_1 = e$. It is worth remarking that the idea of matching is that the inner and outer solutions should agree for values of x in an intermediate region, i.e. where $\delta(\varepsilon) \ll x \ll 1$. In other words, we require the outer limit of the inner solution to match the inner limit of the outer solution, namely $\lim\limits_{X\to\infty} Y_0 = \lim\limits_{x\to 0} y_0$. It remains to note that the determination of $\delta(\varepsilon)$ needs the dominant-balance argument as illustrated in this example; the thickness δ need not be of order ε; there are cases where $\delta = O(\varepsilon^{1/2})$, $\delta = O(\varepsilon^{2/3})$, and so on. Thus, the leading-order inner solution (1.67) assumes the form

$$Y_0 = e(1 - e^{-X}). \tag{1.68}$$

We restrict the analysis of the problem (1.50) to the leading-order approximation in this subsection for the sake of simplicity; however, it is straightforward to perform the calculations to first order in powers of ε.

Uniformly valid composite solution. A formula representing $y(x, \varepsilon)$ on the entire interval $x \in [0, 1]$, the so-called uniformly valid composite solution, may be established as follows

$$y(x, \varepsilon) = \{\text{outer solution}\} + \{\text{inner solution}\} - \{\text{common part}\}. \tag{1.69}$$

Here the 'common part' is the expansion of either the inner or outer approximations in the matching region. In the example considered above, we have

$$y_{\text{common part}} = e. \tag{1.70}$$

Substituting (1.55), (1.56), (1.68) and (1.70) into (1.69), we obtain

$$y(x, \varepsilon) = e^{1-x} - e^{1-x/\varepsilon}.$$

The problem studied above is a simple example since it consists of a single equation dependent on only one variable x, and there is one boundary layer in the solution. The complicated problems arising in fluid dynamics may contain several co-dependent variables in a system of

several equations, and/or with several boundary layers in the solution. It is often advantageous to calculate more terms in the asymptotic expansions of both the outer and the inner solutions. Based on the intricate nature of the problem, the appropriate form of the asymptotic expansions in the inner and outer regions is not always explicit: while a power-series expansion in ε may work, sometimes the appropriate form involves fractional powers of ε, functions like $\varepsilon \ln(\varepsilon)$, etc.

1.4 Numerical methods

Throughout this thesis, a variety of numerical methods will be implemented to solve problems involving linear and nonlinear ordinary differential equations in one variable. In addition, these will be applied to solve nonlinear eigenvalue problems, in cases coupled to linear and nonlinear partial differential equations. A comprehensive discussion of the numerical methods will be provided whenever they are encountered in this thesis. However, in this section, we will give a brief overview of the numerical techniques used throughout.

1.4.1 Finite difference methods

Finite-difference methods are widely used in numerical analysis, particularly for solving differential equations by discretizing them over the domain with difference equations wherein finite differences approximate the derivatives. This method involves the reduction of a linear/non-linear ordinary or partial differential equations to a system of algebraic equations, which can then be solved easily by matrix algebra techniques. To apply this method to approximate the solution of a differential equation, we first discretize the domain of the problem, which is usually accomplished by dividing the domain into a uniform grid of certain step size. There are several ways to approximate the derivatives by considering differences between the points on the discretized grid as we shall see shortly.

Suppose that f is an analytic function. The derivatives of $f(x)$ are based on forward and backward Taylor series expansions of $f(x)$ around the point x, such as

$$f(x+h) = f(x) + hf'(x) + \frac{h^2}{2!}f''(x) + \frac{h^3}{3!}f'''(x) + \cdots, \tag{1.71}$$

$$f(x-h) = f(x) - hf'(x) + \frac{h^2}{2!}f''(x) - \frac{h^3}{3!}f'''(x) + \cdots, \tag{1.72}$$

$$f(x+2h) = f(x) + 2hf'(x) + \frac{(2h)^2}{2!}f''(x) + \frac{(2h)^3}{3!}f'''(x) + \cdots, \tag{1.73}$$

$$f(x-2h) = f(x) - 2hf'(x) + \frac{(2h)^2}{2!}f''(x) - \frac{(2h)^3}{3!}f'''(x) + \cdots, \tag{1.74}$$

valid for sufficiently small h. Rearranging these formulas yields multiple expressions for $f'(x)$ and $f''(x)$:

$$f'(x) = \frac{f(x+h) - f(x-h)}{2h} + O(h^2), \tag{1.75}$$

$$f'(x) = \frac{f(x+h) - f(x)}{h} + O(h), \tag{1.76}$$

$$f'(x) = \frac{f(x) - f(x-h)}{h} + O(h), \tag{1.77}$$

$$f'(x) = \frac{-f(x+2h) + 4f(x+h) - 3f(x)}{2h} + O(h^2), \tag{1.78}$$

$$f'(x) = \frac{f(x-2h) - 4f(x-h) + 3f(x)}{2h} + O(h^2), \tag{1.79}$$

$$f''(x) = \frac{f(x+h) - 2f(x) + f(x-h)}{h^2} + O(h^2), \tag{1.80}$$

$$f''(x) = \frac{f(x+2h) - 2f(x+h) + f(x)}{h^2} + O(h), \tag{1.81}$$

$$f''(x) = \frac{f(x-2h) - 2f(x-h) + f(x)}{h^2} + O(h), \tag{1.82}$$

$$f''(x) = \frac{4f(x+2h) - 5f(x+h) + 2f(x) - f(x+3h)}{h^2} + O(h^2), \tag{1.83}$$

$$f''(x) = \frac{4f(x-2h) - 5f(x-h) + 2f(x) - f(x-3h)}{h^2} + O(h^2), \tag{1.84}$$

where the terms $O(h)$ and $O(h^2)$ indicate that the truncation error behaves as h and h^2. Equations (1.75) and (1.80) are referred to as the first central difference approximation for $f'(x)$ and $f''(x)$ since the function $f(x)$ is computed at values that lie to the left and right of x. This method gives a truncation error $O(h^2)$ which provides more accuracy in the approximation of derivatives. The forms (1.76) and (1.81) are the first forward difference approximation, while the schemes (1.78) and (1.83) are termed as the second forward difference approximation for the first and second derivatives. This method involves evaluations of the function only on one side of x, namely at $x + h$ and x, and has the truncation error $O(h)$ and $O(h^2)$. Its implementation is straightforward but can suffer from strict stability requirements such as Courant–Friedrichs–Lewy condition in the heat equation and hyperbolic equations. Equations (1.77), (1.82) are the first backward difference approximation, while the forms (1.79) and (1.84) are the second backward difference approximation for $f'(x)$ and $f''(x)$. In contrast to the previous method discussed, this uses the function values at x and $x - h$, however, the truncation error has also order of $O(h)$ and $O(h^2)$. It is worth noting that the local truncation error is a function of the step size h, so care should be taken otherwise choosing h large may create instabilities and affect the accuracy of the solution.

1.4.2 Spectral methods

Spectral methods are a class of techniques widely used in applied mathematics and scientific computing to numerically solve ordinary and partial differential equations. In contrast to the finite difference method, derivatives of a function are discretized using an interpolating polynomial. The idea is to seek a solution of the differential equation in the form of a series involving "basis functions" (for example, as a Chebyshev series which is a sum of Chebyshev polynomials or as a Fourier series which is a sum of sinusoids). The method that has been used in this thesis is Chebyshev collocation spectral method since it is advantageous to use Chebyshev polynomials in a bounded domain. The Chebyshev polynomials of first kind, $T_n(y)$, in terms of trigonometric functions is given by the explicit formula

$$T_n(y) = \cos(n \cos^{-1}(y)), \tag{1.85}$$

which are solutions of the singular Sturm-Liouville problem

$$\frac{d}{dy}\left(\sqrt{1-y^2}\frac{d}{dy}T_n(y)\right)+\frac{n^2}{\sqrt{1-y^2}}T_n(y) = 0. \tag{1.86}$$

It is easily seen that $T_0(y) = 1$ and $T_1(y) = y$, while the remaining polynomials may be obtained from recurrence relation, i.e.

$$T_{n+1}(y) = 2yT_n(y) - T_{n-1}(y), \quad n \geq 1, \tag{1.87}$$

or by using a direct formula

$$T_n(y) = \frac{1}{2}\left[(y+\sqrt{y^2-1})^n + (y-\sqrt{y^2-1})^n\right]. \tag{1.88}$$

In addition, Chebyshev polynomials satisfy an orthogonal condition

$$\int_{-1}^{1} \frac{T_n(y)T_m(y)}{\sqrt{1-y^2}}dy = D_n\delta_{nm}, \quad D_0 = \pi, \quad D_n = \frac{\pi}{2}\ (n \neq 0), \tag{1.89}$$

where δ_{nm} is the Kronecker delta. In order to apply the spectral collocation method, the dependent variables are approximated by a Chebyshev expansion

$$f(y) = \sum_{n=0}^{N} a_n T_n(y), \tag{1.90}$$

where the Chebyshev polynomials are calculated at the extrema of $T_n(y)$ so called Gauss–Lobatto points y_j given by

$$y_j = \cos\left(\frac{j\pi}{N}\right), \quad j = 0, 1, \ldots, N. \tag{1.91}$$

Discretization of the governing equations requires us to express the derivatives in terms of Chebyshev polynomials as well, which is achieved by using the following recurrence relations:

$$T_0^{(k)}(y) = 0, \tag{1.92}$$

$$T_1^{(k)}(y) = T_0^{(k-1)}(y), \tag{1.93}$$

$$T_2^{(k)}(y) = 4T_1^{(k-1)}(y), \tag{1.94}$$

$$T_n^{(k)}(y) = 2nT_{n-1}^{(k-1)}(y) + \frac{n}{n-2}T_{n-2}^{(k)}(y), \quad n = 3, 4, \ldots, \tag{1.95}$$

where the superscript $k \geq 1$ represents the order of differentiation. It follows that the kth derivative of $f(y)$ in (1.90) can be approximated as

$$f^{(k)}(y) = \sum_{n=0}^{N} a_n T_n^{(k)}(y). \tag{1.96}$$

Equations for coefficients a_n are determined by substituting (1.90) together with (1.96) into the governing equations and corresponding boundary conditions, using the recurrence relations (1.87), (1.92)-(1.95), re-expanding in terms of Chebyshev polynomials and equating the coefficients of the various $T_n(y)$ for $n = 0, 1, 2, \ldots, N$ to zero. We then require these equations to be evaluated at the collocation points. We obtain a system of $N + 1$ algebraic equations, which in matrix notation assumes the form

$$\mathbf{Aa} = c\mathbf{Ba}, \tag{1.97}$$

where $\mathbf{a} = (a_0, a_1, \ldots, a_N)^T$, $\mathbf{A}$ and $\mathbf{B}$ are $(N + 1) \times (N + 1)$ matrices. The generalized eigenvalue problem (1.97) can be solved easily using standard software to yield eigenvalues c and associated eigenfunctions. It is worth remarking that errors in the Chebyshev collocation method decrease more rapidly than any power of $1/N$ in the limit $N \to \infty$.

1.4.3 Solving linear and nonlinear algebraic equations

Throughout this thesis, we will apply the Newton–Raphson method several times to solve a set of linear and nonlinear algebraic equations arising from the application of discretization methods, namely finite difference and Chebyshev collocation methods to ordinary or partial differential equations. The Newton–Raphson method, named after mathematicians Isaac Newton and Joseph Raphson, is the famous root-finding algorithm which yields better approximations to the zeroes of a real-valued analytic function $f(x)$. The only drawback of the method is that it involves usage of an analytical expression for the derivative $f'(x)$ which may not be easily obtainable in some situations. In these cases, it may be suitable to approximate the derivative using the secant method whose convergence is relatively slower. The Newton–Raphson formula in one dimension can be derived by considering the Taylor series expansion of a function around the solution, $x_{n+1} = x_n + \delta x_n$, where δx_n is small. We find that

$$f(x_{n+1}) = f(x_n) + f'(x_n)(x_{n+1} - x_n) + O(\delta x_n^2). \tag{1.98}$$

If x_{n+1} is a root of $f(x) = 0$, equation (1.98) becomes

$$0 = f(x_n) + f'(x_n)(x_{n+1} - x_n) + O(\delta x_n^2). \tag{1.99}$$

Since we have assumed that δx_n is small, the last term in (1.99) can be ignored and solving for x_{n+1}, we obtain

$$x_{n+1} = x_n - \frac{f(x_n)}{f'(x_n)}. \tag{1.100}$$

Letting x denote the desired solution to $f(x) = 0$, the error in x_n is $E_n = x - x_n$. Hence, it follows from equation (1.100) that

$$E_{n+1} = -\frac{f''(x_n)}{2f'(x_n)} E_n^2, \tag{1.101}$$

implying that the Newton–Raphson method converges quadratically, i.e. for sufficiently small δx_n, we have $\delta x_{n+1} = O(\delta x_n^2)$ on the assumption that $f'(x) \neq 0$. The idea of the method is to repeatedly apply equation (1.100), starting with an initial guess x_0, until the following criterion

$$|x_{n+1} - x_n| < \epsilon, \tag{1.102}$$

is attained, ϵ being the error tolerance. We store only the latest value of x in the computer.

Until now, we restricted our attention to finding a root to the single equation $f(x) = 0$. The solution of n simultaneous, nonlinear equations is a mammoth task and requires the n-dimensional version of the Newton–Raphson method. The scheme follows analogously in higher dimensions, and to derive the formula we begin with the Taylor expansion of $f_i(\mathbf{x})$, $i = 1, 2, \ldots, n$, around the point $\mathbf{x}$, where $\mathbf{x} = (x_1, x_2, \ldots, x_n)^T$:

$$f_i(\mathbf{x} + \delta\mathbf{x}) = f_i(\mathbf{x}) + \sum_{j=1}^{n} \frac{\partial f_i}{\partial x_j} \delta x_j + O(|\delta\mathbf{x}|^2), \tag{1.103}$$

where $\delta\mathbf{x}$ is assumed to be small. We find by dropping terms of order $|\delta\mathbf{x}|^2$ that

$$\mathbf{f}(\mathbf{x} + \delta\mathbf{x}) = \mathbf{f}(\mathbf{x}) + \mathbf{J}(\mathbf{x})\delta\mathbf{x}, \tag{1.104}$$

where $\mathbf{J}(\mathbf{x})$ is the Jacobian matrix (of size $n \times n$) consisting of the partial derivatives

$$J_{ij} = \frac{\partial f_i}{\partial x_j}. \tag{1.105}$$

Suppose that $\mathbf{x} + \delta\mathbf{x}$ satisfies the equation $\mathbf{f}(\mathbf{x}) = 0$ and hence we obtain the following expression for the correction $\delta\mathbf{x}$:

$$\delta\mathbf{x} = -\mathbf{J}^{-1}(\mathbf{x})\mathbf{f}(\mathbf{x}). \tag{1.106}$$

The convergence is quadratic provided that the Jacobian matrix is non-degenerate, and this property of convergence makes the Newton–Raphson approach effective and reliable. It can be difficult or impractical, and time-consuming, to derive the expression for each $\partial f_i/\partial x_j$ analytically. To overcome this complication, it is fruitful to compute the partial derivatives from the finite difference approximation

$$\frac{\partial f_i}{\partial x_j} \approx \frac{f_i(\mathbf{x} + \mathbf{e}_j h) - f_i(\mathbf{x})}{h}, \tag{1.107}$$

where h is a small increment applied to x_j and $\mathbf{e}_j$ indicates a unit vector in the direction of x_j. This form will come in useful at various points in the thesis.

1.4.4 Runge–Kutta methods

The Runge–Kutta methods, named after the German mathematicians Carl Runge and Wilhelm Kutta, is an explicit iterative method based on truncated Taylor series used to approximate solutions of ordinary differential equations. In this thesis, we confine our attention to the Runge–Kutta 4th order method whose derivation is skipped owing to cumbersome calculations involved. This numerical technique is used to solve first or higher-order ordinary differential equations or coupled differential equations. In this thesis, we apply this method to solve the initial value problem of the form

$$\frac{d\mathbf{y}}{dx} = \mathbf{F}(x, \mathbf{y}), \quad \mathbf{y}(a) = \mathbf{b}, \tag{1.108}$$

where

$$\mathbf{F}(x, \mathbf{y}) = \begin{bmatrix} y_2 \\ y_3 \\ \vdots \\ y_n \\ f(x, \mathbf{y}) \end{bmatrix} = \begin{bmatrix} y' \\ y'' \\ \vdots \\ y^{(n-1)} \\ f(x, \mathbf{y}) \end{bmatrix}, \quad \mathbf{b} = \begin{bmatrix} b_1 \\ b_2 \\ \vdots \\ b_n \end{bmatrix}, \quad \mathbf{y} = \begin{bmatrix} y_1 \\ y_2 \\ \vdots \\ y_n \end{bmatrix},$$

$y_1 = y$ and a is a constant. The method requires the following sequence of operations:

$$\begin{aligned} \mathbf{L}_1 &= h\mathbf{F}(x, \mathbf{y}), \\ \mathbf{L}_2 &= h\mathbf{F}\left(x + \frac{h}{2}, \mathbf{y} + \frac{\mathbf{L}_1}{2}\right), \\ \mathbf{L}_3 &= h\mathbf{F}\left(x + \frac{h}{2}, \mathbf{y} + \frac{\mathbf{L}_2}{2}\right), \\ \mathbf{L}_4 &= h\mathbf{F}(x + h, \mathbf{y} + \mathbf{L}_3), \\ \mathbf{y}(x + h) &= \mathbf{y}(x) + \frac{1}{6}(\mathbf{L}_1 + 2\mathbf{L}_2 + 2\mathbf{L}_3 + \mathbf{L}_4), \end{aligned}$$

where $h = h(y)$ is the discretization step, which is guessed or determined by error and trial. In order to demonstrate how the method works, we shall consider, as an example, the following initial-value problem:

$$\frac{d^2y}{dx^2} = x\left(\frac{dy}{dx}\right)^2 - y^2, \quad y(0) = 1, \quad y'(0) = 0. \tag{1.109}$$

The task is to evaluate $y(0.2)$ by integrating (1.109) from $x = 0$ to 0.2 in increments of $h = 0.2$. Letting $y_1 = y$ and $y_2 = y'$, the equivalent first-order equations are

$$\mathbf{F}(x, \mathbf{y}) = \begin{bmatrix} y_2 \\ xy_2^2 - y_1^2 \end{bmatrix}, \tag{1.110}$$

subject to the initial conditions $y_1(0) = 1$ and $y_2(0) = 0$. Letting $\mathbf{L}_i = (l_i^{(1)}, l_i^{(2)})^T$, $i = 1, 2, 3, 4$, we see that

$$\begin{aligned} l_1^{(1)} = 0, \quad & l_1^{(2)} = -0.2, \\ l_2^{(1)} = -0.02, \quad & l_2^{(2)} = -0.1998, \\ l_3^{(1)} = -0.01998, \quad & l_3^{(2)} = -0.1958, \\ l_4^{(1)} = -0.03916, \quad & l_4^{(2)} = -0.19055. \end{aligned}$$

Substituting these values into the formula for $\mathbf{y}(x + h)$ allows to calculate $y(0.2)$ as

$$y(0.2) = y_1(0) + \frac{1}{6}(l_1^{(1)} + 2l_2^{(1)} + 2l_3^{(1)} + l_4^{(1)}) = 0.9801.$$

As a final remark, there are cases where the numerical solution might suffer from numerical instability due to the sensitivity of the solution to initial conditions, so we need to be sensible with the results of numerical integration.

1.4.5 Frobenius method

The method advanced by German mathematician Ferdinand Georg Frobenius is a powerful technique used to obtain series expansions for a second-order ordinary differential equation represented by the form

$$\frac{d^2y}{dx^2} + \left(\frac{p(x)}{x - x_0}\right)\frac{dy}{dx} + \left(\frac{q(x)}{(x - x_0)^2}\right)y = 0, \tag{1.111}$$

in the neighbourhood of the regular singular point $x = x_0$. Here $p(x)$ and $q(x)$ are analytic at $x = x_0$, so a Taylor series representation of these functions about $x = x_0$ may be expressed in the form: $p(x) = \sum_{n=0}^{\infty} p_n(x - x_0)^n$, $q(x) = \sum_{n=0}^{\infty} q_n(x - x_0)^n$. A solution of the linear homogeneous differential equation (1.111) is sought in the form of a Frobenius series, namely

$$y(x) = \sum_{n=0}^{\infty} E_n(x - x_0)^{n+\zeta}, \tag{1.112}$$

where ζ indicates an indicial exponent. Here E_n denotes the nth coefficient of the series, and it is conventional to assume that the leading coefficient E_0 is non-zero. We substitute the Frobenius series (1.112) together with Taylor expansions of $p(x)$ and $q(x)$ into (1.111) and differentiate term by term which leads to the result

$$\sum_{n=0}^{\infty}(n+\zeta)(n+\zeta-1)E_n(x-x_0)^{n+\zeta-2}+\left(\sum_{n=0}^{\infty}p_n(x-x_0)^n\right)\left(\sum_{n=0}^{\infty}(n+\zeta)E_n(x-x_0)^{n+\zeta-2}\right)$$
$$+\left(\sum_{n=0}^{\infty}q_n(x-x_0)^n\right)\left(\sum_{n=0}^{\infty}E_n(x-x_0)^{n+\zeta-2}\right)=0.$$

Equating the coefficients of $(x-x_0)^{n+\zeta-2}$ for $n=0,1,2,...$, we obtain a set of simple algebraic equations:

$$\begin{aligned}
(x-x_0)^{\zeta-2}:&\quad [\zeta^2+(p_0-1)\zeta+q_0]E_0=0,\\
(x-x_0)^{\zeta-1}:&\quad [(\zeta+1)^2+(p_0-1)(\zeta+1)+q_0]E_1+[\zeta p_1+q_1]E_0=0,\\
(x-x_0)^{\zeta}:&\quad [(\zeta+2)^2+(p_0-1)(\zeta+2)+q_0]E_2+\sum_{k=0}^{1}[(\zeta+k)p_{2-k}+q_{2-k}]E_k=0,\\
(x-x_0)^{n+\zeta-2}:&\quad [(\zeta+n)^2+(p_0-1)(\zeta+n)+q_0]E_n+\sum_{k=0}^{n-1}[(\zeta+k)p_{n-k}+q_{n-k}]E_k=0,\qquad n=3,4,...,
\end{aligned}\tag{1.113}$$

which can be solved in closed form. Since we have assumed that $E_0\neq 0$, it follows that the indicial polynomial for (1.111) is

$$P(\zeta)=\zeta^2+(p_0-1)\zeta+q_0,\tag{1.114}$$

whose roots are denoted by ζ_1 and ζ_2 and ordered so that $\mathrm{Re}(\zeta_1)>\mathrm{Re}(\zeta_2)$, where Re denotes the real part. In this thesis, we consider the case when the two roots of the indicial equation differ by an integer say M; therefore, we omit the discussion of the cases: the difference of the two roots is not an integer, or the two roots of the indicial equation are equal. Thus, there are two linearly independent solutions of (1.111) in Frobenius form. Note that $P(\zeta_1+n)\neq 0$ for $n=1,2,...$, and so the last recurrence relation in (1.113) can be solved for E_n in terms of E_0 for all n. This explains that the first solution of (1.111) is the Frobenius series (1.112) evaluated at $\zeta=\zeta_1$. The method employed to find a second linearly independent solution in which logarithms appear is worked out in detail below. The main underlying idea is to observe that the second solution can be determined by differentiating (1.112) with respect to the indicial exponent ζ. To prepare for the process of differentiation with respect to ζ, the first recurrence relation in (1.113) is disregarded for the moment which leaves ζ arbitrary and then the remaining recursion relations are solved for E_n as a function of E_0 and ζ. Henceforth, we express (1.112) by $y(x,\zeta)$:

$$y(x,\zeta)=\sum_{n=0}^{\infty}E_n(\zeta)(x-x_0)^{n+\zeta}.\tag{1.115}$$

At this stage, it is convenient to adopt the shorthand notation

$$L \equiv \frac{d^2}{dx^2} + \left(\frac{p(x)}{x - x_0} \right) \frac{d}{dx} + \frac{q(x)}{(x - x_0)^2}. \tag{1.116}$$

Instead of $Ly(x, \zeta) = 0$, we have that $y(x, \zeta)$ now satisfies

$$Ly(x, \zeta) = E_0(\zeta)(x - x_0)^{\zeta - 2} P(\zeta), \tag{1.117}$$

since the first equation in (1.113) is ignored. If we differentiate both sides of (1.117) with respect to ζ and then let $\zeta = \zeta_1$, we conclude that

$$\begin{aligned} L\left[\frac{\partial}{\partial \zeta} y(x, \zeta) \Big|_{\zeta = \zeta_1} \right] &= E_0[P'(\zeta)(x - x_0)^{\zeta - 2} + P(\zeta)(x - x_0)^{\zeta - 2} \ln(x - x_0)] \Big|_{\zeta = \zeta_1}, \\ &= E_0 P'(\zeta_1)(x - x_0)^{\zeta_1 - 2}, \\ &= E_0 P'(\zeta_1)(x - x_0)^{\zeta_2 + M - 2}, \end{aligned} \tag{1.118}$$

where we have used the fact that E_0 is a constant and $E_0(\zeta_1) = E_0(\zeta) \Big|_{\zeta = \zeta_1}$.

The right side of this equation does not vanish because $P'(\zeta_1)$ is nonzero and therefore $\frac{\partial}{\partial \zeta} y(x, \zeta)$ calculated at $\zeta = \zeta_1$ is not the second solution of (1.111). We now proceed to construct a solution to the homogeneous part of (1.118). It is obvious that the first particular solution of (1.118) is $(\partial / \partial \zeta) y(x, \zeta)|_{\zeta = \zeta_1}$ and for the present we examine (1.118) which suggests that its second particular solution has a Frobenius expansion

$$\frac{\partial}{\partial \zeta} y(x, \zeta) \Big|_{\zeta = \zeta_1} = \sum_{n=0}^{\infty} F_n (x - x_0)^{\zeta_2 + n}, \tag{1.119}$$

where F_n denotes the nth coefficient of this series with $F_0 \neq 0$. Substituting this series into (1.118) and equating the coefficients of $(x - x_0)^{\zeta_2 + n - 2}$ leads to

$$(x - x_0)^{\zeta_2 - 2} : \qquad P(\zeta_2) F_0 = 0, \tag{1.120}$$

$$(x - x_0)^{\zeta_2 + n - 2} : \qquad P(n + \zeta_2) F_n + \sum_{k=0}^{n-1} [(\zeta_2 + k) p_{n-k} + q_{n-k}] F_k = 0, \quad n \neq 0, M, \tag{1.121}$$

$$(x - x_0)^{\zeta_2 + M - 2} : \quad P(M + \zeta_2) F_M + \sum_{k=0}^{M-1} [(\zeta_2 + k) p_{M-k} + q_{M-k}] F_k = E_0 P'(\zeta_1). \tag{1.122}$$

The first equation (1.120) is automatically satisfied for $n = 0$, while the last equation (1.122) for $n = M$ does not determine F_M because $P(\zeta_2 + M) = 0$ and it follows that the value of E_0 is related to the coefficients $F_0, F_1, \ldots, F_{M-1}$ via

$$E_0 = \frac{1}{P'(\zeta_1)} \sum_{k=0}^{M-1} [(\zeta_2 + k) p_{M-k} + q_{M-k}] F_k. \tag{1.123}$$

Differentiating both sides of (1.115) with respect to ζ and then setting $\zeta = \zeta_1$, we get

$$\frac{\partial}{\partial\zeta}y(x,\zeta)\bigg|_{\zeta=\zeta_1} = y(x,\zeta_1)\,\ln(x-x_0) + \sum_{n=0}^{\infty} H_n(\zeta_1)(x-x_0)^{\zeta_1+n},$$

$$= \bigg(\sum_{n=0}^{\infty} E_n(\zeta_1)(x-x_0)^{n+\zeta_1}\bigg)\ln(x-x_0) + \sum_{n=0}^{\infty} H_n(\zeta_1)(x-x_0)^{\zeta_1+n}, \quad (1.124)$$

where

$$H_n(\zeta_1) = \frac{\partial}{\partial\zeta}E_n(\zeta)\bigg|_{\zeta=\zeta_1}.$$

Subtraction of (1.124) from (1.119) finally establishes the solution to equation (1.111), namely

$$y(x) = \sum_{n=0}^{\infty} F_n(x-x_0)^{\zeta_2+n} - \ln(x-x_0)\sum_{n=0}^{\infty} E_n(\zeta_1)(x-x_0)^{\zeta_1+n} - \sum_{n=0}^{\infty} H_n(\zeta_1)(x-x_0)^{\zeta_1+n}. \quad (1.125)$$

The constants F_0, F_M are arbitrary, and we can calculate the other coefficients in terms of these unknowns. Differentiating the last relation in (1.113) with respect to ζ yields the expression for $H_n(\zeta_1)$ as

$$H_n(\zeta_1) = -\frac{1}{[(\zeta_1+n)^2 + (p_0-1)(\zeta_1+n) + q_0]}\bigg(\sum_{k=0}^{n-1} p_{n-k}E_k(\zeta_1) + \sum_{k=0}^{n-1}[(\zeta_1+k)p_{n-k} + q_{n-k}]H_k$$

$$+ [2(\zeta_1+n) + (p_0-1)]E_n(\zeta_1)\bigg) \text{ for } n \geq 1. \quad (1.126)$$

The expressions for $E_n(\zeta_1)$ and F_n can be determined from the relations (1.113) and (1.121) as

$$E_n(\zeta_1) = -\frac{1}{[(\zeta_1+n)^2 + (p_0-1)(\zeta_1+n) + q_0]}\sum_{k=0}^{n-1}[(\zeta_1+k)p_{n-k} + q_{n-k}]E_k \text{ for } n \geq 1, \quad (1.127)$$

$$F_n = -\frac{1}{P(n+\zeta_2)}\sum_{k=0}^{n-1}[(\zeta_2+k)p_{n-k} + q_{n-k}]F_k \text{ for } n \neq 0, M. \quad (1.128)$$

The results (1.126)–(1.128) will play a pivotal role in determining the coefficients of the series expansion (1.125) explicitly. We close our discussion of the Frobenius method by writing the series solution of $y(x)$ for $x < x_0$ which is obtained if we replace $\ln(x-x_0)$ with $\ln(x_0-x)$ in (1.125),

$$y(x) = \sum_{n=0}^{\infty} F_n(x-x_0)^{\zeta_2+n} - \ln(x_0-x)\sum_{n=0}^{\infty} E_n(\zeta_1)(x-x_0)^{\zeta_1+n} - \sum_{n=0}^{\infty} H_n(\zeta_1)(x-x_0)^{\zeta_1+n}.$$

1.5 Summary of this thesis

Chapter 2 will focus on the linear stability of plane Poiseuille–Couette flow asymptotically at large values of the Reynolds numbers and numerically at finite Reynolds numbers. The linear stability of this flow (the exact Navier–Stokes solution arising from the constant pressure-gradient driven flow through a plane channel with sliding walls) is a flow of practical interest with applications in micro-electro-mechanical systems, magnetohydrodynamic power generation, aerodynamics heating, electrostatic precipitation. The linear stability of this flow, through use of the celebrated Orr–Sommerfeld equation, has been extensively studied previously by Potter (1966), Hains (1967), Reynolds and Potter (1967) among others. These authors found a unique neutral curve, demonstrating that for a given sliding speed V, there exist a band of unstable wavelengths above a critical Reynolds number. Potter showed that no linear neutral curve could be found for this flow above a certain cut-off value of sliding speed V_c with the region of linear stability retreating to infinity as $V \to V_c^-$. In terms of the scalings adopted in this paper the value of $V_c \simeq 0.34$ and it was anticipated in Cowley & Smith (1985) based on an asymptotic approach that multiple neutral curves should coexist at large Reynolds numbers R for non-zero V below V_c. We will show that these findings are consistent with numerical computations of the Orr–Sommerfeld equation at finite Reynolds numbers in section 2.2 where we find multiple neutral curves over a range of $O(1)$ sliding speeds. All the studies mentioned here, including our own, reinforce the conclusion that PPCF is stable to all linear disturbances provided $V \geq V_c$. The linear high Reynolds numbers asymptotic theory appropriate to the upper and lower branches of the main neutral curve and the additional new curve is developed in this chapter and the results obtained are compared with finite R results.

In chapter 3, we will examine the nonlinear stability of plane Poiseuille–Couette flow. We will investigate how the critical layer dynamics alter as the disturbance size is increased, starting from the classical linear form which is relevant for small sliding speeds to an intermediate weakly nonlinear stage and ultimately onto the shorter-scaled strongly nonlinear regime, which holds for $O(1)$ values of the wall sliding velocity. The details of the strongly nonlinear critical layer(s) on the upper branch and hybrid scaling is presented in sections 3.1 and 3.2, respectively, providing motivation for the scalings and asymptotic structure of the strongly nonlinear upper and hybrid modes which follow in the subsequent chapter.

In chapter 4, we present a novel method involving the classical balancing of phase shifts for determining the amplitude-dependence of these modes. In addition, we describe the corresponding numerical techniques for calculating the phase speed and streamwise wavenumber of the disturbance as functions of amplitude, with the methods taking into account the asymmetric nature of the basic flow. Furthermore, we provide a comprehensive description of the numerical results for a range of values of disturbance amplitudes, spanwise wavenumbers and sliding velocities. It transpires that the asymptotic structure of the strongly nonlinear hybrid modes breaks down in the limit $V \to 2$ when the disturbance streamwise wavelength decreases to $O(R^{-1/3})$ and the maximum of the basic flow becomes located at the upper

wall, while the strongly nonlinear upper-branch mode structure breaks down in the limit of large disturbance amplitude (where the two critical layers merge) and the limit in which the maximum of the basic flow becomes located at the upper wall. Finally, we draw the main inferences and suggest avenues for further study.

It is well known that for plane Poiseuille flow, finite-amplitude two-dimensional travelling waves exist and map out a neutral surface in the parameter space formed by Reynolds numbers, wavenumbers and amplitude (see Herbert (1977)). Weakly nonlinear stability analysis carried out by Reynolds & Potter (1967), Cowley & Smith (1985) suggested that PPCF may become unstable to finite-amplitude disturbances for $V > V_c$ and this was confirmed to be the case in the nonlinear numerical studies of Ehrenstein, Nagata & Rincon (2008), Balakumar (1997). The numerical study of Ehrenstein, Nagata & Rincon (2008) used Poiseuille–Couette homotopy to continue a path through the equilibrium states for plane Poiseuille flow to Couette flow although it remains unclear whether these solutions are fully resolved. In Balakumar (1997), two-dimensional nonlinear equilibrium surfaces were mapped out by gradually increasing the value of V. These solutions were computed by starting from the main neutral curve for PPCF and it was concluded that such solutions do not exist beyond $V \approx 0.96$ in our non-dimensionalization. However there are no such numerical studies investigating how nonlinearity affects the additional neutral curves that we compute in section 2.2 of this paper. To this end, in chapter 5, we solve the fully nonlinear unsteady two-dimensional Navier–Stokes equations in order to confirm that the nonlinear hybrid neutral modes exist at finite Reynolds numbers. We compare the results of our asymptotic theory with the corresponding Navier–Stokes solutions.

Chapter 2

Linear stability of plane Poiseuille–Couette flow

2.1 Introduction

In this chapter we will discuss the linear stability of plane Poiseuille–Couette flow asymptotically at large values of the Reynolds number and numerically at finite Reynolds number. PPCF has been investigated extensively at asymptotically large Reynolds number by Cowley & Smith (1985) and numerically at finite Reynolds number by Hains (1967), Potter (1966) and Reynolds & Potter (1967), and the general conclusion of these studies is that this linear combination of the classical Poiseuille and Couette flows is stable to all infinitesimal disturbances above a cut-off value of wall sliding speed $V_c \simeq 0.34$ in our non-dimensionalization. Based on their asymptotic analysis, Cowley & Smith (1985) suggested that multiple neutral curves should coexist at large values of the Reynolds number for non-zero wall speeds below V_c: this was confirmed recently by the numerical work of Kumar & Walton (2019) (figure 2.3). Our aim in this chapter is to find an asymptotic description for these linear solutions which describes how the modes self-sustain due to critical layer/wall layer interactions.

The governing Orr–Sommerfeld equation for linear perturbations in two-dimensions was derived in Lin (1945), Potter (1966), Hains (1967), Reynolds and Potter (1967) among others. We will formulate the three-dimensional version of the Orr–Sommerfeld equation to include three-dimensional effects and account for our different scalings for the basic flow. We begin by solving this equation numerically at finite Reynolds number in the next section and then the linear stability equations are analysed asymptotically in the limit of large Reynolds number in section 2.3. It is stressed that the asymptotic analysis of these equations in detail is necessary for an extension to the non-linear regime as we shall see in chapters 3 and 4. In the remainder of this section, we introduce the basic flow under study bearing in mind that the governing non-dimensional Navier–Stokes equations (1.1) are presented in chapter 1.

The steady basic flow is taken to be in the streamwise direction and subject to a uniform

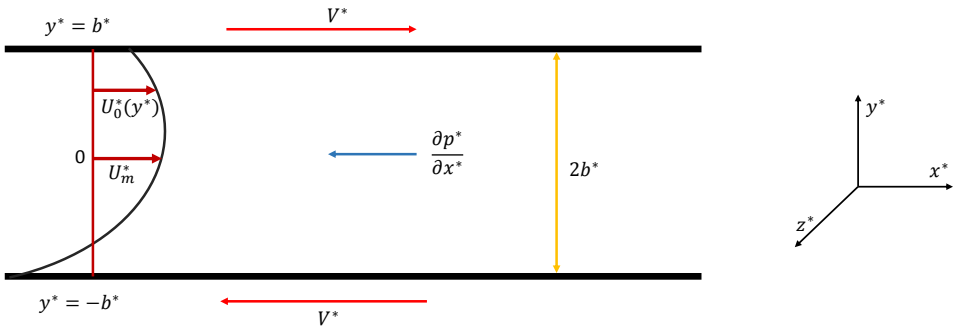

Figure 2.1: Diagram illustrating positive coordinate axes and the basic PPCF in dimensional form. The pressure gradient $(\partial p^*/\partial x^*)$ acts in the negative x^* direction and $U_0^*(y^*)$ is the basic dimensional flow.

streamwise pressure gradient. In addition, the upper wall represented by the scaled location $y = 1$ and the lower wall denoted by $y = -1$ move with the same constant non-dimensional speed V (corresponding to the dimensional speed $V^* = U_m^* V$) but in opposite directions. The no-slip condition of viscous flow then implies that the appropriate boundary conditions are

$$u = \pm V, v = 0 \text{ and } w = 0 \text{ on } y = \pm 1. \tag{2.1}$$

Substituting the unidirectional velocity field into (1.1) and using (2.1), we find that the basic plane Poiseuille-Couette flow is given by

$$(u, v, w, p) = (U_0(y), 0, 0, p(x)) = (1 - y^2 + Vy, 0, 0, (p_0 - 2x)/R), \tag{2.2}$$

where p_0 is a constant. This basic flow is illustrated in figure 2.1. Having obtained the basic flow, we are now concerned with the stability of the basic parallel flow solution (2.2) to a disturbance (perturbations). In the next section, we will perform linear stability analysis to plane Poiseuille–Couette flow for various values of the sliding speed V. This will lead to the formulation of the linear disturbance equations corresponding to this flow which act as the fundamental building blocks of the ensuing analysis.

2.2 Linear stability of plane Poiseuille–Couette flow at finite Reynolds numbers

In order to investigate the stability of plane Poiseuille–Couette flow, a small three-dimensional disturbance harmonic in x, z and t and of amplitude Δ is superimposed upon the basic flow, and the perturbed flow is written as

$$(u, v, w, p) = (U_0(y), 0, 0, p(x)) + \Delta E(\hat{u}, \hat{v}, \hat{w}, \hat{p}). \tag{2.3}$$

Here the hatted variables $\hat{u}$, $\hat{v}$, $\hat{w}$ and $\hat{p}$ are assumed to only depend on the wall-normal coordinate y, the amplitude of the perturbation $\Delta \ll 1$, and E symbolizes the travelling

wave component

$$E = \exp(\mathrm{i}\alpha(x - ct) + \mathrm{i}\beta z), \tag{2.4}$$

with the streamwise wavenumber α and the spanwise wavenumber β prescribed to be real, while the wavespeed c is complex as we are considering the temporal stability problem. We write the complex wavespeed c in the form $c = c_r + \mathrm{i}c_i$ where c_r and c_i represent the real part and the imaginary part of c, respectively. The real part of the complex wavespeed, c_r, indicates the phase speed with which the perturbations propagate obliquely to the streamwise direction. The quantity αc_i represents the temporal growth rate. The temporal growth rate contains important information regarding the stability of modes. Its value determines whether a mode is stable or unstable, thereby enabling us to gain insight into the behaviour of the disturbance. There are three possibilities which we consider in turn. The disturbance with $\alpha c_i > 0$ are unstable modes, whereas the disturbance with the negative temporal growth rate corresponds to stable modes. The disturbance with the imaginary part of the complex wavespeed $c_i = 0$ are referred to as neutral modes which neither grow, nor decay.

The governing equations for the disturbance are obtained by substituting the perturbed flow (2.3) into the non-dimensional Navier-Stokes equations (1.1), neglecting terms which are quadratic in the perturbations and equating coefficients of Δ, leading to the following linearised Navier-Stokes equations:

$$\mathrm{i}\alpha\hat{u} + D\hat{v} + \mathrm{i}\beta\hat{w} = 0, \tag{2.5a}$$

$$\mathrm{i}\alpha(U_0 - c)\hat{u} + \hat{v}DU_0 = -\mathrm{i}\alpha\hat{p} + R^{-1}(D^2 - \alpha^2 - \beta^2)\hat{u}, \tag{2.5b}$$

$$\mathrm{i}\alpha(U_0 - c)\hat{v} = -D\hat{p} + R^{-1}(D^2 - \alpha^2 - \beta^2)\hat{v}, \tag{2.5c}$$

$$\mathrm{i}\alpha(U_0 - c)\hat{w} = -\mathrm{i}\beta\hat{p} + R^{-1}(D^2 - \alpha^2 - \beta^2)\hat{w}, \tag{2.5d}$$

subject to the no-slip boundary conditions

$$\hat{u} = \hat{v} = \hat{w} = 0 \text{ on } y = \pm 1. \tag{2.6}$$

The symbol D stands for differentiation with respect to the wall-normal coordinate y. Equations (2.5) constitute a set of linear equations satisfied by the perturbation ($\hat{u}$, $\hat{v}$, $\hat{w}$, $\hat{p}$). As the disturbance velocities grow above a certain limit, nonlinear effects come into play and the linearised disturbance equations no longer accurately forecast the growth of the disturbance. This signifies that these linear equations have a limited domain of validity. However, these equations are useful as a first step in analyzing the sensitivity of the neutral modes to finite disturbances.

The set of linear equations (2.5) can be simplified further by eliminating the streamwise perturbation $\hat{u}$, the spanwise perturbation $\hat{w}$ and the pressure perturbation $\hat{p}$ to leave a single governing equation for the wall-normal perturbation $\hat{v}$. This is achieved by performing some manipulations on (2.5) which involve multiplying (2.5b) and (2.5d) by $\mathrm{i}\alpha$ and $\mathrm{i}\beta$,

respectively, adding these equations together and using the continuity balance (2.5a), we obtain the following equation for $\hat{v}$ in terms of $\hat{p}$, namely

$$\mathrm{i}\alpha((U_0 - c)D - U_0')\hat{v} = -(\alpha^2 + \beta^2)\hat{p} + R^{-1}(D^2 - \alpha^2 - \beta^2)(D\hat{v}). \tag{2.7}$$

Further, differentiating (2.7) with respect to y, multiplying $(\alpha^2+\beta^2)$ to (2.5c) and finally the subtraction of these two resulting equations formulates a single equation for $\hat{v}$, specifically

$$[(U_0 - c)(D^2 - \alpha^2 - \beta^2) - U_0'' - (\mathrm{i}\alpha R)^{-1}(D^2 - \alpha^2 - \beta^2)^2]\hat{v} = 0. \tag{2.8}$$

This equation is subject to the homogeneous boundary conditions which are easily established by using the no slip boundary condition (2.6) and the continuity equation (2.5a) as

$$\hat{v} = D\hat{v} = 0 \text{ on } y = \pm 1. \tag{2.9}$$

Equation (2.8) is the famous Orr–Sommerfeld equation, which will be useful to examine the linear stability of this flow at finite Reynolds numbers. This is an eigenvalue equation which describes the linear three-dimensional modes of disturbance to this flow. There are many useful methods that can be used to determine numerical solutions to this eigenvalue equation subject to the full set of the boundary conditions (2.9). However, we will use a 'Chebyshev-collocation method', which is discussed in section 1.2.2 of chapter 1. This method enables us to calculate the neutral stability curve defined as the curve along which the growth rate of the disturbance is zero. The modes with zero temporal growth rate lie on the neutral stability curve which is of particular interest since the disturbance (perturbation) corresponding to these modes represents a wave of constant amplitude propagating with speed c_r obliquely to the streamwise direction. Let us denote the region bounded by the upper and lower branches of a neutral curve by U. The modes with positive temporal growth rate lie inside the neutral curve (this, therefore, indicates that U is the region where the flow is unstable), while those with negative temporal growth rate lie everywhere outside this curve (region of stability). In addition, there exists a minimum value of the Reynolds number (also known as the critical Reynolds number denoted by R_c) on the neutral curve. It is worthwhile to mention that when $R < R_c$ the flow is stable for any streamwise wavenumber α since the perturbations decay in this case. On the contrary, if $R > R_c$, then the perturbations are unstable for the set of wavenumbers confined within the region U and consequently the flow is said to be linearly unstable. Figure 2.2 shows the neutral curve for plane Poiseuille flow in (α, R) plane. It consists of a lower branch and an upper branch which can be described asymptotically for large Reynolds number and both branches tend to zero in the limit $R \to \infty$ (see Lin 1945). For plane Poiseuille flow, it is known from Orszag (1971), who applied a Chebyshev spectral method to solve the famous Orr-Sommerfeld equation that the value of R_c is approximately 5772.2. Application of Squire's theorem shows that the value of the critical Reynolds number R_c effectively changes from this value when non-zero values of the spanwise wavenumber are considered. In addition, it follows easily from Squire's transformation that the effect of changing β is only to scale the problem. It should, however, be noted that there is only one neutral curve in plane Poiseuille flow, while two extra neutral curves are found to exist as

wall sliding speed V is increased (Cowley and Smith (1985)). On the other hand, it is well known that plane Couette flow is linearly stable for all Reynolds numbers. In fact, Romanov (1973) has pointed out a proof of the linear stability of this flow at all R.

Equations (2.8), (2.9) constitute an eigenvalue problem for c in terms of α, β, R and V. As far as numerical computations are concerned, we will only consider the case $\beta = 0$ as an application of Squire's transformation allows us to gain insight into the effect of increasing β on the numerical results obtained for zero spanwise wavenumber. As mentioned in the introduction, various authors have tackled this linear stability problem before. Potter (1966) found one neutral stability curve for various V by solving (2.8) using a mixture of asymptotic and numerical methods. His results for $V = 0$ agreed very well with those obtained by Lin (1945) for plane Poiseuille flow. For non-zero V, he concluded that the flow was stable at all R provided $V > V_c$ where $V_c \simeq 0.34$ in our notation. The results given in Potter (1966) were confirmed when the Orr–Sommerfeld equation was solved numerically by Reynolds & Potter (1967) and Hains (1967). Cowley & Smith (1985) predicted exclusively on the basis of a high-Reynolds-number asymptotic approach that multiple neutral curves should exist at large Reynolds number for non-zero sliding speeds which are below V_c. They conjectured that at a certain small value of V two extra neutral curves emerge, and at a slightly larger value of V one of these new neutral curves then disappears, whereas the two remaining ones disappear at $O(1)$ values of V. Being guided by the key asymptotic findings of Cowley & Smith (1985) and the preliminary investigation of Dempsey (2016), a numerical exploration of the parameter space (α, R, V) was undertaken using a Chebyshev collocation approach to solve (2.8) and we have found additional neutral curves (represented by the upper curves in figure 2.3). We investigate the behaviour as V increases and the following features emerge from our finite-Reynolds-numbers computations. The neutral curve for the case when the walls are at rest is presented in figure 2.2. In this situation, there is a single region of linear instability extending from the critical Reynolds number $R_c \approx 5772.2$ (as calculated in Orszag 1971) to infinity. Increasing V slightly from zero, we notice that a pocket of stability in the range $2 \times 10^6 \lesssim R < \infty$, develops within the main neutral curve - see figure 2.3(a). From the sequence of figures 2.3(b)–2.3(c) we observe that as V increases to around $0.0185 - 0.0190$, a stable intrusion forms within the main neutral curve and advances from right to left, eventually slicing this curve into two. We now see that there are two disjoint regions of instability spreading from some finite value of R to infinity: for example, in figure 2.3(c), the upper curve has the critical Reynolds number $R_c \approx 6 \times 10^5$. As V is increased further, the upper curve splits into two, with one part closing up at $R \approx 2 \times 10^6$ while the other part extends from $R \approx 5.8 \times 10^6$ to infinity as captured in figure 2.3(d) for $V \approx 0.025$. It is found that beyond this value of V these two distinct fragments of the upper curve disappear completely, leaving the lower curve (the main neutral curve) to govern the stability properties of the flow. This curve then retreats to $R = \infty$ as $V \to V_c$, in accordance with Potter's results, demonstrating that PPCF exhibits linear stability at all Reynolds numbers for all V beyond this critical value.

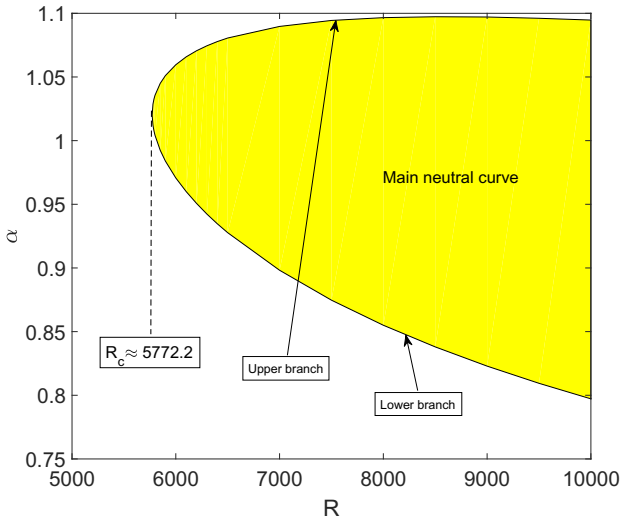

Figure 2.2: Neutral curve for plane Poiseuille flow consisting of a lower and an upper branch as indicated schematically in the plot. The shaded area represents the region of parameter space (α, R) where unstable solutions exist. The modes with negative temporal growth rate lie everywhere outside the shaded area.

2.3 The solution of the linear stability equations at large Reynolds numbers

The disturbance equations (2.5) are also amenable to a high-Reynolds-number asymptotic analysis which complements the finite-R numerical approach seen in the previous section. The advantage of using an asymptotic approach is that it provides useful physical insight, theoretical understanding of underlying physical mechanisms, and gives an easier access to the non-linear regime which is our ultimate interest. We will study the stability properties near the upper and lower branch of the main curve as well as the upper neutral curve (depicted in figures 2.3(c) and (d)). The following analysis has been performed already in Cowley & Smith (1985), but this work lacks the details necessary for an extension to the non-linear regime. In this regard, the work we present here necessitates an extension and modification of the original analysis with the eventual aim of establishing the connections between the linear main/upper curve modes and their non-linear counterparts as Δ is increased. We start by applying Rayleigh's inflection point criterion to study the inviscid instability of this flow before considering the viscous instability at high Reynolds number.

2.3.1 Inviscid instability

When the Reynolds number is assumed large, viscous effects are negligible in the flow, leading to the inviscid version of (2.8), namely

$$(U_0 - c)(D^2 - \alpha^2 - \beta^2)\hat{v} - U_0''\hat{v} = 0, \tag{2.10}$$

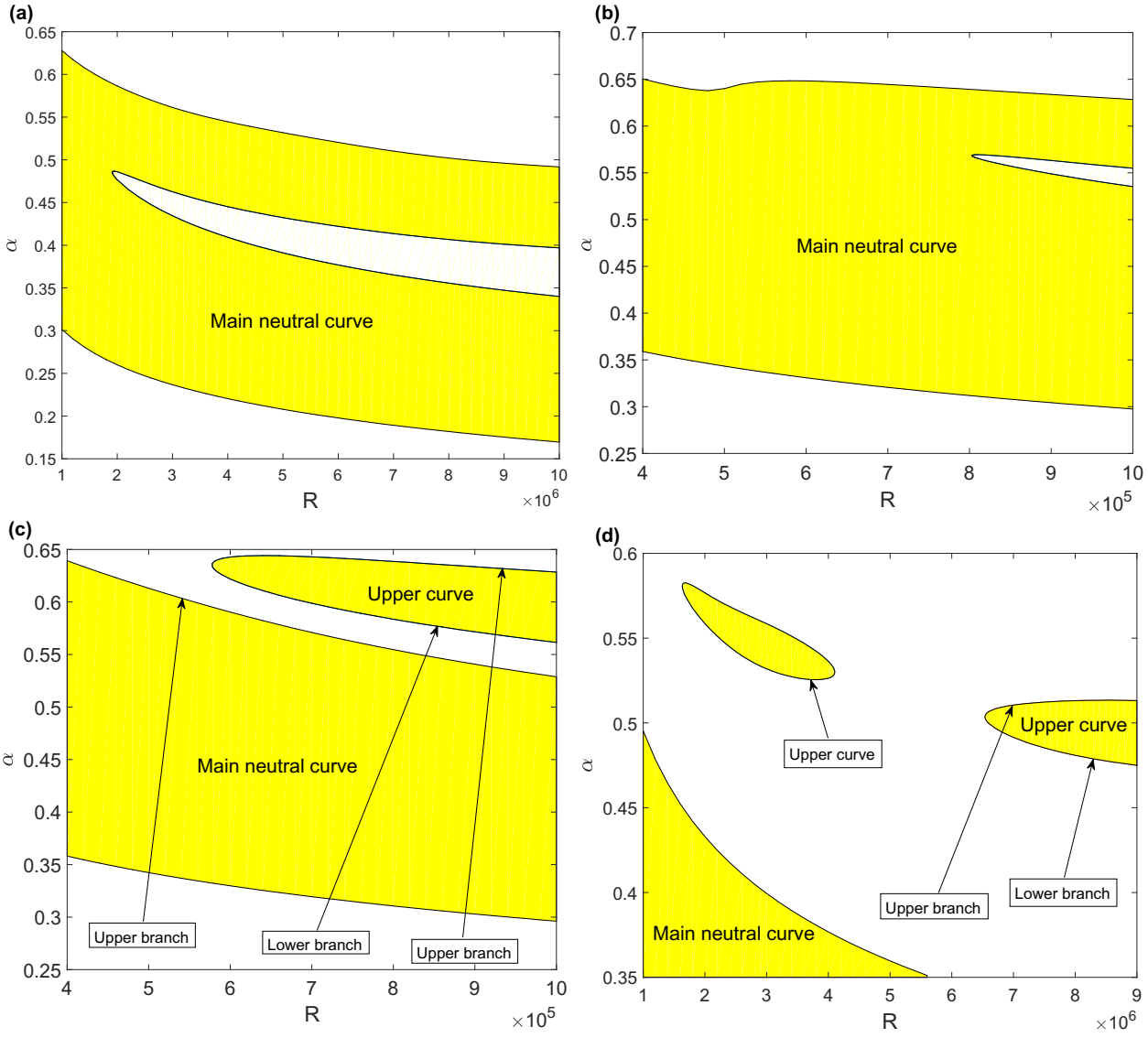

Figure 2.3: (a) Birth of the main neutral curve ($V \approx 0.017$), (b) Pinching off from the main neutral curve ($V \approx 0.0185$), (c) Splitting of the main neutral curve ($V \approx 0.019$), (d) Break off, closing and receding of the surviving branch ($V \approx 0.025$). The shaded regions are unstable.

where a prime ($'$) denotes a y-derivative. This is the Rayleigh equation named after Lord Rayleigh, who introduced it in 1880. The Rayleigh equation (2.10), together with the appropriate boundary conditions (2.9), poses an eigenvalue problem with c as the complex eigenvalue. The coefficients of the second-order linear ordinary differential equation (2.10) are real which implies if c is an eigenvalue of the Rayleigh equation, so is its complex conjugate c^* (where $*$ denotes complex conjugate). This means that any complex eigenvalue c will appear in complex conjugate pairs.

Rayleigh's inflection point criterion relates the existence of a mode with the positive temporal growth rate, that is, an unstable mode, to the occurrence of an inflection point in the basic flow $U_0(y)$ in a bounded plane Poiseuille–Couette flow domain with $y \in [-1, 1]$. It states that given there exist perturbations with the imaginary part of the complex wavespeed c_i positive, a necessary condition for an inviscid instability in this flow is that $U_0''(y) = 0$ for some $-1 \leq y \leq 1$. Thus, inviscid instability is only possible if $U_0''(y)$ changes its sign for some $y \in [-1, 1]$. But the quantity $U_0''(y) = -2$ for plane Poiseuille-Couette flow is, in fact, constant and therefore this flow is inviscidly stable. This completes the proof.

Having now established that any linear instability of the basic streamwise velocity, $U_0(y)$, is viscous in nature, we turn our attention to the viscous instability problem of this flow at high Reynolds number, which is our main interest.

2.3.2 Viscous instability

As already mentioned when the Reynolds number is assumed asymptotically large, viscous effects are negligible in the flow across the majority of the channel and also we have already shown that this flow is inviscidly stable. Therefore, to address the linear instability of the basic flow, which is viscous in nature, it would be sensible to anticipate that viscous effects are confined to the proximity of the plane walls. That is why it is worthwhile to consider the near-wall behaviour of the basic flow, $U_0(y)$, for small values of the sliding speed of the walls V. Letting $V = \varepsilon^2 V_0$, we have

$$U_0(y) = U_{00}(y) + \varepsilon^2 U_{01}(y), \qquad U_{00}(y) = 1 - y^2, \qquad U_{01}(y) = V_0 y. \tag{2.11}$$

Here ε is a small positive parameter. The application of the Taylor series determines the behaviour of the basic flow in the vicinity of the plane walls situated at $y = \pm 1$. Through making use of the Taylor expansions we obtain the following important results:

As $y \to 1^-$:

$$U_{00} \sim \lambda_+^{(0)}(1 - y) + \lambda_+^{(1)}(1 - y)^2, \qquad U_{01} = V_0 y, \tag{2.12}$$

with

$$\lambda_+^{(0)} = 2, \qquad \lambda_+^{(1)} = -1.$$

As $y \to -1^+$:

$$U_{00} \sim \lambda_-^{(0)}(1+y) + \lambda_-^{(1)}(1+y)^2, \qquad U_{01} = V_0 y, \tag{2.13}$$

with

$$\lambda_-^{(0)} = 2, \qquad \lambda_-^{(1)} = -1.$$

These asymptotic forms will play a pivotal role at various points in the analysis while applying the method of matched asymptotic expansions.

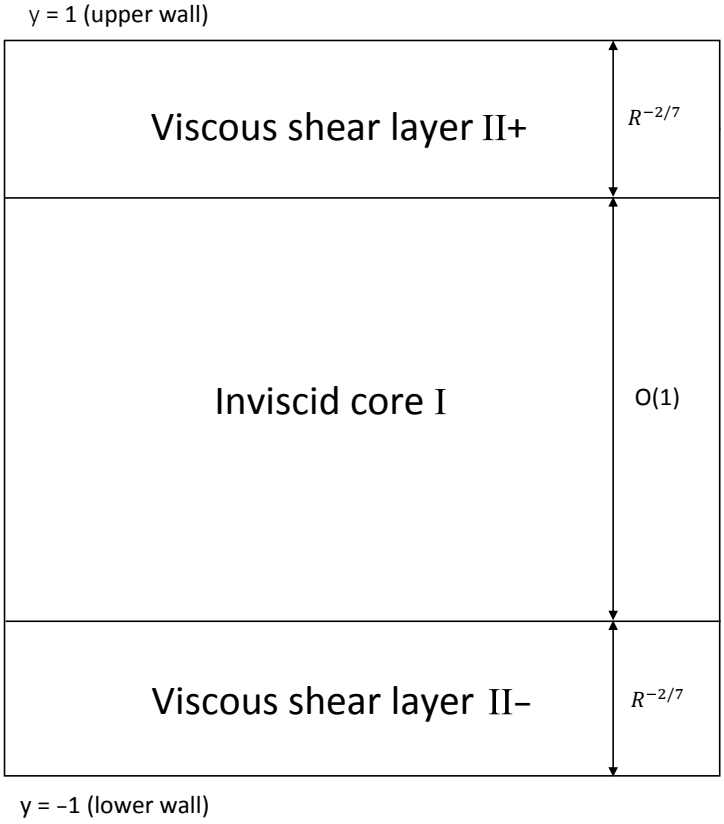

Figure 2.4: The high-Reynolds-numbers asymptotic structure of the lower-branch modes.

2.3.3 Lower-branch analysis

The ensuing analysis and the scalings follow from Smith (1979), although the present problem is difficult owing to the inclusion of three-dimensionality here. We have adopted a similar notation to Walton (2004) wherever possible, who studied the linear stability of circular Poiseuille-Couette flow. The aim is to set out the asymptotic structure corresponding to the lower branch of such a curve at high Reynolds number and to derive the eigenrelation analogous to the lower branch neutral mode. Typically, the high Reynolds number asymptotic structure of the lower-branch modes consists of a three-zone structure: a core region

and two viscous wall layers (see Cowley & Smith (1985)). The distinguishing feature of the lower branch mode behaviour is that the two critical layers are embedded within the viscous wall layers because the typical value of the disturbance wavespeed is small. In addition, the inviscid core region is surrounded above and below by a viscous wall layer. In this scenario, the disturbance survives due to an interaction between the viscous shear layers as we shall see later. Having now established the asymptotic structure corresponding to the lower branch neutral mode, we will describe the dominant physical processes in each region, solve the equations governing dynamics in each and finally avail the method of matched asymptotic expansions in order to match these solutions. Figure 2.4 illustrates the three-zone asymptotic structure of the lower-branch mode. We seek the asymptotic solution to (2.5) at high Reynolds number and

$$V = \varepsilon^2 V_0, \quad \varepsilon \ll 1,$$

which implies that the sliding speed of walls is assumed small. The parameter ε is to be determined in terms of the Reynolds number.

(i) Core region I. The fundamental characteristic of the core region is that the wavespeed of the perturbation is much smaller than the basic flow. This is equivalent to saying that in view of equations (2.5), one may interpret $U_0 - c \approx U_0$. As discussed previously, the viscosity is insignificant across the majority of the channel in the limit of large Reynolds numbers. The consequence of all of this is that there is simplification to the governing disturbance equations (2.5) because the terms multiplied by R^{-1} in these equations can be omitted while carrying out the asymptotic analysis at leading order. The appropriate disturbance expansion, to leading order, is

$$\hat{u} = F_0, \quad \hat{v} = \varepsilon G_0, \quad \hat{w} = \varepsilon^2 H_0, \quad \alpha = \varepsilon \alpha_0, \quad \beta = \varepsilon \beta_0, \tag{2.14}$$

$$c = \varepsilon^2 c_0, \quad \hat{p} = \varepsilon^2 P_0. \tag{2.15}$$

Substituting these expressions into the disturbance equations, with U_0 given by (2.11), we arrive at the following set of inviscid balances

$$\mathrm{i}\alpha_0 F_0 + G_0' = 0, \tag{2.16a}$$
$$\mathrm{i}\alpha_0 U_{00} F_0 + U_{00}' G_0 = 0, \tag{2.16b}$$
$$\mathrm{i}\alpha_0 U_{00} G_0 = -P_0', \tag{2.16c}$$
$$\alpha_0 U_{00} H_0 = -\beta_0 P_0. \tag{2.16d}$$

We start the analysis of the set of equations (2.16) by differentiating (2.16b) with respect to y, followed by elimination of G_0 and G_0' in the resulting equation from use of (2.16a) and (2.16b), and thus the first order linear differential equation satisfied by F_0 is found to be:

$$U_{00}' F_0' = U_{00}'' F_0. \tag{2.17}$$

It follows easily from the method of separation of variables or the method of solving a linear differential equation of the first-order that the solution of (2.17) is

$$F_0 = A_0 U_{00}', \tag{2.18}$$

where the constant A_0 is an undetermined amplitude factor. In order to determine G_0, P_0 and H_0 explicitly, we perform some manipulations on (2.16) which is composed of a few steps. Substitution of the expression for F_0 in (2.16b) yields G_0 and further we can use (2.16c) to determine P_0 up to an arbitrary constant $\hat{P}_0$. Finally, the form for H_0 immediately follows from (2.16d). Therefore, the solution to the core wave system (2.16) is

$$G_0 = -\mathrm{i}\alpha_0 A_0 U_{00}, \quad P_0 = \hat{P}_0 + \alpha_0^2 A_0 I(y), \quad H_0 = -\frac{\beta_0 P_0}{\alpha_0 U_{00}}, \tag{2.19}$$

with F_0 given by (2.18). The integral $I(y)$ is defined by

$$I(y) = \int_y^1 U_{00}^2 \, \mathrm{d}y. \tag{2.20}$$

The expression for $I(y)$ can be calculated analytically, in fact, it is evident that specifically for plane Poiseuille–Couette flow

$$I(y) = -\frac{1}{15}(y-1)^3(3y^2+9y+8). \tag{2.21}$$

The pressure constant $\hat{P}_0$ in (2.19) can be chosen without loss of generality and the proceeding analysis will point out that the eigenrelation for the lower branch neutral mode is unaffected by its value. Using the asymptotic forms (2.12), (2.13) for U_0 we arrive at the following useful results:

As $y \to 1^-$:

$$F_0 \sim -\lambda_+^{(0)} A_0, \quad G_0 \sim -\mathrm{i}\alpha_0 A_0 \lambda_+^{(0)}(1-y), \tag{2.22}$$

$$P_0 \sim \hat{P}_0, \quad H_0 \sim -\left(\frac{\beta_0 \hat{P}_0}{\alpha_0 \lambda_+^{(0)}(1-y)}\right), \tag{2.23}$$

while as $y \to -1^+$:

$$F_0 \sim \lambda_-^{(0)} A_0, \quad G_0 \sim -\mathrm{i}\alpha_0 A_0 \lambda_-^{(0)}(1+y), \tag{2.24}$$

$$P_0 \sim \hat{P}_0 + \alpha_0^2 A_0 I(-1), \quad H_0 \sim -\left(\frac{\beta_0(\hat{P}_0 + \alpha_0^2 A_0 I(-1))}{\alpha_0 \lambda_-^{(0)}(1+y)}\right). \tag{2.25}$$

These forms will come in useful while applying the method of matched asymptotic expansions. Next we aim to identify ε in terms of the Reynolds number and consider the dynamics of the viscous shear layers in detail.

(ii) Viscous shear layers. Suppose that the thickness of the inner viscous shear layers is h which is to be determined in terms of the Reynolds number. To illustrate the main ideas and concepts of the singular perturbation methods let us denote the scaled inner variable for the upper/lower viscous shear layers by $\bar{y}_+/\bar{y}_-$ and thus the relationship between the scaled inner variables and the outer variable y (non-dimensional wall-normal coordinate) is

$$\bar{y}_\pm = \frac{1 \mp y}{h},$$

since these boundary layers have the same thickness h. The physical balance within the inner viscous shear layers arises from the comparable sizes of the inertial term $\mathrm{i}\alpha(U_0 - c)\hat{u}$, the pressure term $\mathrm{i}\alpha\hat{p}$ and the viscous term $R^{-1}\hat{u}''$. Note that α_0, c_0, F_0 and P_0 in (2.14) and (2.15) are $O(1)$ terms and application of the chain rule yields

$$\frac{d^2}{dy^2} = h^{-2}\frac{d^2}{d\bar{y}_\pm^2},$$

which implies that the order of magnitude of the viscous term is $R^{-1}h^{-2}$ since $\bar{y}_\pm$ is $O(1)$, and the pressure term is ε^3 since α is $O(\varepsilon)$ and $\hat{p}$ is $O(\varepsilon^2)$. In order to determine the size of the basic streamwise velocity U_0 within the boundary layers, we express the Taylor expansions (2.12) and (2.13) in terms of the introduced inner variables and therefore find that, to leading order, $(U_0 - c)$ is $O(h)$ and hence, this reveals that the order of the magnitude of the inertial term is εh. Thus an inertial-pressure-viscous balance is achieved provided

$$\varepsilon = R^{-1/7},$$

which then fixes the thickness of the inner viscous shear layers in terms of the Reynolds number, that is, $h = R^{-2/7}$. It immediately follows in view of (2.14) and (2.15) that

$$\alpha = R^{-1/7}\alpha_0, \quad \beta = R^{-1/7}\beta_0, \quad c = R^{-2/7}c_0, \quad V = R^{-2/7}V_0. \tag{2.26}$$

These scalings date back to Lin's analysis of plane Poiseuille flow and are in agreement with Cowley and Smith (1985) for PPCF and identical to those found for circular Poiseuille–Couette flow by Walton (2004). A consequence of the scaling of $R^{-2/7}$ in V is that the effects of the plane walls motion succeed in affecting the viscous shear layers at $y = \pm 1$. Having established the magnitude of the various parameters we aim to investigate the dynamics of these viscous shear layers in turn below.

(a) Viscous shear layer II+

The expansions within the upper viscous shear layer, where $y = 1 - \varepsilon^2\bar{y}_+$, to leading order, take the following form

$$\hat{u} = \bar{u}_+, \ \hat{v} = -\varepsilon^3\bar{v}_+, \ \hat{w} = \bar{w}_+, \ \hat{p} = \varepsilon^2\bar{p}_+, \ U_0 = \varepsilon^2(\lambda_+^{(0)}\bar{y}_+ + V_0). \tag{2.27}$$

Substituting these expansions into the linearised Navier-Stokes equations (2.5), we find the governing equations for the upper viscous wall layer are

$$\mathrm{i}\alpha_0\bar{u}_+ + \frac{d\bar{v}_+}{d\bar{y}_+} + \mathrm{i}\beta_0\bar{w}_+ = 0, \tag{2.28a}$$

$$\mathrm{i}\alpha_0(\lambda_+^{(0)}\bar{y}_+ + V_0 - c_0)\bar{u}_+ + \lambda_+^{(0)}\bar{v}_+ = -\mathrm{i}\alpha_0\bar{p}_+ + \frac{d^2\bar{u}_+}{d\bar{y}_+^2}, \tag{2.28b}$$

$$\frac{d\bar{p}_+}{d\bar{y}_+} = 0, \tag{2.28c}$$

$$\mathrm{i}\alpha_0(\lambda_+^{(0)}\bar{y}_+ + V_0 - c_0)\bar{w}_+ = -\mathrm{i}\beta_0\bar{p}_+ + \frac{d^2\bar{w}_+}{d\bar{y}_+^2}, \tag{2.28d}$$

with these equations subject to the classical no-slip condition of viscous flow

$$\bar{u}_+ = \bar{v}_+ = \bar{w}_+ = 0 \text{ on } \bar{y}_+ = 0, \tag{2.28e}$$

and the far field matching conditions

$$\bar{u}_+ \to -\lambda_+^{(0)}A_0, \quad \bar{w}_+ \to 0 \text{ as } \bar{y}_+ \to \infty, \tag{2.28f}$$

in view of the core behaviour (2.22) and (2.23). From (2.28c) we infer that the wave pressure is independent of the inner variable across the viscous shear layer and so $\bar{p}_+ =$ constant. Matching the pressure within the shear layer (2.27) as $\bar{y}_+ \to \infty$ with the core flow pressure (2.15) as $y \to 1^-$, we obtain

$$\bar{p}_+ = \hat{P}_0, \tag{2.29}$$

where use has been made of the asymptotic form (2.23), which determines the core behaviour of the pressure in the vicinity of the upper wall situated at $y = 1$.

(b) Viscous shear layer II–

The appropriate forms for the velocity and pressure within the lower viscous shear layer, where $y = -1 + \varepsilon^2\bar{y}_-$, to leading order, are

$$\hat{u} = \bar{u}_-,\ \hat{v} = \varepsilon^3\bar{v}_-,\ \hat{w} = \bar{w}_-,\ \hat{p} = \varepsilon^2\bar{p}_-,\ U_0 = \varepsilon^2(\lambda_-^{(0)}\bar{y}_- - V_0). \tag{2.30}$$

Substitution of these expansions into the disturbance equations (2.5) leads to the viscous balances

$$\mathrm{i}\alpha_0\bar{u}_- + \frac{d\bar{v}_-}{d\bar{y}_-} + \mathrm{i}\beta_0\bar{w}_- = 0, \tag{2.31a}$$

$$\mathrm{i}\alpha_0(\lambda_-^{(0)}\bar{y}_- - V_0 - c_0)\bar{u}_- + \lambda_-^{(0)}\bar{v}_- = -\mathrm{i}\alpha_0\bar{p}_- + \frac{d^2\bar{u}_-}{d\bar{y}_-^2}, \tag{2.31b}$$

$$\frac{d\bar{p}_-}{d\bar{y}_-} = 0, \tag{2.31c}$$

$$\mathrm{i}\alpha_0(\lambda_-^{(0)}\bar{y}_- - V_0 - c_0)\bar{w}_- = -\mathrm{i}\beta_0\bar{p}_- + \frac{d^2\bar{w}_-}{d\bar{y}_-^2}, \tag{2.31d}$$

with the usual no-slip condition of viscous flow

$$\bar{u}_- = \bar{v}_- = \bar{w}_- = 0 \text{ on } \bar{y}_- = 0, \tag{2.31e}$$

and the far field matching condition

$$\bar{u}_- \to \lambda_-^{(0)} A_0, \quad \bar{w}_- \to 0 \text{ as } \bar{y}_- \to \infty, \tag{2.31f}$$

in view of the core behaviour (2.24) and (2.25). Equation (2.31c) reveals that the pressure is constant to leading order throughout the lower viscous shear layer. Matching the pressure within the shear layer (2.30) as $\bar{y}_- \to \infty$ with the core flow pressure (2.15) as $y \to -1^+$, we find that

$$\bar{p}_- = \hat{P}_0 + \alpha_0^2 A_0 I(-1), \tag{2.32}$$

upon using the asymptotic form of the core pressure (2.25).

The aim is to derive a solvability condition for the systems (2.28) and (2.31) which depends only on the wave pressures $\bar{p}_\pm$. Smith (1979) outlines the well-known procedure of obtaining the solvability conditions corresponding to these linear wall problems. This leads to important relations which are fundamental to the derivation of a lower branch eigenrelation for plane Poiseuille–Couette flow, namely

$$(\alpha_0^2 + \beta_0^2)\bar{p}_+ = (\mathrm{i}\alpha_0 \lambda_+^{(0)})^{5/3} \frac{\mathrm{Ai}'(\xi_+)}{\kappa(\xi_+)} A_0, \tag{2.33a}$$

$$(\alpha_0^2 + \beta_0^2)\bar{p}_- = -(\mathrm{i}\alpha_0 \lambda_-^{(0)})^{5/3} \frac{\mathrm{Ai}'(\xi_-)}{\kappa(\xi_-)} A_0, \tag{2.33b}$$

where Ai is the Airy function, $\kappa(\xi) = \int_\xi^\infty \mathrm{Ai}(\xi)\, \mathrm{d}\xi$, and ξ_+, ξ_- are given by

$$(\xi_+, \xi_-) = -\mathrm{i}^{1/3}(s_+, s_-) \text{ with } s_+ = \frac{\alpha_0(c_0 - V_0)}{(\alpha_0 \lambda_+^{(0)})^{2/3}}, \quad s_- = \frac{\alpha_0(c_0 + V_0)}{(\alpha_0 \lambda_-^{(0)})^{2/3}}. \tag{2.34}$$

Observe that s_+ can be positive or negative depending on whether $c_0 > V_0$ or $c_0 < V_0$, respectively, while s_- is always positive. Subtraction of (2.33a) and (2.33b) establishes a relationship between the pressure in the upper and lower wall layers, specifically

$$(\alpha_0^2 + \beta_0^2)(\bar{p}_+ - \bar{p}_-) = (\mathrm{i}\alpha_0 \lambda_+^{(0)})^{5/3} \frac{\mathrm{Ai}'(\xi_+)}{\kappa(\xi_+)} A_0 + (\mathrm{i}\alpha_0 \lambda_-^{(0)})^{5/3} \frac{\mathrm{Ai}'(\xi_-)}{\kappa(\xi_-)} A_0. \tag{2.35}$$

Considering the difference between (2.29) and (2.32) leads to the determination of a pressure-displacement relation and we find that

$$\bar{p}_+ - \bar{p}_- = -\alpha_0^2 A_0 I(-1). \tag{2.36}$$

Then, from substitution of (2.36) into (2.35), after some manipulation, we finally obtain the eigenrelation corresponding to the lower branch neutral mode, that is

$$\alpha_0^{1/3}(\alpha_0^2+\beta_0^2)J_0+\lambda_0^{5/3}M_0=0, \tag{2.37}$$

where

$$M_0=\mathrm{i}^{5/3}\left(\frac{\mathrm{Ai}'(\xi_+)}{\kappa(\xi_+)}+\frac{\mathrm{Ai}'(\xi_-)}{\kappa(\xi_-)}\right), \tag{2.38}$$

and

$$J_0=I(-1)=\int_{-1}^{1}U_{00}^2\mathrm{d}y=\frac{16}{15}, \tag{2.39}$$

upon using (2.21) and denoting $\lambda_-^{(0)}=\lambda_+^{(0)}=\lambda_0$. Numerical solution of the lower-branch eigenrelation for given V_0 and spanwise wavenumber β_0 enables us to identify the possible neutral solutions for α_0, which is of our particular interest. Before we carry out this numerical study, it is convenient to introduce functions $g(s_+)$ and $g(s_-)$ defined as

$$g(s_+)=\mathrm{i}^{5/3}\frac{\mathrm{Ai}'(\xi_+)}{\kappa(\xi_+)}\text{ and }g(s_-)=\mathrm{i}^{5/3}\frac{\mathrm{Ai}'(\xi_-)}{\kappa(\xi_-)}. \tag{2.40}$$

Therefore the lower-branch eigenrelation, (2.37), may be expressed in the form

$$\alpha_0^{1/3}(\alpha_0^2+\beta_0^2)J_0+\lambda_0^{5/3}(g(s_+)+g(s_-))=0. \tag{2.41}$$

Subtraction of s_- and s_+ leads to determination of an explicit expression for α_0, namely

$$\alpha_0^{1/3}=\left(\frac{s_--s_+}{2^{1/3}V_0}\right), \tag{2.42}$$

where we have used $\lambda_-^{(0)}=\lambda_+^{(0)}=\lambda_0=2$.

Using (2.42) to eliminate the explicit α_0-dependence in (2.41), we find that

$$(s_--s_+)^7J_0+2^2V_0^6\beta_0^2J_0(s_--s_+)+2^4V_0^7(g(s_+)+g(s_-))=0. \tag{2.43}$$

Taking the real and imaginary parts of (2.43) leads to the important results

$$(s_--s_+)^7J_0+2^2V_0^6\beta_0^2J_0(s_--s_+)+2^4V_0^7(\mathrm{Re}(g(s_+))+\mathrm{Re}(g(s_-)))=0, \tag{2.44a}$$

$$\mathrm{Im}(g(s_+))+\mathrm{Im}(g(s_-))=0. \tag{2.44b}$$

We now investigate the solutions to the system of equations (2.44a) and (2.44b) for given values of the parameters V_0 and β_0. In order to determine the number of solutions of these equations, it is instructive to plot (as functions of s_- and s_+) contours corresponding to

(2.44a) and (2.44b). We consider a set of values for s_+ and s_-, bearing in mind that the former can be positive or negative, while the latter is always positive since c_0 and V_0 are taken to be positive, and plot these contours by making use of the numerical values of $g(s)$ already computed for a range of values of s in Appendix A. In order to identify the neutral values of s_- and s_+ we look at the intersection of these contours, which determines the number of solutions to the system of equations (2.44) and equivalently, establishes the number of solutions to (2.43). This therefore allows us to determine the corresponding neutral values of α_0 from (2.42).

Figure 2.5 illustrates results for the scaled spanwise wavenumber $\beta_0 = 0$ and explores the contours as V_0 increases. From figure 2.5(a) it can be seen that for $V_0 = 0$ which represents plane Poiseuille flow, there is just one intersection of the contours and hence one solution to the lower-branch eigenrelation (2.41). Figure 2.5(b) shows that when $V_0 \simeq 2.061$, two new solutions emerge and interestingly enough, it is observed as V_0 is further increased, one of these intersection points advances so that s_- tends to infinity as $V_0 \to \infty$, with s_+ remaining finite and positive, indicating that the scaled streamwise wavenumber α_0 approaches ∞ from (2.42) and therefore it becomes apparent that the wavelength of this mode is shortening with increasing V. As evident from figure 2.5(d) around $V_0 \simeq 6.45$, two further solutions arise and hence there are four intersections of the contours corresponding to this case. However, from figure 2.5(f) it can be concluded that only three solutions persist as $V_0 \to \infty$. Our main interest here is to investigate the effect of increasing β_0 on the number of solutions to the dispersion relation (2.41). Figures 2.6, 2.7 and 2.8 show the corresponding situation for $\beta_0 = 1, 3$ and 5 respectively. The main conclusions are as follows. For $V_0 = 0$, there is a unique solution for all three values of β_0. As V_0 is increased, two new solutions arise (figures 2.6(b), 2.7(b) and 2.8(b)). In addition, it can be deduced from figures 2.6(c), 2.7(c) and 2.8(c) that the wavelength of one of these modes decreases as $V_0 \to \infty$. As V_0 is further increased, we have four solutions as demonstrated in figures 2.6(d), 2.7(d) and 2.8(d). It should be noted that in the limit of large V_0 only three solutions continue to exist as displayed in figures 2.6(f), 2.7(f) and 2.8(f), analogous to the case when $\beta_0 = 0$. It is useful to examine the eigenrelation (2.43) in the limit $V_0 \to \infty$ as this allows us to gain insight into the ultimate fate of these modes as V is increased. It is assumed that s_+ and s_- remain $O(1)$ in this limit, therefore simplifying the lower-branch eigenrelation to

$$\Lambda\left(\frac{J_0}{4}\right)(s_- - s_+) + g(s_+) + g(s_-) \simeq 0, \tag{2.45}$$

where the new variable Λ is defined by

$$\Lambda = \frac{\beta_0^2}{V_0}.$$

In figure 2.9 we plot contours along which the real and imaginary parts of the left-hand side of (2.45) are zero. Comparison of figures 2.5(f), 2.6(f), 2.7(f) and 2.8(f) with figure 2.9 strongly confirm that we have three solutions in the limit $V_0 \to \infty$. Cubing both sides of (2.42) establishes the asymptotic form for the scaled streamwise wavenumber α_0 in the limit

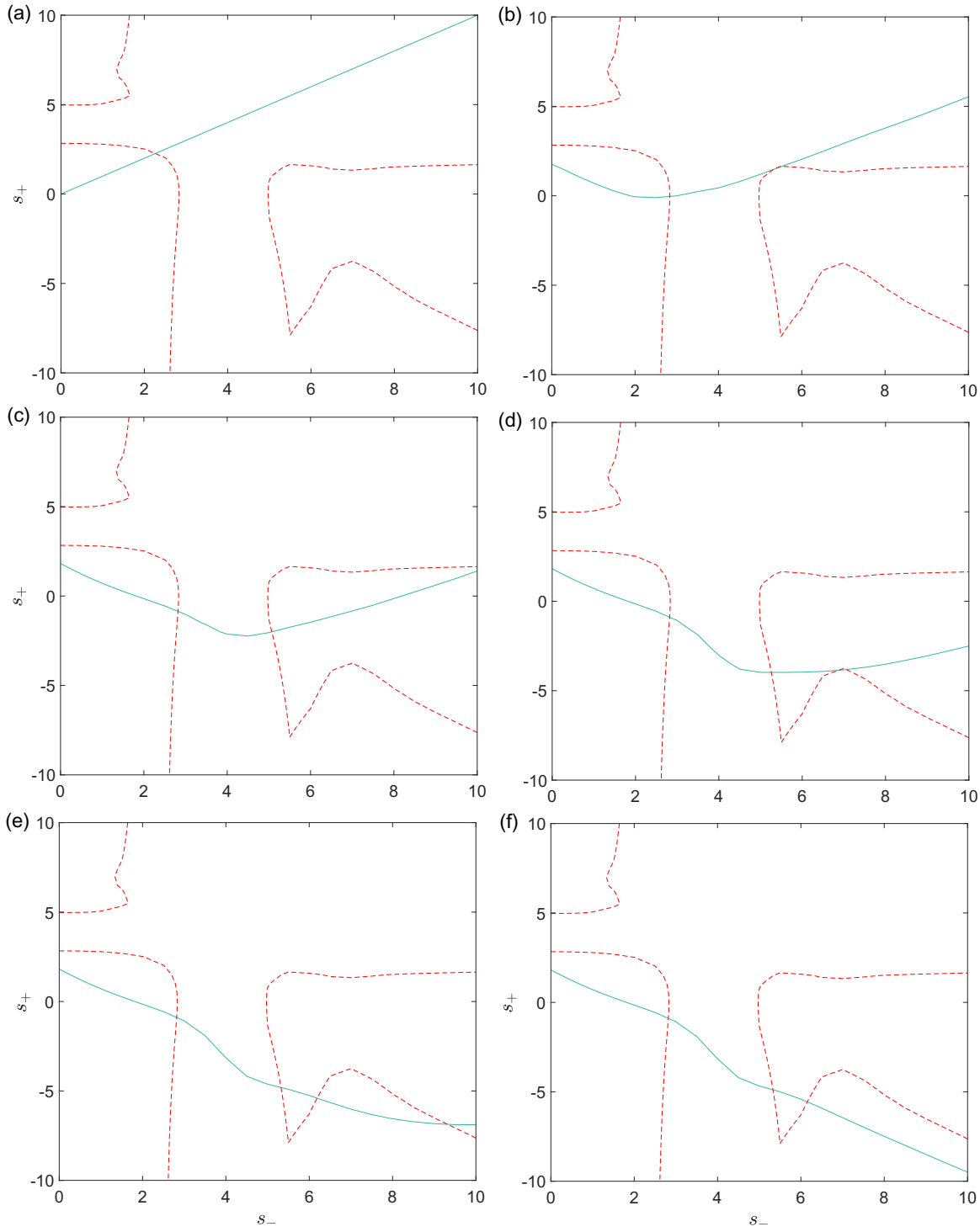

Figure 2.5: Solutions of the lower-branch eigenrelation (2.37) with $\beta_0 = 0$ for various values of the wall sliding speed V_0. (a) $V_0 = 0$; (b) $V_0 = 2.061$; (c) $V_0 = 4.2$; (d) $V_0 = 6.45$; (e) $V_0 = 10$; (f) $V_0 = 20$. Along the dashed curves the imaginary part of the left-hand side of (2.43) is zero, while along the bold curves the real part is zero.

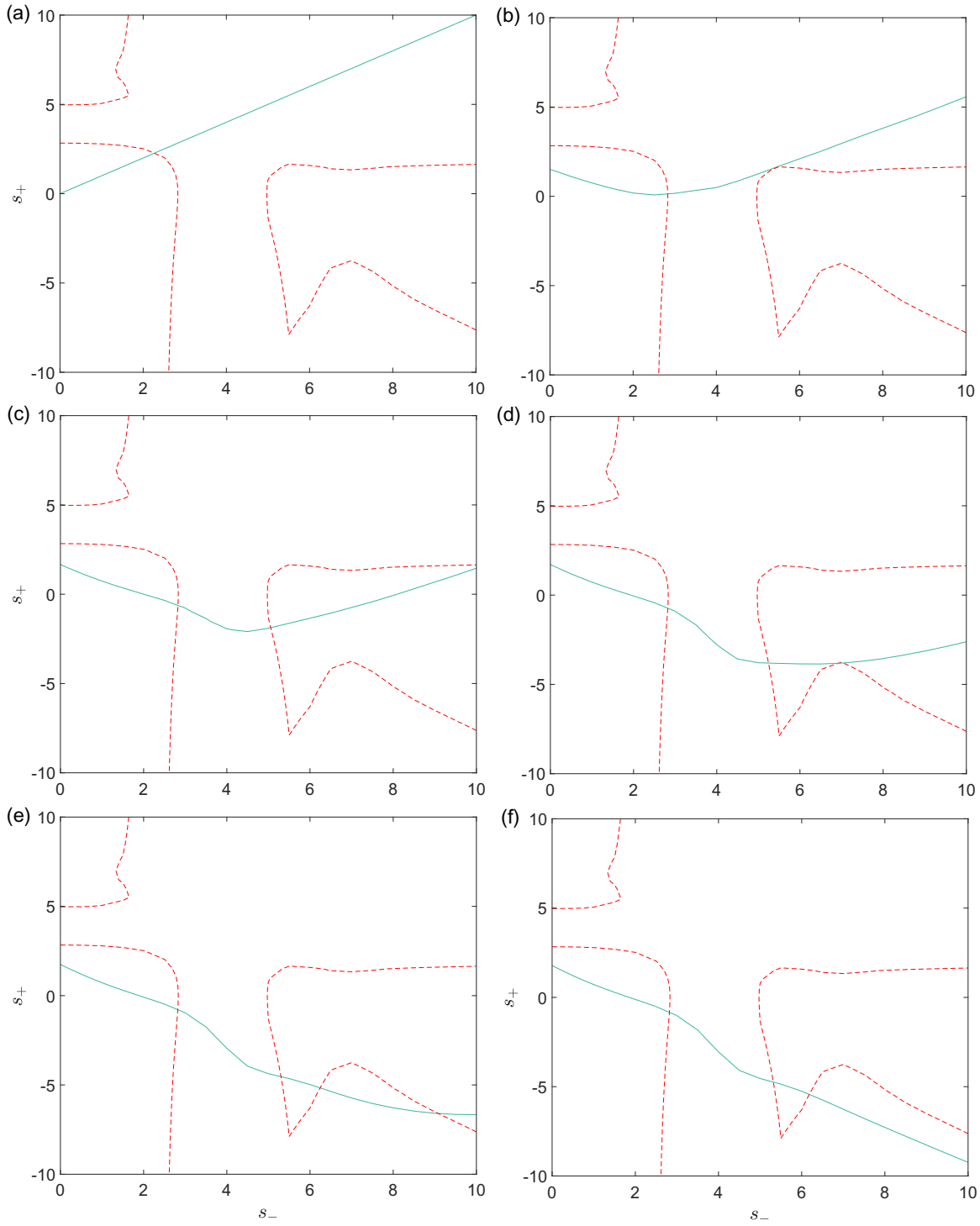

Figure 2.6: Solutions of the lower-branch eigenrelation (2.37) with $\beta_0 = 1$ for various values of the wall sliding speed V_0. (a) $V_0 = 0$; (b) $V_0 = 2.061$; (c) $V_0 = 4.2$; (d) $V_0 = 6.60$; (e) $V_0 = 10$; (f) $V_0 = 20$. Along the dashed curves the imaginary part of the left-hand side of (2.43) is zero, while along the bold curves the real part is zero.

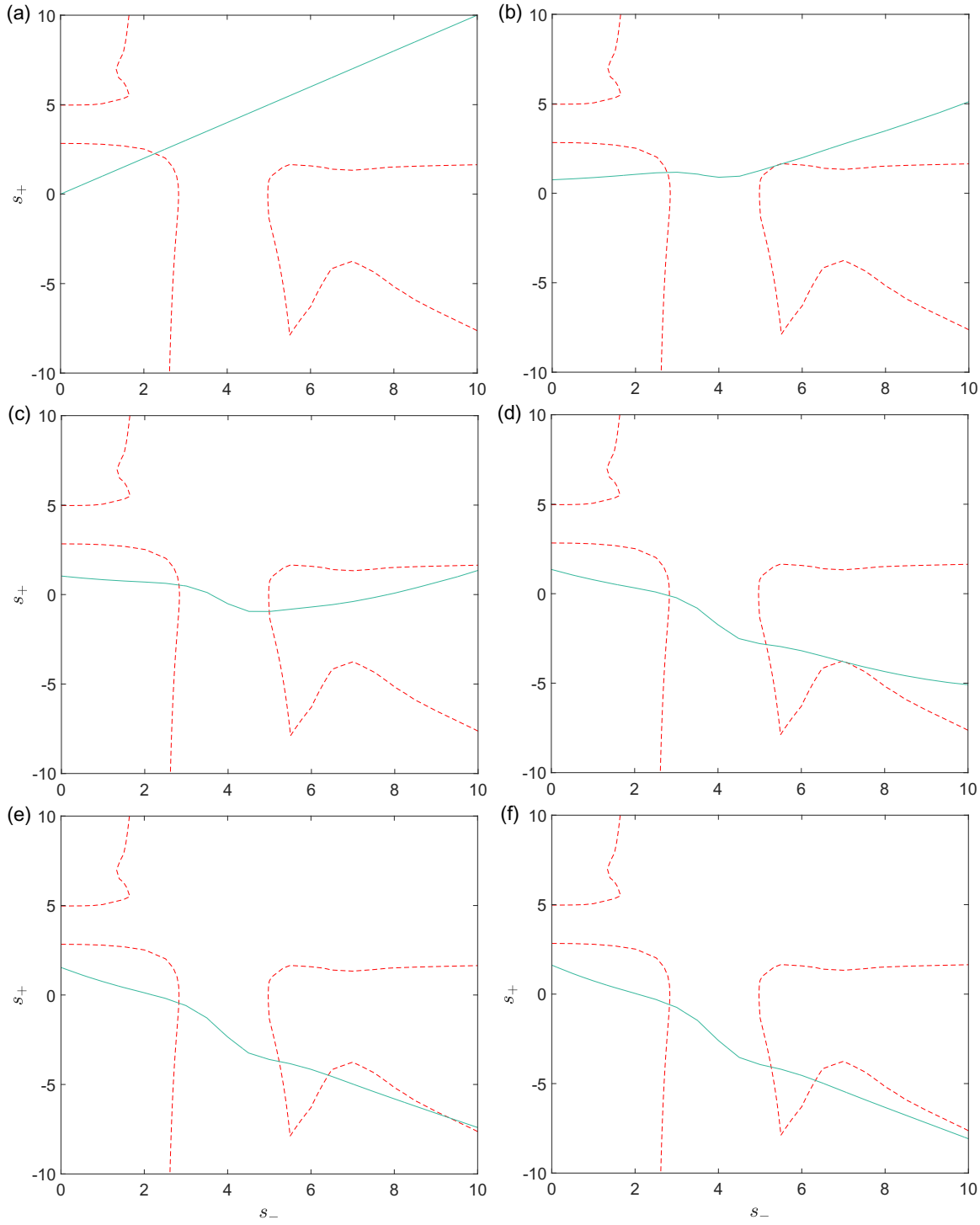

Figure 2.7: Solutions of the lower-branch eigenrelation (2.37) with $\beta_0 = 3$ for various values of the wall sliding speed V_0. (a) $V_0 = 0$; (b) $V_0 = 2.4$; (c) $V_0 = 4.6$; (d) $V_0 = 10.4$; (e) $V_0 = 20$; (f) $V_0 = 30$. Along the dashed curves the imaginary part of the left-hand side of (2.43) is zero, while along the bold curves the real part is zero.

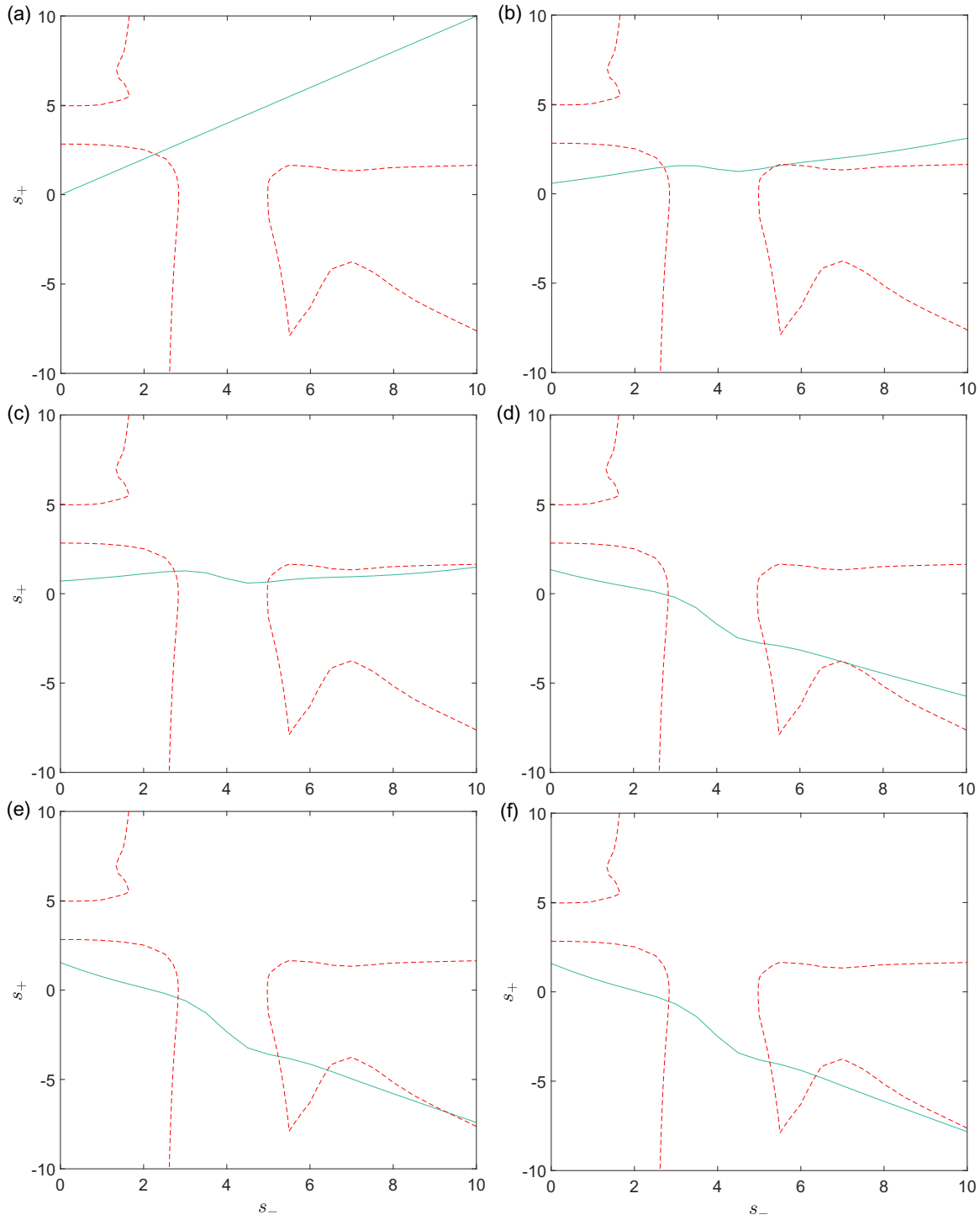

Figure 2.8: Solutions of the lower-branch eigenrelation (2.37) with $\beta_0 = 5$ for various values of the wall sliding speed V_0. (a) $V_0 = 0$; (b) $V_0 = 4.5$; (c) $V_0 = 6$; (d) $V_0 = 28$; (e) $V_0 = 55$; (f) $V_0 = 70$. Along the dashed curves the imaginary part of the left-hand side of (2.43) is zero, while along the bold curves the real part is zero.

of large sliding speed V_0, namely

$$\alpha_0 \sim \frac{(s_- - s_+)^3 V_0^{-3}}{\lambda_0} \text{ as } V_0 \to \infty. \tag{2.46}$$

From (2.46) we infer that α_0 is decreasing with asymptotically increasing V_0, implying that these modes all have an increasing wavelength.

It is important to reiterate that in addition to these solutions, a solution is also found for which $s_- \to \infty$ with s_+ remaining of order one in the limit of large V_0. It is straightforward to show that in this limit the function $g(s_-)$ defined in (2.40) takes the following asymptotic form

$$g(s_-) \sim -s_- + \mathrm{e}^{\mathrm{i}\pi/4} s_-^{-1/2} \text{ as } s_- \to \infty. \tag{2.47}$$

This indicates that, to leading order, $g(s_-)$ is real but $g(s_+)$ is imaginary since s_+ is $O(1)$ as $V_0 \to \infty$. Therefore in order to balance terms in (2.43) the imaginary part of $g(s_+)$ must be zero and from the plot of the imaginary part of the function $g(s)$ in Appendix A, we conclude that there is a unique value of s_+, s_0 say, at which $g(s_+)$ is purely real, namely

$$s_+ = s_0 \simeq 2.2972. \tag{2.48}$$

Setting the value of $s_+ = s_0$ in (2.42) provides the corresponding expression for s_-:

$$s_- = s_0 + \lambda_0^{1/3} \alpha_0^{1/3} V_0. \tag{2.49}$$

Since $g(s_+) = g(s_0)$ and, to leading order, $g(s_-) = -s_-$ from (2.47), the appropriate limiting form of the eigenrelation (2.41) is found to be

$$-\alpha_0^{1/3}(\alpha_0^2 + \beta_0^2) J_0 \sim -\lambda_0((\lambda_0)^{2/3} s_0 + 2\alpha_0^{1/3} V_0) + (\lambda_0)^{5/3} g(s_0), \tag{2.50}$$

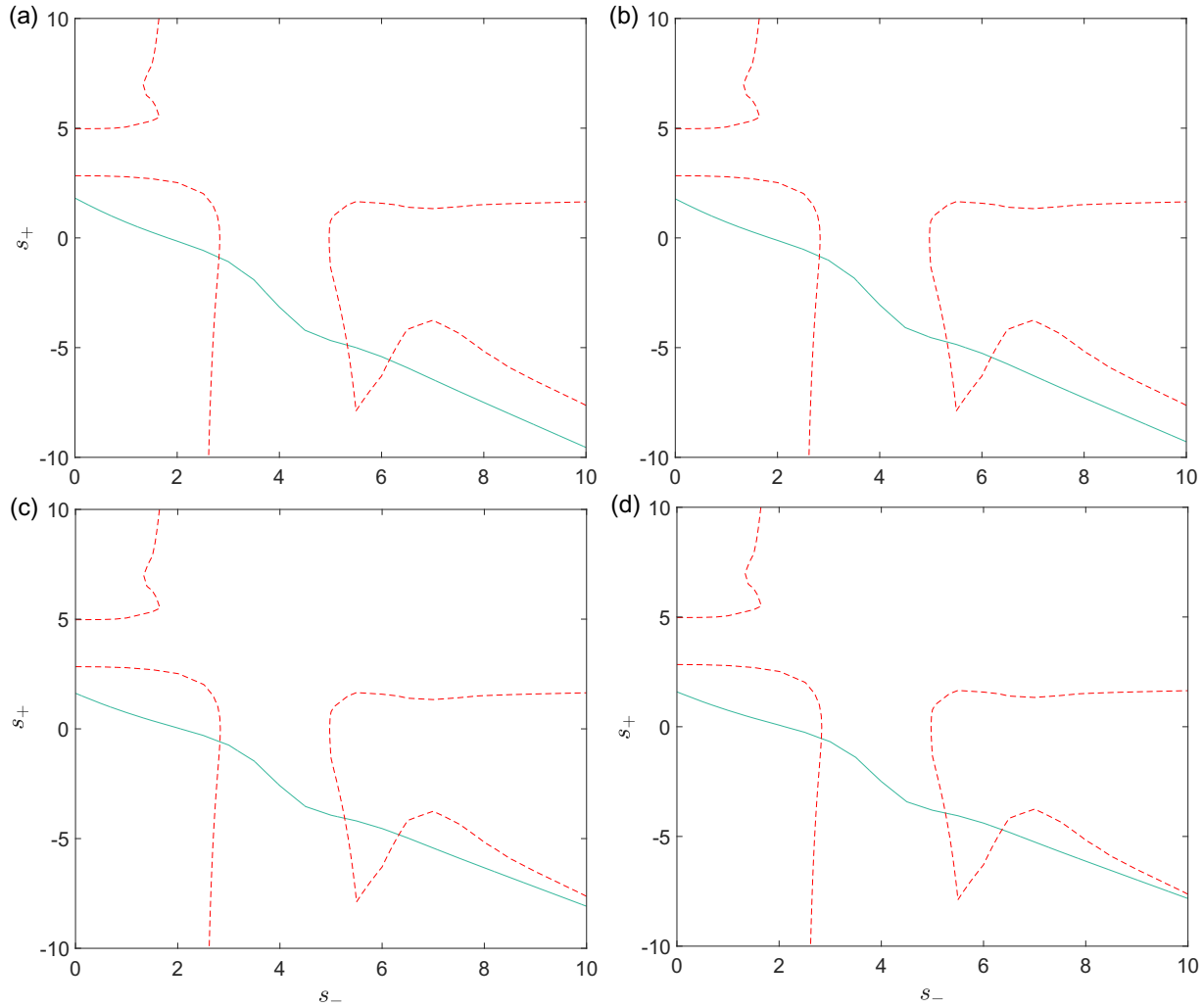

Figure 2.9: Solution of the lower-branch eigenrelation (2.45) with for asymptotically large V_0, for the following values of Λ: (a) 0; (b) 1/20; (c) 9/30; (d) 25/70. Along the dashed curves the imaginary part of the left-hand side of (2.45) is zero, while along the bold curves the real part is zero.

where we have used (2.49) to substitute for s_-. In order to gain insight into how this mode shortens its wavelength as V_0 is increased, we rearrange (2.50) and obtain the result

$$V_0 \sim \frac{(\alpha_0^2 + \beta_0^2)}{2\lambda_0} J_0 + O(\alpha_0^{-1/3}) \text{ as } V_0 \to \infty. \tag{2.51}$$

It follows from (2.34) (after putting $s_+ = s_0$) that the expression for the wavespeed is

$$c_0 = V_0 + (\lambda_0^{2/3})\alpha_0^{-1/3} s_0. \tag{2.52}$$

Combining (2.51) and (2.52) establishes the asymptotic behaviour of the wavespeed c_0 in

the limit of asymptotically large V_0, specifically

$$c_0 \sim V_0 + \left(\frac{2\lambda_0}{J_0} - \Lambda\right)^{-1/6} (\lambda_0)^{2/3} s_0 V_0^{-1/6} \text{ as } V_0 \to \infty. \tag{2.53}$$

As mentioned earlier, for this mode the quantity s_+ remains $O(1)$ and positive and hence from (2.53) it can be deduced that the wavespeed also increases with increasing V_0. Two important remarks may be made at this stage:

(i) It is worthwhile to mention that for this mode the wavespeed increases with increasing sliding speed V, implying that the lower critical layer is moving away from the lower wall since it can be inferred from (2.53) that the quantity $c_0 + V_0 \to \infty$ as $V_0 \to \infty$. However, the upper critical layer remains embedded within its viscous layer because the quantity $c_0 - V_0 \to 0$ as $V_0 \to \infty$. Putting a different way, we recall from the systems (2.28) and (2.31) that the lower and upper critical layers are located at

$$y_- = \frac{c_0 + V_0}{\lambda_-^{(0)}}, \qquad y_+ = \frac{c_0 - V_0}{\lambda_+^{(0)}}. \tag{2.54}$$

Equation (2.54) demonstrates explicitly the variation of the locations of these critical layers with V_0 and it is clearly seen that $y_- \to \infty$ and $y_+ \to 0$ as $V_0 \to \infty$, thus reinforcing the conclusions drawn above. This therefore suggests that the lower part of the the high-Reynolds-number asymptotic structure corresponding to the lower branch of the neutral curve is turning into an upper-branch-type mode while the upper part still remains essentially intact and follows the lower-branch structure. This leads to the formation of a hybrid mode which will be examined further in detail later.

(ii) From numerical and asymptotic studies carried out above, we come to the conclusion that there are two types of mode in the limit $V_0 \to \infty$. The first type behaves according to (2.46), that is, it has an increasing wavelength and the number of solutions found is three corresponding to different values of β_0. Obviously, in this situation the critical layers remain sited within their respective viscous wall layers since it has been assumed that s_+ and s_- remain $O(1)$ as $V_0 \to \infty$. It is interesting to notice that the asymptotic structure remains unaltered until the order of magnitude of V becomes one, in other words, when $V_0 \sim O(R^{2/7})$ as evident from the appropriate scalings (2.26). The second type of mode has a wavelength that decreases as V_0 increases and equation (2.51) predicts the behaviour of this mode. The asymptotic scaling of the upper branch of the main neutral curve will be the focus of the next subsection.

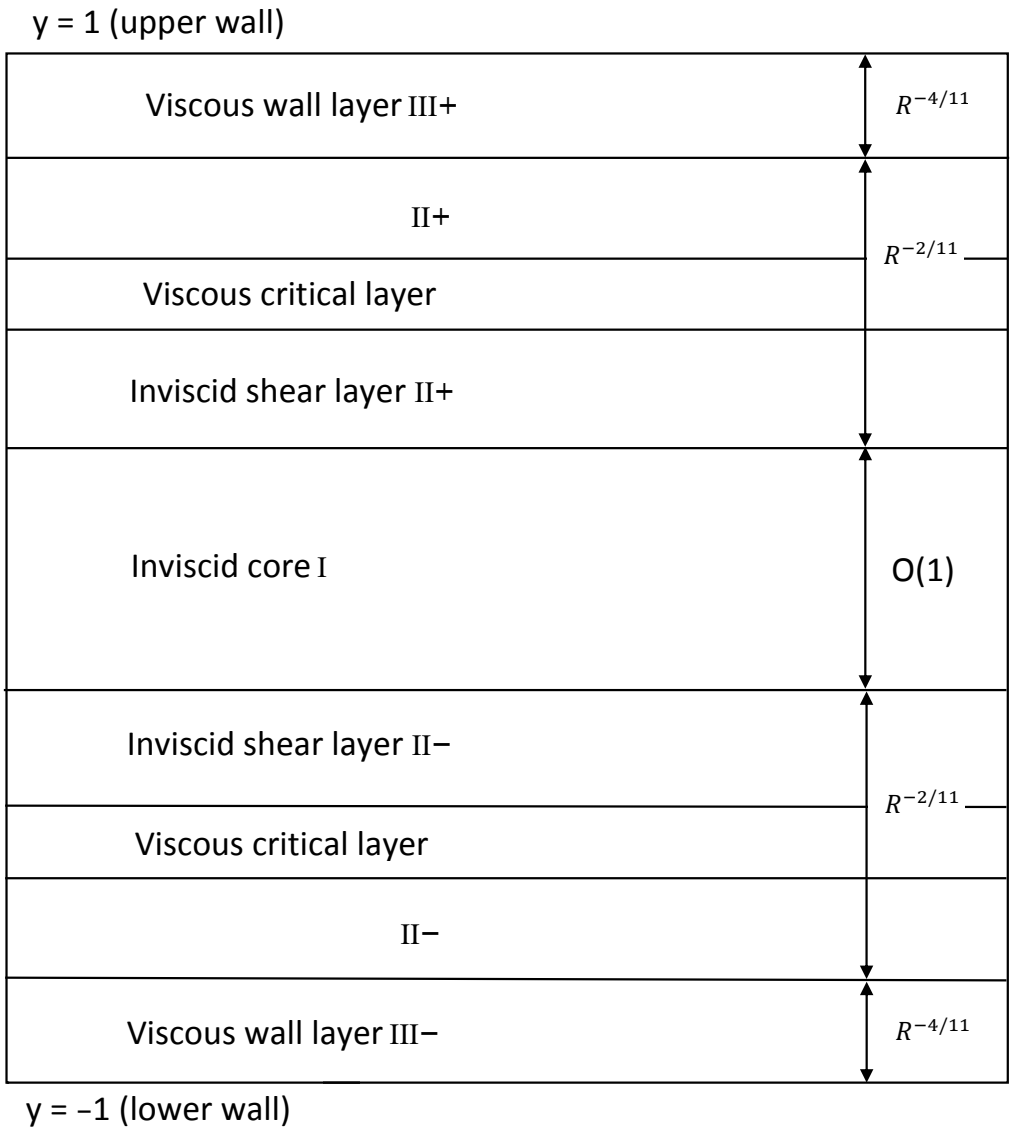

Figure 2.10: The high-Reynolds-numbers asymptotic structure of the upper-branch modes.

2.3.4 Upper-branch analysis

In this subsection, we will focus on the high-Reynolds-number asymptotic analysis of the upper branch of the main neutral stability curve. Before we carry out the asymptotic analysis, it is necessary to describe the asymptotic structure of the upper-branch mode at small values of V. The important contrasting feature of the upper-branch behaviour is that the typical value of the disturbance wavespeed is large, and consequently, the two critical layers are readily distinguishable from the viscous wall layers. This leads to a nine-zone structure in accordance with etiquette: an invisicid core region (I), two invisicid shear layers (regions II+, II–), two viscous wall layers (III+, III–). In this scenario, the disturbance survives

due to an interaction between the linear critical layers (positioned where the basic velocity $U_0(y)$ coincides with the phase speed c of the disturbance) and the viscous Stokes layers adjacent to each wall. It must be pointed out that the viscous critical layers are embedded within their respective shear layers to smooth out the singular behaviour of the solutions in II+, II–. Figure 2.10 shows the nine zone asymptotic structure of the upper-branch-mode. Having now provided a brief introduction of the asymptotic structure corresponding to the upper branch neutral mode, we will explore the dynamics of underlying dominant physical processes in each region as we did for the lower-branch modes. Once again, we seek the asymptotic solution to (2.5) at high Reynolds number with $V = \varepsilon^2 V_0,\ \varepsilon \ll 1$, and we need to determine the small parameter ε in terms of the Reynolds number.

(i) Inviscid Core region I. The principal feature of the core region is that the basic flow velocity is much larger than the wavespeed of the perturbation. This indicates $U_0 - c \approx U_0$ in view of equations (2.5). The dynamics are predominantly inviscid in the core region of the main flow, similar to what we have observed for the lower branch case. At this stage, it is necessary, however, to calculate higher-order terms in the expansions for the normal velocity and pressure. The purpose of consideration of higher-order terms in each of these expansions is of central importance to our investigation of the upper branch mode behaviour and this will become apparent with the proceeding analysis. Unsurprisingly, the disturbance expansions are in the familiar form, namely

$$\left.\begin{aligned} \hat{u} = F_0 + \varepsilon^2 F_1 + \cdots,\ \hat{v} = \varepsilon G_0 + \varepsilon^3 G_1 + \cdots,\ \hat{w} = \varepsilon^2 H_0 + \varepsilon^4 H_1 + \cdots, \\ \hat{p} = \varepsilon^2 P_0 + \varepsilon^4 P_1 + \cdots, \quad \alpha = \varepsilon\alpha_0 + \varepsilon^3\alpha_1 + \cdots, \quad U = U_{00} + \varepsilon^2 U_{01}, \\ c = \varepsilon^2 c_0 + \varepsilon^4 c_1 + \cdots, \quad \beta = \varepsilon\beta_0 + \varepsilon^3\beta_1 + \cdots. \end{aligned}\right\} \tag{2.55}$$

The solutions for F_0, G_0, H_0 and P_0 are as given in (2.18) and (2.19), with A_0 and $\hat{P}_0$ taken to be real without loss of generality. We are particularly interested in deducing the form for the higher-order terms G_1 and P_1 (also known as the correction terms). At the next order the governing equations are found to be

$$\mathrm{i}\alpha_0 F_1 + \mathrm{i}\alpha_1 F_0 + \frac{dG_1}{dy} + \mathrm{i}\beta_0 H_0 = 0, \tag{2.56a}$$

$$U_{00}(\mathrm{i}\alpha_0 F_1 + \mathrm{i}\alpha_1 F_0) + (U_{01} - c_0)\mathrm{i}\alpha_0 F_0 + G_0\frac{dU_{01}}{dy} + G_1\frac{dU_{00}}{dy} = -\mathrm{i}\alpha_0 P_0, \tag{2.56b}$$

$$U_{00}(\mathrm{i}\alpha_0 G_1 + \mathrm{i}\alpha_1 G_0) + (U_{01} - c_0)\mathrm{i}\alpha_0 G_0 = -\frac{dP_1}{dy}, \tag{2.56c}$$

$$U_{00}(\mathrm{i}\alpha_0 H_1 + \mathrm{i}\alpha_1 H_0) + (U_{01} - c_0)\mathrm{i}\alpha_0 H_0 = -\mathrm{i}\beta_0 P_1 - \mathrm{i}\beta_1 P_0. \tag{2.56d}$$

Substitution of the expression for $\mathrm{i}\alpha_0 F_1 + \mathrm{i}\alpha_1 F_0$ from the continuity equation (2.56a) into (2.56b) allows us to formulate the first order differential equation satisfied by G_1 as

$$\frac{dG_1}{dy} - G_1\frac{U_{00}'}{U_{00}} = (U_{01} - c_0)\frac{\mathrm{i}\alpha_0 F_0}{U_{00}} + G_0\frac{U_{01}'}{U_{00}} + \frac{\mathrm{i}\alpha_0 P_0}{U_{00}} - \mathrm{i}\beta_0 H_0. \tag{2.57}$$

The solution can be found by multiplying both sides of (2.57) by the integrating factor $1/U_{00}$, inserting the leading order solutions (2.18), (2.19) and it follows after integration by parts that the correction term G_1 takes the form

$$G_1 = -\mathrm{i}\alpha_0 A_1 U_{00} - \mathrm{i}\alpha_0 A_0 (U_{01} - c_0) + \mathrm{i}\alpha_0 U_{00}\left(1 + \frac{\beta_0^2}{\alpha_0^2}\right)\int_0^y \frac{P_0}{U_{00}^2} dy, \tag{2.58}$$

where $-\mathrm{i}\alpha_0 A_1$ is the constant of integration, with the complex constant A_1 unknown. It should be noted that the lower limit of the integral on the right-hand side is arbitrarily set to zero. Consequently upon substituting the expression for G_1, G_0 from (2.19) into the normal momentum equation (2.56c) and then integrating we obtain the correction term P_1:

$$\begin{aligned} P_1 = P_+^{(1)} + \alpha_0(\alpha_1 A_0 + \alpha_0 A_1)\int_y^1 U_{00}^2 dy \; + 2\alpha_0^2 A_0 \int_y^1 (U_{01} - c_0) U_{00} dy \\ + (\alpha_0^2 + \beta_0^2)\int_1^y U_{00}^2 \left[\int_0^y \frac{P_0}{U_{00}^2} dy\right] dy, \end{aligned} \tag{2.59}$$

where $P_+^{(1)}$ is the complex unknown constant. This suggests that the higher order terms G_1 and P_1 may be expressed in the form

$$G_1 = -\mathrm{i}\alpha_0 A_1 U_{00} + \text{purely imaginary terms}, \tag{2.60a}$$

$$P_1 = P_+^{(1)} + \alpha_0^2 A_1 I(y) + \text{purely real terms}. \tag{2.60b}$$

Considering the near-wall behaviour of these solutions, it is found that (2.22–2.25) continue to hold, and taking the imaginary parts of (2.60b) we obtain

$$\mathrm{Im}(P_1) \to \mathrm{Im}(P_+^{(1)}) \text{ as } y \to 1, \tag{2.61a}$$

$$\mathrm{Im}(P_1) \to \mathrm{Im}(P_+^{(1)}) + \alpha_0^2 \mathrm{Im}(A_1) I(-1) \text{ as } y \to -1. \tag{2.61b}$$

From this latter result, we see that there is a jump in the imaginary part of P_1 across the core, with

$$\Big[\mathrm{Im}(P_1)\Big]_-^+ \equiv \lim_{y\to 1} \mathrm{Im}(P_1) - \lim_{y\to -1} \mathrm{Im}(P_1) = -\alpha_0^2 \mathrm{Im}(A_1) I(-1). \tag{2.62}$$

(ii) The inviscid shear region II+. In contrast to the core region, the invisicid shear region is characterised by the basic near-wall shear flow being of the same size as the wavespeed of the perturbation. Put a different way, a balance is achieved between the first term in the basic flow expansion (2.11) and the disturbance wavespeed c, that is, $U_{00} \sim c$. In addition, it is evident that this takes place at a distance of $O(\varepsilon^2)$ from the upper wall $y = 1$. Now we consider the dynamics of the upper inviscid shear region.

The expansions within the upper inviscid region take the form

$$\left.\begin{aligned} U_0 = \varepsilon^2(2Y_+ + V_0) + \varepsilon^4(-Y_+^2 - V_0 Y_+), \quad y = 1 - \varepsilon^2 Y_+, \\ \hat{u} = u_+^{(0)} + \varepsilon^2 u_+^{(1)} + \cdots, \quad \hat{v} = -\varepsilon^3 v_+^{(0)} - \varepsilon^5 v_+^{(1)} - \cdots, \\ \hat{w} = w_+^{(0)} + \varepsilon^2 w_+^{(1)} + \cdots, \quad \hat{p} = \varepsilon^2 p_+^{(0)} + \varepsilon^4 p_+^{(1)} + \cdots. \end{aligned}\right\} \tag{2.63}$$

Here the velocity and pressure components depend purely on the scaled wall normal coordinate Y_+. Substituting these expansions into the disturbance equations (2.5), to leading order, yields the following set of inviscid balances

$$\mathrm{i}\alpha_0 u_+^{(0)} + \frac{dv_+^{(0)}}{dY_+} + \mathrm{i}\beta_0 w_+^{(0)} = 0, \tag{2.64a}$$

$$\mathrm{i}\alpha_0(\lambda_+^{(0)}Y_+ + V_0 - c_0)u_+^{(0)} + \lambda_+^{(0)}v_+^{(0)} = -\mathrm{i}\alpha_0 p_+^{(0)}, \tag{2.64b}$$

$$\frac{dp_+^{(0)}}{dY_+} = 0, \tag{2.64c}$$

$$\mathrm{i}\alpha_0(\lambda_+^{(0)}Y_+ + V_0 - c_0)w_+^{(0)} = -\mathrm{i}\beta_0 p_+^{(0)}. \tag{2.64d}$$

We start the analysis of the linear problem (2.64) with consideration of the the disturbance normal momentum equation (2.64c). Equation (2.64c) implies that $p_+^{(0)}$ is constant in region II+. Matching the pressure $p_+^{(0)}$ within the upper inviscid region (2.63) as $Y_+ \to \infty$ with the core pressure (2.55) as $y \to 1^-$, we conclude that

$$p_+^{(0)} = \hat{P}_0, \tag{2.65}$$

in view of the core behaviour (2.23).

Our task is to formulate the governing differential equation for the disturbance normal velocity $v_+^{(0)}$. For convenience let us introduce a new variable τ_+ defined by

$$\tau_+ = \lambda_+^{(0)}Y_+ + V_0 - c_0. \tag{2.66}$$

To eliminate the disturbance velocity components $u_+^{(0)}$ and $w_+^{(0)}$ from the continuity equation (2.64a), it remains to substitute for $u_+^{(0)}$, $p_+^{(0)}$ from (2.64a) and (2.65), along with (2.64d) for $w_+^{(0)}$ and we find that

$$\frac{dv_+^{(0)}}{dY_+} - \frac{\lambda_+^{(0)}v_+^{(0)}}{\tau_+} = \frac{\mathrm{i}(\alpha_0^2 + \beta_0^2)\hat{P}_0}{\alpha_0\tau_+}. \tag{2.67}$$

It is obvious that (2.67) can be solved by the usual method of solving a linear differential equation of the first-order. The integrating factor of (2.67) is given by

$$e^{-\int \frac{\lambda_+^{(0)}}{\tau_+} dY_+} = \frac{1}{\tau_+}, \tag{2.68}$$

in view of (2.66). Multiplying both sides of equation (2.67) by the integrating factor and then on integrating the resulting equation with respect to Y_+, we get

$$v_+^{(0)} = -\frac{\mathrm{i}(\alpha_0^2 + \beta_0^2)\hat{P}_0}{\alpha_0\lambda_+^{(0)}} + C_1\tau_+, \tag{2.69}$$

where C_1 is to be determined using the matching procedure. Matching the normal velocity within the invisicid core region (2.55) as $y \to 1^+$ with the expansion for the normal velocity in the upper inviscid region (2.63) as $Y_+ \to \infty$ leads to the evaluation of the constant C_1 as

$$C_1 = \mathrm{i}\alpha_0 A_0,$$

where use has been made of the asymptotic form (2.22), which signifies the core behaviour of the normal velocity in the vicinity of the upper wall. Thus it follows that the solution of (2.67) is

$$v_+^{(0)} = \mathrm{i}\alpha_0 A_0 \tau_+ - \frac{\mathrm{i}(\alpha_0^2 + \beta_0^2)\hat{P}_0}{\alpha_0 \lambda_+^{(0)}}. \tag{2.70}$$

The form for $w_+^{(0)}$ immediately follows from equation (2.64d) upon substituting the expression for $p_+^{(0)}$ from (2.65). Further, substitution of $v_+^{(0)}$ from (2.70) and $p_+^{(0)}$ from (2.65) into the disturbed streamwise momentum equation (2.64b) determines $u_+^{(0)}$ explicitly. Thus the solution to the upper inviscid shear wave system (2.64) can be summarized in the form:

$$u_+^{(0)} = -A_0 \lambda_+^{(0)} + \frac{\beta_0^2 \hat{P}_0}{\alpha_0^2 \tau_+}, \quad w_+^{(0)} = -\frac{\beta_0 \hat{P}_0}{\alpha_0 \tau_+}, \tag{2.71}$$

with $v_+^{(0)}$, $p_+^{(0)}$ given by (2.70) and (2.65) respectively. There are two important observations to be made here:

(i) Two components of wave velocity $u_+^{(0)}$ and $w_+^{(0)}$ exhibit discontinuity at $\tau_+ = 0$. Therefore it becomes clear that in order to smooth out this singularity, an upper viscous critical layer must be introduced in the vicinity of $\tau_+ = 0$ and hence in view of (2.66) this implies that this thin critical layer is located at

$$Y_+ = \frac{c_0 - V_0}{\lambda_+^{(0)}}.$$

This indicates that the position of the critical layer depends on the value V of the wall sliding speed.

(ii) It is interesting to point out that although these two components are singular at the critical level, the linear combination $u_+^{(0)} + (\beta_0/\alpha_0) w_+^{(0)}$ remains finite.

It is easily seen from (2.63) that when $y = 1$, the scaled normal coordinate Y_+ is zero. Applying the wall-normal condition that $v_+^{(0)} = 0$ on the upper wall $y = 1$, we obtain

$$A_0(c_0 - V_0) + \left(1 + \frac{\beta_0^2}{\alpha_0^2}\right) \frac{\hat{P}_0}{\lambda_+^{(0)}} = 0, \tag{2.72}$$

providing a first pressure-displacement relation.

Having understood the key role of the upper viscous critical layer, we aim to formulate the next-order problem. At the next order we obtain the following equations which are forced by the leading order solutions

$$\mathrm{i}\alpha_0 u_+^{(1)} + \mathrm{i}\alpha_1 u_+^{(0)} + \frac{dv_+^{(1)}}{dY_+} + \mathrm{i}\beta_0 w_+^{(1)} + \mathrm{i}\beta_1 w_+^{(0)} = 0, \tag{2.73a}$$

$$\tau_+(\mathrm{i}\alpha_0 u_+^{(1)} + \mathrm{i}\alpha_1 u_+^{(0)}) + \lambda_+^{(0)} v_+^{(1)} + \left(\frac{d\xi_+}{dY_+}\right) v_+^{(0)} + \mathrm{i}\alpha_0 \xi_+ u_+^{(0)} + \mathrm{i}\alpha_0 p_+^{(1)} + \mathrm{i}\alpha_1 p_+^{(0)} = 0, \tag{2.73b}$$

$$\frac{dp_+^{(1)}}{dY_+} = 0, \tag{2.73c}$$

$$\tau_+(\mathrm{i}\alpha_0 w_+^{(1)} + \mathrm{i}\alpha_1 w_+^{(0)}) + \mathrm{i}\alpha_0 \xi_+ w_+^{(0)} + \mathrm{i}\beta_0 p_+^{(1)} + \mathrm{i}\beta_1 p_+^{(0)} = 0, \tag{2.73d}$$

where the new variable $\xi_+ = \lambda_+^{(1)} Y_+^2 - V_0 Y_+ - c_1$. From (2.73c) we conclude that the wave pressure at next order is independent of the scaled variable Y_+ across the upper inviscid region and so $p_+^{(1)} =$ constant. Matching the pressure within the upper inviscid layer (2.63) as $Y_+ \to \infty$ with the inviscid core flow pressure (2.55) as $y \to 1^-$ yields

$$p_+^{(1)} = P_+^{(1)}, \tag{2.74}$$

in view of (2.60b) since $I(1) = 0$ and the contributions from purely real terms are identically zero.

Examining the spanwise momentum equation (2.73d) gives us the next-order term $w_+^{(1)}$ in the asymptotic expansion of the spanwise velocity (2.63) as

$$w_+^{(1)} = -\left(\frac{\alpha_1}{\alpha_0} + \frac{\xi_+}{\tau_+}\right) w_+^{(0)} - \left(\frac{\beta_0 p_+^{(1)} + \beta_1 p_+^{(0)}}{\alpha_0 \tau_+}\right). \tag{2.75}$$

Turning to the streamwise momentum equation (2.73b) now, substitution of the expression for $\mathrm{i}\alpha_0 u_+^{(1)} + \mathrm{i}\alpha_1 u_+^{(0)}$ from the continuity equation (2.73a) into (2.73b) yields a balance of the form

$$\frac{dv_+^{(1)}}{dY_+} - \frac{\lambda_+^{(0)} v_+^{(1)}}{\tau_+} = \mathrm{i}\left(\frac{\alpha_1\beta_0 - \alpha_0\beta_1}{\alpha_0}\right) w_+^{(0)} + \frac{\mathrm{i}(\alpha_0^2 + \beta_0^2) p_+^{(1)}}{\alpha_0 \tau_+} + \frac{\mathrm{i}(\alpha_0\alpha_1 + \beta_0\beta_1)\hat{P}_0}{\alpha_0 \tau_+} + \left(\frac{d\xi_+}{dY_+}\right)\frac{v_+^{(0)}}{\tau_+} - \frac{\mathrm{i}\lambda_+^{(0)} \alpha_0 A_0 \xi_+}{\tau_+},$$

upon substituting for $w_+^{(1)}$ from (2.75) and simply quoting the result from (2.71) that $\alpha_0 u_+^{(0)} + \beta_0 w_+^{(0)} = -\alpha_0 A_0 \lambda_+^{(0)}$. Substituting the expression for $v_+^{(0)}$, $w_+^{(0)}$ from (2.70) and (2.71) respectively, multiplying both sides of the resulting equation by the integrating factor

$1/\tau_+$, and then integrating with respect to Y_+, we obtain the solution for $v_+^{(1)}$ which may be expressed in the form

$$v_+^{(1)} = \mathrm{i}\alpha_0 A_+^{(1)}\tau_+ + \text{imaginary terms} - \frac{\mathrm{i}(\alpha_0^2+\beta_0^2)p_+^{(1)}}{\alpha_0\lambda_+^{(0)}} - \frac{2\mathrm{i}\alpha_0\lambda_+^{(1)}\hat{P}_0}{\lambda_+^{(0)3}}\left(\frac{\beta_0^2}{\alpha_0^2}+1\right)\tau_+ \ln \tau_+, \tag{2.76}$$

with

$$\text{imaginary terms} = -\mathrm{i}A_0\alpha_0\left(\frac{c_0^2+\tau_+^2-V_0^2}{\lambda_+^{(0)2}}\right) - \mathrm{i}\alpha_0 A_0 c_1 + \left(\frac{\alpha_1\beta_0-\alpha_0\beta_1}{\alpha_0^2\lambda_+^{(0)}}\right)\mathrm{i}\beta_0\hat{P}_0 - \frac{\mathrm{i}(\alpha_0\alpha_1+\beta_0\beta_1)\hat{P}_0}{\alpha_0\lambda_+^{(0)}} - \frac{\mathrm{i}(\alpha_0^2+\beta_0^2)c_0\hat{P}_0}{\lambda_+^{(0)2}\alpha_0}.$$

The details of the calculations involving the derivation of the expression for $v_+^{(1)}$ are omitted here for the sake of brevity. Here $A_+^{(1)}$ is an unknown complex constant and the final logarithmic term indicates that the result (2.76) holds for $\tau_+ > 0$. It is important to reiterate that the thin critical layer located at $\tau_+ = 0$ smooths out the singularity arising from the final logarithmic term in the expression for $v_+^{(1)}$. In order to match the normal velocity between the upper inviscid region and the upper viscous wall layer we need to deduce the form for the disturbance normal velocity $v_+^{(1)}$ on the other side of the viscous critical layer, that is, when $\tau_+ < 0$. The dynamics of such a layer have been thoroughly investigated already (Lin 1955; Stuart 1963; Reid 1965) and the implication of this is that the solution for $v_+^{(1)}$ is reproduced when $\tau_+ < 0$, just below the critical layer, with $\ln \tau_+$ replaced by $\ln|\tau_+| - \mathrm{i}\pi$. Consequently, we arrive at the following useful result

$$v_+^{(1)} = \mathrm{i}\alpha_0 A_+^{(1)}\tau_+ + \text{imaginary terms} - \frac{\mathrm{i}(\alpha_0^2+\beta_0^2)p_+^{(1)}}{\alpha_0\lambda_+^{(0)}} - \frac{2\mathrm{i}\alpha_0\lambda_+^{(1)}\hat{P}_0}{\lambda_+^{(0)3}}\left(\frac{\beta_0^2}{\alpha_0^2}+1\right)\tau_+(\ln|\tau_+| - \mathrm{i}\pi) \text{ for } \tau_+ < 0. \tag{2.77}$$

Matching the real part of the first term in (2.77) as $\tau_+ \to \infty$ with the real part of the first term in the expression (2.60a) for G_1 as $y \to 1$, we obtain

$$\mathrm{Im}(A_+^{(1)}) = \mathrm{Im}(A_1). \tag{2.78}$$

Matching the behaviour in the inviscid shear region below the critical layer (i.e. for $\tau_+ < 0$) to the flow in the viscous wall layer III+ at $y = 1$ leads to the determination of the size of the small amplitude parameter ε in terms of the Reynolds number. In the viscous wall layer III+ we have $U_0 - c \simeq V - c$ from (2.2). In this region there is a dominant balance between the

inertial term $\mathrm{i}\alpha(U_0-c)\hat{u}$ and the viscous term $R^{-1}\hat{u}''$. Let q denote the thickness of this layer and then from following similar reasoning as outlined earlier in the lower-branch analysis we can see that $\alpha(V-c)\sim O(\varepsilon^3)$ and $R^{-1}\hat{u}''\sim O(R^{-1}q^{-2})$ and therefore the inertial-viscous balance implies that $q\sim O(R^{-1/2}\varepsilon^{-3/2})$. Also it is easily seen that the scaled streamwise perturbation $\hat{u}$ within this layer must be of $O(1)$ to match with that of the inviscid region II+ and by use of the continuity equation we infer that the order of magnitude of the normal velocity in region III+ is εq. Finally matching this to the second term of the normal velocity $\hat{v}$ in (2.63) yields $\varepsilon q\sim\varepsilon^5$, which establishes the scaling for the upper branch, namely

$$\varepsilon = R^{-1/11}.$$

Having identified the scaling for ε, we now turn to explore the dynamics of the wall layer III+.

(ii) Viscous wall layer III+. The viscous wall layer in the upper region ensures that the disturbance satisfies the no-slip condition on the upper wall $y=1$. In the upper wall layer the appropriate flow expansions, to leading order, are

$$\left.\begin{aligned} U_0=\varepsilon^2 V_0, \quad \hat{u}=\bar{u}_+, \quad \hat{v}=-\varepsilon^5\bar{v}_+,\\ \hat{w}=\bar{w}_+, \quad \hat{p}=\varepsilon^2\hat{p}_0, \quad y=1-\varepsilon^4\bar{y}_+. \end{aligned}\right\} \tag{2.79}$$

Substitution of these expansions into the disturbance equations (2.5) leads to the viscous balances

$$\mathrm{i}\alpha_0\bar{u}_+ + \frac{d\bar{v}_+}{d\bar{y}_+} + \mathrm{i}\beta_0\bar{w}_+ = 0, \tag{2.80a}$$

$$\mathrm{i}\alpha_0(V_0-c_0)\bar{u}_+ = -\mathrm{i}\alpha_0\hat{p}_0 + \frac{d^2\bar{u}_+}{d\bar{y}_+^2}, \tag{2.80b}$$

$$\frac{d\hat{p}_0}{d\bar{y}_+} = 0, \tag{2.80c}$$

$$\mathrm{i}\alpha_0(V_0-c_0)\bar{w}_+ = -\mathrm{i}\beta_0\hat{p}_0 + \frac{d^2\bar{w}_+}{d\bar{y}_+^2}, \tag{2.80d}$$

subject to the usual no-slip wall conditions

$$\bar{u}_+ = \bar{v}_+ = \bar{w}_+ = 0 \text{ on } \bar{y}_+ = 0. \tag{2.80e}$$

From matching of the streamwise and spanwise velocity within the upper viscous wall layer (2.79) as $\bar{y}_+\to\infty$ with the upper shear layer velocity components (2.63) as $Y_+\to 0$ we find that

$$\bar{u}_+ \to \frac{\hat{P}_0}{(c_0-V_0)}, \quad \bar{w}_+ \to \frac{\beta_0\hat{P}_0}{\alpha_0(c_0-V_0)}, \text{ as } \bar{y}_+\to\infty, \tag{2.80f}$$

in view of the first pressure–displacement relation (2.72). Equation (2.80c) reveals that the viscous pressure is constant to leading order in region III+. Matching the pressure within

the upper viscous wall layer (2.79) as $\bar{y}_+ \to \infty$ with the upper shear flow pressure (2.63) as $Y_+ \to 0$, we obtain

$$\hat{p}_0 = \hat{P}_0, \tag{2.81}$$

implied by (2.65). Substituting the expression for $\hat{p}_0$ into (2.80b) yields the second-order inhomogeneous ordinary differential equation satisfied by $\bar{u}_+$:

$$\frac{d^2\bar{u}_+}{d\bar{y}_+^2} - \mathrm{i}\alpha_0(V_0 - c_0)\bar{u}_+ = \mathrm{i}\alpha_0\hat{P}_0. \tag{2.82}$$

The general solution is the sum of a particular solution of (2.82) and two complementary solutions of the homogeneous part of (2.82). Being guided by this discussion, the disturbance streawise velocity $\bar{u}_+$ can be represented as

$$\bar{u}_+ = a_1 e^{r_1\bar{y}_-} + a_2 e^{r_2\bar{y}_-} + \frac{\hat{P}_0}{c_0 - V_0}, \tag{2.83}$$

with

$$r_1 = \left(\frac{1}{2}\alpha_0(c_0 - V_0)\right)^{1/2}(1 - \mathrm{i}), \quad r_2 = -\left(\frac{1}{2}\alpha_0(c_0 - V_0)\right)^{1/2}(1 - \mathrm{i}).$$

Here a_1 and a_2 are arbitrary constants to be determined. An assumption has been made that the wavespeed of the perturbation c_0 is larger than the sliding speed of the upper wall V_0 while finding the roots of the characteristic equation corresponding to the homogeneous part of (2.82). Note that the real part of r_1 is positive, whereas the real part of r_2 is negative. Applying the no-slip condition that $\bar{u}_+ = 0$ on the upper wall $\bar{y}_+ = 0$ establishes a relationship between unknown constants, we find that

$$a_1 + a_2 = -\frac{\hat{P}_0}{c_0 - V_0}. \tag{2.84}$$

Since the real part of r_1 is positive and as a result $\bar{u}_+$ becomes exponentially large as $\bar{y}_+ \to \infty$. Thus, we set $a_1 = 0$ and this evaluates the constant a_2. Substituting the values of a_1 and a_2 into (2.83) we deduce that the disturbance velocity $\bar{u}_+$ takes the form:

$$\bar{u}_+ = \frac{\hat{P}_0}{c_0 - V_0}(1 - e^{r_2\bar{y}_+}). \tag{2.85}$$

A similar procedure establishes that the general solution of the disturbance spanwise momentum (2.80d) satisfying the no-slip on $\bar{y}_+ = 0$ and boundedness condition as $\bar{y}_+ \to \infty$ is

$$\bar{w}_+ = \frac{\beta_0\hat{P}_0}{\alpha_0(c_0 - V_0)}(1 - e^{r_2\bar{y}_+}). \tag{2.86}$$

Examining equations (2.85) and (2.86) in the limit $\bar{y}_+ \to \infty$ shows that the matching conditions (2.80f) are satisfied automatically. Since our task is to determine the normal velocity

let us now return to the continuity equation (2.80a) which formulates the first-order problem for $\bar{v}_+$:

$$\frac{d\bar{v}_+}{d\bar{y}_+} = -\left(\frac{\mathrm{i}(\alpha_0^2+\beta_0^2)\hat{P}_0}{\alpha_0(c_0-V_0)}\right)(1-e^{r_2\bar{y}_+}), \tag{2.87}$$

upon substituting for $\bar{u}_+$, $\bar{w}_+$ from (2.85) and (2.86) respectively. Integrating this equation and imposing the classical no-slip condition (2.80e) it follows that the disturbance velocity in the normal direction is

$$\bar{v}_+ = -\left(\frac{\mathrm{i}(\alpha_0^2+\beta_0^2)\hat{P}_0}{\alpha_0(c_0-V_0)}\right)\left(\bar{y}_+ - \frac{e^{r_2\bar{y}_+}}{r_2} + \frac{1}{r_2}\right). \tag{2.88}$$

We can conclude that the first purely imaginary part in $\bar{v}_+$ matches automatically to the corresponding term in the solution for $v_+^{(0)}$ in the upper inviscid shear region, in view of the first pressure–displacement relation (2.72). Matching the real part of $\bar{v}_+$ as $\bar{y}_+ \to \infty$ with the real part of $v_+^{(1)}$ in (2.76) as $\tau_+ \to (V_0 - c_0)$, we arrive at the result

$$\begin{aligned}-\left(\frac{\hat{P}_0}{(2\alpha_0(c_0-V_0)^3)^{1/2}}\right) = (c_0-V_0)\mathrm{Im}(A_1)\left(1+\frac{\beta_0^2}{\alpha_0^2}\right)^{-1} + \frac{\mathrm{Im}(p_+^{(1)})}{\lambda_+^{(0)}} \\ + \left(\frac{2\lambda_+^{(1)}\hat{P}_0}{\lambda_+^{(0)3}}\right)\pi(c_0-V_0),\end{aligned} \tag{2.89}$$

where use has been made of (2.78) to eliminate $A_+^{(1)}$.

(iv) The inviscid shear region II–. The main feature of the lower invisicid shear region is that there is a balance between the first term in the basic flow expansion (2.11) and the disturbance wavespeed c, that is, $U_{00} \sim c$ and it is obvious that this takes place at a distance of $O(\varepsilon^2)$ from the lower wall $y = -1$. The appropriate flow expansions within the lower inviscid region are

$$\left.\begin{aligned} U_0 = \varepsilon^2(2Y_- - V_0) + \varepsilon^4(-Y_-^2 + V_0Y_-), \quad y = -1+\varepsilon^2 Y_-, \\ \hat{u} = u_-^{(0)} + \varepsilon^2 u_-^{(1)} + \cdots, \quad \hat{v} = \varepsilon^3 v_-^{(0)} + \varepsilon^5 v_-^{(1)} + \cdots, \\ \hat{w} = w_-^{(0)} + \varepsilon^2 w_-^{(1)} + \cdots, \quad \hat{p} = \varepsilon^2 p_-^{(0)} + \varepsilon^4 p_-^{(1)} + \cdots. \end{aligned}\right\} \tag{2.90}$$

Here the velocity components and pressure components depend on the scaled wall normal coordinate Y_-. Substituting these expansions into the linearised Navier-Stokes equations

(2.5), to leading order, provide a set of inviscid balances

$$\mathrm{i}\alpha_0 u_-^{(0)} + \frac{dv_-^{(0)}}{dY_-} + \mathrm{i}\beta_0 w_-^{(0)} = 0, \tag{2.91a}$$

$$\mathrm{i}\alpha_0(\lambda_-^{(0)}Y_- - V_0 - c_0)u_-^{(0)} + \lambda_-^{(0)}v_-^{(0)} = -\mathrm{i}\alpha_0 p_-^{(0)}, \tag{2.91b}$$

$$\frac{dp_-^{(0)}}{dY_-} = 0, \tag{2.91c}$$

$$\mathrm{i}\alpha_0(\lambda_-^{(0)}Y_- - V_0 - c_0)w_-^{(0)} = -\mathrm{i}\beta_0 p_-^{(0)}. \tag{2.91d}$$

We are now ready to proceed with the solution of equations (2.91). We start with the disturbance normal momentum equation (2.91c), which shows that the pressure is constant to leading order throughout region II–. Matching the pressure $p_-^{(0)}$ within the lower inviscid region (2.90) as $Y_- \to \infty$ with the core pressure (2.55) as $y \to -1^+$, we obtain

$$p_-^{(0)} = \hat{P}_0 + \alpha_0^2 A_0 J_0, \tag{2.92}$$

in view of the core behaviour (2.25). At this stage it is convenient to introduce a new variable τ_- defined by

$$\tau_- = \lambda_-^{(0)}Y_- - V_0 - c_0. \tag{2.93}$$

Eliminating $u_-^{(0)}$ and $w_-^{(0)}$ from the continuity equation (2.91a) formulates the governing equation for the disturbance normal velocity $v_-^{(0)}$:

$$\frac{dv_-^{(0)}}{dY_-} - \frac{\lambda_-^{(0)}v_-^{(0)}}{\tau_-} = \frac{\mathrm{i}(\alpha_0^2+\beta_0^2)p_-^{(0)}}{\alpha_0\tau_-}, \tag{2.94}$$

where use has been made of (2.91b), (2.91d) to substitute for $u_-^{(0)}$ and $w_-^{(0)}$, respectively. Multiplying both sides of this equation by the integrating factor $1/\tau_-$ and then integrating the resulting equation with respect to Y_-, we find that

$$v_-^{(0)} = -\frac{\mathrm{i}(\alpha_0^2+\beta_0^2)(\hat{P}_0 + \alpha_0^2 A_0 J_0)}{\alpha_0\lambda_-^{(0)}} + C_2\tau_-, \tag{2.95}$$

where C_2 is to be evaluated. The requirement that the normal velocity within the invisicid core region (2.55) as $y \to -1^+$ should match with the expansion for the normal velocity in the lower inviscid region (2.90) as $Y_- \to \infty$ enables us to calculate C_2 as

$$C_2 = -\mathrm{i}\alpha_0 A_0,$$

where we have used the asymptotic form (2.24), which indicates the core behaviour of the normal velocity near the lower wall. It remains to substitute C_2 into (2.95), which leads to the conclusion that the expression for $v_-^{(0)}$ is

$$v_-^{(0)} = -\mathrm{i}\alpha_0 A_0\tau_- - \frac{\mathrm{i}(\alpha_0^2+\beta_0^2)(\hat{P}_0 + \alpha_0^2 A_0 J_0)}{\alpha_0\lambda_-^{(0)}}. \tag{2.96}$$

The form for $w_-^{(0)}$ immediately follows from equation (2.91d) upon substituting the expression for $p_-^{(0)}$ from (2.92) and after that substitution of $v_-^{(0)}$ and $p_-^{(0)}$ into (2.91b) determines $u_-^{(0)}$. Thus the leading order solution to the inviscid system (2.91) can be written in the form:

$$u_-^{(0)} = A_0\lambda_-^{(0)} + \frac{\beta_0^2(\hat{P}_0 + \alpha_0^2 A_0 J_0)}{\alpha_0^2\tau_-}, \quad w_-^{(0)} = -\frac{\beta_0(\hat{P}_0 + \alpha_0^2 A_0 J_0)}{\alpha_0\tau_-}, \tag{2.97}$$

with $v_-^{(0)}$, $p_-^{(0)}$ given by (2.96) and (2.92) respectively.

It is obvious from (2.90) that when $y = -1$, the scaled normal coordinate Y_- is zero. Applying the wall-normal condition that $v_-^{(0)} = 0$ on the lower wall $y = -1$ yields a second pressure–displacement relation

$$A_0(c_0 + V_0) - \left(1 + \frac{\beta_0^2}{\alpha_0^2}\right)\frac{(\hat{P}_0 + \alpha_0^2 A_0 J_0)}{\lambda_-^{(0)}} = 0. \tag{2.98}$$

It should be noted that similar remarks apply here as for the upper region II+. Having determined the leading order solution to the inviscid system we will now investigate the behaviour of the higher order terms in expansions (2.90) which is of particular importance. Our ultimate aim is to find the next order term $v_-^{(1)}$ in the asymptotic expansion (2.90) of the normal velocity $\hat{v}$. At next order we get the following equations which are forced by these leading order solutions

$$\mathrm{i}\alpha_0 u_-^{(1)} + \mathrm{i}\alpha_1 u_-^{(0)} + \frac{dv_-^{(1)}}{dY_-} + \mathrm{i}\beta_0 w_-^{(1)} + \mathrm{i}\beta_1 w_-^{(0)} = 0, \tag{2.99a}$$

$$\tau_-(\mathrm{i}\alpha_0 u_-^{(1)} + \mathrm{i}\alpha_1 u_-^{(0)}) + \lambda_-^{(0)} v_-^{(1)} + \left(\frac{d\xi_-^{(1)}}{dY_-}\right) v_-^{(0)} + \mathrm{i}\alpha_0\xi_- u_-^{(0)} + \mathrm{i}\alpha_0 p_-^{(1)} + \mathrm{i}\alpha_1 p_-^{(0)} = 0, \tag{2.99b}$$

$$\frac{dp_-^{(1)}}{dY_-} = 0, \tag{2.99c}$$

$$\tau_-(\mathrm{i}\alpha_0 w_-^{(1)} + \mathrm{i}\alpha_1 w_-^{(0)}) + \mathrm{i}\alpha_0\xi_- w_-^{(0)} + \mathrm{i}\beta_0 p_-^{(1)} + \mathrm{i}\beta_1 p_-^{(0)} = 0, \tag{2.99d}$$

where the new variable $\xi_- = \lambda_-^{(1)} Y_-^2 + V_0 Y_- - c_1$. It is easily seen that (2.99d) may be rearranged to yield the next order term $w_-^{(1)}$:

$$w_-^{(1)} = -\left(\frac{\alpha_1}{\alpha_0} + \frac{\xi_-}{\tau_-}\right) w_-^{(0)} - \left(\frac{\beta_0 p_-^{(1)} + \beta_1 p_-^{(0)}}{\alpha_0\tau_-}\right). \tag{2.100}$$

From (2.99c) we deduce that the wave pressure at next order is constant. Matching the pressure within the lower inviscid layer (2.90) as $Y_- \to \infty$ with the core flow pressure (2.55) as $y \to -1^+$, we obtain

$$p_-^{(1)} = P_+^{(1)} + \alpha_0^2 A_1 J_0 + \text{real constant}, \tag{2.101}$$

in view of (2.60b) since $I(-1) = J_0$. It should be noted that real constant incorporates the contributions arising from the remaining terms on the right-hand side of (2.59) as $y \to -1^+$. It is interesting to notice that its value does not affect the upper-branch eigenrelation to be derived later.

To simplify the task of formulating the differential equation for $v_-^{(1)}$, we shall insert the expression for $\mathrm{i}\alpha_0 u_-^{(1)} + \mathrm{i}\alpha_1 u_-^{(0)}$ from the continuity equation (2.99a) into the streamwise momentum equation (2.99b). This leads to

$$\frac{dv_-^{(1)}}{dY_-} - \frac{\lambda_-^{(0)} v_-^{(1)}}{\tau_-} = \mathrm{i}\left(\frac{\alpha_1\beta_0 - \alpha_0\beta_1}{\alpha_0}\right) w_-^{(0)} + \frac{\mathrm{i}(\alpha_0^2 + \beta_0^2) p_-^{(1)}}{\alpha_0 \tau_-} + \frac{\mathrm{i}(\alpha_0\alpha_1 + \beta_0\beta_1) p_-^{(0)}}{\alpha_0 \tau_-} + \left(\frac{d\xi_-}{dY_-}\right)\frac{v_-^{(0)}}{\tau_-} + \frac{\mathrm{i}\lambda_-^{(0)}\alpha_0 A_0 \xi_-}{\tau_-},$$

upon substituting for $w_-^{(1)}$ from (2.100) and using the fact that $\alpha_0 u_-^{(0)} + \beta_0 w_-^{(0)} = \alpha_0 A_0 \lambda_-^{(0)}$. Substituting for $v_-^{(0)}$, $w_-^{(0)}$ from (2.96) and (2.97) respectively, multiplying both sides of the resulting equation by the integrating factor $1/\tau_-$, and then integrating with respect to Y_+, after extensive algebra we find that

$$v_-^{(1)} = -\mathrm{i}\alpha_0 A_-^{(1)} \tau_- + \text{imaginary terms} - \frac{\mathrm{i}(\alpha_0^2 + \beta_0^2) p_-^{(1)}}{\alpha_0 \lambda_-^{(0)}} - \frac{2\mathrm{i}\alpha_0 \lambda_-^{(1)} p_-^{(0)}}{\lambda_-^{(0)3}} \left(\frac{\beta_0^2}{\alpha_0^2} + 1\right) \tau_- \ln \tau_-, \tag{2.102}$$

with

$$\text{imaginary terms} = \mathrm{i}A_0\alpha_0 \left(\frac{c_0^2 + \tau_-^2 - V_0^2}{\lambda_-^{(0)2}}\right) + \mathrm{i}\alpha_0 A_0 c_1 + \left(\frac{\alpha_1\beta_0 - \alpha_0\beta_1}{\alpha_0^2 \lambda_-^{(0)}}\right)\mathrm{i}\beta_0 p_-^{(0)} - \frac{\mathrm{i}(\alpha_0\alpha_1 + \beta_0\beta_1) p_-^{(0)}}{\alpha_0 \lambda_-^{(0)}} - \frac{\mathrm{i}(\alpha_0^2 + \beta_0^2) c_0 p_-^{(0)}}{\lambda_-^{(0)2}\alpha_0},$$

given here for $\tau_- > 0$ and $A_-^{(1)}$ is an unknown complex constant analogous to $A_+^{(1)}$. The details of the calculations concerning the derivation of the higher order term $v_-^{(1)}$ are omitted here. Applying the classical phase shift of $-\pi$ (Lin 1955; Stuart 1963; Reid 1965) it follows that the term $\ln \tau_-$ in (2.102) is replaced by $\ln|\tau_-| - i\pi$ when $\tau_- < 0$. As a consequence we deduce that

$$v_-^{(1)} = -\mathrm{i}\alpha_0 A_-^{(1)} \tau_- + \text{imaginary terms} - \frac{\mathrm{i}(\alpha_0^2 + \beta_0^2) p_-^{(1)}}{\alpha_0 \lambda_-^{(0)}} - \frac{2\mathrm{i}\alpha_0 \lambda_-^{(1)} p_-^{(0)}}{\lambda_-^{(0)3}} \left(\frac{\beta_0^2}{\alpha_0^2} + 1\right) \tau_- (\ln|\tau_-| - \mathrm{i}\pi) \text{ for } \tau_- < 0. \tag{2.103}$$

Matching the real part of the first term in (2.103) as $\tau_- \to \infty$ with the real part of the first term in the expression (2.60a) for G_1 as $y \to -1$, we find that $A_-^{(1)}$ is connected to A_1 via

$$\mathrm{Im}(A_-^{(1)}) = \mathrm{Im}(A_1). \tag{2.104}$$

It is obvious that the relationship between the wave amplitude parameter ε and the Reynolds number R remain unaltered, namely $\varepsilon = R^{-1/11}$ due to symmetry in the high-Reynolds-number asymptotic structure of the upper-branch modes across the inviscid core region I. We now aim to examine the dynamics of the lower viscous wall layer III–.

(v) Viscous wall layer III–. The viscous wall layer in the lower region ensures that the disturbance satisfies the no-slip condition on the lower wall $y = -1$. The disturbance expansion, to leading order, is

$$\left.\begin{aligned} U_0 = -\varepsilon^2 V_0, \quad \hat{u} = \bar{u}_-, \quad \hat{v} = \varepsilon^5 \bar{v}_-, \\ \hat{w} = \bar{w}_-, \quad \hat{p} = \varepsilon^2 \tilde{p}_0, \quad y = -1 + \varepsilon^4 \bar{y}_-. \end{aligned}\right\} \tag{2.105}$$

Substituting these expansions into the disturbance equations (2.5) we obtain the governing equations for the lower viscous wall layer

$$\mathrm{i}\alpha_0 \bar{u}_- + \frac{d\bar{v}_-}{d\bar{y}_-} + \mathrm{i}\beta_0 \bar{w}_- = 0, \tag{2.106a}$$

$$-\mathrm{i}\alpha_0 (V_0 + c_0)\bar{u}_- = -\mathrm{i}\alpha_0 \tilde{p}_0 + \frac{d^2 \bar{u}_-}{d\bar{y}_-^2}, \tag{2.106b}$$

$$\frac{d\tilde{p}_0}{d\bar{y}_-} = 0, \tag{2.106c}$$

$$-\mathrm{i}\alpha_0 (V_0 + c_0)\bar{w}_- = -\mathrm{i}\beta_0 \tilde{p}_0 + \frac{d^2 \bar{w}_-}{d\bar{y}_-^2}, \tag{2.106d}$$

with the no-slip condition on the lower wall:

$$\bar{u}_- = \bar{v}_- = \bar{w}_- = 0 \text{ on } \bar{y}_- = 0. \tag{2.106e}$$

Matching of the streamwise and spanwise velocity within the lower viscous wall layer (2.105) as $\bar{y}_- \to \infty$ with the lower shear layer velocity components (2.90) as $Y_- \to 0$ leads to the conclusion that

$$\bar{u}_- \to \frac{(\hat{P}_0 + \alpha_0^2 A_0 I(-1))}{(c_0 + V_0)}, \quad \bar{w}_- \to \frac{\beta_0 (\hat{P}_0 + \alpha_0^2 A_0 I(-1))}{\alpha_0 (c_0 + V_0)}, \text{ as } \bar{y}_- \to \infty, \tag{2.106f}$$

in view of the second pressure-displacement relation (2.98).

Our aim is to find the general solution of the linear set of equations (2.106) subject to the boundary conditions (2.106e,f). We start by noting that according to (2.106c) the viscous pressure is constant across the lower wall layer. Matching the pressure within the lower viscous wall layer (2.105) as $\bar{y}_- \to \infty$ with the lower shear flow pressure (2.90) as $Y_- \to 0$ yields the expression for $\tilde{p}_0$

$$\tilde{p}_0 = \hat{P}_0 + \alpha_0^2 A_0 J_0, \tag{2.107}$$

from (2.92). Substituting for $\tilde{p}_0$ into (2.106b) we deduce that $\bar{u}_-$ satisfies the equation

$$\frac{d^2\bar{u}_-}{d\bar{y}_-^2} + \mathrm{i}\alpha_0(V_0 + c_0)\bar{u}_- = \mathrm{i}\alpha_0(\hat{P}_0 + \alpha_0^2 A_0 J_0). \tag{2.108}$$

This is a second-order linear inhomogeneous ordinary differential equation. Its general solution is composed of a particular solution of (2.108) and two complementary solutions of the homogeneous part of (2.108). Thus the general solution of leading-order equation (2.108) has the form

$$\bar{u}_- = a_3 e^{r_3\bar{y}_-} + a_4 e^{r_4\bar{y}_-} + \left(\frac{\hat{P}_0 + \alpha_0^2 A_0 J_0}{c_0 + V_0}\right), \tag{2.109}$$

with

$$r_3 = \left(\frac{1}{2}\alpha_0(c_0 + V_0)\right)^{1/2}(1 - \mathrm{i}), \quad r_4 = -\left(\frac{1}{2}\alpha_0(c_0 + V_0)\right)^{1/2}(1 - \mathrm{i}).$$

On the contrary to the analysis carried out for the upper viscous wall layer, no assumption has been made while finding the roots of the characteristic equation corresponding to the homogeneous part of (2.108) since the quantity $(c_0 + V_0)$ is positive. It is worth noting that the real part of r_3 is positive, whereas the real part of r_4 is negative. Now we need to calculate the constants of integration a_3 and a_4. Using the boundary condition (2.106e) and setting $a_3 = 0$ to ensure that $\bar{u}_-$ remains finite as $\bar{y}_- \to \infty$, we obtain

$$\bar{u}_- = \left(\frac{\hat{P}_0 + \alpha_0^2 A_0 J_0}{c_0 + V_0}\right)(1 - e^{r_4\bar{y}_-}). \tag{2.110}$$

It serves to find $\bar{w}_-$ from the disturbance spanwise momentum equation (2.106d). We find that

$$\bar{w}_- = \frac{\beta_0(\hat{P}_0 + \alpha_0^2 A_0 J_0)}{\alpha_0(c_0 + V_0)}(1 - e^{r_4\bar{y}_-}). \tag{2.111}$$

Let us now investigate the solutions (2.110) and (2.111) in the limit $\bar{y}_- \to \infty$. As $\bar{y}_- \to \infty$, the second term in (2.110) and (2.111) tend to zero, reducing these to (2.106f), which proves that the matching conditions are satisfied automatically. Now we can turn to the continuity equation (2.106a) to determine $\bar{v}_-$ explicitly. Substitution of (2.110) and (2.111) into (2.106a) formulates the governing differential equation for $\bar{v}_-$:

$$\frac{d\bar{v}_-}{d\bar{y}_-} = -\left(\frac{\mathrm{i}(\alpha_0^2 + \beta_0^2)(\hat{P}_0 + \alpha_0^2 A_0 J_0)}{\alpha_0(c_0 + V_0)}\right)(1 - e^{r_4\bar{y}_-}). \tag{2.112}$$

Integrating this equation and applying the no-slip condition (2.110e) we arrive at the following the form for $\bar{v}_-$:

$$\bar{v}_- = -\left(\frac{\mathrm{i}(\alpha_0^2+\beta_0^2)(\hat{P}_0+\alpha_0^2 A_0 J_0)}{\alpha_0(c_0+V_0)}\right)\left(\bar{y}_- - \frac{e^{r_4\bar{y}_-}}{r_4}+\frac{1}{r_4}\right). \tag{2.113}$$

It can be easily seen that the first purely imaginary part in $\bar{v}_-$ matches automatically to the corresponding term in the solution for $v_-^{(0)}$ in region II–, in view of the second pressure–displacement relation (2.98). Matching the real part of $\bar{v}_-$ as $\bar{y}_- \to \infty$ with the real part of $v_-^{(1)}$ in (2.103) as $\tau_- \to -(V_0+c_0)$ we obtain

$$\begin{aligned}-\left(\frac{\hat{P}_0+\alpha_0^2 A_0 J_0}{(2\alpha_0(c_0+V_0)^3)^{1/2}}\right) = -(c_0+V_0)\mathrm{Im}(A_1)\left(1+\frac{\beta_0^2}{\alpha_0^2}\right)^{-1} + \frac{\mathrm{Im}(p_-^{(1)})}{\lambda_-^{(0)}} \\ + \left(\frac{2\lambda_-^{(1)}(\hat{P}_0+\alpha_0^2 A_0 J_0)}{\lambda_-^{(0)3}}\right)\pi(c_0+V_0),\end{aligned} \tag{2.114}$$

where we have used (2.104) to eliminate $A_-^{(1)}$. Elimination of the undetermined amplitude factor A_0 between the first pressure-displacement relation (2.72) and the second pressure-displacement relation (2.98) leads to establishment of a first relation between c_0 and α_0, namely

$$c_0 = \left(\frac{J_0}{4}\right)(\alpha_0^2+\beta_0^2), \tag{2.115}$$

where we have used $\lambda_-^{(0)} = \lambda_+^{(0)} = 2$. We are now finally in a position to determine the upper-branch eigenrelation explicitly. Observe that A_0 can be eliminated from (2.114) by utilising the relation obtained from manipulation of (2.72), namely

$$A_0 = -\frac{(\alpha_0^2+\beta_0^2)\hat{P}_0}{\lambda_+^{(0)}\alpha_0^2(c_0-V_0)}. \tag{2.116}$$

After having eliminated A_0 from (2.114), multiplying the resulting equation by $\lambda_-^{(0)}$ and multiplying (2.89) by $\lambda_+^{(0)}$, followed by the subtraction of these two equations yields an important result, namely

$$\begin{aligned}\frac{\lambda_-^{(0)}}{(2\alpha_0(c_0+V_0)^3)^{1/2}} - \frac{\lambda_+^{(0)}}{(2\alpha_0(c_0-V_0)^3)^{1/2}} - \frac{\lambda_-^{(0)}J_0}{(2\alpha_0(c_0+V_0)^3)^{1/2}}\left(\frac{\alpha_0^2+\beta_0^2}{\lambda_+^{(0)}(c_0-V_0)}\right) \\ = \frac{2\lambda_+^{(1)}}{\lambda_+^{(0)2}}\pi(c_0-V_0) - \frac{2\lambda_-^{(1)}}{\lambda_-^{(0)2}}\pi(c_0+V_0) + \frac{2\lambda_-^{(1)}J_0\pi(\alpha_0^2+\beta_0^2)(c_0+V_0)}{\lambda_-^{(0)2}\lambda_+^{(0)}(c_0-V_0)},\end{aligned}$$

where use has been made of the relation (2.115) to eliminate the unknown imaginary part of A_1 and (2.62) to substitute for the net jump in pressure across the core region I.

Finally recalling that $\lambda_-^{(0)} = \lambda_+^{(0)} = 2$ and $\lambda_-^{(1)} = \lambda_+^{(1)} = -1$, after some manipulation we obtain the upper-branch eigenrelation

$$\frac{1}{(c_0+V_0)^{1/2}} + \frac{1}{(c_0-V_0)^{1/2}} = \frac{\pi}{4}(8\alpha_0)^{1/2}(c_0^2+V_0^2). \tag{2.117}$$

This is to be solved in conjunction with (2.115) and gives α_0 and c_0 as functions of V_0 and β_0. This is most easily accomplished by eliminating c_0 between the eigenrelations (2.115) and (2.117) to obtain

$$\Big(RH+V_0\Big)^{-1/2} + \Big(RH-V_0\Big)^{-1/2} = \frac{\pi}{4}(8\alpha_0)^{1/2}\Big(RH^2+V_0^2\Big), \tag{2.118}$$

where $RH = (J_0/4)(\alpha_0^2+\beta_0^2)$. Confidence in the validity of (2.118) is provided by the fact that it reduces correctly to equation (A 13b) of Cowley & Smith (1985) after taking account for our different scalings for the basic flow and setting $\beta_0 = 0$. For a given value of V_0 and β_0, the unique value of α_0 can be found from (2.118) by applying the Newton-Raphson method, with c_0 then following from (2.115). Figures 2.11–2.13 shows α_0 and c_0 plotted versus V_0 for various values of β_0. It can be seen easily that as V_0 is increased from zero, the value of α_0 falls slightly and then increases monotonically with $\alpha_0 \to \infty$ as $V_0 \to \infty$ for selected values of β_0 between 0 and 2. This indicates that the wavelength of the neutral mode is shortening with increasing V and hence the upper-branch asymptotic structure is breaking down. This can be demonstrated explicitly by examining the eigenrelations (2.115), (2.117) in the limit $V_0 \to \infty$. The results of the asymptotic analysis in this limit are presented below. The appropriate expansions are sought in the form

$$\alpha_0 \sim A_1 V_0^{1/2} + A_2 V_0^{-5}, \quad \beta_0 \sim \Omega V_0^{1/2}, \quad c_0 \sim V_0 + B_2 V_0^{-9/2} \text{ as } V_0 \to \infty, \tag{2.119}$$

where A_1, A_2 and B_2 are arbitrary constants to be determined in terms of a new variable Ω. Substituting the scaled streamwise wavenumber and wavespeed expansions (2.119) into (2.115) and equating terms at $O(V_0)$ and $O(V_0^{-9/2})$, we obtain a sequence of simpler equations, namely

At $O(V_0)$,

$$1 = \frac{J_0}{4}(A_1^2+\Omega), \tag{2.120}$$

At $O(V_0^{-9/2})$,

$$B_2 = \left(\frac{J_0}{2}\right) A_1 A_2. \tag{2.121}$$

Substituting the asymptotic expansions (2.120), (2.121) into the upper branch eigenrelation (2.117) and working with $O(V_0^{9/4})$ terms we find that

$$\frac{1}{B_2^{1/2}} = \frac{\pi}{2}(8A_1)^{1/2}. \tag{2.122}$$

The constant A_1 is easily found from (2.120) to be

$$A_1 = \left(\frac{4}{J_0} - \Omega\right)^{1/2}. \tag{2.123}$$

It remains to substitute the expression for A_1 in (2.123) into (2.122) and we conclude that the constant B_2 is

$$B_2 = \frac{1}{2\pi^2}\left(\frac{4}{J_0} - \Omega\right)^{-1/2}. \tag{2.124}$$

Consequently, the corresponding value of A_2 is determined by substituting (2.123) and (2.124) into (2.121) and we have

$$A_2 = \frac{1}{\pi^2 J_0}\left(\frac{4}{J_0} - \Omega\right)^{-1}. \tag{2.125}$$

After inserting the constants A_1, A_2 and B_2 into (2.119), the asymptotic expansions for α_0 and c_0 can be stated explicitly as

$$\alpha_0 \sim \left(\frac{4}{J_0} - \Omega\right)^{1/2} V_0^{1/2} + \frac{1}{\pi^2 J_0}\left(\frac{4}{J_0} - \Omega\right)^{-1} V_0^{-5} \text{ as } V_0 \to \infty, \tag{2.126a}$$

$$c_0 \sim V_0 + \frac{1}{2\pi^2}\left(\frac{4}{J_0} - \Omega\right)^{-1/2} V_0^{-9/2} \text{ as } V_0 \to \infty. \tag{2.126b}$$

The numerical solution of the eigenrelation confirms the validity of these results in figures 2.11, 2.12 and 2.13 below. It is obvious from (2.126b) that $c_0 - V_0 \to 0$ as $V_0 \to \infty$ which provides compelling evidence that for this upper branch mode the upper critical layer positioned at $Y_+ = (c_0 - V_0)/\lambda_+^{(0)}$ will move inside the viscous wall layer III+, turning the upper part of the high-Reynolds-number asymptotic structure into a lower-branch-type structure. However, the lower critical layer located at $Y_- = (c_0 + V_0)/\lambda_-^{(0)}$ remains embedded within the inviscid shear region II– since $c_0 + V_0 \to \infty$ in the limit $V_0 \to \infty$. This therefore suggests that the lower part of the structure still retains the upper-branch structure. Essentially, the new structure is composed of half of the lower branch asymptotic structure and half of the upper branch asymptotic structure set out in figures 2.4 and 2.10, respectively. For this reason, this type of neutral curve (the upper curve in figure 2.3) is sometimes referred to as a 'hybrid' curve (Walton 2004). The study of the hybrid modes will be the focus of the next subsection.

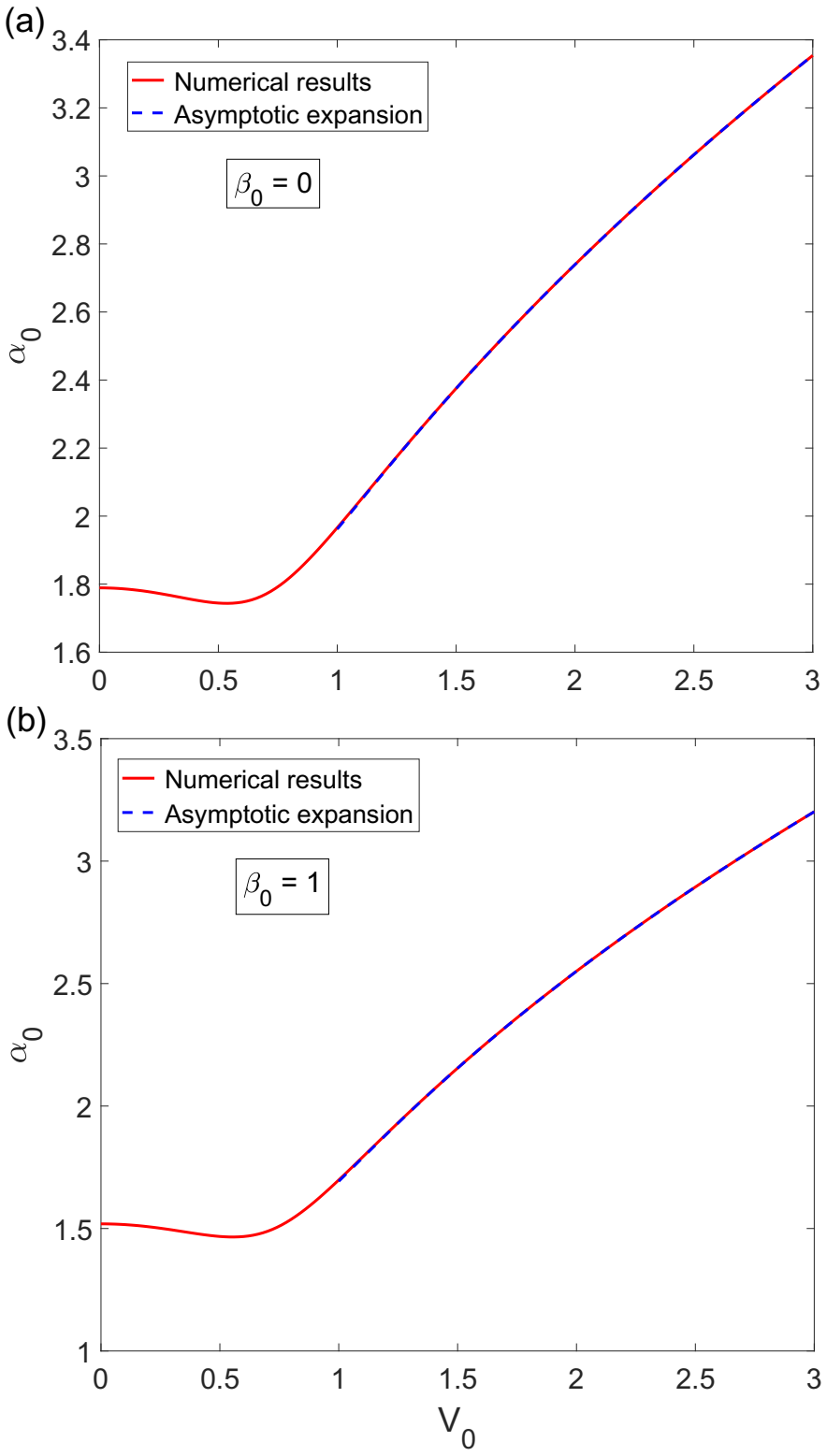

Figure 2.11: Comparison between numerical solutions of the upper-branch eigenrelations (2.118) and plots of the asymptotic behaviour of α_0 for asymptotically large V_0 in (2.126a).

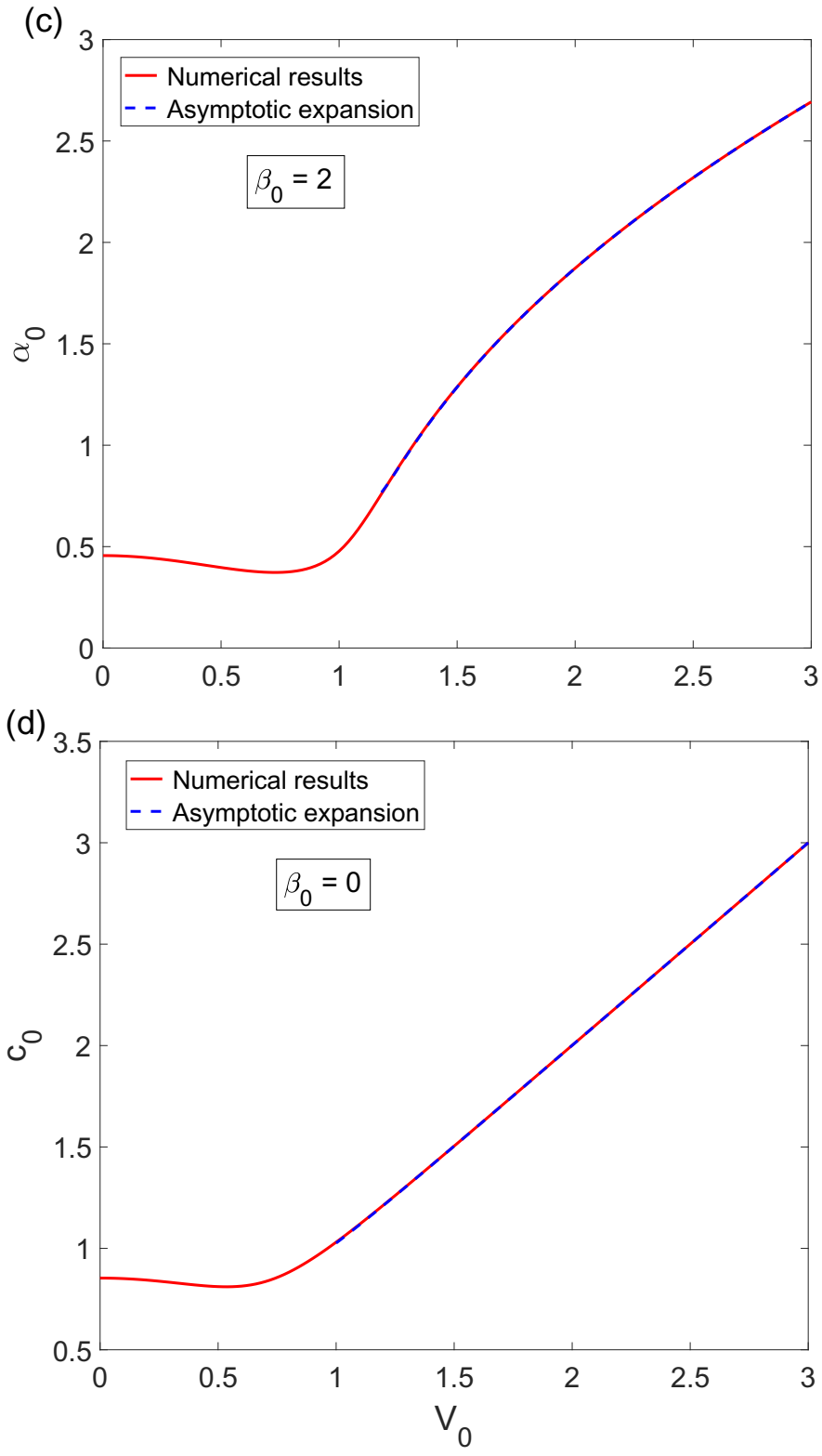

Figure 2.12: Comparison between numerical solutions of the upper-branch eigenrelations (2.118) and plots of the asymptotic behaviour of α_0 and c_0 for asymptotically large V_0 in (2.126).

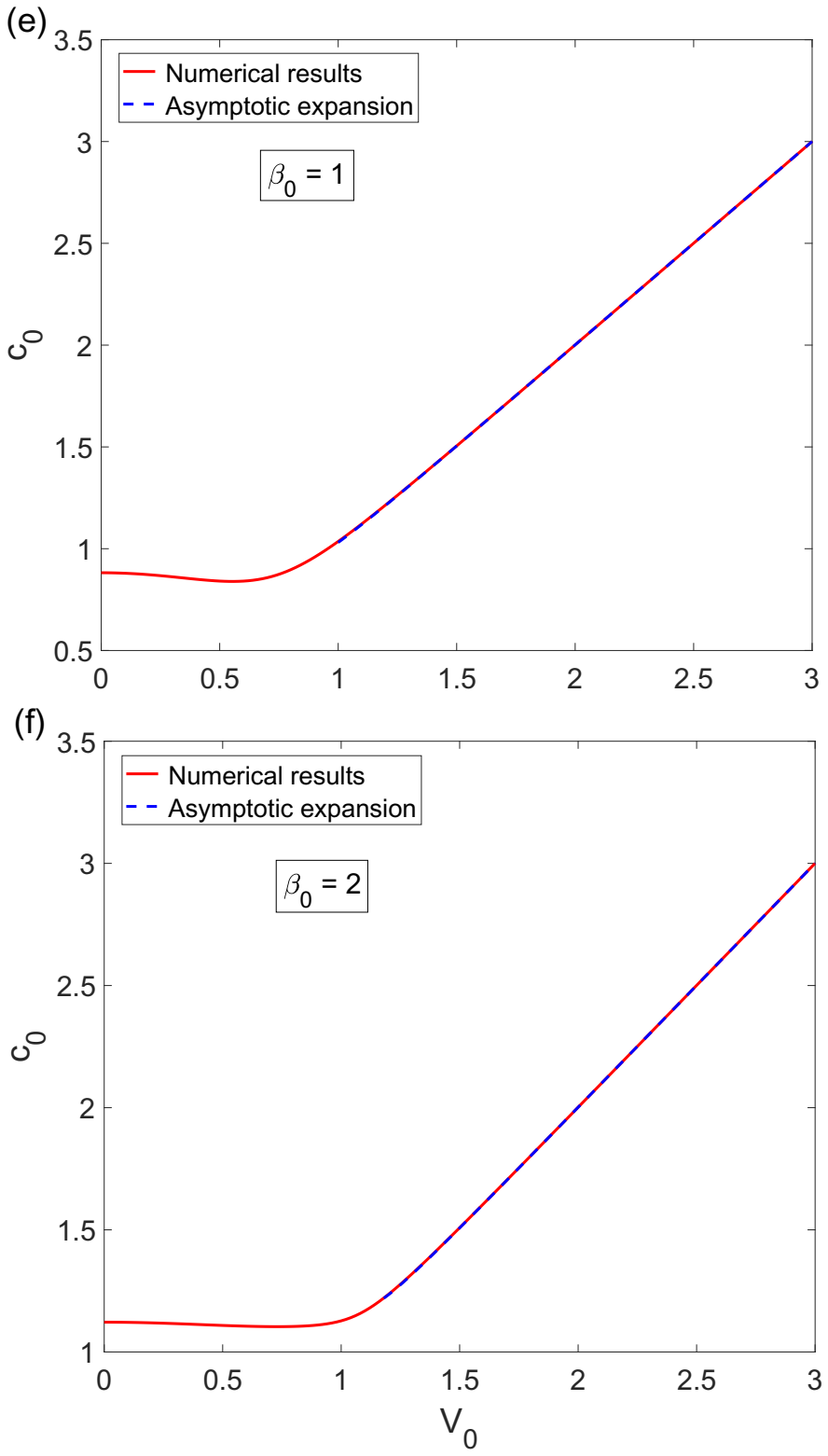

Figure 2.13: Comparison between numerical solutions of the upper-branch eigenrelations (2.118) and plots of the asymptotic behaviour of c_0 for asymptotically large V_0 in (2.126b).

2.3.5 The hybrid scaling

It is convenient to take as our starting point the behaviour on the upper branch of the main neutral curve. The normal scalings for regions II+ and II– in figure 2.10 are $y = 1-R^{-2/11}Y_+$ and $y = -1+R^{-2/11}Y_-$, respectively. Since $c_0 \to V_0+$ as $V_0 \to \infty$ from (2.126b), it is evident that when V_0 is sufficiently large the upper critical layer positioned at $Y_+ = (c_0 - V_0)/2$ moves inside the upper viscous wall layer III+ and the resulting layer then merges with the inviscid shear layer II+ to form a new boundary layer with normal variable $Y = (1-y)/k_3$, whose thickness k_3 is to be determined. By contrast, the lower critical layer located at $Y_- = (c_0 + V_0)/2$ remains sited within the lower inviscid shear layer II– since $c_0 + V_0 \to \infty$ in the limit $V_0 \to \infty$. Considering the behaviour of the term $(U_0 - c)$ as $y \to 1^-$ and using (2.126) we arrive at the following balance

$$U_0 - c \;\sim\; 2(1-y) - R^{-2/11}(c_0 - V_0) \;\sim\; 2k_3 - R^{-2/11}\left(\frac{1}{2\pi^2}\left(\frac{4}{J_0} - \Omega\right)^{-1/2} V_0^{-9/2}\right), \quad (2.127)$$

which holds provided $k_3 \sim R^{-2/11}V_0^{-9/2}$. Further, the crucial balance within the boundary layer near the upper wall is between the term $\alpha(U_0 - c)$ and the viscous operator $R^{-1}\partial^2/\partial y^2$. We thereby conclude from (2.55), (2.126) and (2.127) that the current upper branch formulation breaks down when

$$V_0 \sim R^{4/143}, \quad \alpha_0 \sim R^{2/143}, \quad c_0 \sim R^{4/143}. \quad (2.128)$$

A new structure therefore arises in which the thickness of the boundary layer (viscous shear layer II+) is $k_3 \sim R^{-4/13}$ as shown in figure 2.14. It consists of six zones: an inviscid core region (I), the viscous critical layer (a thin layer centred at the location where $U_0(y) = c$ with $c_i = 0$) sited within an inviscid shear layer (II–), a viscous shear layer (II+) and a viscous wall layer (III–). An asymptotic solution to the linear stability equations (2.5) is sought when $R \gg 1$ with α, β, c and V expanded in terms of $\varepsilon = R^{-1/13}$ as

$$\left.\begin{aligned} \alpha = \varepsilon\overline{\alpha}_0 + \varepsilon^3\overline{\alpha}_1 + \cdots, \quad \beta = \varepsilon\overline{\beta}_0 + \varepsilon^3\overline{\beta}_1 + \cdots, \\ c = \varepsilon^2\overline{c}_0 + \varepsilon^4\overline{c}_1 + \cdots, \quad V = \varepsilon^2\overline{V}_0, \quad \overline{c}_0 = \overline{V}_0, \end{aligned}\right\} \quad (2.129)$$

with these scalings being implied by (2.55), (2.126) and (2.128). We write the basic flow as $U_0(y) = U_{00}(y) + \varepsilon^2 U_{01}(y)$, where $U_{00} = 1 - y^2$, $U_{01} = \overline{V}_0 y$. Next we investigate briefly the dynamics of each asymptotic region in turn and determine the appropriate eigenrelation governing the hybrid modes at large R.

(i) Inviscid Core region I. The main characteristics of the core region are that $U_0 - c \approx U_0$ and the dynamics are predominantly inviscid. The appropriate disturbance expansions are

$$\left.\begin{aligned} \hat{u} = \overline{F}_0 + \varepsilon^2\overline{F}_1 + \cdots, \quad \hat{v} = \varepsilon\overline{G}_0 + \varepsilon^3\overline{G}_1 + \cdots, \\ \hat{w} = \varepsilon\overline{H}_0 + \varepsilon^3\overline{H}_1 + \cdots, \quad \hat{p} = \varepsilon^2\overline{P}_0 + \varepsilon^4\overline{P}_1 + \cdots, \end{aligned}\right\} \quad (2.130)$$

so that at leading order (2.5) yields a set of inviscid balances with solutions

$$\overline{F}_0 = A_0 U_{00}', \ \overline{G}_0 = -\mathrm{i}\overline{\alpha}_0 A_0 U_{00}, \ \overline{P}_0 = \hat{P}_0 + \overline{\alpha}_0^2 A_0 I(y), \text{ with } I(y) = \int_y^1 U_{00}^2 \, \mathrm{d}y, \tag{2.131}$$

where the constants A_0 and $\hat{P}_0$ are taken to be real without loss of generality. To complete the analysis it is necessary to proceed to next order where, after some algebra, it can be shown that $\overline{G}_1$ and $\overline{P}_1$ may be expressed in the form

$$\overline{G}_1 = -\mathrm{i}\overline{\alpha}_0 A_1 U_{00} + \text{purely imaginary terms}, \tag{2.132a}$$

$$\overline{P}_1 = P_+^{(1)} + \overline{\alpha}_0^2 A_1 I(y) + \text{purely real terms}, \tag{2.132b}$$

where A_1 and $P_+^{(1)}$ are unknown complex constants. Hence we find that there is a jump in the imaginary part of $\overline{P}_1$ across the core, with

$$\big[\mathrm{Im}(\overline{P}_1)\big]_-^+ \equiv \lim_{y\to 1} \ \mathrm{Im}(\overline{P}_1) - \lim_{y\to -1} \ \mathrm{Im}(\overline{P}_1) = -\overline{\alpha}_0^2 \mathrm{Im}(A_1) I(-1). \tag{2.133}$$

(ii) The inviscid shear region II–. Here $U_{00} \sim c$, and in view of (2.130)–(2.132), the relevant flow expansions are

$$\left.\begin{aligned} U_0 = \varepsilon^2 \tau_0 + \varepsilon^4(-Y_-^2 + \overline{V}_0 Y_-), \ \hat{u} = u_-^{(0)} + \varepsilon^2 u_-^{(1)} + \cdots, \ y = -1 + \varepsilon^2 Y_-, \\ \hat{v} = \varepsilon^3 v_-^{(0)} + \varepsilon^5 v_-^{(1)} + \cdots, \ \hat{w} = w_-^{(0)} + \varepsilon^2 w_-^{(1)} + \cdots, \ \hat{p} = \varepsilon^2 p_-^{(0)} + \varepsilon^4 p_-^{(1)} + \cdots. \end{aligned}\right\} \tag{2.134}$$

Substituting these expansions into (2.5), at leading order, we obtain the governing equations whose solution subject to the condition of matching with (2.130) is given by:

$$\left.\begin{aligned} u_-^{(0)} = 2A_0 + \frac{\overline{\beta}_0^2 p_-^{(0)}}{\overline{\alpha}_0^2 \tau_-}, \quad w_-^{(0)} = -\frac{\overline{\beta}_0 p_-^{(0)}}{\overline{\alpha}_0 \tau_-}, \\ v_-^{(0)} = -\mathrm{i}\overline{\alpha}_0 A_0 \tau_- - \frac{\mathrm{i}(\overline{\alpha}_0^2 + \overline{\beta}_0^2) p_-^{(0)}}{2\overline{\alpha}_0}, \quad p_-^{(0)} = \hat{P}_0 + \overline{\alpha}_0^2 A_0 I(-1), \end{aligned}\right\} \tag{2.135}$$

where for brevity we put $\tau_- = \tau_0 - \overline{c}_0$ and $\tau_0 = 2Y_- - \overline{V}_0$. Applying the wall-normal condition that $v_-^{(0)} = 0$ on the lower wall $y = -1$ provides a pressure–displacement relation

$$2A_0(\overline{c}_0 + \overline{V}_0) - (1 + \overline{\beta}_0^2/\overline{\alpha}_0^2)(\hat{P}_0 + \overline{\alpha}_0^2 A_0 I(-1)) = 0. \tag{2.136}$$

Substituting for the leading order solution from (2.135) we deduce, after extensive algebra, that the second term in the normal velocity expansion is of the form

$$\begin{aligned} v_-^{(1)} = -\mathrm{i}\overline{\alpha}_0 A_-^{(1)} \tau_- + \text{purely imaginary terms} - \frac{\mathrm{i}(\overline{\alpha}_0^2 + \overline{\beta}_0^2) p_-^{(1)}}{2\overline{\alpha}_0} \\ + \left(\frac{\mathrm{i}\overline{\alpha}_0 p_-^{(0)}}{4}\right)\left(1 + \frac{\overline{\beta}_0^2}{\overline{\alpha}_0^2}\right)\tau_- \ \ln \ \tau_-, \end{aligned} \tag{2.137}$$

where the higher-order pressure term $p_-^{(1)} = P_+^{(1)} + \overline{\alpha}_0^2 A_1 I(-1)$ up to an additive real constant whose value does not affect the eigenrelation to be derived later. Here $A_-^{(1)}$ is an unknown complex constant, and the final logarithmic term indicates that the result (2.137) only holds for $\tau_- > 0$. To smooth out the singularity in (2.137), a viscous critical layer must be introduced in the vicinity of $\tau_- = 0$, implying that the position of the critical layer is a function of the scaled sliding speed $\overline{V}_0$. Also of importance here is to establish a connection between $A_-^{(1)}$ and A_1: this is achieved by matching the real part of (2.137) as $\tau_- \to \infty$ with the real part of the first term in the expression (2.132a) for $\overline{G}_1$ as $y \to -1$, yielding

$$\mathrm{Im}(A_-^{(1)}) = \mathrm{Im}(A_1). \tag{2.138}$$

In order to match the normal velocity $\hat{v}$ between layers II– and III– we need to consider the form for $v_-^{(1)}$ on the other side of the viscous critical layer, that is, when $\tau_- < 0$. The dynamics of such a classical linear critical layer have been thoroughly investigated already for related flows (e.g. Lin (1955); Stuart (1963); Reid (1965)) and those studies have shown that the solution for $v_-^{(1)}$ is reproduced when $\tau_- < 0$, just below the critical layer, with $\ln \tau_-$ replaced by $\ln|\tau_-| - \mathrm{i}\pi$, so that the critical layer induces a phase shift of magnitude π. We will see later that the phase shift also plays a crucial role in the nonlinear dynamics where its value becomes dependent on the perturbation amplitude. Next we examine the dynamics of the lower viscous wall layer III–.

(iii) Viscous wall layer III–. Here we have $y = -1 + \varepsilon^5 \bar{y}_-$. The scalings (2.134) in II–, together with the solution (2.135) as $Y_- \to 0$, suggest a flow expansion of the form

$$U_0 = -\varepsilon^2 \overline{V}_0, \quad \hat{u} = \bar{u}_-, \quad \hat{v} = \varepsilon^6 \bar{v}_-, \quad \hat{w} = \bar{w}_-, \quad \hat{p} = \varepsilon^2 \bar{p}_-. \tag{2.139}$$

Substituting into the linear disturbance equations (2.5) leads to a set of viscous balances

$$\mathrm{i}\overline{\alpha}_0 \bar{u}_- + \mathrm{i}\overline{\beta}_0 \bar{w}_- = -\frac{d\bar{v}_-}{d\bar{y}_-}, \quad -\mathrm{i}\overline{\alpha}_0(\overline{V}_0 + \bar{c}_0)\bar{u}_- = -\mathrm{i}\overline{\alpha}_0 \bar{p}_- + \frac{d^2\bar{u}_-}{d\bar{y}_-^2},$$
$$\frac{d\bar{p}_-}{d\bar{y}_-} = 0, \quad -\mathrm{i}\overline{\alpha}_0(\overline{V}_0 + \bar{c}_0)\bar{w}_- = -\mathrm{i}\overline{\beta}_0 \bar{p}_- + \frac{d^2\bar{w}_-}{d\bar{y}_-^2},$$

with

$$\bar{u}_- = \bar{v}_- = \bar{w}_- = 0 \quad \text{on} \quad \bar{y}_- = 0,$$
$$\bar{u}_- \to 2A_0(1 + \overline{\beta}_0^2/\overline{\alpha}_0^2)^{-1}, \quad \bar{w}_- \to 2A_0(\overline{\beta}_0/\overline{\alpha}_0)(1 + \overline{\beta}_0^2/\overline{\alpha}_0^2)^{-1} \quad \text{as} \quad \bar{y}_- \to \infty,$$

for no slip and to match with II– as $Y_- \to 0$. From matching the pressure between (2.134) and (2.139), we find $\bar{p}_- = \hat{P}_0 + \overline{\alpha}_0^2 A_0 I(-1)$ and hence we obtain the solutions

$$\bar{u}_- = 2A_0\left(1 + \frac{\overline{\beta}_0^2}{\overline{\alpha}_0^2}\right)^{-1}(1 - e^{m\bar{y}_-}),\ \bar{v}_- = -2\mathrm{i}A_0\left(\bar{y}_- - \frac{e^{m\bar{y}_-}}{m} + \frac{1}{m}\right)\overline{\alpha}_0,\ \bar{w}_- = (\overline{\beta}_0/\overline{\alpha}_0)\bar{u}_-, \tag{2.140}$$

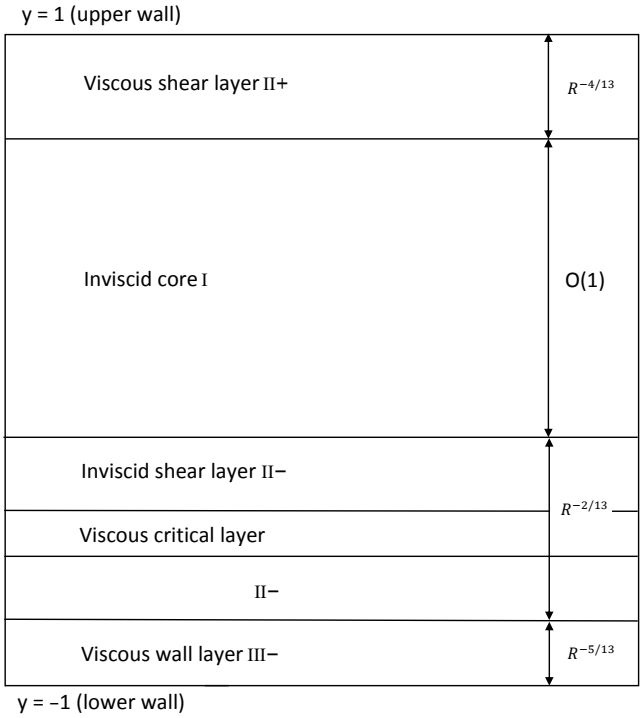

Figure 2.14: The asymptotic structure of the hybrid modes.

upon using (2.136), where $m = -\{\overline{\alpha}_0(\overline{c}_0 + \overline{V}_0)\}^{1/2}e^{-\mathrm{i}\pi/4}$. We match the real part of $\bar{v}_-$ as $\bar{y}_- \to \infty$ with the real part of $v_-^{(1)}$ in (2.137) as $\tau_- \to -(\bar{V}_0 + \bar{c}_0)$. Taking into account the phase shift of magnitude π, and using (2.138) to eliminate $A_-^{(1)}$, we finally obtain

$$-(\overline{c}_0 + \overline{V}_0)\ \mathrm{Im}(A_1) + \left(1 + \frac{\overline{\beta}_0^2}{\overline{\alpha}_0^2}\right)\frac{\mathrm{Im}(p_-^{(1)})}{2} = \left(1 + \frac{\overline{\beta}_0^2}{\overline{\alpha}_0^2}\right)\left(\frac{\hat{P}_0 + \overline{\alpha}_0^2 A_0 I(-1)}{4(\overline{c}_0 + \overline{V}_0)^{-1}}\right)\pi. \tag{2.141}$$

(iv) Viscous shear layer II+. Here $y = 1 - \varepsilon^4 Y_+$, and from (2.130)–(2.132) we have

$$\hat{u} = u_+^{(0)} + \cdots, \quad \hat{v} = -\varepsilon^5 v_+^{(0)} + \cdots, \quad \hat{w} = w_+^{(0)} + \cdots, \quad \hat{p} = \varepsilon^2 p_+^{(0)} + \varepsilon^4 p_+^{(1)} + \cdots, \tag{2.142}$$

with $U_0 = \varepsilon^2 \overline{V}_0 + 2\varepsilon^4 Y_+ + \cdots$ for the basic flow. Substitution of (2.142) into (2.5) reveals that $p_+^{(0)} = 0$, and therefore on matching the shear layer pressure (2.142) as $Y_+ \to \infty$ with the core pressure (2.130) as $y \to 1$, we deduce from (2.131) that $\hat{P}_0 = 0$. Hence from the pressure–displacement relation (2.136) a connection between the leading-order scaled streamwise wavenumber $\overline{\alpha}_0$ and the scaled sliding speed $\overline{V}_0$ is established through the equation

$$\overline{\alpha}_0^2 + \overline{\beta}_0^2 = (15\overline{V}_0/4). \tag{2.143}$$

Determination of a second relation linking wavenumber, sliding speed and phase speed requires investigation of the leading-order balances within the layer which are found to be

$$\left.\begin{aligned} \mathrm{i}\overline{\alpha}_0 u_+^{(0)} + \frac{dv_+^{(0)}}{dY_+} + \mathrm{i}\overline{\beta}_0 w_+^{(0)} = 0, \quad \mathrm{i}\overline{\alpha}_0(2Y_+ - \overline{c}_1)u_+^{(0)} + 2v_+^{(0)} = -\mathrm{i}\overline{\alpha}_0 p_+^{(1)} + \frac{d^2u_+^{(0)}}{dY_+^2}, \\ \frac{dp_+^{(1)}}{dY_+} = 0, \quad \mathrm{i}\overline{\alpha}_0(2Y_+ - \overline{c}_1)w_+^{(0)} = -\mathrm{i}\overline{\beta}_0 p_+^{(1)} + \frac{d^2w_+^{(0)}}{dY_+^2}, \end{aligned}\right\} \tag{2.144}$$

with

$$u_+^{(0)} = v_+^{(0)} = w_+^{(0)} = 0 \quad \text{on} \quad Y_+ = 0, \text{ and } u_+^{(0)} \to -2A_0, \quad w_+^{(0)} \to 0 \quad \text{as} \quad Y_+ \to \infty, \tag{2.145}$$

upon matching to the core region I. A solvability condition for the system (2.144)–(2.145) which depends only on the wave pressure $p_+^{(1)}$ can be obtained from the well-known procedure outlined in Smith (1979) and this leads us to the relation

$$(\overline{\alpha}_0^2 + \overline{\beta}_0^2)p_+^{(1)} = (2\mathrm{i}\overline{\alpha}_0)^{5/3}\left(\frac{\mathrm{Ai}'(\overline{\xi})}{\kappa(\overline{\xi})}\right)A_0, \tag{2.146}$$

where Ai is the Airy function, $\kappa(\overline{\xi}) = \int_{\overline{\xi}}^{\infty} \mathrm{Ai}(\xi)\ \mathrm{d}\xi$, and $\overline{\xi} = -\mathrm{i}^{1/3}\overline{s}$, with

$$\overline{s} = \frac{\overline{\alpha}_0\overline{c}_1}{(2\overline{\alpha}_0)^{2/3}}. \tag{2.147}$$

Taking the imaginary part of (2.146), noting that $\mathrm{Im}(p_+^{(1)}) - \mathrm{Im}(p_-^{(1)}) = -\overline{\alpha}_0^2\mathrm{Im}(A_1)I(-1)$ from (2.133) upon matching (2.130) with (2.142), and using (2.141), (2.143), we derive the desired second eigenrelation:

$$\overline{V}_0^2 = (2\overline{\alpha}_0)^{-1/3}\frac{\mathrm{Im}(g(\overline{s}))}{\pi}, \quad \text{where} \quad g(\overline{s}) = \mathrm{i}^{5/3}\left(\frac{\mathrm{Ai}'(\overline{\xi})}{\kappa(\overline{\xi})}\right). \tag{2.148}$$

In order to help solve (2.143), (2.148) numerically, we use a differential equation representation for $g(\overline{s})$ derived in appendix A and calculate the imaginary part of g as shown in figure 2.15. For given $\overline{V}_0$ and $\overline{\beta}_0$, the value of $\overline{\alpha}_0$ can be calculated from (2.143); consequently the task is to determine the corresponding value(s) of $\overline{c}_1$ from (2.148) by solving the equation $\mathrm{Im}(g(\overline{s})) = \Upsilon$ where Υ is a positive constant. Figure 2.16 shows plots of the wavespeed correction $\overline{c}_1$ versus the scaled sliding speed $\overline{V}_0$ for zero and unit scaled spanwise wavenumber, $\overline{\beta}_0 = 0$ and $\overline{\beta}_0 = 1$.

The important results may be summarized as follows.
(i) For $\Upsilon = 0$, the unique (finite) root of the equation is $\overline{s} \simeq 2.2972$. It turns out that for $0 < \Upsilon < 0.232$ there are two solutions to this equation, while for $0.232 < \Upsilon < 0.302$ two more solutions arise and hence we see four solutions in this interval.
(ii) For values of Υ in the range $0.302 < \Upsilon < 1.241$, there are only two solutions and finally,

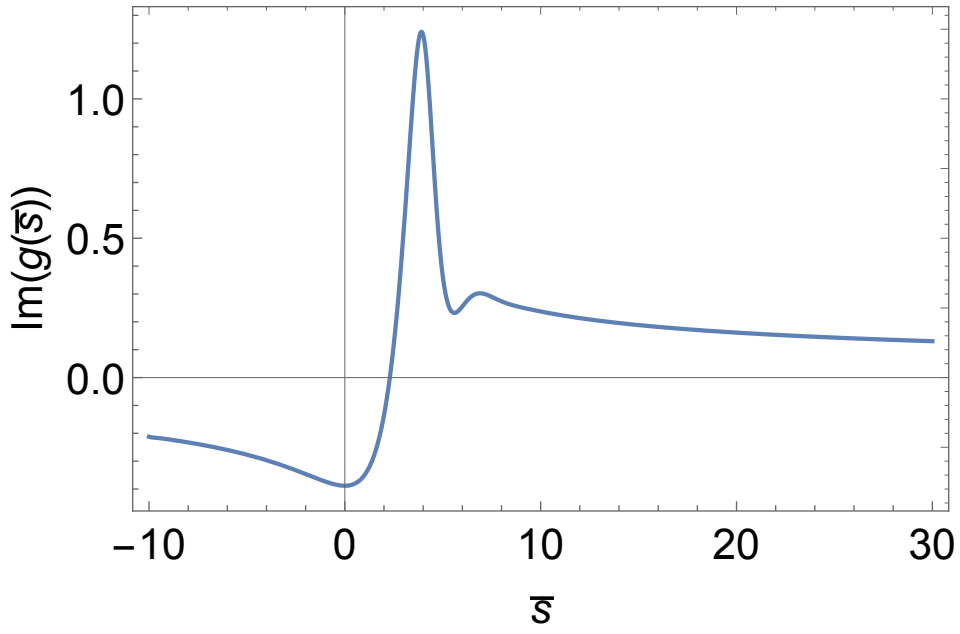

Figure 2.15: The imaginary part of the function $g(\overline{s})$ and solution of the hybrid eigenrelations.

for $\Upsilon > 1.241$ it is found that no solutions exist. At the value $\Upsilon = 1.241$, the neutral curve turns around sharply for the first time, thus creating the first turning point, above which these modes are no longer neutral, in the graph of $\overline{c}_1$ plotted versus $\overline{V}_0$ in figure 2.16. In addition, the number of solutions increases from two to four as a consequence of the remaining two turning points.

In order to demonstrate how the emergence of the two typical modes on this scaling is linked to the upper-branch and lower-branch forms, it is revealing to examine analytically the hybrid-branch eigenrelation in the limit $\overline{V}_0 \to (\overline{\beta}_0^2 J_0)/4$. This limit is obtained by letting $\overline{\alpha}_0 \to 0$ in (2.143) and using the fact that $J_0 = 16/15$ from (2.39). It follows from (2.148) that in this limit, $\mathrm{Im}(g(\overline{s})) \to 0$, resulting in two possibilities which we consider in turn below: (i) $\overline{s} \to s_0 \simeq 2.2972$ (see (2.48)).

It remains to substitute for $\overline{s}$ in (2.147) and after some manipulation we obtain the asymptotic form for the wavespeed correction $\overline{c}_1$ in the limit V_0, namely

$$\overline{c}_1 \sim (\lambda_+^{(0)})^{2/3}\ \overline{\alpha}_0{}^{-1/3} s_0 \quad \text{as } \overline{V}_0 \to \frac{\overline{\beta}_0^2 J_0}{4}. \tag{2.149}$$

Elimination of the explicit $\overline{\alpha}_0$-dependence in (2.149) is achieved by making use of (2.143) and we find that

$$\overline{c}_1 \sim \left(\frac{4}{J_0} - \Lambda\right)^{-1/6} (\lambda_+^{(0)})^{2/3} s_0 \overline{V}_0{}^{-1/6} \text{ as } \overline{V}_0 \to \frac{\overline{\beta}_0^2 J_0}{4}, \tag{2.150}$$

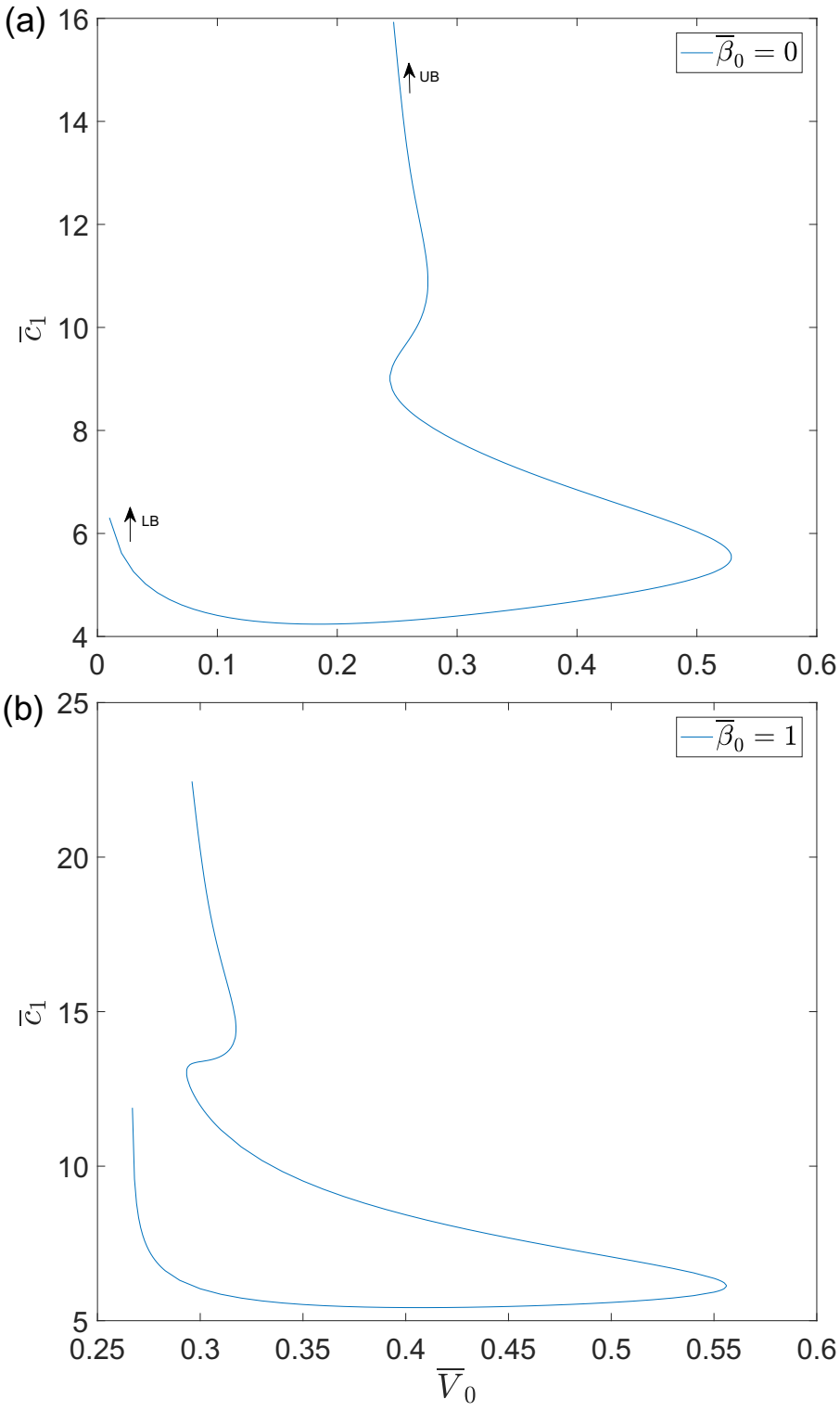

Figure 2.16: Solutions of the hybrid-branch eigenrelation (2.148). The arrows in (a) point out how the two branches of each neutral curve match back to the lower branch (LB) and upper branch (UB) scalings.

where the new variable $\Lambda = \overline{\beta}_0^2/\overline{V}_0$. From comparison with the asymptotic expression (2.53), it is apparent that this mode is the continuation of the lower-branch mode on the new scaling.

(ii) $\overline{s} \to \infty$.

It can be shown that in this limit the asymptotic form of $g(\overline{s})$ is

$$g(\overline{s}) \sim -\overline{s} + \mathrm{e}^{\mathrm{i}\pi/4}(\overline{s})^{-1/2} \text{ as } \overline{s} \to \infty. \tag{2.151}$$

Taking the imaginary part of (2.151) leads to an important result

$$\mathrm{Im}(g(\overline{s})) \sim \sin\left(\frac{\pi}{4}\right)(\overline{s})^{-1/2} \text{ as } \overline{s} \to \infty, \tag{2.152}$$

and upon substituting for $\overline{s}$ from (2.147), this expression simplifies to

$$\mathrm{Im}(g(\overline{s})) \sim \left(\frac{1}{\sqrt{2}}\right)(\overline{\alpha}_0)^{-1/6}(\overline{c}_1)^{-1/2}(\lambda_+^{(0)})^{1/3} \text{ as } \overline{s} \to \infty.$$

Finally, using this result in (2.148) and taking into account the limit $\overline{V}_0 \to (\overline{\beta}_0^2 J_0)/4$, we can deduce the asymptotic behaviour of the eigenrelation, namely

$$\overline{V}_0^2 \sim \frac{(2\overline{\alpha}_0)^{-1/3}}{\pi}\left(\frac{1}{\sqrt{2}}\right)(\overline{\alpha}_0)^{-1/6}(\overline{c}_1)^{-1/2}(\lambda_+^{(0)})^{1/3} \text{ as } \overline{V}_0 \to \frac{\overline{\beta}_0^2 J_0}{4}. \tag{2.153}$$

Upon rearrangement, we obtain the result

$$\overline{c}_1 \sim \frac{1}{2\pi^2}\left(\frac{\overline{V}_0^{-4}}{\overline{\alpha}_0}\right) \text{ as } \overline{V}_0 \to \frac{\overline{\beta}_0^2 J_0}{4}. \tag{2.154}$$

Equation (2.153) describes how the wavelength of this mode decreases as $\overline{V}_0$ increases. It is shown below that this mode is the continuation of the upper-branch mode on the new scaling.

Squaring both sides of (2.122) determines explicitly a relationship between the constants B_2 and A_1 as

$$B_2 = \frac{1}{2\pi^2 A_1}. \tag{2.155}$$

Observing that, to leading order, $A_1 \sim \alpha_0 V_0^{-1/2}$ as $V_0 \to \infty$ from (2.119) and as a result equation (2.155) turns into

$$B_2 \sim \frac{V_0^{1/2}}{2\pi^2 \alpha_0} \text{ as } V_0 \to \infty. \tag{2.156}$$

At this stage, it is necessary to recall the asymptotic expansion for the wavespeed c_0 stated in (2.119), that is

$$c_0 \sim V_0 + B_2 V_0^{-9/2} \text{ as } V_0 \to \infty.$$

Combining this expression with (2.156) yields a very important result

$$c_0 \sim V_0 + \frac{1}{2\pi^2}\left(\frac{V_0^{-4}}{\alpha_0}\right) \text{ as } V_0 \to \infty. \tag{2.157}$$

Thus comparison of (2.154) with (2.157) confirms that the mode which behaves according to (2.154) is in fact the continuation of the upper-branch mode whose behaviour is predicted by (2.157) as claimed earlier. These two modes form the upper and lower branches of a single neutral curve on the hybrid scaling, as can been seen in figure 2.16.

2.3.6 Comparison of asymptotic and numerical results

We are now in a position to consider a quantitative comparison of finite Reynolds number computations and the corresponding solutions to the asymptotic eigenrelation for various small values of V, and we will only consider the case $\beta = 0$. After substitution for $\overline{\alpha}_0$ from (2.143) it is readily seen that (2.147) and (2.148) become

$$\overline{c}_1 = 2\overline{s}(15\overline{V}_0)^{-1/6}, \quad \mathrm{Im}(g(\overline{s})) = \pi(15\overline{V}_0^{13})^{1/6}. \tag{2.165a,b}$$

We note that for given R with V prescribed, the corresponding value for $\overline{V}_0$ is $R^{2/13}V$. We can then return to (2.165a) and (2.165b) to determine $\overline{s}$ and $\overline{c}_1$ as functions of $\overline{V}_0$. Hence the wavespeed c is fixed for a given R from the expansion (2.129). In figures 2.17(a,b) the corresponding plots are labelled by 'Asymptotes' and compared with the upper curves found in the (R, c) plane from the numerical solution of the eigenvalue problem (2.8). Evidently, the asymptotic theory at large Reynolds number yields values of c that are in excellent agreement with the lower branch of the upper curve. By contrast, on the upper branch the asymptotic and finite R wavespeeds differ approximately by 0.02; nevertheless this is still a favourable agreement and would presumably become even better where R is further increased. In the next chapter we will elaborate on how the asymptotic structures of the upper curve and the upper-branch modes shown schematically in figures 2.14 and 2.10 respectively provide a firm foundation on which we can develop a mathematical framework addressing vital aspects associated with the onset of weakly nonlinear effects along the two branches of the upper curve and the upper-branch of the main curve as the disturbance size Δ is increased. The aim is to establish a link between the linear and weakly nonlinear theories by investigating the effect of increasing Δ on the dynamics of the viscous critical layer(s) in the inviscid shear region(s) II–/II+, since the neutral stability state in the linear regime is controlled by the phase shift(s) across it, and determine the appropriate scaling for Δ when weakly nonlinear effects in the flow come into play. It is thus instructive to discuss the properties of the critical layer(s) in detail.

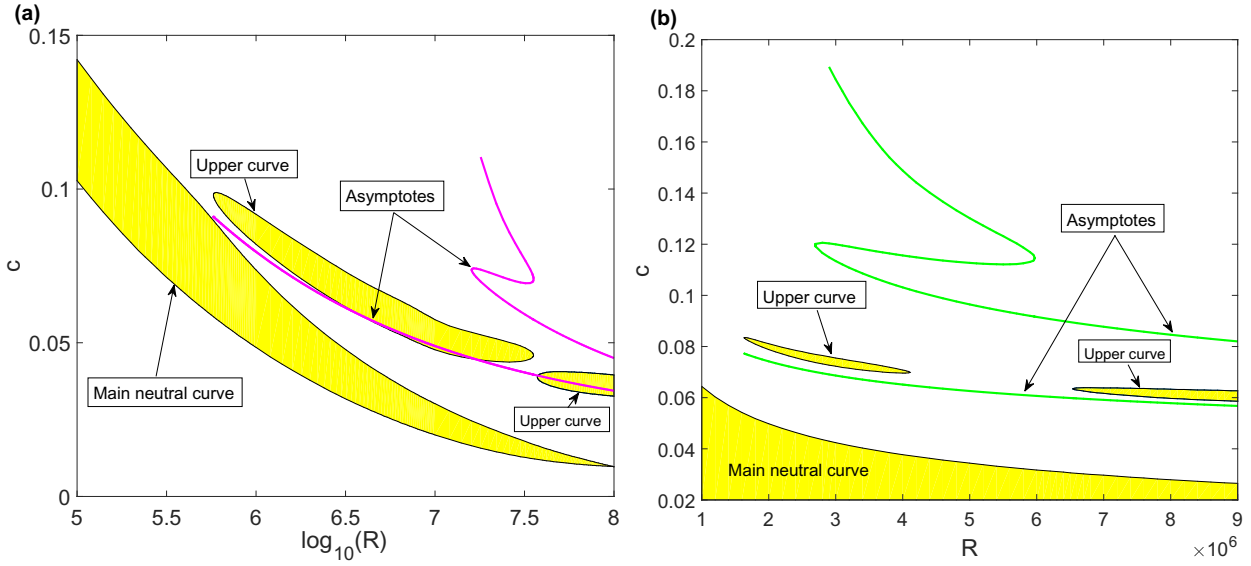

Figure 2.17: Comparison of finite Reynolds numbers computations and the corresponding solutions to the hybrid branch eigenrelations (2.143) and (2.148) for (a) $V \approx 0.019$; (b) $V \approx 0.025$.

2.3.7 Summary of the numerical and asymptotic results

To examine the linear stability of plane Poiseuille–Couette flow at finite Reynolds number, the Orr–Sommerfeld equation has been solved numerically using a standard 'Chebyshev–collocation method'. The number of linear neutral curves for plane Poiseuille–Couette flow is a function of the sliding speed V. Although there is a unique neutral curve when $V = 0$, it is found that for small non-zero values of the sliding speed, multiple neutral curves exist in the two-dimensional problem ($\beta = 0$) at large Reynolds number consistent with the predictions of Cowley & Smith (1985) exclusively based on a high-Reynolds-number asymptotic approach to the flow. Finite-Reynolds-number numerical results were summarized. The asymptotic study in the limit of large Reynolds number identifies that these curves retreat to infinity provided the non-dimensional wall speed V (corresponding to the dimensional speed $V^* = U_m V$) is approximately 0.34 in line with Reynolds & Potter's (1967) conclusions. The analysis aimed at studying the asymptotic behaviours of the upper and lower branches of the main neutral curve and both branches of the upper curve was considered. The governing equations corresponding to each asymptotic region were solved analytically, thus establishing the upper, lower and hybrid-branch eigenrelations. Comparison of finite Reynolds number computations of the two-dimensional problem and the corresponding solutions to the hybrid-branch eigenrelation was presented and discussed for various small values of sliding velocity.

Chapter 3

Viscous and strongly nonlinear critical layer theory for long-wavelength modes

In subsection 2.3.4, we established the form of the upper-branch eigenrelation by balancing the phase shifts across the wall and critical layers. There we made use of the result that the phase shifts of π are induced upon crossing the critical layers (e.g. Lin (1955); Stuart (1963); Reid (1965)). It has been shown that the phase shifts are modified and become a function of the disturbance size Δ in the presence of a larger disturbance (Benney & Bergeron 1969; Haberman 1972). In this chapter we will demonstrate specifically how the reduced phase shift plays an essential role in the subsequent nonlinear evolution of our particular basic flow. We begin by discussing the linear critical layers and then show how the dynamics are altered as the disturbance size is increased.

3.1 The dynamics of the strongly nonlinear critical layers on the upper branch scaling

3.1.1 The strongly nonlinear critical layers

The purpose of this study is to investigate how the dynamics of the lower linear viscous critical layer (see figure 2.10) of the upper-branch mode (where $\varepsilon = R^{-1/11}$) are modified as the disturbance size Δ in (2.3) is increased. The dominant balance in this layer is between the viscous term $R^{-1}\partial^2/\partial y^2$ and the inertial term $(U_0 - c)\partial/\partial x$, with $\partial/\partial x \sim O(\varepsilon)$. As remarked earlier this thin layer is located at $Y_- = (V_0 + c_0)/\lambda_-^{(0)}$ which indicates that its position is a function of sliding speed of walls V. Suppose that the thickness of the critical layer is q which is to be determined in terms of the parameter ε. In order to apply the method of matched asymptotic expansions we introduce the appropriate inner variable $\tilde{y}$

defined by

$$\tilde{y} = q^{-1}\left\{Y_- - \left(\frac{c_0 + V_0}{\lambda_-^{(0)}}\right)\right\}. \tag{3.1}$$

Recall that the normal scaling in the inviscid shear layer II– is $y = -1 + \varepsilon^2 Y_-$. Hence in view of (3.1) this implies that the outer variable y is related to the inner variable $\tilde{y}$ via

$$y = -1 + \varepsilon^2\left(\frac{c_0 + V_0}{\lambda_-^{(0)}}\right) + \varepsilon^2 q\tilde{y}. \tag{3.2}$$

Expanding the term $(U_0 - c)$ in terms of the variable Y_- we find that

$$U_0 - c = \varepsilon^2(\lambda_-^{(0)}Y_- - V_0 - c_0) + \varepsilon^4(V_0 Y_- - Y_-^2 - c_1), \tag{3.3}$$

implying that the order of magnitude of $(U_0 - c)$ is $\varepsilon^2 q$ from consideration of (3.1) since $\tilde{y}$ is the $O(1)$ variable. It follows from (3.2) that $\partial^2/\partial y^2 \sim O(\varepsilon^{-4}q^{-2})$ and thus the inertial-viscous balance is achieved provided $\varepsilon^3 q \sim R^{-1}(\varepsilon^2 q)^{-2}$, which establishes the critical-layer thickness $q \sim \varepsilon^{4/3}$. It remains to substitute for Y_- from (3.1) into the basic flow U_0 and after regrouping the terms according to their orders of magnitude we can conclude that the basic flow within the critical layer takes the form

$$U_0 = \varepsilon^2 c_0 + \varepsilon^{10/3}\lambda_-^{(0)}\tilde{y} + \varepsilon^4\left(\frac{V_0^2 - c_0^2}{\lambda_-^{(0)2}}\right) + \varepsilon^{16/3}\lambda_-^{(1)}c_0\tilde{y} + \varepsilon^{20/3}\lambda_-^{(1)}\tilde{y}^2. \tag{3.4}$$

The velocities and pressure in the linear critical layer expand as follows:

$$u = U_0 + \Delta\hat{u} = U_0 + \Delta\varepsilon^{4/3}u_1(\tilde{y})\cos(\xi) + \Delta\varepsilon^2 u_{cl}(\xi,\tilde{y}) + \cdots, \tag{3.5a}$$

$$v = \Delta\hat{v} = \Delta(\varepsilon^3\alpha_0 A_0(c_0 + V_0)\sin(\xi)) + \cdots - \Delta\varepsilon^{19/3}v_{cl}(\xi,\tilde{y}) + \cdots, \tag{3.5b}$$

$$w = \Delta\hat{w} = \Delta\varepsilon^{4/3}w_1(\tilde{y})\cos(\xi) + \Delta\varepsilon^2 w_{cl}(\xi,\tilde{y}) + \cdots, \tag{3.5c}$$

$$p = \Delta\hat{p} = \Delta\left(\varepsilon^2\left(1 + \frac{\beta_0^2}{\alpha_0^2}\right)^{-1}A_0\lambda_-^{(0)}(c_0 + V_0)\right)\cos(\xi) + \Delta\varepsilon^{10/3}p_{cl}(\xi,\tilde{y}) + \cdots, \tag{3.5d}$$

where $\xi = \alpha(x - ct) + \beta z$ with $\alpha = \varepsilon\alpha_0$, $\beta = \varepsilon\beta_0$ and $c = \varepsilon^2 c_0$, to leading order (these are the upper-branch scalings for α, β and c). Here, the first terms in the expansions for u and w satisfy forced Airy equations and from the continuity equation they are related via

$$\alpha_0 u_1 + \beta_0 w_1 = 0. \tag{3.6}$$

The terms with subscript cl are contributions arising from the logarithmic behaviour evident in the final terms of the velocity expansions in (2.90) (see (2.102), for instance) in the inviscid layer II–.

If we examine the perturbation expansion (3.5a) for u, we observe that weakly nonlinear effects come into play when the basic flow curvature term proportional to $\varepsilon^{20/3}$ becomes comparable with the term with subscript cl: this identifies a critical disturbance size, $\Delta \sim \varepsilon^{14/3}\overline{\Delta}$, with $\overline{\Delta}$ of $O(1)$. We therefore conclude that linear stability theory (and hence the Orr–Sommerfeld approach) is rendered invalid at the stage $\Delta = O(R^{-14/33})$, and weakly nonlinear effects become important and have to be taken into account at leading order. If we consider the continuity and Navier–Stokes equations (1.1) with $\Delta = O(R^{-14/33})$ in (2.3) and the flow expansions (2.63), (2.79), (2.90) and (2.105) it transpires that the dynamics in regions II+, III+, II– and III– remain essentially unchanged by this increase in disturbance size, and so we can concentrate in the remainder of this subsection on the behaviour within the critical layer.

Substitution of these expansions into (1.1) together with $\Delta = \varepsilon^{14/3}\overline{\Delta}$ results in the following balances within the nonlinear critical layer

$$\alpha_0 \frac{\partial u_{cl}}{\partial \xi} - \frac{\partial v_{cl}}{\partial \tilde{y}} + \beta_0 \frac{\partial w_{cl}}{\partial \xi} = 0, \tag{3.7a}$$

$$\begin{aligned}(\overline{\Delta}\alpha_0\lambda_-^{(0)}\tilde{y})\frac{\partial u_{cl}}{\partial \xi} - (\overline{\Delta}\alpha_0\lambda_-^{(1)}c_0\tilde{y})u_1\sin(\xi) - \overline{\Delta}\lambda_-^{(0)}v_{cl} \\ + \overline{\Delta}\alpha_0 A_0(c_0+V_0)\sin(\xi)\left(2\lambda_-^{(1)}\tilde{y} + \overline{\Delta}\frac{\partial u_{cl}}{\partial \tilde{y}}\right) = 2\lambda_-^{(1)} + \overline{\Delta}\frac{\partial^2 u_{cl}}{\partial \tilde{y}^2},\end{aligned} \tag{3.7b}$$

$$\frac{\partial p_{cl}}{\partial \tilde{y}} = 0, \tag{3.7c}$$

$$\begin{aligned}(\overline{\Delta}\alpha_0\lambda_-^{(0)}\tilde{y})\frac{\partial w_{cl}}{\partial \xi} - (\overline{\Delta}\alpha_0\lambda_-^{(1)}c_0\tilde{y})w_1\sin(\xi) \\ + \overline{\Delta}^2\alpha_0 A_0(c_0+V_0)\sin(\xi)\frac{\partial w_{cl}}{\partial \tilde{y}} = \overline{\Delta}\frac{\partial^2 w_{cl}}{\partial \tilde{y}^2}.\end{aligned} \tag{3.7d}$$

It should be pointed out that the nonlinear effects in the critical layer are marked by the presence of various terms proportional to $\overline{\Delta}^2$ in these system of equations. Equation (3.6) suggests that the streamwise and spanwise momentum balances (3.7b) and (3.7d) can be suitably combined if we multiply the former equation by α_0, the latter form of the equation by β_0 and add the results together. This leads to a simpler equation, namely

$$\begin{aligned}(\overline{\Delta}\alpha_0\lambda_-^{(0)}\tilde{y})\left(\alpha_0\frac{\partial u_{cl}}{\partial \xi} + \beta_0\frac{\partial w_{cl}}{\partial \xi}\right) + \overline{\Delta}^2\alpha_0 A_0(c_0+V_0)\sin(\xi)\left(\alpha_0\frac{\partial u_{cl}}{\partial \tilde{y}} + \beta_0\frac{\partial w_{cl}}{\partial \tilde{y}}\right) \\ + 2\overline{\Delta}\lambda_-^{(1)}\alpha_0^2 A_0(c_0+V_0)\tilde{y}\sin(\xi) - \overline{\Delta}\alpha_0\lambda_-^{(0)}v_{cl} = 2\lambda_-^{(1)}\alpha_0 + \overline{\Delta}\left(\alpha_0\frac{\partial^2 u_{cl}}{\partial \tilde{y}^2} + \beta_0\frac{\partial^2 u_{cl}}{\partial \tilde{y}^2}\right).\end{aligned} \tag{3.8}$$

Inspection of the continuity balance (3.7a) motivates defining a streamfunction Ψ such that

$$\alpha_0(\overline{\Delta}u_{cl} - \tilde{y}^2) + \beta_0\overline{\Delta}w_{cl} = \frac{\partial \Psi}{\partial \tilde{y}}, \quad \overline{\Delta}v_{cl} = \frac{\partial \Psi}{\partial \xi}. \tag{3.9}$$

Using this formulation, equation (3.8) can be expressed in the form

$$(\alpha_0\lambda_-^{(0)}\tilde{y})\frac{\partial^2\Psi}{\partial\xi\partial\tilde{y}} + \overline{\Delta}\alpha_0 A_0(c_0+V_0)\,\sin(\xi)\frac{\partial^2\Psi}{\partial\tilde{y}^2} - \alpha_0\lambda_-^{(0)}\frac{\partial\Psi}{\partial\xi} = \frac{\partial^3\Psi}{\partial\tilde{y}^3}. \tag{3.10}$$

Differentiating (3.10) with respect to $\tilde{y}$ we obtain the governing equation in the streamfunction form

$$(\alpha_0\lambda_-^{(0)}\tilde{y})\frac{\partial^3\Psi}{\partial\xi\partial\tilde{y}^2} + \overline{\Delta}\alpha_0 A_0(c_0+V_0)\,\sin(\xi)\frac{\partial^3\Psi}{\partial\tilde{y}^3} = \frac{\partial^4\Psi}{\partial\tilde{y}^4}. \tag{3.11}$$

The appropriate matching conditions to the surrounding shear region II– are

$$\frac{\partial\Psi}{\partial\tilde{y}} \sim -\alpha_0\tilde{y}^2 + \overline{\Delta}^{1/2}\hat{\lambda}^+\tilde{y} - \overline{\Delta}\alpha_0 A_0(c_0+V_0)(\ln\,\tilde{y})(\cos(\xi)) \quad \text{as } \tilde{y}\to+\infty, \tag{3.12a}$$

$$\frac{\partial\Psi}{\partial\tilde{y}} \sim -\alpha_0\tilde{y}^2 + \overline{\Delta}^{1/2}\hat{\lambda}^-\tilde{y} - \overline{\Delta}\alpha_0 A_0(c_0+V_0)(\ln\,|\tilde{y}|\,\cos(\xi) - J(\xi)) \quad \text{as } \tilde{y}\to-\infty. \tag{3.12b}$$

Here the non-monochromatic velocity jump $J(\xi)$ is calculated as part of the solution, while the second term proportional to $\overline{\Delta}^{1/2}$ is included in anticipation of a jump $\hat{\lambda}^+ - \hat{\lambda}^-$ in the vorticity $\partial^2\Psi/\partial\tilde{y}^2$ across the critical layer. From substituting (2.90) into (2.3) and matching its real part as $Y_- \to ((c_0+V_0)/2)^\pm$ with (3.5) as $\tilde{y}\to\pm\infty$ we obtain the first term proportional to $\tilde{y}^2$ in (3.12) and also the asymptotic behaviours $\overline{\Delta}u_{cl} \sim \overline{\Delta}u_-^{(1)}\cos(\xi)$ and $\overline{\Delta}w_{cl} \sim \overline{\Delta}w_-^{(1)}\cos(\xi)$. Then, analysis of the continuity equation (2.99a) in the limit $\tilde{y}\to\pm\infty$, along with use of (2.97), (2.98) and (2.102), yields the balance $\alpha_0 u_-^{(1)} + \beta_0 w_-^{(1)} \sim -\vartheta\,\ln|\tilde{y}|$, explaining the logarithmic contributions present in (3.12). Despite the fact that the velocity jump becomes non-monochromatic once weakly nonlinear effects are included, the concept of a phase shift ϕ^- can be retained provided $J(\xi)$ is represented by a Fourier series and ϕ^- is defined to be the coefficient of $\sin(\xi)$ in that series, i.e.

$$\phi^- = \frac{1}{\pi}\int_0^{2\pi} J(\xi)\,\sin(\xi)\,\mathrm{d}\xi.$$

Integrating (3.11) twice with respect to $\tilde{y}$, once with respect to ξ from 0 to 2π and then taking finite parts as $\tilde{y}\to\pm\infty$, leads to the establishment of a relation between the velocity and vorticity jumps, namely

$$\overline{\Delta}\alpha_0 A_0(c_0+V_0)\int_0^{2\pi}\left[\left[\frac{\partial\Psi}{\partial\tilde{y}}\right]\right]_{-\infty}^{\infty}\sin(\xi)\,\mathrm{d}\xi = \int_0^{2\pi}\left[\left[\frac{\partial^2\Psi}{\partial\tilde{y}^2}\right]\right]_{-\infty}^{\infty}\mathrm{d}\xi, \tag{3.13}$$

where [[ ]] represents the finite part of the jump. It is important to note that the integrated contributions from the first term on the left hand side of (3.11) is identically zero owing to the periodicity requirement of Ψ in ξ, that is, $\Psi(\xi=0,\tilde{y}) = \Psi(\xi=2\pi,\tilde{y})$.

From the asymptotic constraint in (3.12) we can deduce the representations of the integrands in (3.13) which are easily found to be

$$\left[\left[\frac{\partial\Psi}{\partial\tilde{y}}\right]\right]_{-\infty}^{\infty} = -\overline{\Delta}\alpha_0 A_0(c_0+V_0)J(\xi), \quad \left[\left[\frac{\partial^2\Psi}{\partial\tilde{y}^2}\right]\right]_{-\infty}^{\infty} = \overline{\Delta}^{1/2}(\hat{\lambda}^+ - \hat{\lambda}^-). \tag{3.14}$$

Inserting (3.14) into (3.13) and using the definition of ϕ^- we obtain the desired expression for the phase shift in terms of the scaled disturbance amplitude $\overline{\Delta}$ and the vorticity jump $(\hat{\lambda}^+ - \hat{\lambda}^-)$ as

$$\phi^- = -\left(\frac{2}{\alpha_0^2 A_0^2 (c_0+V_0)^2}\right)(\hat{\lambda}^+ - \hat{\lambda}^-)\overline{\Delta}^{\frac{-3}{2}}. \tag{3.15}$$

The following questions arise naturally: what is the disturbance amplitude Δ at which strong nonlinear effects are provoked within the critical layer? How is the stability structure associated with the nonlinear neutral mode modified as the disturbance size is increased from $O(R^{-14/33})$? We will explore the answers to these questions shortly. Of particular interest next is to examine the critical layer equation (3.11) in the limit $\overline{\Delta} \to \infty$ and obtain a relationship between ϕ^- and $\overline{\Delta}$. This will serve as an all-important guide to forming the scalings for the strongly nonlinear regime to be considered in chapter 4.

3.1.2 The solution of the critical layer problem at large disturbance amplitude

Our approach to analysing (3.11), (3.12) as $\overline{\Delta} \to \infty$ is based on the work of Haberman (1972), Smith & Bodonyi (1982b) for a two-dimensional accelerating boundary layer flow, but with some modifications to account for our different basic flow. In this limit the main change to the stability properties we encounter is that the inertia terms play a dominant role over the viscous effects in (3.11) and correspondingly the critical-layer variable $\tilde{y}$ is transformed as $\tilde{y} = \overline{\Delta}^{1/2} y^*$, with the scaled variable $y^* \sim O(1)$. Thus, the streamfunction equation can be rewritten in the form

$$(\alpha_0 \lambda_-^{(0)} y^*)\frac{\partial^3\Psi}{\partial\xi\partial y^{*2}} + \vartheta \sin(\xi)\frac{\partial^3\Psi}{\partial y^{*3}} = \overline{\Delta}^{\frac{-3}{2}}\frac{\partial^4\Psi}{\partial y^{*4}}, \tag{3.16}$$

where $\vartheta = \alpha_0 A_0(c_0+V_0)$. We seek the solution in the form of a perturbation series in powers of $\overline{\Delta}$:

$$\frac{\partial^2\Psi}{\partial y^{*2}} = \overline{\Delta}^{3/2}\chi_0(\xi, y^*) + \chi_1(\xi, y^*) + \cdots. \tag{3.17}$$

Substituting (3.17) into (3.16) and equating coefficients of powers of $\overline{\Delta}^{3/2}$ we obtain a linear partial differential equation for χ_0:

$$\alpha_0 \lambda_-^{(0)} y^* \frac{\partial\chi_0}{\partial\xi} + \vartheta \sin(\xi)\frac{\partial\chi_0}{\partial y^*} = 0. \tag{3.18}$$

It is easily verified through the application of the method of characteristics (Benney & Bergeron 1969) that (3.18) has the solution

$$\chi_0 = M(\hat{\eta}), \quad \hat{\eta} = \alpha_0 y^{*2} + \vartheta \cos(\xi). \tag{3.19}$$

The physical interpretation of (3.19) is that the unknown vorticity $M(\hat{\eta})$ is conserved along the streamlines $\hat{\eta} =$ constant. The streamlines, which are closed for $\hat{\eta} < \vartheta$, strongly resemble the structure of the Kelvin cat's eye. According to the Prandtl–Batchelor theorem, the vorticity is constant in such a region and thus we can infer that within the cat's eye

$$\chi_0 = M(\hat{\eta}) = M_0 \quad \text{for} \quad \hat{\eta} < \vartheta, \tag{3.20}$$

where M_0 is a constant to be determined. To fix the vorticity variation outside the eye, we need to proceed to the next order where we obtain the equation satisfied by the correction χ_1, namely

$$\alpha_0 \lambda_-^{(0)} y^* \frac{\partial \chi_1}{\partial \xi} + \vartheta \sin(\xi) \frac{\partial \chi_1}{\partial y^*} = \frac{\partial^2 \chi_0}{\partial y^{*2}}. \tag{3.21}$$

The ensuing analysis can be simplified by performing the transformation from (ξ, y^*) to $(\hat{\xi}, \hat{\eta})$ coordinates, with $\xi = \hat{\xi}$, which results in the governing equation for χ_1 as

$$\frac{\partial \chi_1}{\partial \hat{\xi}} = \pm (2\alpha_0 \lambda_-^{(0)})^{1/2} \frac{\partial}{\partial \hat{\eta}} \left((\hat{\eta} - \vartheta \cos(\hat{\xi}))^{1/2} M'(\hat{\eta}) \right), \tag{3.22}$$

where use has been made of the following useful results:

$$\frac{\partial}{\partial \xi} = \frac{\partial}{\partial \hat{\xi}} - \vartheta \sin(\xi) \frac{\partial}{\partial \hat{\eta}}, \quad \frac{\partial}{\partial y^*} = 2\alpha_0 y^* \frac{\partial}{\partial \hat{\eta}}, \quad y^* = \pm \left(\frac{\hat{\eta} - \vartheta \cos(\xi)}{\alpha_0} \right)^{1/2}. \tag{3.23}$$

Here the $\pm$ notation refers to the upper and lower parts of the critical layer, where $y^* > (\vartheta/\overline{\alpha}_0)^{1/2}(1-\cos(\xi))^{1/2}$ and $y^* < -(\vartheta/\overline{\alpha}_0)^{1/2}(1-\cos(\xi))^{1/2}$, respectively. Integrating equation (3.22) with respect to $\hat{\xi}$ from 0 to 2π and imposing periodicity of χ_1 we obtain

$$\frac{\partial}{\partial \hat{\eta}} \left(M'(\hat{\eta}) \int_0^{2\pi} (\hat{\eta} - \vartheta \cos(q))^{1/2} \, \mathrm{d}q \right) = 0, \tag{3.24}$$

which can be integrated with respect to $\hat{\eta}$ to yield

$$M'(\hat{\eta}) = \frac{M^{\pm}}{\hat{I}(\hat{\eta})}, \quad \hat{I}(\hat{\eta}) = \int_0^{2\pi} (\hat{\eta} - \vartheta \cos(q))^{1/2} \, \mathrm{d}q, \tag{3.25}$$

where $M^{\pm}$ are unknown constants. In order to calculate their value it is instructive to express the asymptotic form (3.12) in terms of the new variable y^* and then differentiate the result with respect to y^* which renders the asymptotic constraint for χ_0 as

$$\chi_0 \sim -2\alpha_0 y^* + \hat{\lambda}^{\pm} + O\left(\frac{1}{y^*} \right) \quad \text{as } y^* \to \pm\infty. \tag{3.26}$$

The asymptotic condition for $M'(\hat{\eta})$ can be obtained by changing (3.26) to characteristic coordinates $(\hat{\xi}, \hat{\eta})$ and differentiating the resulting form with respect to $\hat{\eta}$. This leaves

$$M'(\hat{\eta}) \sim \mp\left(\frac{\alpha_0^{1/2}}{(\hat{\eta} - \vartheta\,\cos(\hat{\xi}))^{1/2}}\right) + O\left(\frac{1}{\hat{\eta}^{\frac{3}{2}}}\right) \quad \text{as } \hat{\eta} \to \infty. \tag{3.27}$$

Multiplying this asymptotic condition by $(\hat{\eta} - \vartheta\,\cos(\hat{\xi}))^{1/2}$ and integrating with respect to $\hat{\xi}$ from 0 to 2π enables us to fix the constants $M^{\pm} = \mp 2\pi\alpha_0^{1/2}$ so that the vorticity gradient $M'(\hat{\eta})$ is given by

$$M'(\hat{\eta}) = \mp\left(\frac{2\pi\alpha_0^{1/2}}{\hat{I}(\hat{\eta})}\right). \tag{3.28}$$

Examining equations (3.20) and (3.28), we see that $M'(\hat{\eta})$ exhibits a discontinuity at the edges of the cat's eye, $\hat{\eta} = \vartheta^{\pm}$, and therefore to make further progress an additional boundary condition on $M(\hat{\eta})$ is required. Fortunately, this dilemma has been resolved already in Brown & Stewartson (1978), where a study of the evolution of the critical layer of a Rossby wave suggested that the vorticity is continuous at the edges of the cat's eye. Hence, from integration of (3.28), we find that the leading order contribution χ_0 takes the form

$$\chi_0 = M(\hat{\eta}) = M_0 \mp 2\pi\alpha_0^{1/2} \int_{\vartheta}^{\hat{\eta}} \frac{\mathrm{d}s}{\hat{I}(s)} \quad \text{for} \quad \hat{\eta} > \vartheta. \tag{3.29}$$

The determination of the vorticity jump now necessitates an examination of the matching condition (3.26) for a second time, which in turn reveals that

$$\hat{\lambda}^+ - \hat{\lambda}^- = [[\chi_0]]_{-\infty}^{+\infty} = -4\pi\alpha_0^{1/2} \fint_{\vartheta}^{\infty} \frac{\mathrm{d}s}{\hat{I}(s)}, \quad M_0 = \left(\frac{\hat{\lambda}^+ + \hat{\lambda}^-}{2}\right),$$

where the bar denotes the finite part of the integral, the value of which is evaluated to be

$$\fint_{\vartheta}^{\infty} \frac{\mathrm{d}s}{\hat{I}(s)} = \frac{(2\vartheta)^{1/2}}{8\pi} C^{(1)}, \quad C^{(1)} \simeq -5.516,$$

as calculated in Smith and Bodonyi (1982b) and Haberman (1972), among others. Thus, it follows immediately that the effective vorticity jump across the nonlinear critical layer is given by

$$\hat{\lambda}^+ - \hat{\lambda}^- = -\left(\frac{\alpha_0\vartheta}{2}\right)^{1/2} C^{(1)} = -\alpha_0\left(\frac{A_0(c_0 + V_0)}{2}\right)^{1/2} C^{(1)}, \tag{3.30}$$

in view of the fact that $\vartheta = \alpha_0 A_0(c_0 + V_0)$. Substituting (3.30) into (3.15) we find the following expression for the phase shift as a function of disturbance amplitude $\overline{\Delta}$:

$$\phi^- \sim \left(\frac{4C^{(1)}}{\alpha_0(2A_0(c_0 + V_0))^{3/2}}\right)\overline{\Delta}^{\frac{-3}{2}} \quad \text{as} \quad \overline{\Delta} \to \infty. \tag{3.31}$$

We will not consider the dynamics of the upper nonlinear critical layer as the details are very similar to those presented above, the only difference being that V_0 in (3.31) is replaced by $-V_0$, and hence we have the analogous result

$$\phi^+ \sim \left(\frac{4C^{(1)}}{\alpha_0(2A_0(c_0-V_0))^{3/2}}\right)\overline{\Delta}^{\frac{-3}{2}} \quad \text{as} \quad \overline{\Delta}\to\infty, \tag{3.32}$$

where ϕ^+ is the phase shift induced across it. The striking feature of the results (3.31) and (3.32) is that the anticipated phase shifts $\phi^{\mp}$ across the critical layers decrease as the scaled disturbance size $\overline{\Delta}$ increases, with $\phi^{\mp}\to 0$ as $\overline{\Delta}\to\infty$. As we shall see in section 4.2.1 of the next chapter, this result is of prime importance for it enables us to identify the scalings in the strongly nonlinear regime and in particular determine the thicknesses of the critical layers in terms of R. In the next section, we examine the effect of increasing the disturbance size Δ on the critical layer in the hybrid region in 2.3.5.

3.2 The dynamics of the strongly nonlinear critical layer on the hybrid scaling

The dominant balance in the linear viscous critical layer (see figure 2.14) is between the viscous term $R^{-1}\partial^2/\partial y^2$ and the inertial operator $(U_0-c)\partial/\partial x$, with $\partial/\partial x\sim O(\varepsilon)$. As remarked earlier this thin layer is located at $Y_-=\overline{V}_0$ in terms of the scalings for the inviscid shear region in 2.3.5(**ii**), and we suppose that the thickness of the critical layer is q which is to be determined in terms of ε. Hence we introduce the appropriate $O(1)$ variable $\tilde{y}=q^{-1}(Y_--\overline{V}_0)$. Recalling that the normal scaling in the region II– is $y=-1+\varepsilon^2Y_-$ we have

$$y=-1+\varepsilon^2\overline{V}_0+\varepsilon^2q\tilde{y}. \tag{3.33}$$

In view of (2.129) and (3.33), the term (U_0-c) assumes the form

$$U_0-c=2\varepsilon^2q\tilde{y}-\varepsilon^4\overline{c}_1-\varepsilon^4\overline{V}_0q\tilde{y}-\varepsilon^4q^2\tilde{y}^2-\cdots, \tag{3.34}$$

implying that the order of magnitude of (U_0-c) is ε^2q. It follows from (3.33) that $\partial^2/\partial y^2\sim O(\varepsilon^{-4}q^{-2})$ and thus an inertial-viscous balance is achieved provided $\varepsilon^3q\sim R^{-1}(\varepsilon^2q)^{-2}$, establishing the critical-layer thickness $q\sim\varepsilon^2$. The disturbance velocities and pressure are

$$u=U_0+\Delta\hat{u}=U_0+\Delta\varepsilon^2\tilde{u}_1(\tilde{y})\cos(\xi)+\Delta\varepsilon^2u_{cl}(\xi,\tilde{y})+\cdots, \tag{3.35a}$$

$$v=\Delta\hat{v}=\Delta(\varepsilon^3\overline{\alpha}_0A_0(\overline{c}_0+\overline{V}_0))\sin(\xi)-\Delta\varepsilon^7v_{cl}(\xi,\tilde{y})+\cdots, \tag{3.35b}$$

$$w=\Delta\hat{w}=\Delta\varepsilon^2\tilde{w}_1(\tilde{y})\cos(\xi)+\Delta\varepsilon^2w_{cl}(\xi,\tilde{y})+\cdots, \tag{3.35c}$$

$$p=\Delta\hat{p}=\Delta\left(\varepsilon^2\left(1+\frac{\overline{\beta}_0^2}{\overline{\alpha}_0^2}\right)^{-1}A_0\lambda_-^{(0)}(\overline{c}_0+\overline{V}_0)\right)\cos(\xi)+\Delta\varepsilon^4p_{cl}(\xi,\tilde{y})+\cdots, \tag{3.35d}$$

where $\xi = \alpha(x - ct) + \beta z$ with $\alpha = \varepsilon\overline{\alpha}_0$, $\beta = \varepsilon\overline{\beta}_0$ and $c = \varepsilon^2\overline{c}_0$, to leading order (these are the hybrid-branch scalings for α, β and c). Here, the leading-order disturbances $\tilde{u}(\tilde{y})$ and $\tilde{w}(\tilde{y})$ satisfy forced Airy equations and from the continuity equation they are related via

$$\overline{\alpha}_0\tilde{u}_1 + \overline{\beta}_0\tilde{w}_1 = 0. \tag{3.36}$$

The terms with subscript cl are known as the logarithmic contributions which arises as an immediate consequence of the principle of continuation and regularization of the logarithmic behaviour noticed in the lower inviscid layer II–.

It is interesting to observe that weakly nonlinear effects come into play when the term proportional to ε^8 in the expansion (3.34) becomes comparable with the $O(\Delta\varepsilon^2)$ term in the perturbation expansion (3.35a), leading to $\Delta \sim \varepsilon^6\overline{\Delta}$, with $\overline{\Delta}$ of $O(1)$. If we consider the continuity and Navier–Stokes equations (1.1) with $\Delta = O(R^{-6/13})$ in (2.3) and the flow expansions (2.134), (2.139), it transpires that the dynamics in regions II– and III– remain essentially unchanged by this increase in disturbance size, and so we can focus in the remainder of this section on the behaviour within the critical layer. Then, from substitution of (3.35) into the Navier–Stokes equations (1.1) together with $\Delta = \varepsilon^6\overline{\Delta}$, the critical-layer problem can be posed in the streamfunction form

$$(2\overline{\alpha}_0\tilde{y})\frac{\partial^3\Psi}{\partial\xi\partial\tilde{y}^2} + \overline{\Delta}\overline{\alpha}_0 A_0(\overline{c}_0 + \overline{V}_0)\sin(\xi)\frac{\partial^3\Psi}{\partial\tilde{y}^3} = \frac{\partial^4\Psi}{\partial\tilde{y}^4}. \tag{3.37}$$

The appropriate matching conditions to the shear region II– can be shown to be

$$\frac{\partial\Psi}{\partial\tilde{y}} \sim -\overline{\alpha}_0\tilde{y}^2 + \overline{\Delta}^{1/2}\hat{\lambda}^+\tilde{y} - \overline{\Delta}\overline{\alpha}_0 A_0(\overline{c}_0 + \overline{V}_0)(\ln\,\tilde{y})(\cos(\xi)) \quad \text{as } \tilde{y} \to +\infty, \tag{3.38a}$$

$$\frac{\partial\Psi}{\partial\tilde{y}} \sim -\overline{\alpha}_0\tilde{y}^2 + \overline{\Delta}^{1/2}\hat{\lambda}^-\tilde{y} - \overline{\Delta}\overline{\alpha}_0 A_0(\overline{c}_0 + \overline{V}_0)(\ln\,|\tilde{y}|\cos(\xi) - J(\xi)) \quad \text{as } \tilde{y} \to -\infty, \tag{3.38b}$$

with the phase shift ϕ given by

$$\phi = \frac{1}{\pi}\int_0^{2\pi} J(\xi)\,\sin(\xi)\,\mathrm{d}\xi.$$

Here, the quantity $\hat{\lambda}^+ - \hat{\lambda}^-$ represents the unknown jump in vorticity across the critical layer. Our interest here lies in the analysis of (3.37), (3.38) in the limit $\overline{\Delta} \to \infty$ which can be performed in a similar manner to that outlined in subsection 3.1.2. Specifically, it can be shown that the phase shift ϕ induced across the critical layer decreases with increasing disturbance amplitude such that

$$\phi \sim \left(\frac{C^{(1)}}{2\overline{\alpha}_0(A_0\overline{V}_0)^{3/2}}\right)\overline{\Delta}^{\,-3/2} \quad \text{as} \quad \overline{\Delta} \to \infty, \tag{3.39}$$

for disturbances of amplitude $\Delta = R^{-6/13}\overline{\Delta}$. As we shall see shortly, how this result allows us to identify the scalings in the strongly nonlinear regime, thus providing the motivation for the nonlinear study to be considered in the next chapter.

Chapter 4

Nonlinear stability of plane Poiseuille–Couette flow

Before we begin our discussion on the nonlinear stability of PPCF, it is worth stating that the accounts in this chapter are the expanded versions of those appearing in two papers, namely Kumar & Walton (2018), Kumar & Walton (2019). In recent years a dynamical systems approach to transition has become fashionable, in which equilibrium solutions of the Navier–Stokes equations play a key role in transitional and turbulent dynamics (see for example the review of Kawahara G, Uhlmann M & van Veen L (2012)). The relevant equilibrium solutions are those in which there is a mutual interaction between a roll flow in the cross-stream plane, a streamwise streak and a wave propagating in the streamwise direction. This interaction is fundamentally three-dimensional in nature and has no obvious two-dimensional analogue. If we wish to consider Tollmien-Schlichting (TS) instabilities, which are inherently two-dimensional, then the roll/streak/wave theories are not directly applicable, even at high Reynolds number, unless a very specific spanwise variation is imposed. In this chapter we investigate a form of self-sustaining process (SSP) that can operate in three dimensions and involves critical layer/wall layer interaction. We develop the theory under the assumption of an asymptotically large Reynolds number, which allows us to identify the crucial scalings and regions where different physical balances dominate and to demonstrate the way in which those regions interact to ensure that the instability is maintained. We develop the theory here for the specific case of plane Poiseuille–Couette flow (PPCF), which is well-known to support a TS form of instability provided that the sliding speed is not too large, although the theory readily generalizes to other base flows. We will see in chapter 5, by comparing Navier–Stokes solutions with asymptotic theory, the nonlinear interaction formulated in section 4.1 accurately describes solutions that bifurcate from one of the additional neutral curves in figure 2.3(d).

We will consider two possible self-sustaining interactions in PPCF. The first assumes that the phasespeed is sufficiently close in value to the sliding speed of the upper wall that the upper critical layer and Stokes layer merge to form a viscous shear layer. In the second scenario, both the wall sliding speed V and the disturbance phasespeed c are $O(1)$ quantities, but

are sufficiently distinct from one another that there exist two critical layers that reside an $O(1)$ distance from both walls, with viscous Stokes layers adjoining the boundaries. In the next section we consider the interaction of the first type, while the latter case is discussed in section 4.2.

4.1 Analysis of the nonlinear hybrid modes

In this section, the nonlinear stability of PPCF to three-dimensional disturbances is investigated asymptotically at large values of the Reynolds number R based on channel half-width and the maximum velocity of the Poiseuille component. The asymptotic theory, aimed at a detailed understanding of the physical mechanisms governing the amplitude-dependent stability properties of the flow, shows that the phase shifts induced across the critical layer and a near-wall shear layer are comparable when the disturbance size $\Delta = O(R^{-4/9})$. In addition, it emerges that at this crucial size both streamwise and spanwise wavelengths of the travelling wave disturbance are comparable with the channel width, with an associated phasespeed of $O(1)$. Neutral solutions are found to exist in the range $0 < V < 2$ with $c_0 = V$ to leading order, where c_0 and V are non-dimensional quantities representing the dominant phasespeed of the nonlinear travelling waves and the wall sliding speed respectively. Moreover, these instability modes exist at sliding speeds well in excess of the linear instability cut-off. The amplitude equation governing these modes is derived analytically and we further find that this asymptotic structure breaks down in the limit $V \to 2$ when the disturbance streamwise wavelength decreases to $O(R^{-1/3})$ and the maximum of the basic flow becomes located at the upper wall.

It is well known that for plane Poiseuille flow, finite amplitude two-dimensional travelling waves exist and map out a neutral surface in the parameter space formed by Reynolds number, wavenumber and amplitude (Herbert 1977). Weakly nonlinear stability analysis (Reynolds & Potter (1967); Cowley & Smith (1985)) suggested that PPCF may become unstable to finite-amplitude disturbances for $V > V_c$ and this was confirmed to be the case in the nonlinear numerical studies of Ehrenstein, Nagata & Rincon (2008), Balakumar (1997). The numerical study of Ehrenstein, Nagata & Rincon (2008) used Poiseuille–Couette homotopy to continue a path through the equilibrium states for plane Poiseuille flow to Couette flow although it remains unclear whether these solutions are fully resolved. In Balakumar (1997), two-dimensional nonlinear equilibrium surfaces were mapped out by gradually increasing the value of V. These solutions were computed by starting from the main neutral curve for PPCF and it was concluded that such solutions do not exist beyond $V \approx 0.96$ in our non-dimensionalization. However there are no such numerical studies investigating how nonlinearity affects the additional neutral curves (the upper curves) that we computed in section 2.2 of this thesis. To investigate this problem we will adopt a high Reynolds number asymptotic approach, which enables us to start from the known linear stability properties along the upper neutral curve. We then seek a structure that incorporates three-dimensionality and nonlinearity and find that the stability properties are determined by the interaction of the

predominantly inviscid critical layer and a viscous shear layer located near the upper wall. It is discovered that this new nonlinear travelling wave structure is supported at $O(1)$ sliding speeds in excess of the linear cutoff V_c and is strongly three-dimensional in the sense that the streamwise and spanwise wavenumbers are comparable with the channel width. A novel feature of the structure is that the amplitude of the waves can be determined almost entirely analytically in terms of the sliding speed and the aforementioned wavenumbers. The critical layer is sited an $O(1)$ distance away from the channel walls and, as such, the asymptotic structure considered here is very different to the lower branch structure assumed in Zhuk & Protsenko (2006), where the sliding speed must necessarily remain asymptotically small.

In subsection 4.1.1 we derive the scalings for the strongly nonlinear hybrid modes, while in 4.1.2 we formulate the equations governing the strongly nonlinear regime. The bulk of the flow is governed by a Rayleigh equation incorporating a nonlinear jump condition across the critical layer which is now sited an $O(1)$ distance from the channel walls. This critical layer possesses a structure very similar to that proposed by Benney and Bergeron (1969) but its behaviour is affected by viscous effects from the near-wall regions which are transmitted through the Rayleigh zone. The critical layer structure is considered in detail and the phase shift across it is determined explicitly. Finally in this subsection the amplitude equation for the nonlinear modes is established as a result of an exact counterbalance between the two small phase shifts produced by the critical layer and the viscous shear layer astride the upper wall. In subsection 4.1.3, a numerical procedure is outlined to solve the Rayleigh equation: this allows us to compute the neutral streamwise wavenumber for a given sliding velocity and spanwise wavenumber. In addition, we discuss numerical solutions to the amplitude equation and conclude that the asymptotic structure associated with these nonlinear modes breaks down as $V \to 2$, at which value the maximum of the basic PPCF flow is located at the upper wall. Finally, we summarize our findings and suggest avenues for further research, including some discussion of the new structure which emerges in the $V \to 2$ limit mentioned above.

4.1.1 Scalings in the strongly nonlinear regime

Before we look for a description of the behaviour of the scaled wavenumber and wavespeed when the scaled disturbance amplitude $\overline{\Delta} \to \infty$, it is useful to write down the corresponding expression for $\overline{\alpha}_0$, $\overline{\beta}_0$ in terms of $\overline{V}_0$ at finite $\overline{\Delta}$. Returning briefly to the linear analysis of subsection 2.3.5 and combining (2.129), (2.143) and (2.148), we obtain the following asymptotic neutral stability criteria for the hybrid curve in the linear regime:

$$\overline{\alpha}_0 = \frac{1}{2}\left\{\frac{\mathrm{Im}(g(\overline{s}))}{\pi \overline{V}_0^2}\right\}^3, \quad \overline{\beta}_0 = \left\{\frac{15\overline{V}_0}{4} - \frac{1}{4}\left(\frac{\mathrm{Im}(g(\overline{s}))}{\pi \overline{V}_0^2}\right)^6\right\}^{\frac{1}{2}}, \quad \overline{c}_0 = \overline{V}_0. \tag{4.1}$$

As the amplitude of the perturbation Δ is increased to $O(R^{-6/13})$, the linear stability structure of the hybrid modes breaks down and the transition from the linear to weakly nonlinear regime takes place. Interestingly, at the $O(R^{-6/13})$ stage, despite the appearance of the

higher harmonics in the critical layer expansions (3.35), the criteria (4.1) continue to hold provided the 'π' in the denominator is replaced by ϕ (Haberman (1976)), and so the weakly nonlinear neutral criteria are simply

$$\overline{\alpha}_0 = \frac{1}{2}\left\{\frac{\mathrm{Im}(g(\overline{s}))}{\phi\overline{V}_0^2}\right\}^3, \quad \overline{\beta}_0 = \left\{\frac{15\overline{V}_0}{4} - \frac{1}{4}\left(\frac{\mathrm{Im}(g(\overline{s}))}{\phi\overline{V}_0^2}\right)^6\right\}^{\frac{1}{2}}, \quad \overline{c}_0 = \overline{V}_0. \tag{4.2}$$

We also note that in the weakly nonlinear regime the following estimates for $\overline{\alpha}_0$, $\overline{\beta}_0$ and $\overline{c}_0$ from (2.143) and (2.129) continue to hold:

$$\overline{c}_0 \sim \overline{V}_0, \quad \overline{\alpha}_0 \sim O(\overline{V}_0^{1/2}), \quad \overline{\beta}_0 \sim O(\overline{V}_0^{1/2}). \tag{4.3}$$

In view of (3.39), the limiting behaviour of the phase shift ϕ can be explicitly stated as

$$\phi \sim O(\overline{\alpha}_0^{-1}\overline{V}_0^{-3/2}\ \overline{\Delta}^{\ -3/2}) \quad \text{as} \quad \overline{\Delta} \to \infty, \tag{4.4}$$

for disturbances of amplitude $\Delta = \varepsilon^6\overline{\Delta}$. Taking this into account, from (4.2) we arrive at the following asymptotic forms for $\overline{\alpha}_0$ and $\overline{\beta}_0$:

$$\overline{\alpha}_0 \sim O(\overline{V}_0^{3/4}\ \overline{\Delta}^{\ -9/4}), \quad \overline{\beta}_0 \sim \left\{\frac{15\overline{V}_0}{4} - \frac{1}{4}(\mathrm{Im}(g(\overline{s})))^{-3}\ \overline{V}_0^{\frac{3}{2}}\ \overline{\Delta}^{-\frac{9}{2}}\right\}^{\frac{1}{2}} \quad \text{as} \quad \overline{\Delta} \to \infty. \tag{4.5}$$

We then consider (4.3) and (4.5), which lead to the amplitude–velocity balance

$$\overline{\Delta} \sim O(\overline{V}_0^{\frac{1}{9}}). \tag{4.6}$$

Analysis of the perturbation expansions (3.35) accompanied by the streamfunction equation (3.37) with the boundary conditions (3.38) reveals that the asymptotic structure of the weakly nonlinear upper curve modes remains intact until $\overline{V}_0 \sim O(\varepsilon^{-2})$, that is to say, until V becomes $O(1)$. We therefore conclude from (4.6) that

$$\overline{\Delta} \sim O(\varepsilon^{-2/9}), \tag{4.7}$$

in the new regime. Simultaneously we observe that in the new regime according to the asymptotic relation (4.3) the scaled wavenumbers $\overline{\alpha}_0$ and $\overline{\beta}_0$ increase to $O(\varepsilon^{-1})$, while the scaled wavespeed $\overline{c}_0$ rises to $O(\varepsilon^{-2})$. Thus for $\overline{s}$ to remain $O(1)$ in (2.147) the wavespeed correction $\overline{c}_1$ must decrease to $O(\varepsilon^{1/3})$. It is apparent from (4.7) that when the transition from the weakly nonlinear to the strongly nonlinear regime occurs the appropriate disturbance amplitude is therefore

$$\Delta = \varepsilon^6\overline{\Delta} \sim O(\varepsilon^6\varepsilon^{-2/9}) \sim O(R^{-4/9}), \tag{4.8}$$

since $\varepsilon = R^{-1/13}$. We infer that when Δ is of this order a new stability structure comes into play involving faster propagating, shorter wavelength disturbances, since the unscaled

wavenumber and wavespeed become $O(1)$ then.

We now have sufficient information to set out the asymptotic structure of the strongly nonlinear hybrid modes and this is shown schematically in figure 4.1. We find that the shear layer II– and inviscid core I indicated in figure 2.14 have merged to form a new inviscid zone (labelled I in figure 4.1) in view of the normal scaling for II–, since $\overline{V}_0 \sim O(\varepsilon^{-2})$ in the nonlinear setting considered here and therefore for U_0 in (2.134) to stay $O(1)$ the variable Y_- must rise to $O(\varepsilon^{-2})$. Additionally the thicknesses of the viscous shear layer II+ and viscous wall layer III– reduce respectively to $O(R^{-1/3})$ and $O(R^{-1/2})$, as we shall see later in subsection 4.1.2. The viscous critical layer now exhibits prominent nonlinear effects and we infer from (4.4) that the phase shift ϕ produced across it is asymptotically small, specifically of $O(R^{-1/3})$. It is demonstrated below that the critical layer is no longer sited near the lower wall and approaches the midst of the inviscid region I.

We now show how to determine the thickness of the nonlinear critical layer II. It is advisable first to summarize the main points concerning the weakly nonlinear version and then we will examine the alteration to its properties, position and thickness caused by the increased disturbance size.

In the weakly nonlinear regime the disturbance size $\Delta = R^{-6/13}\overline{\Delta}$ with $\overline{\Delta} \sim O(1)$, and the critical layer is situated at $Y_- = \overline{V}_0$ and has thickness $O(\varepsilon^2)$. As $\overline{\Delta} \to \infty$, the inertial effects control its dynamics to a large extent and the transformation $\tilde{y} = \overline{\Delta}^{1/2} y^*$ is introduced, where $y^* \sim O(1)$ as seen just above (3.16). This implies the variable $\tilde{y}$ increases as $\overline{\Delta}$ increases and hence the relation (3.33) becomes

$$y \sim -1 + \varepsilon^2 \overline{V}_0 + \ \varepsilon^2 q \overline{\Delta}^{1/2} y^* \quad \text{as} \quad \overline{\Delta} \to \infty. \tag{4.9}$$

Turning our attention to the strongly nonlinear regime, the result (4.7) reflects the fact that with the increase of the scaled disturbance size $\overline{\Delta}$ to $O(\varepsilon^{-2/9})$, intense nonlinear effects are induced within the critical layer. Since we now have $\overline{\alpha}_0 \sim O(\varepsilon^{-1})$, $\overline{c}_0 \sim O(\varepsilon^{-2})$ in this regime we notice from (3.23) that

$$\underbrace{\frac{\partial}{\partial \xi}}_{\mathrm{O}(1)} = \underbrace{\frac{\partial}{\partial \hat{\xi}}}_{\mathrm{O}(1)} - \underbrace{\vartheta \sin(\xi)}_{\mathrm{O}(\varepsilon^{-3})} \frac{\partial}{\partial \hat{\eta}}, \quad y^* = \pm \underbrace{\left(\frac{1}{\overline{\alpha}_0}\right)^{1/2}}_{\mathrm{O}(\varepsilon^{1/2})} \underbrace{(\hat{\eta} - \vartheta \cos(\xi))^{1/2}}_{\mathrm{O}(\varepsilon^{-3/2})},$$

indicating that $\hat{\eta}$ must increase to $O(\varepsilon^{-3})$ and hence the size of the variable y^* is $O(\varepsilon^{-1})$ in contrast to its $O(1)$ status in the weakly nonlinear regime. Taking this into consideration, the estimation of the quantity $\varepsilon^2 q \overline{\Delta}^{1/2} y^*$ is $O(R^{-2/9})$, and if we define $y^* = \varepsilon^{-1} Y_1$ with $Y_1 \sim O(1)$, we find the relation (4.9) then becomes

$$y = V - 1 + R^{-2/9} Y_1, \tag{4.10}$$

suggesting that the strongly nonlinear critical layer is positioned at $V-1$ and has thickness $O(R^{-2/9})$. It is worth stating that it is assumed that $V<2$. It remains to note that the streamfunction forms in the present case are precisely as given in (3.9) (with $\overline{\alpha}_0$, $\overline{\beta}_0$ replacing α_0, β_0). Keeping this in mind, it is not hard to show from (3.9) and (4.7) that $v_{cl}\sim O(\varepsilon^{2/9})$, $u_{cl}\sim O(\varepsilon^{7/3})$ in this regime since now ξ is $O(1)$ and $\tilde{y}$ is $O(\varepsilon^{-10/9})$. It is notable that the orders of magnitude of the final terms in (3.35) are then: $\varepsilon^8\overline{\Delta}u_{cl}\sim O(R^{-7/9})$, $\varepsilon^8\overline{\Delta}w_{cl}\sim O(R^{-7/9})$, $\varepsilon^{13}\overline{\Delta}v_{cl}\sim O(R^{-1})$ from (4.7) which should be compared with the last terms in (4.23) below, thus establishing in an elegant manner that the phase shift in the strongly nonlinear critical layer should arise from the $m=4$ stage. The validity of this argument will be confirmed through a strict mathematical analysis in subsection 4.1.2.

To summarise, in the strongly nonlinear regime, we should seek solutions with α, V and c of $O(1)$, to leading order, and an $O(R^{-4/9})$ disturbance amplitude, leading to an induced $O(R^{-1/3})$ phase shift across the critical layer as demonstrated above. This provides the incentive for the study of the nonlinear neutral hybrid modes whose asymptotic composition, illustrated in figure 4.1, is described by a five-zone structure consisting of a strongly non-linear critical layer in the midst of the Rayleigh inviscid zone (I), and surrounded above and below by a viscous shear layer (IV) and a viscous wall layer (III) respectively. We will consider this novel structure in detail in the next subsection.

4.1.2 The nonlinear instability structure

(a) The Rayleigh inviscid region I

We begin by considering the Rayleigh region I where the dynamics are predominantly inviscid and the normal variable y is $O(1)$. An unsteady three-dimensional fundamental disturbance of size $\Delta=O(\epsilon^2)$ is superimposed upon the basic flow (2.2), with ϵ to be identified in terms of R shortly. Asymptotic studies of fully-developed and developing pipe flow (Smith and Bodonyi (1982a), Walton (2002)) have established that this induces a larger $O(\epsilon)$ steady flow distortion. Although the present study focuses on PPCF, the same principles apply equally well here. This suggests that the appropriate flow expansions in the inviscid region are

$$u=U_0(y)+\epsilon u_{1M}(y)+\epsilon^2u_2(\xi,y)+\epsilon^2u_{2M}(y)+\cdots+\epsilon^2R^{-1/3}u_4(\xi,y)+\cdots, \tag{4.11a}$$

$$v=\epsilon^2v_2(\xi,y)+\cdots+\epsilon^2R^{-1/3}v_4(\xi,y)+\cdots, \tag{4.11b}$$

$$w=\epsilon w_{1M}(y)+\epsilon^2w_2(\xi,y)+\epsilon^2w_{2M}(y)+\cdots+\epsilon^2R^{-1/3}w_4(\xi,y)+\cdots, \tag{4.11c}$$

$$p=\epsilon^2p_2(\xi,y)+\cdots+\epsilon^2R^{-1/3}p_4(\xi,y)+\cdots, \tag{4.11d}$$

with $U_0(y)$ given by (2.2) and the fundamental disturbances (u_2,v_2,w_2,p_2) take the form of travelling waves

$$\tilde{A}_0[F_2(y)\cos(\xi),G_2(y)\sin(\xi),H_2(y)\cos(\xi),P_2(y)\cos(\xi)],\quad \xi=\alpha(x-ct)+\beta z. \tag{4.12}$$

Here the unknown amplitude functions F_2, G_2, H_2, P_2 and the mean flow corrections u_{1M}, u_{2M}, w_{1M}, w_{2M} only depend on y, while the presence of the higher order terms u_4, v_4, w_4, p_4

anticipates the occurrence of the induced $O(R^{-1/3})$ phase shift across the nonlinear critical layer II predicted by the large amplitude analysis of the strongly nonlinear critical layer in subsection 4.1.1 and this will be emphasized in detail later. It has also been inferred that $\overline{c}_1 \sim O(R^{1/3})$, $\overline{V}_0 \sim O(\varepsilon^{-2})$ in the strongly nonlinear regime so we write the wavespeed as

$$c = V + R^{-1/3} c_1, \tag{4.13}$$

in view of (2.129). The central problem is to determine the O(1) real amplitude $\tilde{A}_0$ of the nonlinear hybrid modes as a function of α, β, V and c_1. It has been shown in the previous subsection that the disturbance size Δ is of order $R^{-4/9}$, implying that

$$\epsilon = R^{-2/9}. \tag{4.14}$$

Substitution of (4.11) into the continuity and Navier–Stokes equations (1.1) leads to the inviscid balances

$$\alpha F_2 - \frac{\mathrm{d}G_2}{\mathrm{d}y} + \beta H_2 = 0, \tag{4.15a}$$

$$\alpha(U_0 - V)F_2 - U_0' G_2 = -\alpha P_2, \tag{4.15b}$$

$$\alpha(U_0 - V)G_2 = -\frac{\mathrm{d}P_2}{\mathrm{d}y}, \tag{4.15c}$$

$$\alpha(U_0 - V)H_2 = -\beta P_2, \tag{4.15d}$$

with a prime denoting the appropriate ordinary derivative. Elimination of F_2, G_2 and H_2 reduces the set of equations (4.15) to the disturbance pressure equation:

$$(U_0 - V)(P_2'' - (\alpha^2 + \beta^2)P_2) = 2U_0' P_2', \tag{4.16}$$

subject to the inviscid conditions of tangential flow as the walls are approached, namely

$$P_2'(-1) = 0, \quad P_2'(1) = 0. \tag{4.17}$$

Equation (4.16) is the Rayleigh pressure equation which has regular singular points at $y_1 = 1$, $y_c = V - 1$ with these values denoting the possible locations of the critical layers. We note that $y_1 = 1$ indicates that there is a critical layer in the vicinity of the upper wall but embedded within the viscous shear layer IV. We now consider the critical layer situated at $y = y_c$ which is located within the Rayleigh inviscid region as shown in figure 4.1.

It is straightforward to derive a series solution of (4.16), valid about the location $y = y_c$. This takes the form as $y \to y_c^+$:

$$P_2(y) = \sum_{n=0}^{\infty} p^{(n)} (\tilde{\epsilon})^n + \ln(\tilde{\epsilon}) \sum_{n=1}^{\infty} P^{(n)} (\tilde{\epsilon})^{n+2}, \tag{4.18}$$

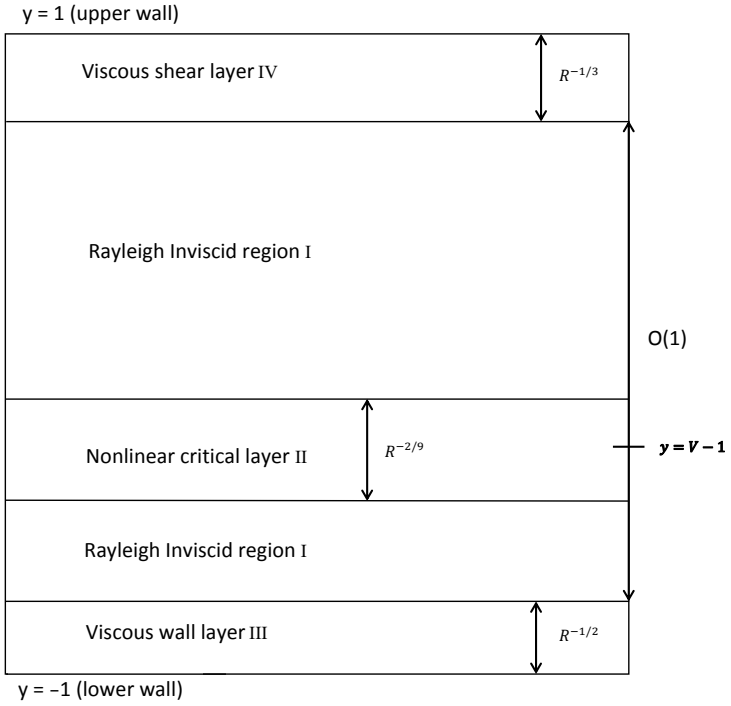

Figure 4.1: The nonlinear neutral mode structure on the hybrid scalings.

where $\tilde{\epsilon} = y - y_c$. The constants $p^{(0)}$ and $p^{(3)}$ are unknowns to be found numerically by solving (4.16) with (4.17), while the remaining constants in (4.18) can be determined once those two unknowns are fixed. From (4.15) it follows that in the same limit

$$\begin{aligned}
F_2(y) &\sim \frac{1}{\alpha^2}\left\{\frac{1}{\tilde{\epsilon}}\left(\frac{\beta^2 p^{(0)}}{1-y_c}\right) + 2P^{(2)}\ln(\tilde{\epsilon}) - \left(\frac{3p^{(3)}}{1-y_c}\right) + \left(\frac{5\alpha^2+2\beta^2}{3(\alpha^2+\beta^2)}\right)P^{(2)}\right\} + O(\tilde{\epsilon}\,\ln\tilde{\epsilon}),\\
G_2(y) &\sim \frac{1}{\alpha}\left\{\frac{3}{2}P^{(1)} + 2P^{(2)}\tilde{\epsilon}\,\ln(\tilde{\epsilon}) - \left(\frac{3p^{(3)}}{1-y_c} + \frac{P^{(2)}}{3}\right)\tilde{\epsilon} + \left(\frac{2P^{(2)}}{y_c-1}\right)\tilde{\epsilon}^2\,\ln(\tilde{\epsilon})\right\} + O(\tilde{\epsilon}^2),\\
H_2(y) &\sim \frac{\beta}{\alpha(\alpha^2+\beta^2)}\left\{-\frac{1}{\tilde{\epsilon}}\left(\frac{3P^{(1)}}{2}\right) + P^{(2)}\right\} + O(\tilde{\epsilon}).
\end{aligned} \tag{4.19}$$

In the series solution, the coefficients $P^{(1)}$, $P^{(2)}$ are given explicitly by

$$P^{(1)} = -\frac{2}{3}(\alpha^2+\beta^2)\left(\frac{p^{(0)}}{V-2}\right), \quad P^{(2)} = -(\alpha^2+\beta^2)\left(\frac{p^{(0)}}{(V-2)^2}\right). \tag{4.20}$$

In order to derive the corresponding behaviour as $y \to y_c^-$, it is necessary to study the dynamics of the critical layer. We will see shortly that a phase shift ϕ, of relative order $O(R^{-1/3})$, is produced across this layer and so we set $\phi = R^{-1/3}\Phi$ where Φ is an $O(1)$ quantity. This behaviour implies that as $y \to y_c^-$, the asymptotic behaviour (4.18)–(4.19) is

reproduced with

$$\mathrm{Re}(\ln(\tilde{\epsilon})\,\exp(\mathrm{i}\xi)) \quad \text{replaced by} \quad \mathrm{Re}((\ln(-\tilde{\epsilon}) - \mathrm{i}R^{-1/3}\Phi)\,\exp(\mathrm{i}\xi)). \tag{4.21}$$

In other words, $\ln(y - y_c)\cos(\xi)$ is effectively replaced by $\ln(y_c - y)\cos(\xi) + R^{-1/3}\Phi\sin(\xi)$ as the critical layer is crossed. In view of (4.21), it is noticeable that the $O(\epsilon^2 R^{-1/3})$ contributions $[u_4, v_4, w_4, p_4]$ in (4.11) are the highest order terms to undergo a non-zero phase shift. The connection formula (4.21) is similar to that used in previous works, e.g. Smith & Bodonyi (1982b), Smith & Bodonyi (1982a), Deguchi & Walton (2013), but the phase shift here is larger, resulting in significant changes to the neutral mode structure compared to those references. The Rayleigh equation (4.16) subject to the boundary conditions (4.17) and the jump condition (4.21) for $P_2(y)$, with Φ set to zero, constitutes a novel eigenvalue problem (Benney & Bergeron (1969)) for $\alpha = \alpha(V, \beta)$ which is tackled numerically in subsection 4.1.3. As far as the series expansion (4.18) is concerned, its continuation to $\tilde{\epsilon} < 0$ is simply given by

$$P_2(y) \sim \sum_{n=0}^{\infty} p^{(n)}(\tilde{\epsilon})^n + \ln|\tilde{\epsilon}| \sum_{n=1}^{\infty} P^{(n)}(\tilde{\epsilon})^{n+2}. \tag{4.22}$$

Of particular interest though is the determination of the scaled phase shift Φ as a function of the amplitude $\tilde{A}_0$ which requires a thorough investigation of the nonlinear critical layer dynamics.

(b) The nonlinear critical layer II

The normal scaling for the critical layer is given in (4.10), and the appropriate flow expansions are posed in the form

$$u = c_0 + \epsilon U_1 + \epsilon^2 \ln\epsilon\; U_{3/2} + \epsilon^2 U_2 + \cdots + \epsilon^{5/2} U_3 + \cdots + \epsilon^{7/2} U_4 + \cdots, \tag{4.23a}$$

$$v = \epsilon^2 V_1 + \epsilon^3 \ln\epsilon\; V_{3/2} + \epsilon^3 V_2 + \cdots + \epsilon^{7/2} V_3 + \cdots + \epsilon^{9/2} V_4 + \cdots, \tag{4.23b}$$

$$w = \epsilon W_1 + (\epsilon^2 \ln\epsilon) W_{3/2} + \epsilon^2 W_2 + \cdots + \epsilon^{5/2} W_3 + \cdots + \epsilon^{7/2} W_4(Y_1, \xi) + \cdots, \tag{4.23c}$$

$$p = \epsilon^2 Q_1 + \epsilon^3 \ln\epsilon\; Q_{3/2} + \epsilon^3 Q_2 + \cdots + \epsilon^{7/2} Q_3 + \cdots + \epsilon^{9/2} Q_4 + \cdots, \tag{4.23d}$$

as implied mainly by (4.11), (4.18) and (4.19). Here the velocity components and pressure are dependent on the scaled normal coordinate Y_1 and the travelling wave coordinate ξ. From substitution of these expansions into the continuity and Navier–Stokes equations (1.1) we find the leading-order nonlinear inviscid balances, cf. Benney & Bergeron (1969):

$$\left.\begin{aligned} \alpha\frac{\partial U_1}{\partial \xi} + \frac{\partial V_1}{\partial Y_1} + \beta\frac{\partial W_1}{\partial \xi} = 0, \quad (\alpha U_1 + \beta W_1)\frac{\partial U_1}{\partial \xi} + V_1\frac{\partial U_1}{\partial Y_1} = -\alpha\frac{\partial Q_1}{\partial \xi}, \\ \frac{\partial Q_1}{\partial Y_1} = 0, \quad (\alpha U_1 + \beta W_1)\frac{\partial W_1}{\partial \xi} + V_1\frac{\partial W_1}{\partial Y_1} = -\beta\frac{\partial Q_1}{\partial \xi}. \end{aligned}\right\} \tag{4.24}$$

Thus from (4.24) the main pressure Q_1 is constant throughout the critical layer. Matching with (4.11d) and using (4.18), its specific form is

$$Q_1 = \tilde{A}_0 p^{(0)} \cos(\xi). \tag{4.25}$$

Comparing the expansions (4.23) within the critical layer to the inviscid regions (4.11) on either side, we obtain the far field matching conditions

$$\left.\begin{aligned} U_1 &\sim (-2y_c + V)Y_1 + u_{1M}(y_c\pm) + \frac{\tilde{A}_0 p^{(0)}\beta^2}{\alpha^2(1-y_c)Y_1}\cos(\xi), \\ V_1 &\sim \frac{3}{2}\left(\frac{\tilde{A}_0 P^{(1)}}{\alpha}\right)\sin(\xi), \\ W_1 &\sim w_{1M}(y_c\pm) - \frac{3}{2}\left\{\frac{\tilde{A}_0 P^{(1)}\beta}{\alpha(\alpha^2+\beta^2)Y_1}\right\}\cos(\xi), \end{aligned}\right\} \quad \text{as} \quad Y_1 \to \pm\infty \qquad (4.26)$$

which follow from the asymptotic behaviour in (4.19). The critical layer problem (4.24–4.26) is fully nonlinear but can be solved analytically which permits the analysis of the higher-order contributions, in (4.23), to be dealt with below. The leading-order solution is readily found to be

$$V_1 = \mu\,\sin(\xi), \quad \overline{u}_1 = \alpha b_1 Y_1 + \alpha\tilde{b}, \quad W_1(Y_1,\xi) = \left(\frac{\alpha\beta}{\alpha^2+\beta^2}\right)(1-y_c)\left(Y_1 + \frac{\tilde{b}}{b_1}\right) + G(\eta),$$
$$U_1 = (\overline{u}_1 - \beta W_1)/\alpha, \quad \text{with} \quad b_1 = V - 2y_c, \quad \mu = \frac{3}{2}\left(\frac{\tilde{A}_0 P^{(1)}}{\alpha}\right). \qquad (4.27)$$

At this point in the analysis $G(\eta)$ is an unknown function of

$$\eta = \mu\,\cos(\xi) + \frac{\alpha b_1}{2}\left(Y_1 + \frac{\tilde{b}}{b_1}\right)^2, \qquad (4.28)$$

and is determined fully at higher order but must be subject to the asymptotic condition

$$G(\eta) \sim \pm\left(\frac{2\alpha\eta}{b_1}\right)^{1/2}\left\{\frac{\beta(y_c-1)}{\alpha^2+\beta^2}\right\} + w_{1M}(y_c\pm) + O(1) \quad \text{as} \quad \eta\to\infty, \qquad (4.29)$$

in order to match to the core asymptotes in (4.26). Here, as in the preceding chapter, the plus and minus signs refer to the upper and lower parts of the critical layer II where

$$Y_1 + \frac{\tilde{b}}{b_1} > \left\{\frac{-2\mu(1+\cos(\xi))}{\alpha b_1}\right\}^{1/2} \quad \text{and} \quad Y_1 + \frac{\tilde{b}}{b_1} < -\left\{\frac{-2\mu(1+\cos(\xi))}{\alpha b_1}\right\}^{1/2},$$

respectively. The quantity $\tilde{b} = u_{1M}(y_c\pm) + (\beta/\alpha)w_{1M}(y_c\pm)$ is a constant and we define the skewed velocity component

$$\overline{u}_m = \alpha U_m + \beta W_m, \quad m = 1, 3/2, 2, \ldots. \qquad (4.30)$$

Having completed the analysis connected with the $m = 1$ stage, we now examine subsequent terms in the critical-layer expansion with the aim of fixing conclusively the phase shift ϕ.

We substitute (4.23) into the continuity and Navier–Stokes equations (1.1) and apply the definition (4.30) to arrive at the equations

$$\frac{\partial \overline{u}_m}{\partial \xi} + \frac{\partial V_m}{\partial Y_1} = 0, \tag{4.31a}$$

$$\overline{u}_1 \frac{\partial U_m}{\partial \xi} + \overline{u}_m \frac{\partial U_1}{\partial \xi} + V_1 \frac{\partial U_m}{\partial Y_1} + V_m \frac{\partial U_1}{\partial Y_1} + \alpha \frac{\partial Q_m}{\partial \xi} = \mathscr{L}_m^{(2)}, \tag{4.31b}$$

$$\frac{\partial Q_m}{\partial Y_1} = \mathscr{L}_m^{(3)}, \tag{4.31c}$$

$$\overline{u}_1 \frac{\partial W_m}{\partial \xi} + \overline{u}_m \frac{\partial W_1}{\partial \xi} + V_1 \frac{\partial W_m}{\partial Y_1} + V_m \frac{\partial W_1}{\partial Y_1} + \beta \frac{\partial Q_m}{\partial \xi} = \mathscr{L}_m^{(4)}, \tag{4.31d}$$

for $m > 1$. The quantities $\mathscr{L}_m^{(n)} (n = 2, 3, 4)$ are referred to as forcing functions generated from (1.1b), (1.1c) and (1.1d), respectively, due to nonlinear interactions between various terms in (4.23) exclusive of the contributions $\partial^2 U_1/\partial Y_1^2$, $\partial^2 W_1/\partial Y_1^2$ in $\mathscr{L}_3^{(2)}$, $\mathscr{L}_3^{(4)}$ and $\partial^2 U_2/\partial Y_1^2$, $\partial^2 W_2/\partial Y_1^2$ in $\mathscr{L}_4^{(2)}$, $\mathscr{L}_4^{(4)}$ which mark the first appearance of viscous effects in the critical layer. It should be noted that the relative simplicity of (1.1a) inhibits the occurrence of forcing terms in (4.31a) and therefore its right-hand-side is identically zero for all values of m. Next, if we differentiate (4.31b) with respect to Y_1 and use the momentum balances (4.31a), (4.31c) followed by substitution of (4.27) we can derive an equation governing the shear $\overline{u}_{mY_1}$. This takes the form

$$\overline{u}_1 \frac{\partial \overline{u}_{mY_1}}{\partial \xi} + V_1 \frac{\partial \overline{u}_{mY_1}}{\partial Y_1} = \frac{\partial}{\partial Y_1}\{\alpha \mathscr{L}_m^{(2)} + \beta \mathscr{L}_m^{(4)}\} - (\alpha^2 + \beta^2) \frac{\partial \mathscr{L}_m^{(3)}}{\partial \xi}. \tag{4.32}$$

The ensuing analysis can be simplified by means of the transformation from (ξ, Y_1) to $(\hat{\xi}, \eta)$ coordinates similar to that used in (3.23), with $\xi = \hat{\xi}$ given by

$$\frac{\partial}{\partial \xi} = \frac{\partial}{\partial \hat{\xi}} - \mu \sin(\xi) \frac{\partial}{\partial \eta}, \quad \frac{\partial}{\partial Y_1} = \overline{u}_1 \frac{\partial}{\partial \eta}. \tag{4.33}$$

In view of (4.27) and (4.33), the terms proportional to $(\partial \overline{u}_{mY_1}/\partial \eta)$ cancel out and as a result the shear equation (4.32) simplifies to

$$\pm(2\alpha b_1(\eta - \mu \cos(\xi)))^{1/2} \frac{\partial \overline{u}_{mY_1}}{\partial \hat{\xi}} = \frac{\partial}{\partial Y_1}\{\alpha \mathscr{L}_m^{(2)} + \beta \mathscr{L}_m^{(4)}\} - (\alpha^2 + \beta^2) \frac{\partial \mathscr{L}_m^{(3)}}{\partial \xi}. \tag{4.34}$$

Following some manipulation of (4.31d) we deduce an equation for W_m which satisfies

$$\overline{u}_1 \frac{\partial W_m}{\partial \hat{\xi}} = \mu \sin(\xi) G'(\eta) \overline{u}_m + V_m \left\{ \left(\frac{\alpha\beta}{\alpha^2 + \beta^2} \right)(y_2 - y_1) - G'(\eta)\overline{u}_1 \right\} + \mathscr{L}_m^{(4)} - \beta \frac{\partial Q_m}{\partial \xi}. \tag{4.35}$$

The aim now is to find the value of m at which a phase shift is first induced across the critical layer. Below the notation 'E' and 'O' is used to represent terms that are even and

odd about $\xi = \pi$. The following analysis is based on the principles put forward in Smith & Bodonyi (1982a). The basic idea is that the determination of the phase shift requires us to identify the first solution $(\overline{u}_m, V_m, W_m, Q_m)$ possessing the following property: $(\overline{u}_m, W_m, Q_m)$ contain an 'O' part with V_m having an 'E' part. As far as the $m = 1$ stage is concerned it is easy to see from (4.25) and (4.27) that $\overline{u}_1$, W_1, Q_1 are 'E', while V_1 is 'O' and so no phase shift occurs at this value of m. This also turns out to be the case at the next level $m = 3/2$: since the solution here plays no further role we omit it for the sake of brevity. The governing equations for the next stage are (4.31) with $m = 2$ and $\mathscr{L}_2^{(2)} = \mathscr{L}_2^{(3)} = \mathscr{L}_2^{(4)} = 0$, coupled with the boundary conditions as $Y_1 \to \pm\infty$:

$$U_2 \sim -Y_1^2 + Y_1 u'_{1M}(y_c\pm) + \frac{\tilde{A}_0}{\alpha^2}\left\{2P^{(2)}\ln|Y_1| - \left(\frac{3p^{(3)}}{y_1 - y_2}\right) + \left(\frac{5\alpha^2 + 2\beta^2}{3(\alpha^2+\beta^2)}\right)P^{(2)}\right\}\cos(\xi) + u_{2M}(y_c\pm), \tag{4.36a}$$

$$V_2 \sim \frac{\tilde{A}_0}{\alpha}\left\{2P^{(2)}\ln|Y_1| - \left(\frac{3p^{(3)}}{y_1 - y_2} + \frac{P^{(2)}}{3}\right)\right\}Y_1\sin(\xi), \tag{4.36b}$$

$$W_2 \sim Y_1 w'_{1M}(y_c\pm) + \frac{\tilde{A}_0}{\alpha}\left\{\left(\frac{\beta}{\alpha^2+\beta^2}\right)P^{(2)}\right\}\cos(\xi) + w_{2M}(y_c\pm), \tag{4.36c}$$

in view of (4.19). Integrating equation (4.34) with respect to $\hat{\xi}$ we obtain

$$\overline{u}_{2Y_1} = K(\eta), \tag{4.37}$$

with $K(\eta)$ being a hitherto unknown shear function, which is determined fully at higher order. From the boundary conditions (4.36a), (4.36c) we find that a requirement of the shear term $\overline{u}_{2Y_1}$ is

$$\overline{u}_{2Y_1} \sim -2\alpha Y_1 + \tilde{\lambda}^{\pm} \quad \text{as} \quad Y_1 \to \pm\infty, \tag{4.38}$$

with the constants $\tilde{\lambda}^{\pm} = \alpha u'_{1M}(y_c\pm) + \beta w'_{1M}(y_c\pm)$ corresponding to the upper and lower regions of the critical layer. The quantity $\tilde{\lambda}^+ - \tilde{\lambda}^-$ is analogous to the vorticity jump $\hat{\lambda}^+ - \hat{\lambda}^-$ across the strongly nonlinear critical layer in section 3.2. From (4.38) and (4.33) we can then deduce the asymptotic behaviour for $K(\eta)$ as

$$K(\eta) \sim \mp\, 2^{3/2}\left(\frac{\alpha\eta}{b_1}\right)^{1/2} + \tilde{\lambda}^{\pm} \quad \text{as} \quad \eta \to \infty. \tag{4.39}$$

It is apparent that $\overline{u}_{2Y_1}$ is 'E' and further integration with respect to Y_1 also gives an arbitrary function of ξ, while application of the matching conditions (4.36a), (4.36c) shows that $\overline{u}_2$ is also 'E'. Consequently, we see that $\partial\overline{u}_2/\partial\xi$ is 'O' and hence V_2, given by the integral of (4.31a) with respect to Y_1, is also 'O' on account of the odd boundary condition (4.36b). If we consider the equation (4.31b) with $m = 2$, we observe that the fourth term $\partial Q_2/\partial\xi$ is 'O' and hence, on integration with respect to ξ we find that Q_2 is 'E'. Inspection of (4.35) shows that $\partial W_2/\partial\hat{\xi}$ is 'O' and, thus integrating with respect to $\hat{\xi}$ and applying the asymptotic

condition (4.36c) point to the fact that the solution for W_2 is 'E'. The implication is that the $m = 2$ solution does not give a phase shift. It is subsequently found that the $m = 5/2$ solution possesses the same symmetry and so we proceed to the next stage, $m = 3$, for which the forcing terms are

$$\mathscr{L}_3^{(2)} = \frac{\partial^2 U_1}{\partial Y_1^2}, \quad \mathscr{L}_3^{(3)} = 0, \quad \mathscr{L}_3^{(4)} = \frac{\partial^2 W_1}{\partial Y_1^2}. \tag{4.40}$$

Examination of (4.40) elucidates that a combination of the velocity perturbations, namely $\alpha\mathscr{L}_3^{(2)} + \beta\mathscr{L}_3^{(4)} = \overline{u}_{1Y_1Y_1}$, is identically zero from (4.27). Substituting (4.40) into (4.34) we find that

$$\overline{u}_{3Y_1} = G_3(\eta), \tag{4.41}$$

with $G_3(\eta)$ an arbitrary function. Hence, on integration of (4.41), $\overline{u}_3$ is 'E' since η is even about $\xi = \pi$. Using the line of reasoning identical to those for the $m = 2$ stage it can be shown from (4.31a), (4.31b) that V_3 is 'O' and P_3 is 'E'. Therefore the [even, odd, even] symmetry of [$\overline{u}_3$, V_3, P_3] about $\xi = \pi$ is retained, however, the equation for W_3 obtained from (4.35) with $m = 3$ then becomes

$$\pm(2\alpha b_1(\eta - \mu\,\cos(\xi)))^{1/2}\left(\frac{\partial W_3}{\partial \hat{\xi}}\right) = \frac{\partial^2 W_1}{\partial Y_1^2} + \text{'O'}. \tag{4.42}$$

From (4.42) and (4.27) we have

$$W_3 = \pm(2\alpha b_1)^{1/2}\frac{\partial}{\partial \eta}\left\{G'(\eta)\int_0^{\hat{\xi}}(\eta - \mu\,\cos(q))^{1/2}\mathrm{d}q\right\} + G_4(\eta) + \text{'E'}, \tag{4.43}$$

since the leading term on the right-hand side is 'O'. The function $G'(\eta)$ readily follows by imposing that W_3 has periodicity of 2π in $\hat{\xi}$ and thus we obtain

$$G'(\eta) = \pm\left(\frac{D_2}{I(\eta)}\right), \quad D_2 = \pi\left(\frac{2\alpha}{b_1}\right)^{1/2}\left\{\frac{\beta(y_c - 1)}{(\alpha^2 + \beta^2)}\right\}, \quad I(\eta) = \int_0^{2\pi}(\eta - \mu\,\cos(q))^{1/2}\,\mathrm{d}q,$$

where the constant D_2 is determined from the matching condition (4.29). We note in passing that although it is clear from (4.43) that W_3 possesses an odd part about $\xi = \pi$, this contribution tends to zero as $Y_1 \to \pm\infty$ taking note of $G'(\eta)$ being proportional to $\eta^{-1/2}$ in this limit. Therefore there is no overall phase shift at level $m = 3$, nor is there at $m = 7/2$. The final crucial stage we consider in the critical layer analysis is $m = 4$ where a non-zero phase shift is encountered. The forcing terms are expressed in the form

$$\begin{aligned}
\mathscr{L}_4^{(2)} &= \frac{\partial^2 U_2}{\partial Y_1^2} - \overline{u}_2\frac{\partial U_3}{\partial \xi} - \overline{u}_3\frac{\partial U_2}{\partial \xi} - V_2\frac{\partial U_3}{\partial Y_1} - V_3\frac{\partial U_2}{\partial Y_1},\\
\mathscr{L}_4^{(3)} &= 0,\\
\mathscr{L}_4^{(4)} &= \frac{\partial^2 W_2}{\partial Y_1^2} - \overline{u}_2\frac{\partial W_3}{\partial \xi} - \overline{u}_3\frac{\partial W_2}{\partial \xi} - V_2\frac{\partial W_3}{\partial Y_1} - V_3\frac{\partial W_2}{\partial Y_1}.
\end{aligned}$$

Leaving aside the contributions $U_{2Y_1Y_1}$ and $W_{2Y_1Y_1}$, it is easy to use the symmetry of the $m = 1, 2, 3$ solutions to show that the rest of $\mathscr{L}_4^{(2)}$ and $\mathscr{L}_4^{(4)}$ are 'O', which implies that the forcing terms at this stage can be written down in the condensed form

$$\mathscr{L}_4^{(2)} = \frac{\partial^2 U_2}{\partial Y_1^2} + \text{'O'}, \quad \mathscr{L}_4^{(3)} = 0, \quad \mathscr{L}_4^{(4)} = \frac{\partial^2 W_2}{\partial Y_1^2} + \text{'O'}. \tag{4.44}$$

Substitution of (4.44) into (4.34), with $m = 4$, followed by use of (4.30) leads to the following equation governing the shear $\overline{u}_{4Y_1}$:

$$\pm(2\alpha b_1(\eta - \mu\cos(\xi)))^{1/2}\left(\frac{\partial \overline{u}_{4Y_1}}{\partial \hat{\xi}}\right) = \overline{u}_{2Y_1Y_1Y_1} + \text{'O'}. \tag{4.45}$$

Applying the chain rule and then integrating both sides with respect to $\hat{\xi}$ we obtain

$$\overline{u}_{4Y_1} = \pm(2\alpha b_1)^{1/2}\frac{\partial}{\partial \eta}\left\{\frac{dK(\eta)}{d\eta}\int_0^{\hat{\xi}}(\eta - \mu\cos(q))^{1/2}\mathrm{d}q\right\} + G_4(\eta) + \text{'E'}, \tag{4.46}$$

with $G_4(\eta)$ an arbitrary function, where we have used equation (4.37) for $\overline{u}_{2Y_1}$. Taking note that the integral in (4.46) is 'O', the leading term on the right-hand side is 'O' and therefore $\overline{u}_4$ is 'E' + 'O', which in turn makes it explicit from (4.31a) that V_4 contains a non-trivial 'E' part and it then follows that Q_4, W_4 both have non-zero 'O' parts, hence confirming that the terms $(\overline{u}_4, V_4, W_4, Q_4)$ indeed undergo a non-zero phase shift. We now continue the analysis with the aim of calculating the shear function $K(\eta)$. This readily follows by imposing that $\overline{u}_{4Y_1}$ has periodicity of 2π in $\hat{\xi}$ and thus we obtain

$$\left(\frac{dK(\eta)}{d\eta}\right)I(\eta) = E_2^{\pm}, \quad \text{with} \quad I(\eta) = \int_0^{2\pi}(\eta - \mu\cos(q))^{1/2}\,\mathrm{d}q. \tag{4.47}$$

By letting $\eta \to \infty$ in (4.47), using $I \sim 2\pi\eta^{1/2}$ as $\eta \to \infty$ and substituting the expression for $K'(\eta)$ obtained from differentiation of the asymptotic condition (4.39) we find that the values of the constants $E_2^{\pm}$ are fixed as $E_2^{\pm} = \mp(8\alpha/b_1)^{1/2}\pi$. Hence our expression for $K(\eta)$ follows from integration of (4.47) and then applying the condition of uniform vorticity $K = K_0$ when $\eta = -\mu$, we have

$$K(\eta) = K_0 \mp 2\pi\left(\frac{2\alpha}{b_1}\right)^{1/2}\int_{-\mu}^{\eta}\frac{\mathrm{d}s}{I(s)}. \tag{4.48}$$

Examining (4.48) in the limit $\eta \to \infty$ provides a second asymptotic formula describing the behavior of $K(\eta)$ at the edges of the critical layer:

$$K(\eta) \sim K_0 \mp 2\pi\left(\frac{2\alpha}{b_1}\right)^{1/2}(\pi^{-1}\eta^{1/2} + J) \quad \text{as} \quad \eta \to \infty, \tag{4.49}$$

where

$$J = -\frac{(-\mu)^{1/2}}{\pi} + \int_{-\mu}^{\infty}\left(\frac{1}{I(\eta)} - \frac{1}{2\pi\eta^{1/2}}\right)d\eta = \frac{(-2\mu)^{1/2}C^{(1)}}{8\pi}, \tag{4.50}$$

and $C^{(1)} \simeq -5.516$, as in subsection 3.1.2. The effective vorticity jump, $\tilde{\lambda}^+ - \tilde{\lambda}^-$, can then be determined by taking the finite part of the jump in $K(\eta)$ across the critical layer as $Y_1 \to \pm\infty$, and hence

$$\tilde{\lambda}^+ - \tilde{\lambda}^- = [[K(\eta)]]_{-\infty}^{\infty} = -4\pi\left(\frac{2\alpha}{b_1}\right)^{1/2} J = -\left(\frac{-\alpha\mu}{b_1}\right)^{1/2} C^{(1)}, \tag{4.51}$$

upon use of (4.39), (4.49) and (4.50). In the remainder of this subsection our objective is to evaluate the phase shift ϕ. We observe that we have an expression for $\overline{u}_4$ in (4.46) from which we can determine its behaviour as $Y_1 \to \pm\infty$. The calculation proceeds in a similar way to that explained in an appendix to Smith & Bodonyi (1982a), so we will present only brief details here. The fundamental idea underlying the calculation concerns representing the finite part of the total velocity jump $\overline{u}_4$ across the nonlinear critical layer as a Fourier series, namely

$$[[\overline{u}_4]]_{-\infty}^{+\infty} = \sum_{m=0}^{\infty}(F_m\,\sin(m\xi) + \tilde{F}_m\,\cos(m\xi)). \tag{4.52}$$

It should be noted that the phase shift integral has to converge, so we need to exclude the singular part in the total velocity jump, and this part matches to the inviscid region. It is clear that the coefficient of relevance to the phase shift is

$$F_1 = \frac{1}{\pi}\int_0^{2\pi}[[\overline{u}_4]]_{-\infty}^{+\infty}\,\sin(\xi)\,\mathrm{d}\xi = \frac{1}{\pi}\int_{-\infty}^{+\infty}\left(\int_0^{2\pi}\overline{u}_{4Y_1}\,\sin(\xi)\,\mathrm{d}\xi\right)\mathrm{d}Y_1. \tag{4.53}$$

Switching to characteristic coordinates, integrating by parts and using (4.45) we find that

$$-\pi\mu F_1 = \int_{\hat{\xi}=0}^{2\pi}\left\{\left[\left[\left[\left(Y_1 + \frac{\tilde{b}}{b_1}\right)\overline{u}_{2Y_1Y_1}\right]\right]\right]_{-\infty}^{\infty} - [[\overline{u}_{2Y_1}]]_{-\infty}^{\infty}\right\}\mathrm{d}\hat{\xi}, \tag{4.54}$$

since the integrated contributions from the 'O' terms in (4.45) are identically zero. Keeping in mind the asymptotic condition (4.38), we deduce that the first term on the right-hand side of (4.54) is identically zero and $[[\overline{u}_{2Y_1}]]_{-\infty}^{\infty} = \tilde{\lambda}^+ - \tilde{\lambda}^-$. Substituting for the vorticity jump (4.51) relates F_1 to the disturbance amplitude $\tilde{A}_0$ via

$$F_1 = \left(\frac{2\alpha C^{(1)}}{\tilde{A}_0^{1/2}(\alpha^2+\beta^2)^{1/2}(-p^{(0)})^{1/2}}\right), \tag{4.55}$$

where we have made use of (4.27) and substituted for $P^{(1)}$ from (4.20) to simplify this expression. The formula for the scaled phase shift Φ can be established by comparing the

Fourier coefficient F_1 in (4.53) with the logarithmic asymptote for $\overline{u}_2$ deduced from the asymptotic forms for U_2, W_2 in (4.36a), (4.36c) and definition (4.30). In a surprisingly simple way the comparison yields the required relation between F_1 and Φ:

$$F_1 = \frac{2\tilde{A}_0}{\alpha}\left\{\frac{(\alpha^2+\beta^2)p^{(0)}}{(y_c-1)^2}\right\}\Phi. \tag{4.56}$$

We then find, upon equating the two values of F_1 in (4.55) and (4.56), that the scaled phase shift Φ is related to the amplitude $\tilde{A}_0$ by

$$\Phi = -\left\{\frac{\alpha^2 C^{(1)}(y_c-1)^2}{\tilde{A}_0^{3/2}(\alpha^2+\beta^2)^{3/2}(-p^{(0)})^{3/2}}\right\}. \tag{4.57}$$

The amplitude dependence of the neutral modes follows from balancing the phase shift just determined with that induced across the wall layers. With this in mind, we move on to discuss the dynamics of the near-wall regions.

(c) The viscous wall layer III

This layer is located in the proximity of the lower wall at $y = -1$ and we assume that it has the thickness m which is to be determined in terms of the Reynolds number. In this connection we introduce the $O(1)$ normal coordinate $Z_1 = (y+1)/m$. The physical balance within the wall layer is between the viscous operator $R^{-1}\partial^2/\partial y^2$ and the inertia term $\alpha(U_0 - c)$ which implies $R^{-1}m^{-2} \sim O(1)$, and determines the normal scaling of region III as $y = -1 + R^{-1/2}Z_1$ as in a classical boundary layer. The corresponding expansions for the velocities, pressure and wavespeed, to leading order, are

$$[u, v, w, p, c] = [-V + \epsilon^2\hat{U}(\xi, Z_1),\ \epsilon^2 R^{-1/2}\hat{V}(\xi, Z_1),\ \epsilon^2\hat{W}(\xi, Z_1),\ \epsilon^2\hat{P}(\xi, Z_1),\ c_0], \tag{4.58}$$

where $c_0 = V$. Substitution of these expansions into the continuity and Navier–Stokes equations (1.1) yields the following unsteady-viscous-pressure force balances

$$\alpha\frac{\partial\hat{U}}{\partial\xi} + \frac{\partial\hat{V}}{\partial Z_1} + \beta\frac{\partial\hat{W}}{\partial\xi} = 0, \tag{4.59a}$$

$$-2\alpha V\frac{\partial\hat{U}}{\partial\xi} = -\alpha\frac{\partial\hat{P}}{\partial\xi} + \frac{\partial^2\hat{U}}{\partial Z_1^2}, \tag{4.59b}$$

$$\frac{\partial\hat{P}}{\partial Z_1} = 0, \tag{4.59c}$$

$$-2\alpha V\frac{\partial\hat{W}}{\partial\xi} = -\beta\frac{\partial\hat{P}}{\partial\xi} + \frac{\partial^2\hat{W}}{\partial Z_1^2}, \tag{4.59d}$$

with these equations subject to the no-slip conditions

$$\hat{U} = \hat{V} = \hat{W} = 0 \quad \text{at} \quad Z_1 = 0. \tag{4.60}$$

Matching the pressure within the viscous wall layer (4.58) as $Z_1 \to \infty$ with the pressure in the inviscid region (4.11d) as $y \to -1$, we obtain $\hat{P} = \tilde{A}_0 P_2(-1)\cos(\xi)$. Inserting the expression for $\hat{P}$ into (4.59b), (4.59d), solving for $(\hat{U}, \hat{V}, \hat{W})$ with the boundary condition (4.60) and no exponential growth as $Z_1 \to \infty$, we find

$$\left.\begin{aligned} \hat{U} = \sigma_1 \tilde{A}_0 \ \mathrm{Re}[(1-\exp(-m_1 Z_1))\ \exp(\mathrm{i}\xi)], \quad \hat{W} = (\beta/\alpha)\hat{U}, \\ \hat{V} = -\sigma_1 \alpha^{-1}(\alpha^2+\beta^2)\tilde{A}_0\ \mathrm{Re}[\ \mathrm{i}(Z_1 + m_1^{-1}\exp(-m_1 Z_1) - m_1^{-1})(\exp(\mathrm{i}\xi))], \end{aligned}\right\} \tag{4.61}$$

where $\sigma_1 = P_2(-1)/(2V)$, $m_1 = (2\alpha V)^{1/2}\exp(-\mathrm{i}\pi/4)$ and Re denotes the real part. The solutions are very similar to those in the linear regime considered in subsection 2.3.5, but the phasespeed and sliding velocities are now $O(1)$ quantities. Taking the limit of the form for $\hat{V}$ in (4.61) as $Z_1 \to \infty$ provides the asymptotic behaviour

$$v \sim \varepsilon^2 R^{-1/2}\sigma_1\alpha^{-1}(\alpha^2+\beta^2)\tilde{A}_0 Z_1\ \sin(\xi) - \varepsilon^2 R^{-1/2}\left(\frac{2^{-1/2}\alpha^{-3/2}(\alpha^2+\beta^2)\sigma_1\tilde{A}_0}{(2V)^{1/2}}\right)(\sin(\xi)+\cos(\xi)), \tag{4.62}$$

in view of (4.58). As $y \to -1$ the expansion for the normal velocity (4.11b) in the inviscid region may be represented as

$$v \sim \varepsilon^2 R^{-1/2}\tilde{A}_0 Z_1 G_2'(-1)\ \sin(\xi) + \cdots + \varepsilon^2 R^{-1/3} v_4 + \cdots, \tag{4.63}$$

since $G_2(-1) = 0$ for zero normal flow at the wall. The first term in (4.62) matches with the behaviour of G_2 in the inviscid region (4.63), but the second term in (4.62) is asymptotically smaller than the term involving v_4 in (4.63). We therefore conclude that

$$G_2'(-1) = \sigma_1\alpha^{-1}(\alpha^2+\beta^2), \quad v_4 \to 0 \quad \text{as} \quad y \to -1, \tag{4.64}$$

affirming that the normal velocity disturbance v in (4.11b) suffers zero phase shift due to the viscous wall layer adjacent to the lower wall in contrast to previous studies of this type. We now turn our attention to the behaviour in the vicinity of the upper wall.

(d) The viscous shear layer IV

It is worth emphasizing that the dynamics here are quite different to those in previous works on equilibrium critical layers where the wall layers are typically of the Stokes form considered in the previous subsection. If we suppose that the thickness of this layer is k_1, then we can introduce the $O(1)$ normal variable $Z_2 = (1-y)/k_1$. The balance within the shear layer is between the viscous operator $R^{-1}\partial^2/\partial y^2$ and the inertia term $\alpha(U_0 - c)$ as in region III. However, the crucial difference here is that the inertia term is now vanishingly small in the vicinity of the upper wall in view of the fact that $c = V$ to leading order. Therefore, it proves necessary to include the higher-order term in the expansion for the wavespeed by writing $c = V + k_2 c_1$ with c_1 being the wavespeed correction and $k_2 = R^{-1/3}$ from (4.13). Considering the near-wall behaviour of the inertia term it is found that $\alpha(U_0 - c) \sim -\alpha(k_1 U_0'(1) Z_2 + k_2 c_1)$

and for the two terms to be in balance we therefore require $k_1 \sim k_2$. Thus an inertial-viscous balance is achieved provided $R^{-1}k_1^{-2} \sim k_1$, resulting in the shear layer thickness $k_1 \sim R^{-1/3}$. In terms of ϵ and R, the appropriate expansions here are

$$u = V - U_0'(1)R^{-1/3}Z_2 + \epsilon^2\overline{U}(\xi, Z_2) + \cdots, \; v = -\epsilon^2 R^{-1/3}\overline{V}(\xi, Z_2) + \cdots, \; w = \epsilon^2\overline{W}(\xi, Z_2) + \cdots,$$
$$p = \epsilon^2\overline{P}_1(\xi, Z_2) + \epsilon^2 R^{-1/3}\overline{P}_2(\xi, Z_2) + \cdots, \; c = V + R^{-1/3}c_1 + \cdots, \tag{4.65}$$

with $y = 1 - R^{-1/3}Z_2$. If we substitute (4.65) into (1.1) and examine the $O(\epsilon^2)$ contribution from the streamwise momentum equation (1.1b), we find $\overline{P}_1 \equiv \overline{P}_1(Z_2)$. Applying the boundary condition of matching with the pressure expansion (4.11d) in the inviscid region leads to the expression

$$\overline{P}_1 = \tilde{A}_0 P_2(1)\cos(\xi). \tag{4.66}$$

Since $\overline{P}_1$ is independent of the variable ξ, the validity of (4.66) can be ensured if and only if $P_2(1) = 0$. Thus $\overline{P}_1 = 0$ and the other leading-order wave balances arising from the substitution of (4.65) into (1.1) are succinctly expressed as

$$\left.\begin{aligned} \alpha\frac{\partial\overline{U}}{\partial\xi} + \frac{\partial\overline{V}}{\partial Z_2} + \beta\frac{\partial\overline{W}}{\partial\xi} = 0, \quad -\alpha(U_0'(1)Z_2 + c_1)\frac{\partial\overline{U}}{\partial\xi} - U_0'(1)\overline{V} = -\alpha\frac{\partial\overline{P}_2}{\partial\xi} + \frac{\partial^2\overline{U}}{\partial Z_2^2}, \\ \frac{\partial\overline{P}_2}{\partial Z_2} = 0, \quad -\alpha(U_0'(1)Z_2 + c_1)\frac{\partial\overline{W}}{\partial\xi} = -\beta\frac{\partial\overline{P}_2}{\partial\xi} + \frac{\partial^2\overline{W}}{\partial Z_2^2}, \end{aligned}\right\} \tag{4.67}$$

with the boundary conditions of no slip at the wall and matching with (4.11a), so that

$$\overline{U} = \overline{V} = \overline{W} = 0 \quad \text{at} \quad Z_2 = 0, \quad \overline{U} \to \tilde{A}_0 F_2(1)\cos(\xi), \quad \overline{W} \to 0 \quad \text{as} \quad Z_2 \to \infty. \tag{4.68}$$

We can express $F_2(1)$ in terms of the pressure by differentiating (4.15c) twice with respect to y, using (4.15a,b) to eliminate $G_2'(y)$ and $G_2(y)$, and then letting $y \to 1^-$ in the resulting equation and taking note of $H_2(1) = 0$, eventually obtaining $F_2(1) = -P_2'''(1)/(2\alpha^2 U_0'(1))$. It is worth noting that, as far as the mean-flow distortion is concerned, $u_{2M}(1) = w_{2M}(y) = 0$ from the no-slip condition on the wall and as a consequence this term does not arise in the matching condition (4.68). The coefficients in equations (4.67) do not depend on ξ which suggests that solutions can be sought in the normal form representation

$$(\overline{U}, \overline{V}, \overline{W}, \overline{P}_2) = \mathrm{Re}((\tilde{U}(Z_2), \tilde{V}(Z_2), \tilde{W}(Z_2), \tilde{P}_2(Z_2))\exp(\mathrm{i}\xi)).$$

Thus the problem (4.67), (4.68) reduces to

$$\left.\begin{aligned} \mathrm{i}\alpha\tilde{U} + \tilde{V}' + \mathrm{i}\beta\tilde{W} = 0, \quad -\mathrm{i}\alpha(U_0'(1)Z_2 + c_1)\tilde{U} - U_0'(1)\tilde{V} = -\mathrm{i}\alpha\tilde{P}_2 + \tilde{U}'', \\ \tilde{P}_2' = 0, \quad -\mathrm{i}\alpha(U_0'(1)Z_2 + c_1)\tilde{W} = -\mathrm{i}\beta\tilde{P}_2 + \tilde{W}'', \end{aligned}\right\} \tag{4.69}$$

subject to

$$\tilde{U} = \tilde{V} = \tilde{W} = 0 \quad \text{at} \quad Z_2 = 0, \quad \tilde{U} \to \tilde{A}_0 F_2(1), \quad \tilde{W} \to 0 \quad \text{as} \quad Z_2 \to \infty. \tag{4.70}$$

The system (4.69), (4.70) constitutes a standard 'lower-deck' problem whose analytical solution can be easily found with some adjustments to the original analysis performed in Smith (1979). The explicit expression for $\tilde{P}_2$ is found to be

$$(\alpha^2+\beta^2)\tilde{P}_2 = (-\mathrm{i}\alpha U_0'(1))^{5/3}\left(\frac{\mathrm{Ai}'(\Theta)}{\kappa(\Theta)}\right)\left(\frac{\tilde{A}_0F_2(1)}{U_0'(1)}\right), \tag{4.71}$$

where Ai is the Airy function, $\kappa(\Theta)=\int_\Theta^\infty \mathrm{Ai}(\xi)\mathrm{d}\xi$ and Θ is given in terms of the streamwise wavenumber, wavespeed correction and basic flow as

$$\Theta = -\mathrm{i}^{1/3}s, \quad \text{with } s=\frac{\alpha c_1}{(-\alpha U_0'(1))^{2/3}}. \tag{4.72}$$

It remains to substitute (4.71) into the normal-mode form for the higher-order pressure term $\overline{P}_2$, to establish that

$$\overline{P}_2 = \left(\frac{(-\alpha U_0'(1))^{5/3}}{\alpha^2+\beta^2}\right)\left(\frac{\tilde{A}_0F_2(1)}{U_0'(1)}\right)\{\mathrm{Re}(g(s))\,\cos(\xi)-\mathrm{Im}(g(s))\,\sin(\xi)\}, \tag{4.73}$$

where $g(s)=\mathrm{i}^{5/3}\mathrm{Ai}'(\Theta)/\kappa(\Theta)$. The requirement that the pressure within the viscous shear layer (4.65) as $Z_2\to\infty$ should match with the expansion for the pressure in the inviscid core (4.11d) as $y\to 1$ then leads to the boundary condition

$$p_4 \to \left(\frac{(-\alpha U_0'(1))^{5/3}}{\alpha^2+\beta^2}\right)\left(\frac{\tilde{A}_0F_2(1)}{U_0'(1)}\right)\{\mathrm{Re}(g(s))\,\cos(\xi)-\mathrm{Im}(g(s))\,\sin(\xi)\} \quad \text{as } y\to 1. \tag{4.74}$$

Thus we see that the term proportional to $\sin(\xi)$ in (4.74) represents the phase shift in the pressure disturbance p (see expansion (4.11d)) induced by the viscous shear layer astride the upper wall. This needs to be in tune with the phase shift, specifically $R^{-1/3}\Phi$, induced in the $O(\epsilon^2R^{-1/3})$ contribution p_4 of (4.11d) across the critical layer. It therefore turns out that the amplitude equation for the nonlinear modes arises as the outcome of the interplay between these two phase shifts and this will form the focus of the next subsection.

(e) Derivation of the amplitude equation for the nonlinear modes

The critical layer analysis has demonstrated that the $O(\epsilon^{9/2})$ contribution Q_4 in (4.23d) contains a non-zero 'O' part, which indicates that the small phase shift induced at the stage $m=4$ induces a $\sin(\xi)$ component in the Fourier series for p_4 in the pressure expansion (4.11d). This means that only the $\sin(\xi)$ Fourier coefficient, denoted by $P_4(y)$, of this series plays a part in fixing the amplitude-dependence of the nonlinear hybrid modes. Hence the key definition is

$$P_4(y)=\frac{1}{\pi}\int_0^{2\pi} p_4(x,y,z,t)\,\sin(\xi)\,d\xi = \frac{1}{\pi}\int_0^{2\pi} p_4(\xi,y)\,\sin(\xi)\,d\xi. \tag{4.75}$$

Here the Fourier component $P_4(y)$ governs the same Rayleigh equation as the amplitude function $P_2(y)$ in subsection 4.1.2(a), namely

$$(U_0 - V)(P_4'' - (\alpha^2 + \beta^2)P_4) = 2U_0'P_4'. \tag{4.76}$$

The determination of the boundary conditions to be imposed on $P_4(y)$ requires inspection of (4.75) along with the asymptotic behaviours (4.64), (4.74) derived earlier. Substitution of the expansions (4.11) into the Navier–Stokes equations (1.1) we obtain at $O(\epsilon^2 R^{-1/3})$:

$$\alpha(U_0 - V)\frac{\partial v_4}{\partial \xi} = -\frac{\partial p_4}{\partial y}. \tag{4.77}$$

Differentiating (4.75) with respect to y, using (4.77), integrating by parts, taking the limit as $y \to -1$ and using the asymptotic constraint (4.64) we conclude that $P_4' \to 0$ as we approach the lower wall. Next, if we let $y \to 1$ in (4.75) and employ (4.74), we find

$$P_4(1) = -\left(\frac{(-\alpha U_0'(1))^{5/3}}{\alpha^2 + \beta^2}\right)\left(\frac{\tilde{A}_0 F_2(1)}{U_0'(1)}\right) \mathrm{Im}(g(s)). \tag{4.78}$$

We now wish to examine what happens to the quantity $P_4(y)$ as we cross the critical layer from $y = y_c^+$ to $y = y_c^-$. To achieve this we consider the finite part of the jump in (4.75) which yields

$$[[P_4]]_-^+ = \lim_{y \to y_c^+} P_4 - \lim_{y \to y_c^-} P_4 = \frac{1}{\pi}\int_0^{2\pi} [[p_4]]_-^+ \sin(\xi)\, d\xi = -\tilde{A}_0 P^{(1)}(y - y_c)^3\, \Phi, \tag{4.79}$$

from the series solution for P_2 in (4.18), the nonlinear jump condition (4.21) and (4.12). We now have sufficient information to derive the amplitude equation and this is achieved through the following steps. Multiplying equation (4.76) by $P_2(y)/(U_0 - V)$, while making use of the Rayleigh equation for $P_2(y)$ in (4.16), leads us to an equation for the Wronskian of $(P_2,\, P_4)$ which may be written as

$$\hat{K}' - \left(\frac{2U_0'}{U_0 - V}\right)\hat{K} = 0, \tag{4.80}$$

where $\hat{K}(y) = P_2P_4' - P_4P_2'$. If we multiply both sides of (4.80) by $1/(U_0 - V)^2$, then straightforward integration leads to

$$\hat{K}(y) = \gamma^{\pm}(U_0 - V)^2, \tag{4.81}$$

where $\gamma^{\pm}$ are constants in the upper and lower regions of the critical layer II. Applying the wall conditions $P_2'(-1) = P_4'(-1) = 0$ we find that $\gamma^- = 0$. We already know that the second critical layer embedded within the viscous shear layer IV lies in the proximity of the upper wall which provides a rationale for evaluating the value of γ^+ from (4.81) as

$$\gamma^+ = \lim_{y \to 1^-} \frac{\hat{K}(y)}{(U_0 - V)^2}. \tag{4.82}$$

A series solution of P_2 about $y = 1$, (given in (4.86) below), confirms that P_2, P_2' and P_2'' all vanish at the upper wall, resulting in $\hat{K}(1) = \hat{K}'(1) = 0$. The limit in (4.82) may be easily evaluated using L'Hospital's Rule, resulting in $\gamma^+ = \hat{K}''(1)/[2(U_0'(1))^2]$. This therefore shows that the function $\hat{K}(y)/(U_0 - V)^2$ defined over $-1 < y < 1$ takes the form

$$\frac{\hat{K}(y)}{(U_0 - V)^2} = \begin{cases} -\{P_2'''(1)P_4(1)\}/\{2(U_0'(1))^2\}, & y > y_c \\ 0, & y < y_c. \end{cases}$$

The constant γ^+ may also be calculated directly by analysing the jump in the relation (4.81) across the critical layer as follows:

$$\gamma^+ = \left[\left[\frac{\hat{K}(y)}{(U_0 - V)^2}\right]\right]_-^+ = \left\{\frac{1}{(y_c - 1)^2}\right\}\left[\left[\frac{\hat{K}(y)}{(y - y_c)^2}\right]\right]_-^+ = -\left(\frac{3p^{(0)}\tilde{A}_0 P^{(1)}}{(y_c - 1)^2}\right)\Phi, \tag{4.83}$$

with the last step following from the asymptotic expansion in (4.18) for P_2 and differentiation of the jump condition (4.79) on P_4 with respect to y. Equating the two values of γ^+ enables us to derive an explicit expression for the scaled phase shift Φ as

$$\Phi = -\frac{1}{\tilde{A}_0}\left\{\frac{(y_c - 1)^3}{(\alpha^2 + \beta^2)(p^{(0)})^2}\right\}\left(\frac{P_2'''(1)P_4(1)}{4(U_0'(1))^2}\right), \tag{4.84}$$

in view of the form for $P^{(1)}$ in (4.20). Equating the two values of Φ in (4.57) and (4.84), and after some manipulation, we deduce the amplitude equation for the nonlinear neutral modes:

$$\tilde{A}_0 = \left(\frac{4(-p^{(0)})^{1/3}(-C^{(1)})^{2/3}\alpha^{14/9}(2 - V)^{8/9}(\alpha^2 + \beta^2)^{1/3}}{(P_2'''(1))^{4/3}(\mathrm{Im}(g(s)))^{2/3}}\right), \tag{4.85}$$

where use has been made of (4.78) to substitute for $P_4(1)$. The value of $P_2'''(1)$ in (4.85) can be normalized to unity and for given sliding velocity V and spanwise wavenumber β, the values of α and $p^{(0)}$ are first computed from a numerical solution of the Rayleigh-like problem set out in (4.16), (4.17). The numerical algorithm employed and the results obtained will be discussed in the next section. Once these quantities are determined, the wavespeed correction c_1 in (4.85) can be determined for a given value of the pressure amplitude $\tilde{A}_0$.

4.1.3 Results for the strongly nonlinear regime

(a) Numerical Method

First we describe the numerical method devised to solve the Rayleigh pressure equation (4.16) for the pressure eigenfunctions P_2 with the boundary conditions (4.17) and the scaled phase shift $\Phi = 0$ in the jump condition (4.21). With the wall sliding speed and spanwise wavenumber prescribed, we guess a value of the streamwise wavenumber α. We then express P_2 in a series expansion about $y = 1$ of the form

$$P_2(y) = \sum_{n=3}^{\infty} \overline{p}^{(n)}(y - 1)^n, \tag{4.86}$$

and impose the phase normalization condition $P_2'''(1) = 1$, which gives $\overline{p}^{(3)} = 1/6$ in (4.86) and fully determines all coefficients in this expansion, enabling us to compute P_2 and its derivative at $y = 1 - \delta$ where δ is taken small, typically 0.001. These values are then used to initiate a Runge-Kutta (RK) solution of (4.16) in the region from $y = 1 - \delta$ to $y = y_c + \delta$. Next we write down the first few terms of the power series (4.18) and its derivative in terms of the unknown constants $p^{(0)}$ and $p^{(3)}$. In order to ensure the continuity of P_2 at the junction $y = y_c + \delta$, the values of P_2 and P_2' calculated from the series solution (4.18) and the RK method are equated which fixes $p^{(0)}$ and $p^{(3)}$. Once this is achieved we can use these values to evaluate the quantities $P_2(y_c - \delta)$ and $P_2'(y_c - \delta)$ using the first few terms of the series solution (4.22). Finally, we apply the RK method to solve (4.16) in the domain from $y = y_c - \delta$ to $y = -1$ and calculate a value for $P_2'(-1)$. The technique of Newton iteration on α is applied until this quantity is zero to some suitable tolerance. We repeat the procedure for a range of values of V and β.

(b) Numerical results

The neutral stability results for $\beta = 0$ giving α as a function of V are shown in figure 4.2(a), which indicates that the streamwise wavenumber increases monotonically as the sliding speed increases. Figure 4.2(b) presents the location of the critical layer y_c versus α from which it can be seen that as V increases, the critical layer is moving away from the lower wall and eventually heading towards the upper wall. Therefore as V increases, the neutral disturbance is characterized by an ever decreasing wavelength, with most of the disturbance activity concentrated near the upper wall. In figure 4.2(c) we show the results for the pressure distribution $P_2(y)$ across the channel at representative values of α. Inspection of these plots suggests that as the sliding speed approaches a value of 2, pressure variations are confined to a thin region near the upper wall. This phenomenon is investigated further by performing an asymptotic analysis in the limit $V \to 2$ in the next subsection. The dependence of the wavespeed correction c_1 on the amplitude $\tilde{A}_0$ for various values of V is given in figure 4.3. We observe that for a given V and for $\tilde{A}_0$ above a threshold amplitude ($\tilde{A}_c$, say), there are firstly two solutions. With further increase in $\tilde{A}_0$, two more solutions exist over a small range of $\tilde{A}_0$, but only two solutions (those labelled 'upper branch' and 'lower branch') persist as $\tilde{A}_0 \to \infty$. For values of V in the range $0.1 \leq V \leq 1.5$, an increase in the threshold amplitude is accompanied by a corresponding increase in the sliding speed of the walls. For the same range of V, for a given $\tilde{A}_0$ the wavespeed correction c_1 along the upper and lower branch decreases monotonically as can be seen in figure 4.3. It is already evident that the behaviour of the nonlinear modes and their dependence upon the values of V and $\tilde{A}_0$ is a complicated issue. The main drawback of the numerical method described in subsection 4.1.3(a) is that it is ill-suited for the purpose of obtaining the neutral values of α once V is in excess of 1.7, as the proximity of the critical layer to the upper wall renders the matching between the RK and series solutions problematical. In order to achieve accurate solutions at larger values of α we turn to an asymptotic approach to the Rayleigh problem in the next subsection.

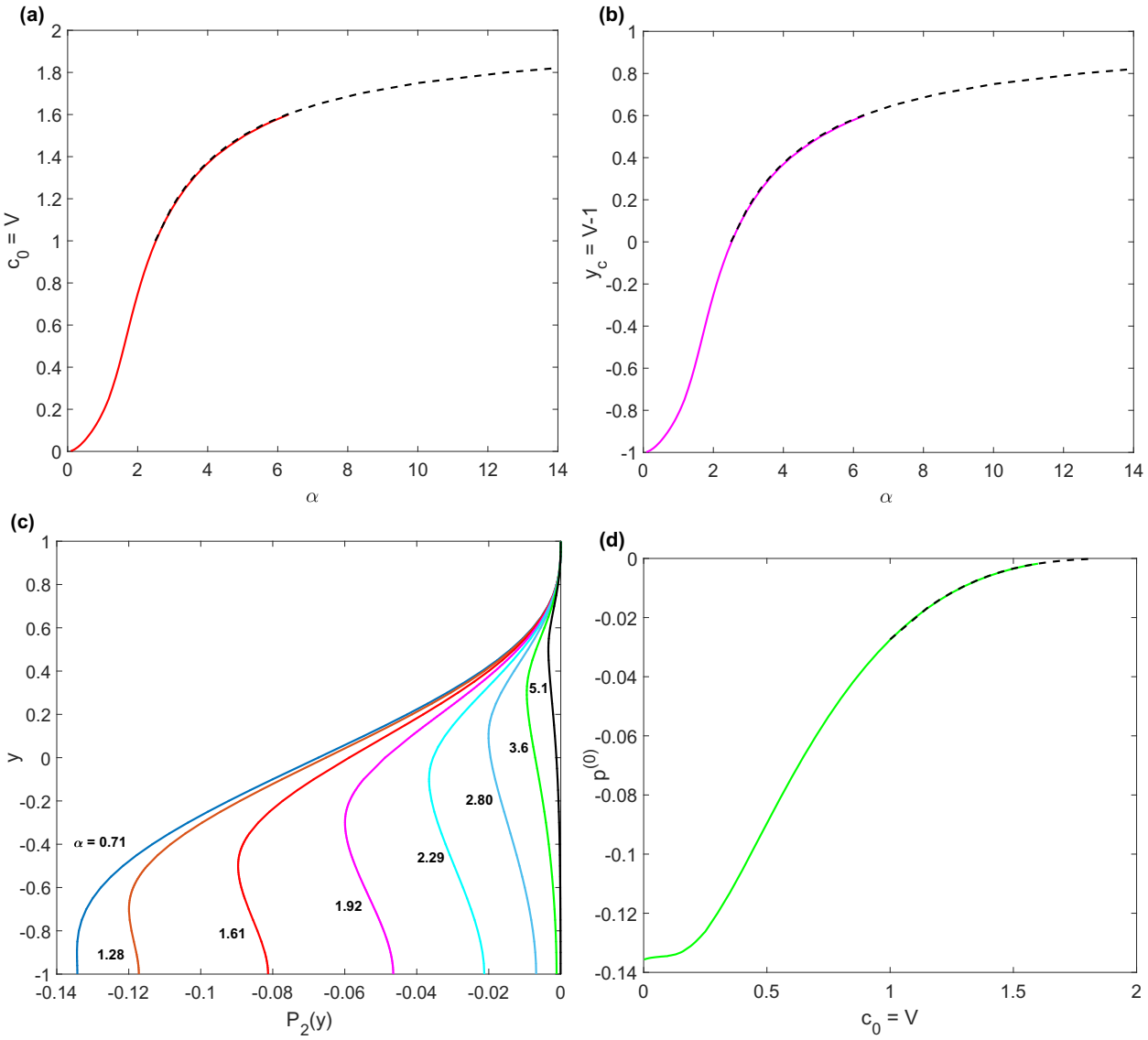

Figure 4.2: Numerical results for the strongly nonlinear regime for the case of zero spanwise wavenumber. (a) streamwise wavenumber α versus sliding speed V; (b) critical layer location y_c versus α; (c) pressure distribution $P_2(y)$ for various V; (d) pressure coefficient $p^{(0)}$ versus V. On figures (a), (b) and (d), the dashed curves are the asymptotic solution as $V \to 2$, from the analysis of subsection 4.1.3(c).

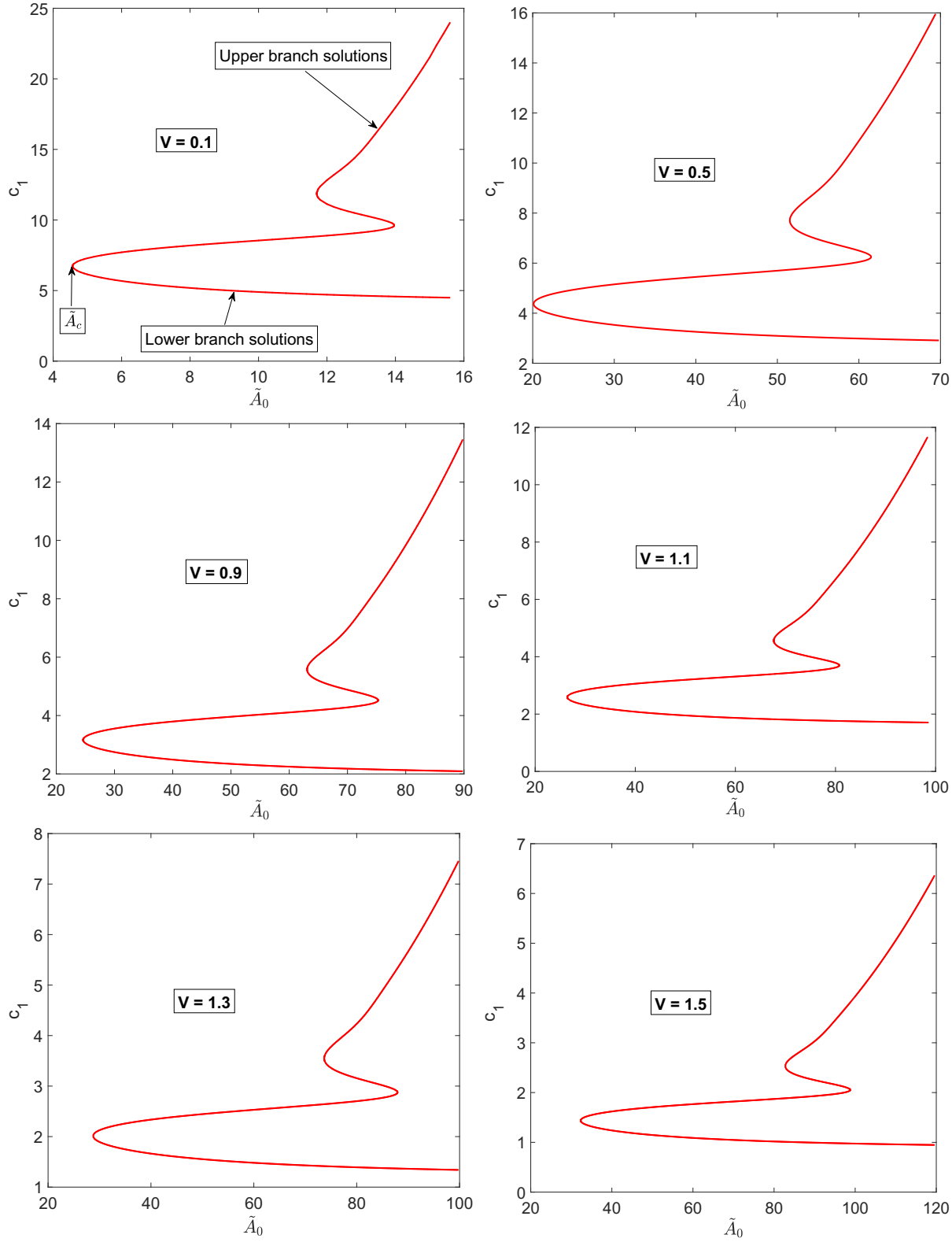

Figure 4.3: Solution of the nonlinear amplitude equation (4.85) for $\beta = 0$, giving the wavespeed correction c_1 as a function of $\tilde{A}_0$ for various values of sliding velocity.

(c) Analysis of the nonlinear neutral modes in the limit $V \to 2$

The results just presented suggest that this limit, in which the maximum of the basic flow is attained on the upper wall, is worthy of further analysis. Examination of figure 4.2 suggests that in this limit we have $\alpha \to \infty$, $y_c \to 1^-$ and $p^{(0)} \to 0^-$. For $|2-V| \ll 1$ we seek solutions of (4.16), (4.17) with the aforementioned properties allowing for the fact that s in (4.72) remains $O(1)$ in this limit as can be verified from our numerical calculations. Then the main variation of P_2 takes place when $(y-1)$ is small, $y = 1-(2-V)\hat{y}$ with $0 \le \hat{y} < \infty$, and hence the dominant scalings are

$$\alpha = (2-V)^{-1}\hat{\alpha}, \quad P_2 = -(2-V)^3\hat{P}_2(\hat{y}), \quad c_1 = (2-V)\hat{c}_1, \quad p^{(0)} = -(2-V)^{\zeta}\hat{p}^{(0)}, \quad (4.87)$$

where the $O(1)$ constants $\hat{\alpha}$, ζ and $\hat{p}^{(0)}$ are to be determined. Under the scaling (4.87), the Rayleigh equation (4.16) becomes to leading order:

$$\frac{d^2\hat{P}_2}{d\hat{y}^2} - \hat{\alpha}^2\hat{P}_2 = \left\{\frac{2(1-2\hat{y})}{(-\hat{y}^2+\hat{y})}\right\}\frac{d\hat{P}_2}{d\hat{y}}, \quad (4.88)$$

while the appropriate boundary conditions (4.17), (4.21) respectively become

$$\hat{P}_2'(\infty) = 0, \quad \hat{P}_2(0) = 0, \quad \text{zero velocity jump at } \hat{y} = 1. \quad (4.89)$$

It is straightforward to deduce series solutions of (4.88) about the points $\hat{y} = 0, 1$ and they can be used as part of a numerical method very similar to that outlined in subsection 4.1.3(a). The numerical solution yields the neutral values $\hat{\alpha} \approx 2.5037$, $\zeta = 3$, $\hat{p}^{(0)} \approx 0.0273$. Careful numerical checks show that taking a boundary at $\hat{y} = 10^6$ as a computational cut-off proves sufficiently large enough to satisfy the condition at infinity. With (4.87) holding, the amplitude equation (4.85) is modified to

$$\tilde{A}_0 = \left(\frac{4(\hat{p}^{(0)})^{1/3}(-C^{(1)})^{2/3}\hat{\alpha}^{20/9}(2-V)^{-1/3}}{(\hat{P}_2'''(0))^{4/3}(\mathrm{Im}(g(s)))^{2/3}}\right), \quad \text{with} \quad s = \hat{\alpha}^{1/3}\hat{c}_1, \quad (4.90)$$

which establishes that $\tilde{A}_0 \propto (2-V)^{-1/3}$ as $V \to 2$. The threshold amplitude is increasing according to $\tilde{A}_c \approx (25.0485)(2-V)^{-1/3}$ and we draw the conclusion that $\tilde{A}_c \to \infty$ as $V \to 2$. In this limit, with $\tilde{A}_0$ finite, we observe that there are two finite values of $\hat{c}_1$ corresponding to the upper and lower branch solutions respectively. The scaled wavespeed correction $\hat{c}_1$ approaches infinity along the upper branch solutions but takes a finite value along the lower branch solutions as $\tilde{A}_0 \to \infty$.

The overall conclusion is that the asymptotic structure associated with the nonlinear hybrid modes breaks down in the limit $V \to 2$ as the critical layer II moves into the viscous shear layer IV. In this limit, as the sliding speed is increased, the critical layer, situated at $y = V-1$, moves ever closer to the $O(R^{-1/3})$ shear layer adjacent to the upper wall. A new distinguished scaling therefore emerges when $V - 1 \sim 1 + O(R^{-1/3})$, i.e. when $V - 2 \sim O(R^{-1/3})$. Simultaneously the streamwise wavenumber is increasing proportional

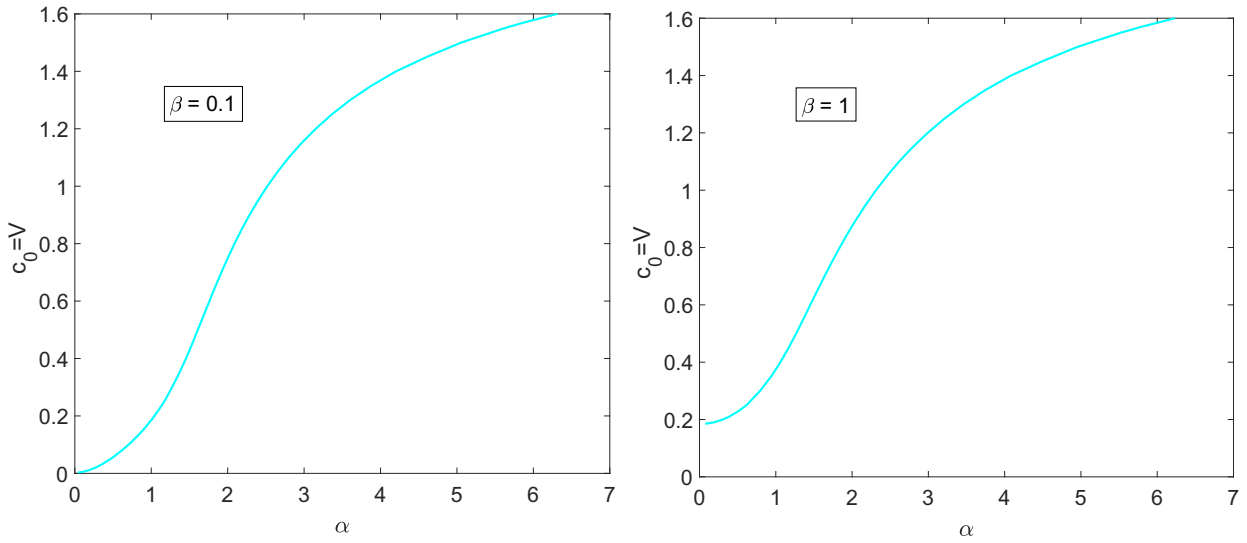

Figure 4.4: Sliding speed V versus α for non-zero values of the spanwise wavenumber β.

to $(2-V)^{-1}$ from (4.87) and therefore rises to $O(R^{1/3})$, so that this new short-scale structure possesses comparable-sized derivatives in the streamwise and wall-normal directions. In addition, the amplitude of the travelling waves can be shown to rise to $O(R^{-1/3})$ while the phasespeed remains $O(1)$. The governing balances in this new nonlinear near-wall region are the full 2D Navier–Stokes equations but with unit Reynolds number and are subject to matching conditions to the $O(1)$ Rayleigh region and a link to the Stokes region (now of thickness $O(R^{-2/3})$) near the lower wall. Even in the case of 3D disturbances, the leading-order equations apparently remain 2D due to the fact that the streamwise and wall-normal scales are shorter than that imposed in the spanwise direction. These equations are reminiscent of those governing the 'production layer' in Deguchi & Hall (2014). This structure will be considered further in future work.

The heart of the matter is that the numerical solutions to the three-dimensional Rayleigh equation exist for a range of the spanwise wavenumbers, for example, $\beta = 0.1, 1$ as illustrated by figure 4.4. It is interesting to observe that for $\beta = 1$ no nonlinear neutral solutions are found until a lower cut-off value $V \approx 0.2$, while for $\beta = 0.1$ these solutions appear to exist in the range $0 \leq V < 2$. For values of $\beta > 1$, it emerges that an increase in lower cut-off value is accompanied by a corresponding increase in the spanwise wavenumber. The main point is that strong three-dimensionality with spanwise wavenumbers comparable with the channel width can be incorporated into our nonlinear neutral mode structure in a rational way.

4.1.4 Conclusions

Figure 4.5 summarizes the different types of stability theories corresponding to the size of disturbance Δ superimposed on the basic state (2.2) of PPCF that have been considered in this paper. Our main conclusions are as follows.

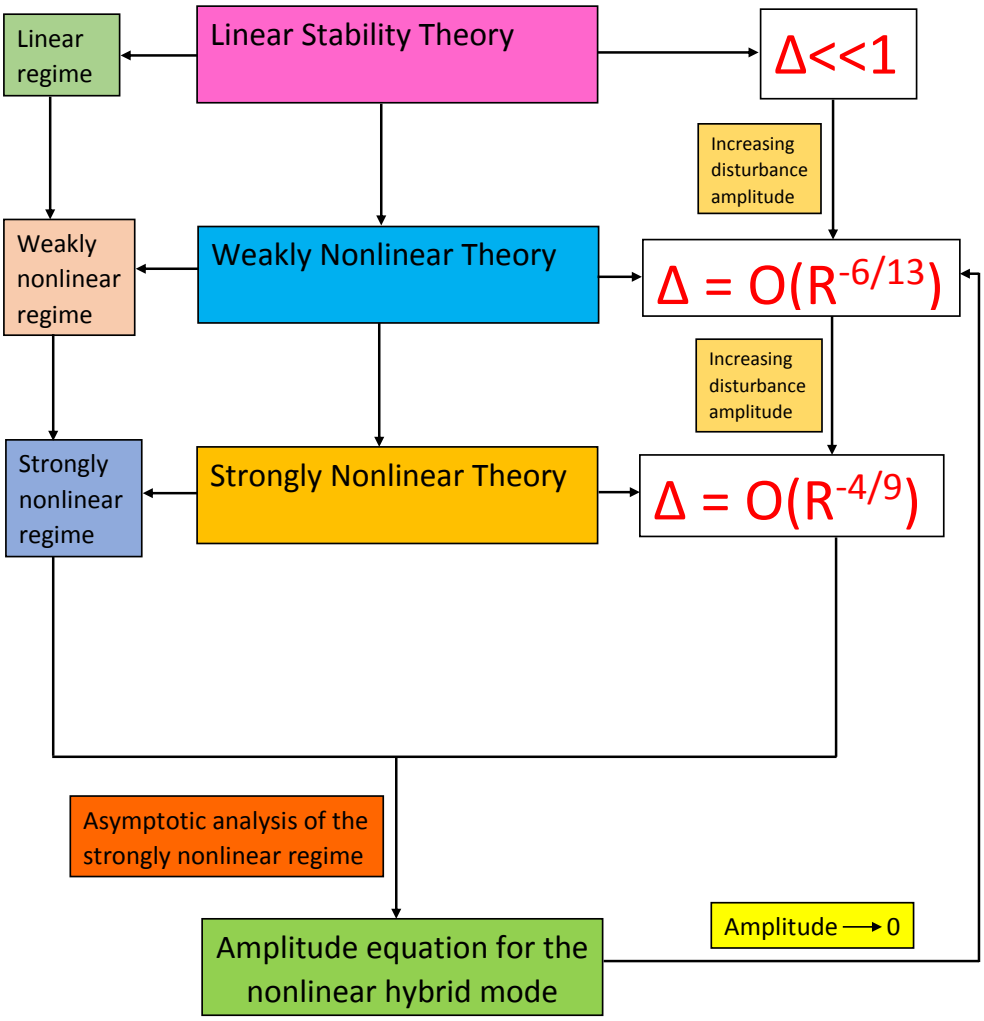

Figure 4.5: Sketch illustrating a relation among the fundamental stability theories as a function of the disturbance amplitude Δ.

(i) For $\Delta \ll 1$, the existence of multiple neutral curves for small sliding speed V below the linear cut-off value of approximately 0.34, is confirmed by the numerical results presented in figure 2.3. Investigation of the dynamics of the linear viscous critical layer in section 3.2 reveals that the linear asymptotic structure of the new upper neutral curve, which is a mixture of a traditional upper branch and lower branch mode, illustrated in figure 2.14, continues to hold until Δ increases to $O(R^{-6/13})$.

(ii) At the stage $\Delta = O(R^{-6/13})$ the main variations are found to take place only within the balances controlling the properties of the viscous critical layer due to the development of weakly nonlinear effects. We find that no significant changes occur in the inviscid shear layer II– and the viscous wall layer III– astride the lower wall. It can therefore be inferred

that in the weakly nonlinear regime the flow stability properties outside the critical layer remain substantially unaltered. In section 3.2 the strongly nonlinear critical-layer problem is posed, and its behaviour at larger amplitude gives the result (3.39), demonstrating that the phase shift decreases as nonlinearity begins to take effect.

(iii) As the disturbance size is increased further from $O(R^{-6/13})$ to $O(R^{-4/9})$, a connection between weakly nonlinear theory and strongly nonlinear theory is established, thus leading to the scalings and recognition of the asymptotic structure for the strongly nonlinear regime as discussed in subsections 4.1.1 and 4.1.2. It emerges that at this stage a dominant flow feature resembling a Kelvin cat's eye containing uniform vorticity develops within the critical layer. Such cat's eye structures have recently been observed in full Navier–Stokes simulations of related flows (see Deguchi & Walton (2013)). Although this asymptotic structure, possessing a strongly nonlinear critical layer in the central region of the channel, bears some similarities to the structures considered by Smith & Bodonyi (1982b), Smith & Bodonyi (1982a), Walton (2002), Walton (2003) among others, there are some novel features here including a viscous shear layer near the upper wall which affects the matching condition on the core region.

(iv) The numerical results for the strongly nonlinear regime presented in subsection 4.1.3 show that nonlinear neutral solutions exist over a wide range of $O(1)$ spanwise and streamwise wavenumbers and for sliding velocities in the range $0 \leq V < 2$. In particular solutions exist above the linear threshold of $V \simeq 0.34$ discussed in section 2.2. For fixed V, threshold amplitudes are determined at which neutral solutions first emerge. As $V \to 2$ the maximum of the basic flow moves ever closer to the upper wall and in this limit the disturbances become more localized in the streamwise direction and it becomes harder to obtain converged solutions using our numerical method. Numerical computation in subsection 4.1.3 demonstrates that the inclusion of three-dimensionality restricts nonlinear neutral solutions to the range $V_b < V < 2$, where V_b is a lower cut-off value and is a function of the spanwise wavenumber.

(v) Further examination of the strongly nonlinear structure in the limit $V \to 2$ is carried out and shows that as the sliding speed is increased, the critical layer, situated at $y = V - 1$, moves ever closer to the $O(R^{-1/3})$ shear layer adjacent to the upper wall. A new distinguished scaling therefore emerges when $V - 1 \sim 1 + O(R^{-1/3})$, i.e. when $V - 2 \sim O(R^{-1/3})$. Simultaneously the streamwise wavenumber is increasing proportional to $(2 - V)^{-1}$ from (4.87) and therefore rises to $O(R^{1/3})$, so that this new short-scale structure possesses comparable-sized derivatives in the streamwise and wall-normal directions. In addition the amplitude of the travelling waves can be shown to rise to $O(R^{-1/3})$ while the phasespeed remains $O(1)$. The governing balances in this new nonlinear near-wall region are the full 2D Navier–Stokes equations but with unit Reynolds number and are subject to matching conditions to the $O(1)$ Rayleigh region and a link to the Stokes region (now of thickness $O(R^{-2/3})$) near the lower wall. Even in the case of 3D disturbances, the leading-order equations apparently remain 2D due to the fact that the streamwise and wall-normal scales are shorter than that imposed in

the spanwise direction. These equations are reminiscent of those governing the 'production layer' in Deguchi & Hall (2014).

(vi) As remarked in **(iv)**, nonlinear neutral modes exist in PPCF for disturbances of $O(R^{-4/9})$ when $R \gg 1$. The next most important step is to solve the fully nonlinear unsteady two-dimensional Navier–Stokes equations in order to confirm that such neutral surfaces exist at finite Reynolds number. Given that the flow is linearly stable for $V > 0.34$, above this critical sliding speed these surfaces must become disconnected from the zero amplitude plane.

Next, we consider the second scenario where both the wall sliding speed V and the disturbance phasespeed c are $O(1)$ quantities, but are sufficiently distinct from one another that there exist two critical layers that reside an $O(1)$ distance from both walls, with viscous Stokes layers adjoining the boundaries. The aim here is to set out the structure of the nonlinear upper branch modes and determine its disturbance amplitude analytically in terms of the streamwise and spanwise wavenumbers and the properties of the basic flow.

4.2 Analysis of the nonlinear upper branch modes

In this section, the nonlinear stability of PPCF subjected to three-dimensional disturbances is studied asymptotically at large Reynolds number R. By analysing the nature of the instability for increasing disturbance size Δ, the scaling $\Delta = O(R^{-1/3})$ is identified at which a strongly nonlinear neutral wave structure emerges, involving the interaction of two inviscid critical layers. The striking feature of this structure is that the travelling wave disturbances have streamwise and spanwise wavelengths both comparable to the channel width, with an associated phase speed of O(1). A novel method of the classical balancing of phase shifts enables the amplitude-dependence of the neutral modes to be determined in terms of the wavenumbers and the properties of the basic flow. Numerical computation of the Rayleigh equation which governs the flow outside of the critical layers shows that neutral solutions exist for non-dimensional wall sliding speeds in the range $0 \leq V < 2$. It transpires that the critical layers merge and the asymptotic structure referred to above breaks down both in the large-amplitude limit and the limit $V \to 2$ when the maximum of the basic flow becomes located at the upper wall.

As far as the nonlinear stability properties of this flow are concerned, Balakumar (1997) has demonstrated numerically that two-dimensional nonlinear equilibrium surfaces exist in the parameter space formed by Reynolds number, wavenumber and amplitude, with these surfaces forming due to the bifurcation of the solution from the linear state as the disturbance amplitude is increased. Our aim in this paper is to find an asymptotic description for such nonlinear solutions which describes how the modes self-sustain due to critical layer/wall layer interactions. Our formulation also allows us to include three-dimensional effects over a lengthscale comparable with the channel width. Our starting point is the classical linear asymptotic structure on the upper branch of the main neutral curve of figure 2.3(c). This

structure was first set out in Cowley & Smith (1985) and is sketched in figure 2.10. As mentioned in subsection 2.3.4, in this scenario the disturbance survives due to an interaction between the linear critical layers (positioned where the basic velocity coincides with the phase speed of the disturbance) and the viscous Stokes layers adjacent to each wall. We study how this interactive structure alters as the disturbance size Δ increases. In particular we will show that when $\Delta = O(R^{-1/3})$ nonlinear modes are supported over an $O(1)$ range of wall sliding speeds and possess streamwise, spanwise wavenumbers and a phase speed all comparable in magnitude with the channel width. A novel feature of this structure is the presence of two strongly three-dimensional nonlinear critical layers in which the dominant physical balances are very similar to those proposed in the pioneering work of Benney & Bergeron (1969). It is discovered that the amplitude of the waves can be determined analytically by balancing the total phase shift across the two critical layers with that induced across the near-wall Stokes layers.

Subsection 4.2.1 concerns briefly the details of the strongly nonlinear critical layers, providing motivation for the scalings and asymptotic structure of the strongly nonlinear upper branch modes which follow in 4.2.2, where we present a method for determining the amplitude-dependence of the neutral modes. In subsection 4.2.3, we present a numerical technique for calculating the phase speed and wavenumber of the disturbance as functions of amplitude, with the method taking into account the asymmetric nature of the basic flow. In addition, we provide a comprehensive description of the numerical results for a range of values of disturbance amplitudes, spanwise wavenumbers and sliding velocities. The rest of this subsection is devoted to a discussion of the new structures encountered in the limit of large disturbance amplitude (where the two critical layers merge) and the limit in which the maximum of the basic flow becomes located at the upper wall. In addition, we draw the main inferences and suggest avenues for further study.

4.2.1 Scalings in the strongly nonlinear regime

In an Appendix to Cowley & Smith (1985), the eigenrelations on the upper-branch of the linear neutral curve for PPCF are formulated. Extended to three dimensions and in terms of our notation (see (2.115), (2.117)) they take the form

$$c_0 = (4/15)(\alpha_0^2 + \beta_0^2), \quad (c_0 + V_0)^{-1/2} + (c_0 - V_0)^{-1/2} = (\phi^{\pm}/\sqrt{2})\alpha_0^{1/2}(c_0^2 + V_0^2). \qquad (4.91)$$

Here $(\alpha_0, \beta_0) = R^{1/11}(\alpha, \beta)$ are the $O(1)$ scaled streamwise and spanwise wavenumbers of the linear disturbance with $c_0 = R^{2/11}c$ the corresponding $O(1)$ scaled phase speed. This long-wave structure holds for a range of small sliding speeds $V = R^{-2/11}V_0$ with V_0 of $O(1)$. The quantities $\phi^{\pm}$ represent the phase shifts induced across the upper and lower critical layers and are both equal to π in the linear setting considered in Cowley & Smith (1985) but can take on smaller values once the effects of nonlinearity are incorporated as first shown by Haberman (1972). A schematic of the full nine-zone asymptotic structure, which includes two critical layers (of thickness $O(R^{-10/33})$) and two wall layers of Stokes form is given in

figure 2.10.

The effect of weak nonlinearity on this upper branch structure was analyzed in section 3.1. It transpires that once the disturbance size is increased to $O(R^{-14/33})$, nonlinearity affects the properties of the critical layers significantly, while leaving the dynamics of the other asymptotic regions essentially unchanged. Specifically, it is shown (see equations (3.31) and (3.32)) that the phase shifts $\phi^{\pm}$ induced across the critical layers decrease with increasing disturbance amplitude such that

$$\phi^{+} \sim O(\alpha_0^{-1}(c_0 - V_0)^{-3/2}\overline{\Delta}^{-3/2}) \text{ and } \phi^{-} \sim O(\alpha_0^{-1}(c_0 + V_0)^{-3/2}\overline{\Delta}^{-3/2}) \text{ as } \overline{\Delta} \to \infty, \quad (4.92)$$

for disturbances of amplitude $\Delta = R^{-14/33}\overline{\Delta}$.

If we now wish to investigate stability at $O(1)$ sliding speeds we require V_0 to increase to $O(R^{2/11})$. From balancing terms in the eigenrelations (4.91) it follows that

$$c_0 \sim O(R^{2/11}),\ \alpha_0 \sim O(R^{1/11}),\ \beta_0 \sim O(R^{1/11}),\ \phi^{\pm} \sim O(R^{-1/2}).$$

Then, from the limiting behaviours (4.92), the scaled disturbance size $\overline{\Delta}$ rises to $O(R^{1/11})$ which implies that the new structure holds for an enhanced disturbance amplitude

$$\Delta = R^{-14/33}\overline{\Delta} = O(R^{-1/3}). \quad (4.93)$$

We are now in a position to set out formally the asymptotic structure of the strongly nonlinear upper-branch modes. In view of the enhanced sliding speed, the inviscid shear layers II−, II+ depicted in figure 2.10 thicken and merge with the inviscid core region to form a Rayleigh inviscid zone of $O(1)$ which is subject to the full velocity profile (2.2). In addition, the viscous wall layers (III−, III+) decrease to an $O(R^{-1/2})$ thickness comparable with the phase shift. It can also be shown using an identical approach to that described in 4.1.1 that the critical layers approach the midst of the Rayleigh region with their thicknesses increasing to $O(R^{-1/6})$, i.e., $\Delta^{1/2}$. The scaling arguments presented above indicate that in this strongly nonlinear regime we should seek solutions with α, β, V and c of $O(1)$ and an $O(R^{-1/3})$ wave amplitude, leading to an induced $O(R^{-1/2})$ phase shift across the critical layers. This provides the motivation for the study of the nonlinear neutral modes whose asymptotic structure, illustrated in figure 4.6(a), consists of five main regions: the strongly nonlinear critical layers (II+, II−) in the midst of the Rayleigh inviscid region I surrounded above and below by the viscous wall layers (III+, III−). We begin by considering the region I where the dynamics are predominantly inviscid before embarking upon the more complicated analysis of the critical layers.

4.2.2 The nonlinear instability structure

(a) The Rayleigh inviscid region I

The analysis for smaller disturbances presented in the preceding subsection has identified a critical wave amplitude of $O(R^{-1/3})$ at which strongly nonlinear effects are activated. In the

bulk of the flow we therefore seek a structure in terms of the small parameter

$$\epsilon = R^{-1/6},$$

in which the appropriate velocity and pressure expansions are

$$u = U_0(y) + \epsilon u_{1M}(y) + \epsilon^2 u_2(\xi, y) + \epsilon^2 u_{2M}(y) + \cdots + \epsilon^2 R^{-1/2} u_5(\xi, y) + \cdots , \tag{4.94a}$$

$$v = \epsilon^2 v_2(\xi, y) + \cdots + \epsilon^2 R^{-1/2} v_5(\xi, y) + \cdots , \tag{4.94b}$$

$$w = \epsilon w_{1M}(y) + \epsilon^2 w_2(\xi, y) + \epsilon^2 w_{2M}(y) + \cdots + \epsilon^2 R^{-1/2} w_5(\xi, y) + \cdots , \tag{4.94c}$$

$$p = \epsilon^2 p_2(\xi, y) + \cdots + \epsilon^2 R^{-1/2} p_5(\xi, y) + \cdots . \tag{4.94d}$$

The fundamental disturbances (u_2, v_2, w_2, p_2) take the form of travelling waves

$$A_0[F_2(y)\cos(\xi), G_2(y)\sin(\xi), H_2(y)\cos(\xi), P_2(y)\cos(\xi)], \quad \xi = \alpha(x - ct) + \beta z. \tag{4.95}$$

Here F_2, G_2, H_2, P_2 are the unknown amplitude functions and u_{1M}, w_{1M}, u_{2M}, w_{2M} are the mean-flow distortions, while the terms with subscript 5 anticipate the occurrence of induced $O(R^{-1/2})$ phase shifts across the nonlinear critical layers, as alluded to in subsection 4.2.1. It is worth remarking that the fundamental disturbance in the core is still of size $O(\epsilon^2)$ as in (4.11), but now the Reynolds number dependence has changed so that $\epsilon = R^{-1/6}$ in this new regime. A feature of this structure is that the induced streamwise and spanwise mean-flow distortions are larger than the fundamental disturbance: this follows from a rigorous examination of the dynamics of each linear viscous critical layer subjected to weakly nonlinear effects in the large amplitude limit referred to in subsection 4.2.1. For prescribed spanwise wavenumber β and sliding velocity V, the real $O(1)$ constant A_0 needs to be determined in terms of the streamwise wavenumber α and phase speed c, with $c = c_0$ to leading order. The scalings (4.94) are identical to those found in asymptotic studies of fully-developed and developing pipe flow Smith & Bodonyi (1982a), Walton (2002). Substitution of (4.94) into the governing equations (1.1) yields the following inviscid balances:

$$\alpha F_2 - G_2' + \beta H_2 = 0, \tag{4.96a}$$

$$\alpha(U_0 - c_0)F_2 - U_0' G_2 = -\alpha P_2, \tag{4.96b}$$

$$\alpha(U_0 - c_0)G_2 = -P_2', \tag{4.96c}$$

$$\alpha(U_0 - c_0)H_2 = -\beta P_2, \tag{4.96d}$$

with a prime denoting the appropriate ordinary derivative. Elimination of F_2, H_2, P_2 in (4.96) leaves the normal velocity perturbations G_2 governed by Rayleigh's equations:

$$(U_0 - c_0)(G_2'' - (\alpha^2 + \beta^2)G_2) = U_0'' G_2, \tag{4.97}$$

subject to the inviscid condition of tangential flow at the walls

$$G_2(-1) = 0, \quad G_2(1) = 0. \tag{4.98}$$

It is evident from (4.96) that the velocity components are singular at $y = y_1, y_2$ where

$$y_1 = \frac{V + \sqrt{V^2 + 4(1 - c_0)}}{2}, \quad y_2 = \frac{V - \sqrt{V^2 + 4(1 - c_0)}}{2}, \tag{4.99}$$

at which points $U_0 = c_0$: critical layers are required to regularize the singularities at these locations. It is worth remarking that as before the bulk of the flow is governed by a Rayleigh equation (for the normal velocity in this case instead of pressure), but now that we have $c_0 \neq V$ to leading order, thus replacing (4.16). We note that the maximum allowable value of c_0 is $1 + V^2/4$ which ensures that the argument of the square root in (4.99) is non-negative. We observe from the plot of the basic velocity profile in figure 4.5(b) that the existence of the two critical layers is possible if and only if $c_0 > V$: this inequality certainly holds on the upper branch in the linear regime (as is clear from (4.91)) and we would expect it to continue to hold as the disturbance amplitude is gradually increased.

In order to match with the critical layer it is necessary to calculate the asymptotic behaviour of the disturbance velocity components and pressure about $y = y_i$, where $i \in \{1, 2\}$, by applying the Frobenius method. The series solution for the normal velocity takes the form

$$G_2(y) = \sum_{n=0}^{\infty} g_i^{(n)} (\tilde{\varepsilon}_i)^n + \ln(\tilde{\varepsilon}_i) \sum_{n=1}^{\infty} \mathscr{G}_i^{(n)} (\tilde{\varepsilon}_i)^n \quad \text{with } \tilde{\varepsilon}_i = y - y_i > 0. \tag{4.100}$$

Here, for given i, the coefficients of the series can be expressed in terms of two unknowns, $g_i^{(0)}$ and $g_i^{(1)}$, with these coefficients determined numerically by solving (4.97) with (4.98) using the numerical method outlined in subsection 4.2.3(a). Alternatively, the coefficients may be expressed analytically in recurrence relation form, and these formulae are given for completeness in Appendix B. For future purposes the coefficients $\mathscr{G}_i^{(1)}$, $\mathscr{G}_i^{(2)}$ may be calculated explicitly to be

$$\mathscr{G}_i^{(1)} = (-1)^{i+1} \left(\frac{2 g_i^{(0)}}{y_1 - y_2} \right), \quad \mathscr{G}_i^{(2)} = \frac{2 g_i^{(0)}}{(y_1 - y_2)^2}. \tag{4.101}$$

Turning now to the other velocity components and pressure, it is straightforward to show from (4.96), (4.100) that as $y \to y_i^+$:

$$F_2(y) \sim \frac{1}{\tilde{\varepsilon}_i} \left(\frac{\beta^2 g_i^{(0)}}{\alpha(\alpha^2 + \beta^2)} \right) + \left(\frac{\mathscr{G}_i^{(1)}}{\alpha} \right) \ln(\tilde{\varepsilon}_i) + \left(\frac{2\alpha^2 + \beta^2}{2\alpha(\alpha^2 + \beta^2)} \right) \mathscr{G}_i^{(1)} + \frac{g_i^{(1)}}{\alpha} + O(\tilde{\varepsilon}_i \ln(\tilde{\varepsilon}_i)), \tag{4.102a}$$

$$H_2(y) \sim -\frac{1}{\tilde{\varepsilon}_i} \left(\frac{\beta g_i^{(0)}}{\alpha^2 + \beta^2} \right) + \left(\frac{\beta}{2(\alpha^2 + \beta^2)} \right) \mathscr{G}_i^{(1)} + O(\tilde{\varepsilon}_i), \tag{4.102b}$$

$$P_2(y) \sim (-1)^i \left\{ \left(\frac{\alpha}{\alpha^2 + \beta^2} \right) (y_1 - y_2) g_i^{(0)} + O(\tilde{\varepsilon}_i^2) \right\}. \tag{4.102c}$$

The continuation of (4.100), (4.102) on the other side $y = y_i^-$ of the critical layers occurs in such a way as to smooth out the irregular behaviour of the logarithmic terms in these series solutions. The principal feature of the nonlinear critical layers is that the velocity and pressure jump induced across them are asymptotically small (as first proposed by Benney & Bergeron (1969)) and the implication of this is that as $y \to y_i^-$, (4.100) and (4.102) are reproduced with

$$\ln(\tilde{\varepsilon}_i) \quad \text{replaced by} \quad \ln(-\tilde{\varepsilon}_i). \tag{4.103}$$

The Rayleigh equation (4.97) for $G_2(y)$ subject to the boundary conditions (4.98) and the jump condition (4.103) constitutes an eigenvalue problem for $\alpha = \alpha(c_0, V, \beta)$ which is treated in 4.2.3. The amplitude-dependence of these modes is not determined explicitly in the core but rather via an interaction with the critical layers and wall layers. The study of the critical layers will be the focus of the next subsection.

(b) The nonlinear critical layers

The critical layers located at $y = y_i$ for $i \in \{1, 2\}$ have thickness $O(\epsilon)$ and so for each critical layer we introduce the $O(1)$ normal wall variable $Y_i = (y - y_i)/\epsilon$. The relevant expansions are

$$u = c_0 + \epsilon U_1^{(i)} + \cdots + \epsilon^2 U_2^{(i)} + \cdots + \epsilon^3 U_3^{(i)} + \cdots + \epsilon^4 U_4^{(i)} + \cdots + \epsilon^5 U_5^{(i)} + \cdots, \tag{4.104a}$$

$$v = \epsilon^2 V_1^{(i)} + \cdots + \epsilon^3 V_2^{(i)} + \cdots + \epsilon^4 V_3^{(i)} + \cdots + \epsilon^5 V_4^{(i)} + \cdots + \epsilon^6 V_5^{(i)} + \cdots, \tag{4.104b}$$

$$w = \epsilon W_1^{(i)} + \cdots + \epsilon^2 W_2^{(i)} + \cdots + \epsilon^3 W_3^{(i)} + \cdots + \epsilon^4 W_4^{(i)} + \cdots + \epsilon^5 W_5^{(i)} + \cdots, \tag{4.104c}$$

$$p = \epsilon^2 P_1^{(i)} + \cdots + \epsilon^3 P_2^{(i)} + \cdots + \epsilon^4 P_3^{(i)} + \cdots + \epsilon^5 P_4^{(i)} + \cdots + \epsilon^6 P_5^{(i)} + \cdots, \tag{4.104d}$$

as implied mainly by (4.94), (4.100) and (4.102). Here the velocity components and pressure depend on Y_i and ξ. The intermediate $\cdots$ in each expansion denotes the occurrence of logarithmic terms which play no role in the determination of the vorticity jump which is our main concern here. Substitution of these expansions into (1.1) results in the following leading-order nonlinear inviscid balances, cf. Benney & Bergeron (1969):

$$\alpha U_{1\xi}^{(i)} + V_{1Y_i}^{(i)} + \beta W_{1\xi}^{(i)} = 0, \tag{4.105a}$$

$$(\alpha U_1^{(i)} + \beta W_1^{(i)}) U_{1\xi}^{(i)} + V_1^{(i)} U_{1Y_i}^{(i)} = -\alpha P_{1\xi}^{(i)}, \tag{4.105b}$$

$$P_{1Y_i}^{(i)} = 0, \tag{4.105c}$$

$$(\alpha U_1^{(i)} + \beta W_1^{(i)}) W_{1\xi}^{(i)} + V_1^{(i)} W_{1Y_i}^{(i)} = -\beta P_{1\xi}^{(i)}, \tag{4.105d}$$

from which we infer that the main pressure disturbance $P_1^{(i)}$ is constant throughout the critical layers and its specific form is

$$P_1^{(i)} = (-1)^i A_0 \left(\frac{\alpha}{\alpha^2 + \beta^2} \right) (y_1 - y_2) g_i^{(0)} \cos(\xi), \tag{4.106}$$

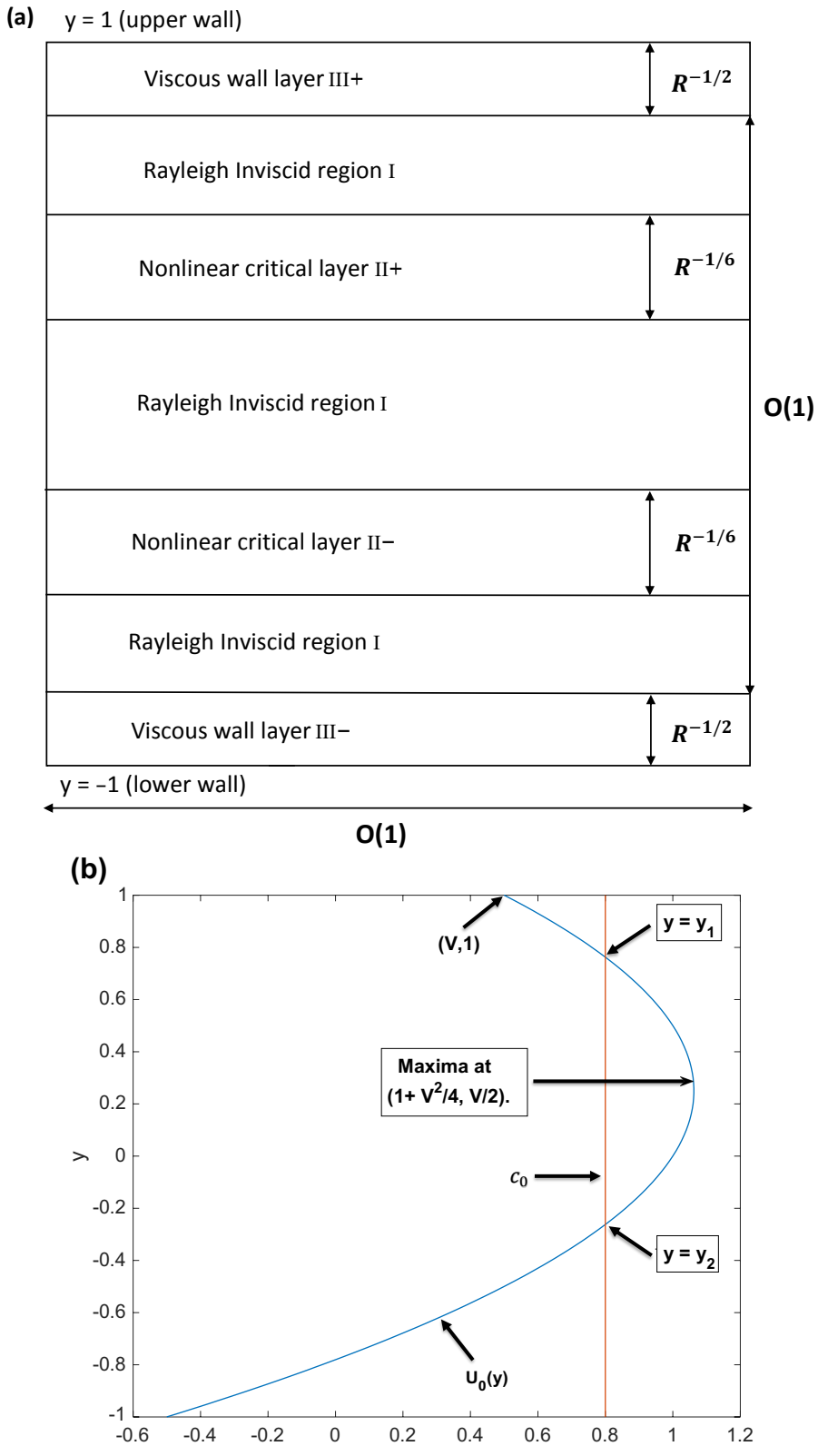

Figure 4.6: (a) The strongly nonlinear neutral mode structure. (b) Plot of the basic velocity profile illustrating that the two critical layers exist only when $V < c_0 < 1 + \frac{V^2}{4}$.

from (4.95), (4.102c). The far field conditions on the velocity components $(U_1^{(i)}, V_1^{(i)}, W_1^{(i)})$ are obtained from matching of (4.104) with the inviscid region expansions (4.94a)–(4.94c) on either side of the critical layers. These are given by

$$\left.\begin{aligned} U_1^{(i)} &\sim (-2y_i + V)Y_i + u_{1M}(y_i\pm) + \frac{A_0 g_i^{(0)}\beta^2}{\alpha(\alpha^2+\beta^2)Y_i}\cos(\xi), \\ V_1^{(i)} &\sim A_0 g_i^{(0)}\sin(\xi), \quad W_1^{(i)} \sim w_{1M}(y_i\pm) - \frac{A_0 g_i^{(0)}\beta}{(\alpha^2+\beta^2)Y_i}\cos(\xi), \end{aligned}\right\} \quad \text{as} \quad Y_i \to \pm\infty \tag{4.107}$$

in view of (4.100), (4.102a) and (4.102b). Equations (4.105)–(4.107) constitute the leading-order fully nonlinear problem whose solution can be shown to be

$$U_1^{(i)} = \left(\frac{\alpha^2 b_i}{\alpha^2+\beta^2}\right)\left(Y_i + \frac{\tilde{b}_i}{b_i}\right) - \left(\frac{\beta}{\alpha}\right)M_i(\eta_i),\ \overline{u}_1^{(i)} = \alpha b_i\left(Y_i + \frac{\tilde{b}_i}{b_i}\right),\ W_1^{(i)} = \frac{1}{\beta}\left(\overline{u}_1^{(i)} - \alpha U_1^{(i)}\right),$$
$$V_1^{(i)} = \lambda_i \sin(\xi), \quad \text{with} \quad \lambda_i = A_0 g_i^{(0)}, \quad b_i = (-1)^i(y_1 - y_2). \tag{4.108}$$

The solution depends on the variable η_i, a function of Y_i and ξ given by

$$\eta_i = \lambda_i \cos(\xi) + \frac{\alpha b_i}{2}\left(Y_i + \frac{\tilde{b}_i}{b_i}\right)^2. \tag{4.109}$$

At this order the function $M_i(\eta_i)$ is arbitrary (it will be determined later in (4.123)), but to match to the inviscid region we require the asymptotic behaviour

$$M_i(\eta_i) \sim \pm(-1)^{i+1}\left(\frac{2\alpha\eta_i}{b_i}\right)^{1/2}\frac{\beta(y_1 - y_2)}{\alpha^2+\beta^2} + O(1) \quad \text{as } \eta_i \to (-1)^i\infty, \tag{4.110}$$

implied by (4.107). Here and below, the notation $\pm$ denotes the upper and lower parts of each critical layer, wherein $Y_i + \tilde{b}_i/b_i > (2\lambda_i((-1)^{i+1} - \cos(\xi))/\alpha b_i)^{1/2}$ and $Y_i + \tilde{b}_i/b_i < -(2\lambda_i((-1)^{i+1} - \cos(\xi))/\alpha b_i)^{1/2}$, respectively. The quantity

$$\tilde{b}_i = u_{1M}(y_i\pm) + \beta w_{1M}(y_i\pm)/\alpha, \tag{4.111}$$

is a constant (in recognition of the continuity of the mean flow distortion across the critical layers) and we define the skewed velocity component

$$\overline{u}_m^{(i)} = \alpha U_m^{(i)} + \beta W_m^{(i)}, \tag{4.112}$$

for $m = 1, 2, \ldots$. It is worth noting that the quantity λ_i is negative since $g_i^{(0)} < 0$ from the solution of the Rayleigh equation (4.97) in subsection 4.2.3, while b_1, b_2 are of opposite signs with $b_1 = -b_2$. The fact that the leading-order solution (4.108) is of relatively simple form facilitates an examination of the behaviour of higher-order contributions in the critical-layer

expansion (4.104) required for the determination of the vorticity jump. From substitution of (4.104) into (1.1) the governing equations for $m > 1$ are found to be

$$\overline{u}^{(i)}_{m\xi} + V^{(i)}_{mY_i} = 0, \tag{4.113a}$$

$$\overline{u}^{(i)}_1 U^{(i)}_{m\xi} + \overline{u}^{(i)}_m U^{(i)}_{1\xi} + V^{(i)}_1 U^{(i)}_{mY_i} + V^{(i)}_m U^{(i)}_{1Y_i} + \alpha P^{(i)}_{m\xi} = \mathscr{L}^{(i)}_{(2,m)}, \tag{4.113b}$$

$$P^{(i)}_{mY_i} = \mathscr{L}^{(i)}_{(3,m)}, \tag{4.113c}$$

$$\overline{u}^{(i)}_1 W^{(i)}_{m\xi} + \overline{u}^{(i)}_m W^{(i)}_{1\xi} + V^{(i)}_1 W^{(i)}_{mY_i} + V^{(i)}_m W^{(i)}_{1Y_i} + \beta P^{(i)}_{m\xi} = \mathscr{L}^{(i)}_{(4,m)}. \tag{4.113d}$$

The quantities $\mathscr{L}^{(i)}_{(n,m)} (n = 2, 3, 4)$ are forcing functions arising due to the nonlinear inertial responses and viscous effects which can be written down for any particular m and n. After taking an appropriate linear combination of the equations (4.113b), (4.113d), we differentiate the resulting equation with respect to Y_i followed by use of (4.108), (4.109), (4.112), (4.113a) and (4.113c) to obtain an equation for the shear $\overline{u}^{(i)}_{mY_i}$ in the form

$$\pm(2\alpha b_i(\eta_i - \lambda_i \cos(\xi)))^{1/2} \frac{\partial \overline{u}^{(i)}_{mY_i}}{\partial \hat{\xi}} = \frac{\partial}{\partial Y_i}\{\alpha \mathscr{L}^{(i)}_{(2,m)} + \beta \mathscr{L}^{(i)}_{(4,m)}\} - (\alpha^2 + \beta^2) \frac{\partial \mathscr{L}^{(i)}_{(3,m)}}{\partial \xi}, \tag{4.114}$$

where the change of variables $(\xi, Y_i) \to (\hat{\xi}, \eta_i)$, with $\xi = \hat{\xi}$ has been performed so that

$$\frac{\partial}{\partial \xi} = \frac{\partial}{\partial \hat{\xi}} - \lambda_i \sin(\xi) \frac{\partial}{\partial \eta_i}, \quad \frac{\partial}{\partial Y_i} = \overline{u}^{(i)}_1 \frac{\partial}{\partial \eta_i}. \tag{4.115}$$

A similar equation for W_m can be obtained from (4.113d) and takes the form

$$\overline{u}^{(i)}_1 \frac{\partial W^{(i)}_m}{\partial \hat{\xi}} = \lambda_i \sin(\xi) M_i' \overline{u}^{(i)}_m - V^{(i)}_m \left\{ \left(\frac{\alpha \beta b_i}{\alpha^2 + \beta^2} \right) + M_i' \overline{u}^{(i)}_1 \right\} + \mathscr{L}^{(i)}_{(4,m)} - \beta P^{(i)}_{m\xi}. \tag{4.116}$$

This equation enables $W^{(i)}_m$ to be determined once the shear term $\overline{u}^{(i)}_{mY_i}$ is found from (4.114). Below, the notation 'E' or 'O' is used to represent contributions that are even or odd about $\xi = \pi$. In order to find the value of m at which a phase shift is induced across the critical layers we need to identify the first solution $(\overline{u}^{(i)}_m, V^{(i)}_m, W^{(i)}_m, P^{(i)}_m)$ possessing the following property: $(\overline{u}^{(i)}_m, W^{(i)}_m, P^{(i)}_m)$ contain an odd part about $\xi = \pi$, with $V^{(i)}_m$ having an even part. Clearly, for each critical layer, the leading-order solution $(\overline{u}^{(i)}_1, V^{(i)}_1, W^{(i)}_1, P^{(i)}_1)$ is ('E', 'O', 'E', 'E'), with this pattern staying intact at higher order until viscous effects come into play. The symmetry here is simply inherited from the form of the fundamental mode (4.95) in the core region. For the next stage the governing equations are (4.113) with $m = 2$ and $\mathscr{L}^{(i)}_{(2,2)} = \mathscr{L}^{(i)}_{(3,2)} = \mathscr{L}^{(i)}_{(4,2)} = 0$, subject to the following matching conditions with the inviscid region as $Y_i \to \pm\infty$:

$$U^{(i)}_2 \sim -Y_i^2 + Y_i u_{1M}'(y_i\pm) + \frac{A_0}{\alpha} \left\{ \left(\frac{2\alpha^2 + \beta^2}{2(\alpha^2 + \beta^2)} \right) \mathscr{G}^{(1)}_i + g^{(1)}_i + \mathscr{G}^{(1)}_i \ln|Y_i| \right\} \cos(\xi) + u_{2M}(y_i\pm),$$

$$V^{(i)}_2 \sim A_0 (g^{(1)}_i + \mathscr{G}^{(1)}_i \ln|Y_i|) Y_i \sin(\xi),$$

$$W^{(i)}_2 \sim Y_i w_{1M}'(y_i\pm) + \frac{A_0}{2} \left\{ \left(\frac{\beta}{\alpha^2 + \beta^2} \right) \mathscr{G}^{(1)}_i \right\} \cos(\xi) + w_{2M}(y_i\pm), \tag{4.117}$$

from (4.94), (4.95), (4.100) and (4.102). Integration of (4.114) with $m = 2$ and use of (4.117) leads us to expressions for the shear $\overline{u}^{(i)}_{2Y_i}$ and its associated asymptotic behaviour. These take the form

$$\overline{u}^{(i)}_{2Y_i} = K_i(\eta_i), \quad \overline{u}^{(i)}_{2Y_i} \sim -2\alpha Y_i + \tilde{\lambda}^{\pm}_i + O(1) \quad \text{as} \quad Y_i \to \pm\infty, \tag{4.118}$$

with the constants $\tilde{\lambda}^{\pm}_i = \alpha u'_{1M}(y_i\pm) + \beta w'_{1M}(y_i\pm)$ corresponding to the upper and lower regions of the critical layers. The difference $\tilde{\lambda}^{+}_i - \tilde{\lambda}^{-}_i$ is the vorticity jump whose determination is the main aim of this analysis. Analogous to the function M_i in the leading order solution (4.108), the function $K_i(\eta_i)$ is at present unknown (it is fully determined at the level $m = 5$); however we can deduce the asymptotic behaviour

$$K_i(\eta_i) \sim \mp\, 2^{3/2}\left(\frac{\alpha\eta_i}{b_i}\right)^{1/2} + \tilde{\lambda}^{\pm}_i + O(1) \quad \text{as} \quad \eta_i \to (-1)^i\infty, \tag{4.119}$$

from (4.109), (4.118). In view of the fact that no viscous effects have entered the analysis at this stage, the ('E', 'O', 'E', 'E') symmetry established for the $m = 1$ solution carries over to the $m = 2$ stage. Next we turn to $m = 3$ where the forcing terms may be expressed in the form

$$\mathscr{L}^{(i)}_{(2,3)} = -\overline{u}^{(i)}_2 U^{(i)}_{2\xi} - V^{(i)}_2 U^{(i)}_{2Y_i},\ \mathscr{L}^{(i)}_{(3,3)} = -\overline{u}^{(i)}_1 V^{(i)}_{1\xi} - V^{(i)}_1 V^{(i)}_{1Y_i},\ \mathscr{L}^{(i)}_{(4,3)} = -\overline{u}^{(i)}_2 W^{(i)}_{2\xi} - V^{(i)}_2 W^{(i)}_{2Y_i}.$$

Taking into account the symmetry of the $m = 1, 2$ solutions, examination of these terms elucidates that $\mathscr{L}^{(i)}_{(2,3)}$, $\mathscr{L}^{(i)}_{(3,3)}$ and $\mathscr{L}^{(i)}_{(4,3)}$ are respectively 'O', 'E', 'O' since these forcing terms stem solely from the nonlinear interactions of various terms in the expansions for the nonlinear critical layer. An important implication of this pattern of the forcing terms is the evenness of the $m = 3$ solution and therefore no phase shift is induced in the terms $\overline{u}^{(i)}_3$, $V^{(i)}_3$, $W^{(i)}_3$ and $P^{(i)}_3$. It emerges that for PPCF a phase shift is not encountered until $m = 5$ stage analogous to previous studies by Smith and Bodonyi (1982) and Walton (2001) for other parallel flows. It turns out that the solutions at $m = 3$ stage give no further information about the unknown functions in the $m = 1, 2$ solutions and so we proceed to the stage $m = 4$. Unsurprisingly, at this stage the forcing terms take convoluted form

$$\begin{aligned}
\mathscr{L}^{(i)}_{(2,4)} &= U^{(i)}_{1Y_iY_i} - \overline{u}^{(i)}_2 U^{(i)}_{3\xi} - \overline{u}^{(i)}_3 U^{(i)}_{2\xi} - V^{(i)}_2 U^{(i)}_{3Y_i} - V^{(i)}_3 U^{(i)}_{2Y_i},\\
\mathscr{L}^{(i)}_{(3,4)} &= -\,\overline{u}^{(i)}_1 V^{(i)}_{2\xi} - \overline{u}^{(i)}_2 V^{(i)}_{1\xi} - V^{(i)}_1 V^{(i)}_{2Y_i} - V^{(i)}_2 V^{(i)}_{1Y_i},\\
\mathscr{L}^{(i)}_{(4,4)} &= W^{(i)}_{1Y_iY_i} - \overline{u}^{(i)}_2 W^{(i)}_{3\xi} - \overline{u}^{(i)}_3 W^{(i)}_{2\xi} - V^{(i)}_2 W^{(i)}_{3Y_i} - V^{(i)}_3 W^{(i)}_{2Y_i}.
\end{aligned}$$

Leaving aside the contributions $U^{(i)}_{1Y_iY_i}$, $W^{(i)}_{1Y_iY_i}$ which mark the first appearance of any viscous effects in the critical layers, we turn our attention to examine the nonlinear terms. A brief explanation concerning the evenness or oddness of these terms is presented below. From the conclusions drawn above for the solution connected with $m = 1, 2$ and 3 we see that

$$\underbrace{\overline{u}^{(i)}_2}_{\text{'E'}}\underbrace{\frac{\partial U^{(i)}_3}{\partial\xi}}_{\text{'O'}} + \underbrace{\overline{u}^{(i)}_3}_{\text{'E'}}\underbrace{\frac{\partial U^{(i)}_2}{\partial\xi}}_{\text{'O'}} + \underbrace{V^{(i)}_2}_{\text{'O'}}\underbrace{\frac{\partial U^{(i)}_3}{\partial Y_i}}_{\text{'E'}} + \underbrace{V^{(i)}_3}_{\text{'O'}}\underbrace{\frac{\partial U^{(i)}_2}{\partial Y_i}}_{\text{'E'}} = \text{'O'},$$

$$\underbrace{\overline{u}_1^{(i)}}_{\text{'E'}}\underbrace{\frac{\partial V_2^{(i)}}{\partial \xi}}_{\text{'E'}} + \underbrace{\overline{u}_2^{(i)}}_{\text{'E'}}\underbrace{\frac{\partial V_1^{(i)}}{\partial \xi}}_{\text{'E'}} + \underbrace{V_1^{(i)}}_{\text{'O'}}\underbrace{\frac{\partial V_2^{(i)}}{\partial Y_i}}_{\text{'O'}} + \underbrace{V_2^{(i)}\frac{\partial V_1^{(i)}}{\partial Y_i}}_{=0} = \text{'E'},$$

$$\underbrace{\overline{u}_2^{(i)}}_{\text{'E'}}\underbrace{\frac{\partial W_3^{(i)}}{\partial \xi}}_{\text{'O'}} + \underbrace{\overline{u}_3^{(i)}}_{\text{'E'}}\underbrace{\frac{\partial W_2^{(i)}}{\partial \xi}}_{\text{'O'}} + \underbrace{V_2^{(i)}}_{\text{'O'}}\underbrace{\frac{\partial W_3^{(i)}}{\partial Y_i}}_{\text{'E'}} + \underbrace{V_3^{(i)}}_{\text{'O'}}\underbrace{\frac{\partial W_2^{(i)}}{\partial Y_i}}_{\text{'E'}} = \text{'O'},$$

where we have taken into consideration

$$\frac{\partial}{\partial \xi}(\text{'O'}) = \text{'E'}, \quad \frac{\partial}{\partial \xi}(\text{'E'}) = \text{'O'}, \quad \frac{\partial}{\partial Y_2}(\text{'O'}) = \text{'O'}, \quad \frac{\partial}{\partial Y_2}(\text{'E'}) = \text{'E'},$$

and used the result that the product of two purely odd contributions or two purely even contributions yields an even contribution. Based on the preceding observation the forcing functions at the $m = 4$ stage may be abbreviated to

$$\mathscr{L}_{(2,4)}^{(i)} = U_{1Y_iY_i}^{(i)} + \text{'O'}, \quad \mathscr{L}_{(3,4)}^{(i)} = \text{'E'}, \quad \mathscr{L}_{(4,4)}^{(i)} = W_{1Y_iY_i}^{(i)} + \text{'O'}. \tag{4.120}$$

Substituting (4.120) into (4.114) we find that the shear $\overline{u}_{4Y_i}^{(i)}$ is governed by

$$\pm(2\alpha b_i(\eta_i - \lambda_i\cos(\xi)))^{1/2}\frac{\partial \overline{u}_{4Y_i}^{(i)}}{\partial \hat{\xi}} = \text{'O'}, \tag{4.121}$$

since $\overline{u}_{1Y_iY_iY_i}^{(i)} = 0$ from (4.108). Hence, on integration of (4.121), $\overline{u}_4^{(i)}$ is 'E', and it follows from (4.113a), (4.113c), (4.120) that $V_4^{(i)}$ is 'O' and $P_4^{(i)}$ is 'E'. Although the solution at this level does not explicitly determine the phase shift, it does allow us to fix the unknown functions M_i in the leading order solutions (4.108) as follows. Integrating (4.116) with respect to $\hat{\xi}$, and inserting the form (4.108) for $W_{1Y_iY_i}^{(i)}$ we obtain

$$W_4^{(i)} = \pm\frac{\partial}{\partial \eta_i}\left\{M_i'(\eta_i)\int_0^{\hat{\xi}}(2\alpha b_i(\eta_i - \lambda_i\,\cos(q)))^{1/2}\mathrm{d}q\right\} + C_i(\eta_i) + \text{'E'}, \tag{4.122}$$

with $C_i(\eta_i)$ an arbitrary function. Imposing the condition of periodicity on $W_4^{(i)}$, we conclude that

$$M_i'(\eta_i)\hat{I}(\eta_i) = D^{(i)\pm}, \quad \text{with} \quad \hat{I}(\eta_i) = \int_0^{2\pi}(|\eta_i - \lambda_i\cos(q)|)^{1/2}\mathrm{d}q, \tag{4.123}$$

where

$$D^{(i)\pm} = \pm(-1)^{i+1}\pi\left(\frac{2\alpha}{|b_i|}\right)^{1/2}\frac{\beta(y_1 - y_2)}{\alpha^2 + \beta^2}, \tag{4.124}$$

from the asymptotic condition (4.110) on M_i established earlier. This fully determines the leading-order solution (4.108) in the critical layers. The expression (4.122) signifies that

both $W_4^{(i)}$, $U_4^{(i)}$ possess non-zero 'O' parts, while the combination $\overline{u}_4^{(i)}$ remains 'E'. This vital aspect gives no contribution to the phase shift, nevertheless, since it can be inferred from (4.122), (4.123) that M_i' is proportional to $|\eta_i|^{-1/2}$ as $Y_i \to \pm\infty$, implying that the 'O' parts of $W_4^{(i)}$, $U_4^{(i)}$ tend to zero in this limit. The final stage we deal with is $m = 5$ where we are able to determine the function K_i introduced in (4.118) and hence determine the phase shifts across the two critical layers. The forcing terms may be written in the form

$$\begin{aligned}
\mathscr{L}_{(2,5)}^{(i)} &= U_{2Y_iY_i}^{(i)} - \overline{u}_4^{(i)}U_{2\xi}^{(i)} - \overline{u}_2^{(i)}U_{4\xi}^{(i)} - \overline{u}_3^{(i)}U_{3\xi}^{(i)} - V_2^{(i)}U_{4Y_i}^{(i)} - V_4^{(i)}U_{2Y_i}^{(i)} - V_3^{(i)}U_{3Y_i}^{(i)},\\
\mathscr{L}_{(3,5)}^{(i)} &= -\,\overline{u}_1^{(i)}V_{3\xi}^{(i)} - \overline{u}_2^{(i)}V_{2\xi}^{(i)} - \overline{u}_3^{(i)}V_{1\xi}^{(i)} - V_1^{(i)}V_{3Y_i}^{(i)} - V_2^{(i)}V_{2Y_i}^{(i)} - V_3^{(i)}V_{1Y_i}^{(i)},\\
\mathscr{L}_{(4,5)}^{(i)} &= W_{2Y_iY_i}^{(i)} - \overline{u}_4^{(i)}W_{2\xi}^{(i)} - \overline{u}_2^{(i)}W_{4\xi}^{(i)} - \overline{u}_3^{(i)}W_{3\xi}^{(i)} - V_2^{(i)}W_{4Y_i}^{(i)} - V_4^{(i)}W_{2Y_i}^{(i)} - V_3^{(i)}W_{3Y_i}^{(i)}.
\end{aligned}$$

Since the solutions $(\overline{u}_m^{(i)}, W_m^{(i)}, U_m^{(i)})$ are 'E' for $m < 4$, while $V_m^{(i)}$ is 'O' for $m < 5$ and so we note that

$$\begin{aligned}
\underbrace{\overline{u}_4^{(i)}}_{\text{'E'}}\underbrace{\frac{\partial U_2^{(i)}}{\partial\xi}}_{\text{'O'}} + \underbrace{\overline{u}_3^{(i)}}_{\text{'E'}}\underbrace{\frac{\partial U_3^{(i)}}{\partial\xi}}_{\text{'O'}} + \underbrace{V_4^{(i)}}_{\text{'O'}}\underbrace{\frac{\partial U_2^{(i)}}{\partial Y_i}}_{\text{'E'}} + \underbrace{V_3^{(i)}}_{\text{'O'}}\underbrace{\frac{\partial U_3^{(i)}}{\partial Y_i}}_{\text{'E'}} &= \text{'O'},\\
\underbrace{\overline{u}_1^{(i)}}_{\text{'E'}}\underbrace{\frac{\partial V_3^{(i)}}{\partial\xi}}_{\text{'E'}} + \underbrace{\overline{u}_2^{(i)}}_{\text{'E'}}\underbrace{\frac{\partial V_2^{(i)}}{\partial\xi}}_{\text{'E'}} + \underbrace{\overline{u}_3^{(i)}}_{\text{'E'}}\underbrace{\frac{\partial V_1^{(i)}}{\partial\xi}}_{\text{'E'}} + \underbrace{V_1^{(i)}}_{\text{'O'}}\underbrace{\frac{\partial V_3^{(i)}}{\partial Y_i}}_{\text{'O'}} + \underbrace{V_2^{(i)}}_{\text{'O'}}\underbrace{\frac{\partial V_2^{(i)}}{\partial Y_i}}_{\text{'O'}} + \underbrace{V_3^{(i)}}_{\text{'O'}}\underbrace{\frac{\partial V_1^{(i)}}{\partial Y_i}}_{\text{'O'}} &= \text{'E'},\\
\underbrace{\overline{u}_4^{(i)}}_{\text{'E'}}\underbrace{\frac{\partial W_2^{(i)}}{\partial\xi}}_{\text{'O'}} + \underbrace{\overline{u}_3^{(i)}}_{\text{'E'}}\underbrace{\frac{\partial W_3^{(i)}}{\partial\xi}}_{\text{'O'}} + \underbrace{V_4^{(i)}}_{\text{'O'}}\underbrace{\frac{\partial W_2^{(i)}}{\partial Y_i}}_{\text{'E'}} + \underbrace{V_3^{(i)}}_{\text{'O'}}\underbrace{\frac{\partial W_3^{(i)}}{\partial Y_i}}_{\text{'E'}} &= \text{'O'}.
\end{aligned}$$

By virtue of exploration of the behaviour of these few terms, it is completely clear that the forcing terms may be written compactly in the form

$$\mathscr{L}_{(2,5)}^{(i)} = U_{2Y_iY_i}^{(i)} - \overline{u}_2^{(i)}U_{4\xi}^{(i)} - V_2^{(i)}U_{4Y_i}^{(i)} + \text{'O'}, \quad \mathscr{L}_{(4,5)}^{(i)} = W_{2Y_iY_i}^{(i)} - \overline{u}_2^{(i)}W_{4\xi}^{(i)} - V_2^{(i)}W_{4Y_i}^{(i)} + \text{'O'},$$

and $\mathscr{L}_{(3,5)}^{(i)} = $ 'E'. By substituting for $\overline{u}_{2Y_i}^{(i)}$ from (4.118) and integrating the shear equation (4.114) for $m = 5$ with respect to $\hat{\xi}$, we obtain

$$\overline{u}_{5Y_i}^{(i)} = \pm(2\alpha|b_i|)^{1/2}\frac{\partial}{\partial\eta_i}\left\{K_i'(\eta_i)\int_0^{\hat{\xi}}(|\eta_i - \lambda_i\cos(q)|)^{1/2}\mathrm{d}q\right\} + T_i(\eta_i) + \text{'E'}, \tag{4.125}$$

where the function $T_i(\eta_i)$ is undetermined at this level. By applying the periodicity condition $[\overline{u}_{5Y_i}^{(i)}]_0^{2\pi} = 0$, we deduce an equation controlling the behaviour of the shear term K_i:

$$K_i'(\eta_i)\hat{I}(\eta_i) = F^{(i)\pm}, \quad F^{(i)\pm} = \mp 2(2\alpha/|b_i|)^{1/2}\pi, \tag{4.126}$$

where the constants $F^{(i)\pm}$ have been evaluated using (4.119). This equation can itself be integrated and after applying the condition of uniform vorticity $K_i = K_0^{(i)}$ when $\eta_i = (-1)^{i+1}\lambda_i$

we obtain

$$K_i = K_0^{(i)} \mp 2\pi \left(\frac{2\alpha}{|b_i|}\right)^{1/2} \int_{(-1)^{i+1}\lambda_i}^{\eta_i} \frac{\mathrm{d}q}{\hat{I}(q)}. \tag{4.127}$$

Letting $\eta_i \to (-1)^i \infty$ in (4.127), the asymptotic form for K_i is determined to be

$$K_i(\eta_i) \sim K_0^{(i)} \mp 2\pi \left(\frac{2\alpha}{|b_i|}\right)^{1/2} \left((-1)^i \pi^{-1} |\eta_i|^{1/2} + J_1^{(i)}\right), \tag{4.128}$$

where

$$J_1^{(i)} = (-1)^{i+1} \frac{|\lambda_i|^{1/2}}{\pi} + \int_{-(-1)^i\lambda_i}^{(-1)^i\infty} \left(\frac{1}{\hat{I}(\eta_i)} - \frac{1}{2\pi|\eta_i|^{1/2}}\right) \mathrm{d}\eta_i = \frac{(2|\lambda_i|)^{1/2} C^{(1)}}{8\pi}, \tag{4.129}$$

and $C^{(1)} \simeq -5.516$ is the same constant that occurs in a number of earlier critical layer studies (e.g. Smith & Bodonyi (1982a)). Examining the finite part of the jump in $K_i(\eta_i)$ across the critical layers in the relations (4.119) and (4.128) allows us to determine the vorticity jump as

$$[[K_i(\eta_i)]]_{-\infty}^{\infty} = \tilde{\lambda}_i^+ - \tilde{\lambda}_i^- = -\left(\frac{\alpha}{|b_i|}\right)^{1/2} |\lambda_i|^{1/2}\ C^{(1)}. \tag{4.130}$$

Our objective is to derive the expression for the phase shift across the critical layers, which we denote by $\phi^{(i)}$ for $i \in \{1, 2\}$, by using a sophisticated approach to that explained in an appendix to Smith and Bodonyi (1982a). The proceeding analysis aims to establish a relationship between $\phi^{(i)}$ and A_0, which will enable us to gain insight into the variation of the phase shift with amplitude. The fundamental idea underlying calculation of the phase shift concerns representing the finite part of the total velocity jump $\overline{u}_5^{(i)}$ as the sum of infinite trigonometric series, namely

$$[[\overline{u}_5^{(i)}]]_{-\infty}^{+\infty} = \sum_{m=1}^{\infty} (F_m^{(i)} \sin(m\xi) + \tilde{F}_m^{(i)} \cos(m\xi)). \tag{4.131}$$

We now pose the problem of determining the coefficients $F_m^{(i)}$, $\tilde{F}_m^{(i)}$ from applying the orthogonal property attributed to the system of trigonometric functions. As the first step, an important observation is made that the coefficient of relevance to the phase shift is the first Fourier sine component, $F_1^{(i)}$, in (4.131). In this regard, we will merely concentrate on finding $F_1^{(i)}$, thus leaving the rest of the coefficients undetermined. The coefficient $F_1^{(i)}$ is obtained from the Fourier series expansion (4.131) by multiplying by $\sin(\xi)$, integrating term by term and noting that the trigonometric functions are pairwise orthogonal. As a consequence, all the integrals in the sum vanish except one involving $F_1^{(i)}$, which puts the definition of the phase shift as

$$A_0\phi^{(i)} = F_1^{(i)} = \frac{1}{\pi} \int_0^{2\pi} [[\overline{u}_5^{(i)}]]_{-\infty}^{+\infty} \sin(\xi) \mathrm{d}\xi = \frac{1}{\pi} \fint_{-\infty}^{+\infty} \left(\int_0^{2\pi} \overline{u}_{5Y_i}^{(i)} \sin(\xi) \mathrm{d}\xi \right) \mathrm{d}Y_i, \tag{4.132}$$

where the notation $\fint$ denotes the finite part of the integral. From substitution of (4.125) into (4.132), and since $(-1)^i(2\alpha|b_i|)^{1/2}\mathrm{d}Y_i = \pm\mathrm{d}\eta_i/(|\eta_i - \lambda_i\cos(\hat{\xi})|)^{1/2}$ for fixed $\hat{\xi}$ and $\overline{u}^{(i)}_{5Y_i}$ is periodic in $\hat{\xi}$, integration by parts with respect to $\hat{\xi}$ therefore gives

$$(-1)^i\pi\lambda_i\alpha b_i\phi^{(i)} = \fint_{Y_i=-\infty}^{+\infty}\int_{\hat{\xi}=0}^{2\pi}\hat{R}(\hat{\xi},\eta_i)\mathrm{d}\hat{\xi}\mathrm{d}\eta_i, \tag{4.133}$$

where $\hat{R}(\hat{\xi},\eta_i)$ is the right-hand side of (4.125). It remains to note that $\mathrm{d}\eta_i = \alpha b_i(Y_i + \frac{\tilde{b}_i}{b_i})\mathrm{d}Y_i$ for fixed ξ from (4.109), and hence (4.133) becomes

$$(-1)^i\pi\lambda_i\phi^{(i)} = \fint_{Y_i=-\infty}^{+\infty}\int_{\hat{\xi}=0}^{2\pi}\left(Y_i + \frac{\tilde{b}_i}{b_i}\right)\hat{R}(\hat{\xi},\eta_i)\mathrm{d}\hat{\xi}\mathrm{d}Y_i. \tag{4.134}$$

Using the definition of $\hat{R}(\hat{\xi},\eta_i)$ and keeping in mind that the integrated contributions from the 'O' terms are identically zero, we find that

$$(-1)^i\pi\lambda_i\phi^{(i)} = \int_{\hat{\xi}=0}^{2\pi}\left\{\left[\left[\left(Y_i + \frac{\tilde{b}_i}{b_i}\right)\overline{u}^{(i)}_{2Y_iY_i}\right]\right]_{-\infty}^{\infty} - [[\overline{u}^{(i)}_{2Y_i}]]_{-\infty}^{\infty}\right\}\mathrm{d}\hat{\xi}. \tag{4.135}$$

Further we note that

$$\left[\left[\left(Y_i + \frac{\tilde{b}_i}{b_i}\right)\overline{u}^{(i)}_{2Y_iY_i}\right]\right]_{-\infty}^{\infty} = 0, \quad [[\overline{u}^{(i)}_{2Y_i}]]_{-\infty}^{\infty} = [[K(\eta_i)]]_{-\infty}^{\infty} = \tilde{\lambda}_i^+ - \tilde{\lambda}_i^-,$$

from consideration of the form (4.118). Substituting for the vorticity jump (4.130) into (4.135) we finally obtain the phase shift $\phi^{(i)}$ as a function of disturbance amplitude A_0, namely

$$\phi^{(i)} = \left(\frac{2C^{(1)}}{A_0^{3/2}|b_i||M_i|^{1/2}}\right) \quad \text{with} \quad M_i = \frac{g_i^{(0)}}{\alpha b_i}. \tag{4.136}$$

In order to determine the amplitude-dependence of the neutral modes we need to calculate the corresponding net phase shift across the viscous Stokes layers which form the focus of our attention in the next subsections.

(c) The upper viscous wall layer

The dominant balance in the wall layer is between the inertia term $\alpha(U_0 - c)$ and the viscous operator $R^{-1}\partial^2/\partial y^2$. Suppose that the thickness of the layer is m which is to be determined in terms of the Reynolds number. The wall layer is located in the proximity of the lower wall at $y = 1$ which suggests the definition of the appropriate inner variable Z_1 as

$$Z_1 = \frac{y-1}{m}, \tag{4.137}$$

where Z_1 is the $O(1)$ normal coordinate within the wall layer. Then the inertial-viscous balance implies that $R^{-1}m^{-2} \sim O(1)$, leading to the wall layer thickness $m \sim R^{-1/2}$ since c, V and α are $O(1)$, and $\partial^2/\partial y^2 \sim O(m^{-2})$ from consideration of (4.137). Thus we introduce the normal scaling of the region III+ as

$$y = 1 + R^{-1/2} Z_1. \tag{4.138}$$

In terms of ϵ and R, the velocities and pressure expand, to leading order, as follows:

$$u = V + \epsilon^2 \hat{U}(\xi, Z_1), \quad v = \epsilon^2 R^{-1/2} \hat{V}(\xi, Z_1), \quad w = \epsilon^2 \hat{W}(\xi, Z_1), \quad p = \epsilon^2 \hat{P}(\xi, Z_1), \tag{4.139}$$

and the wavespeed takes the form $c = c_0$. Substitution of these expansions into the Navier-Stokes equations (1.1) yields the following unsteady-viscous-pressure force balances

$$\alpha \frac{\partial \hat{U}}{\partial \xi} + \frac{\partial \hat{V}}{\partial Z_1} + \beta \frac{\partial \hat{W}}{\partial \xi} = 0, \tag{4.140a}$$

$$\alpha (V - c_0) \frac{\partial \hat{U}}{\partial \xi} = -\alpha \frac{\partial \hat{P}}{\partial \xi} + \frac{\partial^2 \hat{U}}{\partial Z_1^2}, \tag{4.140b}$$

$$\frac{\partial \hat{P}}{\partial Z_1} = 0, \tag{4.140c}$$

$$\alpha (V - c_0) \frac{\partial \hat{W}}{\partial \xi} = -\beta \frac{\partial \hat{P}}{\partial \xi} + \frac{\partial^2 \hat{W}}{\partial Z_1^2}, \tag{4.140d}$$

with these equations subject to the no-slip conditions

$$\hat{U} = \hat{V} = \hat{W} = 0 \quad \text{on } Z_1 = 0. \tag{4.140e}$$

It follows from (4.140c) that the pressure depends purely on ξ. Matching the pressure within the viscous wall layer (4.139) as $Z_1 \to -\infty$ with the pressure in the inviscid region (4.94d) as $y \to 1$, we find that

$$\hat{P} = A_0 P_2(1) \cos(\xi). \tag{4.141}$$

Inserting the expression for $\hat{P}$ into (4.140b) and (4.140d) leads to a set of linear equations, namely

$$\alpha (V - c_0) \frac{\partial \hat{U}}{\partial \xi} = \alpha A_0 P_2(1) \sin(\xi) + \frac{\partial^2 \hat{U}}{\partial Z_1^2}, \tag{4.142a}$$

$$\alpha (V - c_0) \frac{\partial \hat{W}}{\partial \xi} = \beta A_0 P_2(1) \sin(\xi) + \frac{\partial^2 \hat{W}}{\partial Z_1^2}. \tag{4.142b}$$

It can be easily seen that $\hat{W} = (\beta/\alpha)\hat{U}$ and hence we aim to solve only equation (4.142a). It is possible to tackle (4.142a) analytically by separating the variables, and seeking solutions in the normal-mode-form

$$\hat{U} = \mathrm{Re}(f_1(Z_1) \exp(\mathrm{i}\xi)), \tag{4.143}$$

where Re denotes the real part. Substitution of (4.143) into (4.142a) yields the following ordinary equation for function f_1:

$$\frac{d^2 f_1}{dZ_1^2} + \mathrm{i}\alpha(c_0 - V) f_1 = \mathrm{i}\alpha A_0 P_2(1). \tag{4.144}$$

The general solution of (4.144) satisfying the no-slip on $Z_1 = 0$ and boundedness conditions as $Z_1 \to -\infty$ is written as

$$f_1(Z_1) = \left(\frac{A_0 P_2(1)}{c_0 - V}\right)(1 - \exp(m_1 Z_1)), \tag{4.145}$$

where $m_1 = (\alpha(c_0 - V))^{1/2} \exp(-i\pi/4)$. Hence, we arrive at a conclusion that the leading-order disturbance streamwise and spanwise velocity components assume the form

$$\hat{U} = \mathrm{Re}\left\{\left(\frac{A_0 P_2(1)}{c_0 - V}\right)(1 - \exp(m_1 Z_1))\exp(\mathrm{i}\xi)\right\}, \tag{4.146a}$$

$$\hat{W} = \mathrm{Re}\left\{\left(\frac{\beta A_0 P_2(1)}{\alpha(c_0 - V)}\right)(1 - \exp(m_1 Z_1))\exp(\mathrm{i}\xi)\right\}. \tag{4.146b}$$

The disturbance normal velocity can be determined from the continuity balance (4.140a) since the other two velocity components $\hat{U}$ and $\hat{W}$ are known. The governing differential equation satisfied by $\hat{V}$ is found to be

$$\frac{\partial \hat{V}}{\partial Z_1} = -\mathrm{Re}\left\{\left(\frac{\mathrm{i}A_0 P_2(1)(\alpha^2 + \beta^2)}{\alpha(c_0 - V)}\right)(1 - \exp(m_1 Z_1))\exp(\mathrm{i}\xi)\right\}.$$

The appropriate solution of this equation satisfying the no-slip condition is

$$\hat{V} = -\mathrm{Re}\left\{\left(\frac{\mathrm{i}A_0 P_2(1)(\alpha^2 + \beta^2)}{\alpha(c_0 - V)}\right)\left(Z_1 - \frac{\exp(m_1 Z_1)}{m_1} + \frac{1}{m_1}\right)\exp(\mathrm{i}\xi)\right\}.$$

Taking the limit of the latter expression as $Z_1 \to -\infty$, we obtain

$$v \sim \varepsilon^2 R^{-1/2}\left(\frac{A_0 P_2(1)(\alpha^2 + \beta^2)}{\alpha(c_0 - V)}\right)\left[Z_1 \sin(\xi) + \left(\frac{2^{-1/2}}{(\alpha(c_0 - V))^{1/2}}\right)(\sin(\xi) + \cos(\xi))\right]. \tag{4.147}$$

As $y \to 1$, the normal velocity from the inviscid region (4.94b) takes the form

$$v \sim \varepsilon^2 R^{-1/2} A_0 Z_1 G_2'(1)\sin(\xi) + \cdots + \varepsilon^2 R^{-1/2} v_5 + \cdots, \tag{4.148}$$

since $G_2(1) = 0$ from (4.98). Matching the asymptotic form for the normal velocity within the upper wall layer (4.147) with the behaviour of the normal velocity in the inviscid region (4.148) leads to the following results

$$G_2'(1) = \frac{P_2(1)(\alpha^2 + \beta^2)}{\alpha(c_0 - V)}, \tag{4.149a}$$

$$v_5 \sim \frac{2A_0 P_2(1)(\alpha^2 + \beta^2)}{(2\alpha(c_0 - V))^{3/2}}(\sin(\xi) + \cos(\xi)) \quad \text{as } y \to 1. \tag{4.149b}$$

(d) The lower viscous wall layer

This section focuses on the study of the dynamics of the lower wall layer, which is of $O(R^{-1/2})$ thickness and located in the vicinity of the lower wall at $y = -1$. The appropriate normal scaling in this region is therefore

$$y = -1 + R^{-1/2} Z_2, \tag{4.150}$$

where Z_2 is the $O(1)$ variable within the wall layer. In the lower layer (III–) we have to leading order

$$u = -V + \epsilon^2 \tilde{U}(\xi, Z_2), \quad v = \epsilon^2 R^{-1/2} \tilde{V}(\xi, Z_2), \quad w = \epsilon^2 \tilde{W}(\xi, Z_2), \quad p = \epsilon^2 \tilde{P}(\xi, Z_2), \tag{4.151}$$

with the wavespeed $c = c_0$. We substitute the expansions (4.151) into the governing three-dimensional unsteady Navier-Stokes equations (1.1) and obtain

$$\alpha \frac{\partial \tilde{U}}{\partial \xi} + \frac{\partial \tilde{V}}{\partial Z_2} + \beta \frac{\partial \tilde{W}}{\partial \xi} = 0, \tag{4.152a}$$

$$-\alpha (V + c_0) \frac{\partial \tilde{U}}{\partial \xi} = -\alpha \frac{\partial \tilde{P}}{\partial \xi} + \frac{\partial^2 \tilde{U}}{\partial Z_2^2}, \tag{4.152b}$$

$$\frac{\partial \tilde{P}}{\partial Z_2} = 0, \tag{4.152c}$$

$$-\alpha (V + c_0) \frac{\partial \tilde{W}}{\partial \xi} = -\beta \frac{\partial \tilde{P}}{\partial \xi} + \frac{\partial^2 \tilde{W}}{\partial Z_2^2}, \tag{4.152d}$$

subject to the usual no-slip conditions

$$\tilde{U} = \tilde{V} = \tilde{W} = 0 \quad \text{on } Z_2 = 0. \tag{4.152e}$$

In view of (4.152c), the pressure throughout the wall layer is independent of Z_2. Matching the pressure within the viscous wall layer (4.151) as $Z_2 \to \infty$ with the pressure in the inviscid region (4.94d) as $y \to -1$ we conclude that

$$\tilde{P} = A_0 P_2(-1) \cos(\xi). \tag{4.153}$$

Substituting the expression for $\tilde{P}$ into (4.152b) and (4.152d) results in a system of linear equations, namely

$$-\alpha (V + c_0) \frac{\partial \tilde{U}}{\partial \xi} = \alpha A_0 P_2(-1) \sin(\xi) + \frac{\partial^2 \tilde{U}}{\partial Z_2^2}, \tag{4.154a}$$

$$-\alpha (V + c_0) \frac{\partial \tilde{W}}{\partial \xi} = \beta A_0 P_2(-1) \sin(\xi) + \frac{\partial^2 \tilde{W}}{\partial Z_2^2}. \tag{4.154b}$$

We note that $\tilde{W} = (\beta/\alpha)\tilde{U}$ which is an immediate consequence of (4.154a) and (4.154b), and hence it suffices to consider only (4.154a). The solution of (4.154a) is sought in the normal-mode-form

$$\tilde{U} = \mathrm{Re}(f_2(Z_2)\exp(\mathrm{i}\xi)). \tag{4.155}$$

Inserting (4.155) into (4.154a) leads to the inhomogeneous second order differential equation satisfied by the function f_2:

$$\frac{d^2 f_2}{dZ_2^2} + \mathrm{i}\alpha(V + c_0)f_2 = \mathrm{i}\alpha A_0 P_2(-1). \tag{4.156}$$

Taking account of the no-slip on $Z_2 = 0$ and boundedness conditions as $Z_2 \to \infty$ the solution of (4.156) can be expressed in the form:

$$f_2(Z_2) = \left(\frac{A_0 P_2(-1)}{V + c_0}\right)(1 - \exp(-m_2 Z_2)), \tag{4.157}$$

where $m_2 = (\alpha(V + c_0))^{1/2}\exp(-i\pi/4)$. It then follows that the leading-order disturbance streamwise and spanwise velocity components take the form

$$\tilde{U} = \mathrm{Re}\left\{\left(\frac{A_0 P_2(-1)}{V + c_0}\right)(1 - \exp(-m_2 Z_2))\exp(\mathrm{i}\xi)\right\}, \tag{4.158a}$$

$$\tilde{W} = \mathrm{Re}\left\{\left(\frac{\beta A_0 P_2(-1)}{\alpha(V + c_0)}\right)(1 - \exp(-m_2 Z_2))\exp(\mathrm{i}\xi)\right\}. \tag{4.158b}$$

Substituting for $\tilde{U}$ and $\tilde{W}$ from (4.158a), (4.158b) into the continuity equation (4.152a), we obtain the differential equation governed by $\tilde{V}$, namely

$$\frac{\partial \tilde{V}}{\partial Z_2} = -\mathrm{Re}\left\{\left(\frac{\mathrm{i}A_0 P_2(-1)(\alpha^2 + \beta^2)}{\alpha(V + c_0)}\right)(1 - \exp(-m_2 Z_2))\exp(\mathrm{i}\xi)\right\}.$$

Imposing the no-slip condition (4.152e) we find that the solution of this equation is

$$\tilde{V} = -\mathrm{Re}\left\{\left(\frac{\mathrm{i}A_0 P_2(-1)(\alpha^2 + \beta^2)}{\alpha(V + c_0)}\right)\left(Z_2 + \frac{\exp(-m_2 Z_2)}{m_2} - \frac{1}{m_2}\right)\exp(\mathrm{i}\xi)\right\}.$$

Analyzing the expression for $\tilde{V}$ in the limit $Z_2 \to \infty$ leaves

$$v \sim \varepsilon^2 R^{-1/2}\left(\frac{A_0 P_2(-1)(\alpha^2 + \beta^2)}{\alpha(c_0 + V)}\right)[Z_2 \sin(\xi) - (2\alpha(c_0 + V))^{-1/2}(\sin(\xi) + \cos(\xi))]. \tag{4.159}$$

From letting $y \to -1$ we see that the normal velocity within the inviscid region (4.94b) has the form

$$v \sim \varepsilon^2 R^{-1/2} A_0 Z_2 G_2'(-1)\sin(\xi) + \cdots + \varepsilon^2 R^{-1/2} v_5 + \cdots, \tag{4.160}$$

since $G_2(-1) = 0$. Here the term proportional to Z_2 in (4.159) provides match with (4.160) which yields the expression for $G_2'(-1)$, while the term independent of Z_2 gives the asymptotic form for v_5 as

$$G_2'(-1) = \frac{P_2(-1)(\alpha^2+\beta^2)}{\alpha(V+c_0)}, \tag{4.161a}$$

$$v_5 \sim -\frac{2A_0P_2(-1)(\alpha^2+\beta^2)}{(2\alpha(V+c_0))^{3/2}}(\sin(\xi)+\cos(\xi)) \quad \text{as } y \to -1. \tag{4.161b}$$

(e) Derivation of the amplitude equation

The critical layer analysis in section 4.2.2(b) has revealed that the components (u_5, v_5, w_5, p_5) contain terms of the form

$$A_0[F_5(y)\sin(\xi), -G_5(y)\cos(\xi), H_5(y)\sin(\xi), P_5(y)\sin(\xi)]. \tag{4.162}$$

After substitution into the Navier–Stokes equations (1.1) and some manipulation we infer that G_5 satisfies the same Rayleigh equation as G_2, namely

$$(U_0 - c_0)(G_5'' - (\alpha^2+\beta^2)G_5) = U_0''G_5, \tag{4.163}$$

subject to the boundary conditions

$$G_5(1) = \frac{2A_0P_2(1)(\alpha^2+\beta^2)}{(2\alpha(c_0-V))^{3/2}}, \quad G_5(-1) = -\frac{2A_0P_2(-1)(\alpha^2+\beta^2)}{(2\alpha(c_0+V))^{3/2}}, \tag{4.164}$$

deduced from the behaviour of v_5 in (4.149b) and (4.161b). The method used to derive the jump conditions on the derivative of G_5 across the critical layers is described in Appendix C and it gives the result that

$$[[G_5']]_{y_1^-}^{y_1^+} = \frac{2C^{(1)}}{A_0^{1/2}b_1M_1^{1/2}}, \quad [[G_5']]_{y_2^-}^{y_2^+} = -\frac{2C^{(2)}}{A_0^{1/2}b_2M_2^{1/2}}. \tag{4.165}$$

Multiplying the equation for $G_5(y)$ by $G_2(y)/(U_0 - c_0)$, integrating with respect to y over the flow domain and using the equation (4.97) for G_2 results in the Wronskian of G_2 and G_5

$$[[G_2G_5' - G_5G_2']]_{-1}^{y_2^-} + [[G_2G_5' - G_5G_2']]_{y_2^+}^{y_1^-} + [[G_2G_5' - G_5G_2']]_{y_1^+}^{1} = 0. \tag{4.166}$$

After some simple manipulations and demanding the inviscid conditions of tangential flow on G_2 namely (4.98) we can write (4.166) in an appropriate form as

$$[[G_2G_5']]_{y_2^+}^{y_2^-} + \underbrace{[[G_5G_2']]_{y_2^-}^{y_2^+}}_{=0} + [[G_2G_5']]_{y_1^+}^{y_1^-} + \underbrace{[[G_5G_2']]_{y_1^-}^{y_1^+}}_{=0} = G_2'(1)G_5(1) - G_5(-1)G_2'(-1),$$

where the underbraced quantities are equal to zero because we have

$$[[G_5G_2']]_{y_1^-}^{y_1^+} = \{\text{finite part of } G_2'\}\underbrace{[[G_5]]_{y_1^-}^{y_1^+}}_{=0} = 0, \quad [[G_5G_2']]_{y_2^-}^{y_2^+} = \{\text{finite part of } G_2'\}\underbrace{[[G_5]]_{y_2^-}^{y_2^+}}_{=0} = 0,$$

in view of the fact that the finite part of the net jump in G_5 across the critical layers is trivial. From the series solution (4.100) for G_2 we draw the inference that

$$[[G_2G_5']]_{y_1^+}^{y_1^-} = g_1^{(0)}[[G_5']]_{y_1^+}^{y_1^-}, \quad [[G_2G_5']]_{y_2^+}^{y_2^-} = g_2^{(0)}[[G_5']]_{y_2^+}^{y_2^-}.$$

Substitution of the boundary and jump conditions on G_5 from (4.164) and (4.165), together with use of (4.149a) and (4.161a), leads to the expression

$$A_0 = 2(-\alpha C^{(1)})^{2/3}\left(\left|\frac{g_1^{(0)}}{b_1}\right|^{1/2} + \left|\frac{g_2^{(0)}}{b_2}\right|^{1/2}\right)^{2/3}\left(\frac{(G_2'(1))^2}{(c_0-V)^{1/2}} + \frac{(G_2'(-1))^2}{(c_0+V)^{1/2}}\right)^{-2/3}, \qquad (4.167)$$

determining explicitly the amplitude dependence of the nonlinear upper branch modes. The value of $G_2'(1)$ is normalized to unity and for given sliding speed V and the spanwise wavenumber β, the normal velocity amplitude A_0 in (4.167) is fixed, once $g_1^{(0)}$, $g_2^{(0)}$, $G_2'(-1)$, α and c_0 are calculated by solving numerically the Rayleigh problem posed in section 4.2.2(a).

4.2.3 Results for the strongly nonlinear regime

(a) Numerical Method

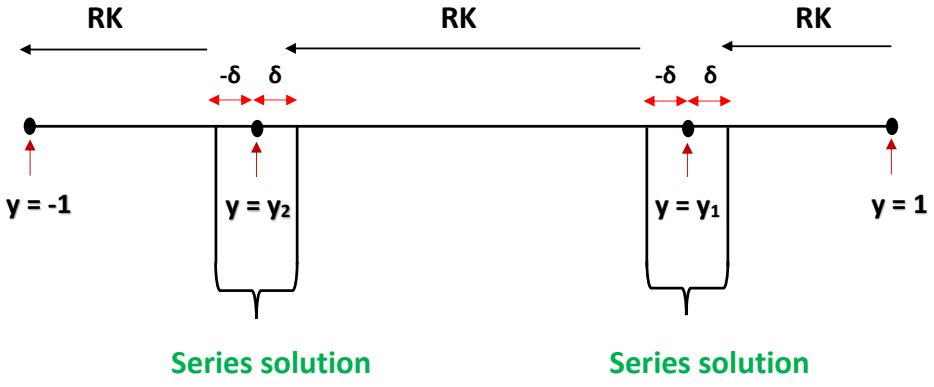

Figure 4.7: Sketch illustrating the procedure used to solve (4.97).

First we describe the numerical method formulated to solve the Rayleigh equation (4.97) for the normal velocity eigenfunctions $G_2(y)$ with the boundary conditions (4.98) and the

jump condition (4.103). Our procedure is as follows. With the wall sliding speed V, spanwise wavenumber β and phase speed c_0 prescribed, we guess a value of the streamwise wavenumber α. Then using the conditions $G_2(1) = 0$, $G_2'(1) = 1$, a Runge–Kutta (RK) solution of (4.97) is initiated in the region from $y = 1$ to $y = y_1 + \delta$ where δ is taken small, typically 0.001. The continuity of G_2 at the junction $y = y_1 + \delta$ is assured by equating the values of G_2, G_2' computed from the series solution (4.100) with those from the RK approach: this determines $g_1^{(0)}$ and $g_1^{(1)}$. Applying the jump condition (4.103), we consider the series solution (4.100) for $y < y_1$ and evaluate $G_2(y_1 - \delta)$, $G_2'(y_1 - \delta)$. These quantities are then used to perform an RK march in the region from $y = y_1 - \delta$ to $y_2 + \delta$. At $y = y_2 + \delta$, the values of G_2, G_2' due to the power series (4.100) with $i = 2$ and those arising from the RK method are equated, thus fixing $g_2^{(0)}$ and $g_2^{(1)}$. These values are then used to calculate $G_2(y_2 - \delta)$ and $G_2'(y_2 - \delta)$ from the series solution (4.100) for $y < y_2$. Finally, we march (4.97) inwards from $y = y_2 - \delta$ to $y = -1$, where we calculate $G_2(-1)$. Newton iteration on α is then applied until this quantity is zero to some suitable tolerance. Once the solution for α is obtained, the value of $G_2'(-1)$ is known and the amplitude A_0 of the neutral modes can then be determined from (4.167). We repeat the procedure for a range of values of V, β and c_0. A schematic of the numerical procedure is given in figure 4.7.

(b) Numerical results

Figure 4.8(a,b) displays the amplitude-dependent neutral stability results giving α, c_0 as functions of the amplitude A_0 for various values of V for the case of zero spanwise wavenumber. We observe that for a given V the streamwise wavenumber and dominant phase speed increase monotonically as the amplitude is increased, indicating that the wavelength of the neutral modes is shortening. In addition, we see that on these plots there are lower cut-off values (α_c and c_c, say), being functions of the sliding speed, and the range of amplitudes over which the instability exists is reduced, particularly at larger values of V. Figure 4.8(c) shows that an increase in the sliding speed results in the movement of the critical layer y_2 away from the lower wall, while the critical layer y_1 heads towards the upper wall. In figure 4.8(d) we show the nonlinear dispersion relation $c_0(\alpha)$ which of course resembles figure 4.8(b) given the monotonic behaviour for $\alpha(A_0)$ mentioned above. The numerical solutions to the three-dimensional Rayleigh equation (4.97) exist for a range of non-zero spanwise wavenumbers, for example, $\beta = 1, 3$, as shown in figures 4.9 and 4.10. The general trends described above for $\beta = 0$ remain unchanged, but it is interesting to notice that c_c is also a function of the spanwise wavenumber, and its value increases with increasing β. In figure 4.11(a-c) we plot the difference in critical layer location versus amplitude for various sliding velocities and spanwise wavenumbers. It is observed that at large amplitude the critical layers appear ever closer together. In order to gain more insight into this potential merging process, it is instructive to examine the Rayleigh problem in the large-amplitude limit $A_0 \gg 1$, and this is carried out in the next subsection. We also found that solutions were confined to sliding velocities in the range $0 \leq V < 2$. As V approaches 2, the maximum of the basic flow (2.2) becomes located on the upper wall, and the numerical results suggest that the asymptotic

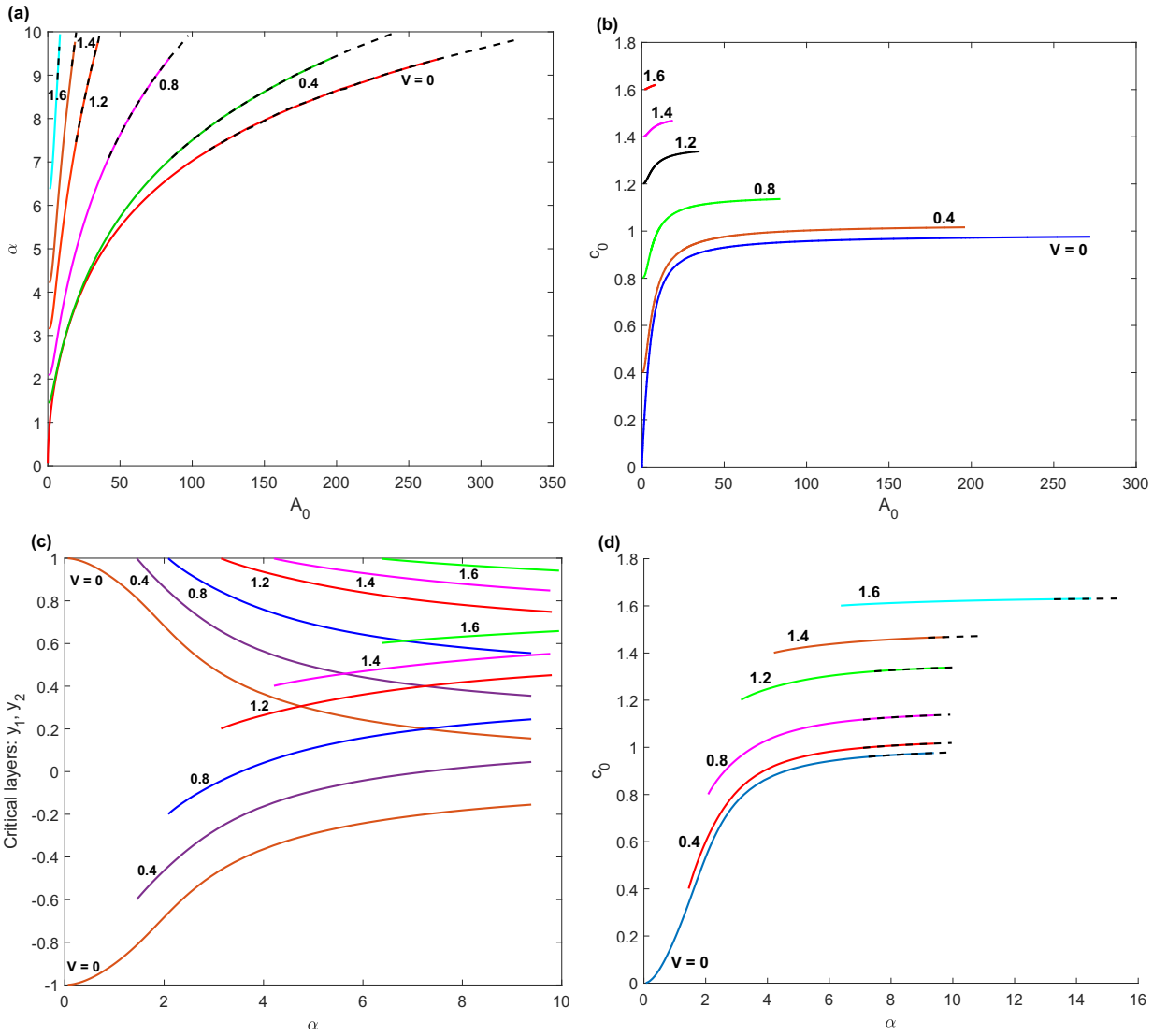

Figure 4.8: Neutral mode results for $\beta = 0$ and various wall sliding speeds V. (a) Streamwise wavenumber α versus amplitude A_0. (b) Phase speed c_0 versus A_0. (c) Critical layers location y_1, y_2 versus α. (d) Phase speed c_0 versus streamwise wavenumber α. Here and in figures 4.9 and 4.10, the dashed curves are the large-amplitude asymptotes computed from the theory of section 4.2.3(c).

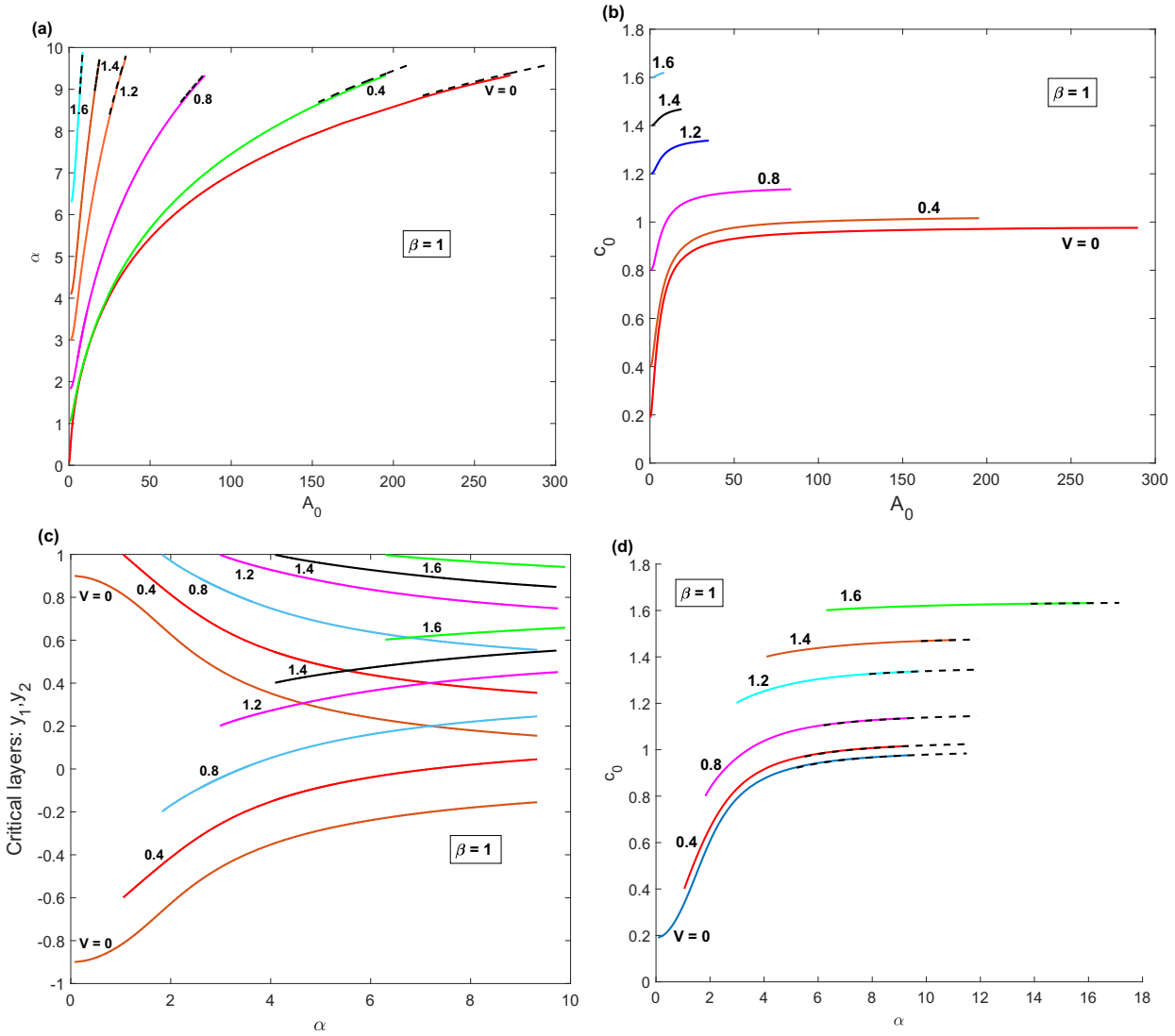

Figure 4.9: Neutral mode results for $\beta = 1, 3$ and various wall sliding speeds V. (a,e) Streamwise wavenumber α versus amplitude A_0. (b,f) Phase speed c_0 versus A_0. (c,g) Critical layers location y_1, y_2 versus α. (d,h) Phase speed c_0 versus streamwise wavenumber α.

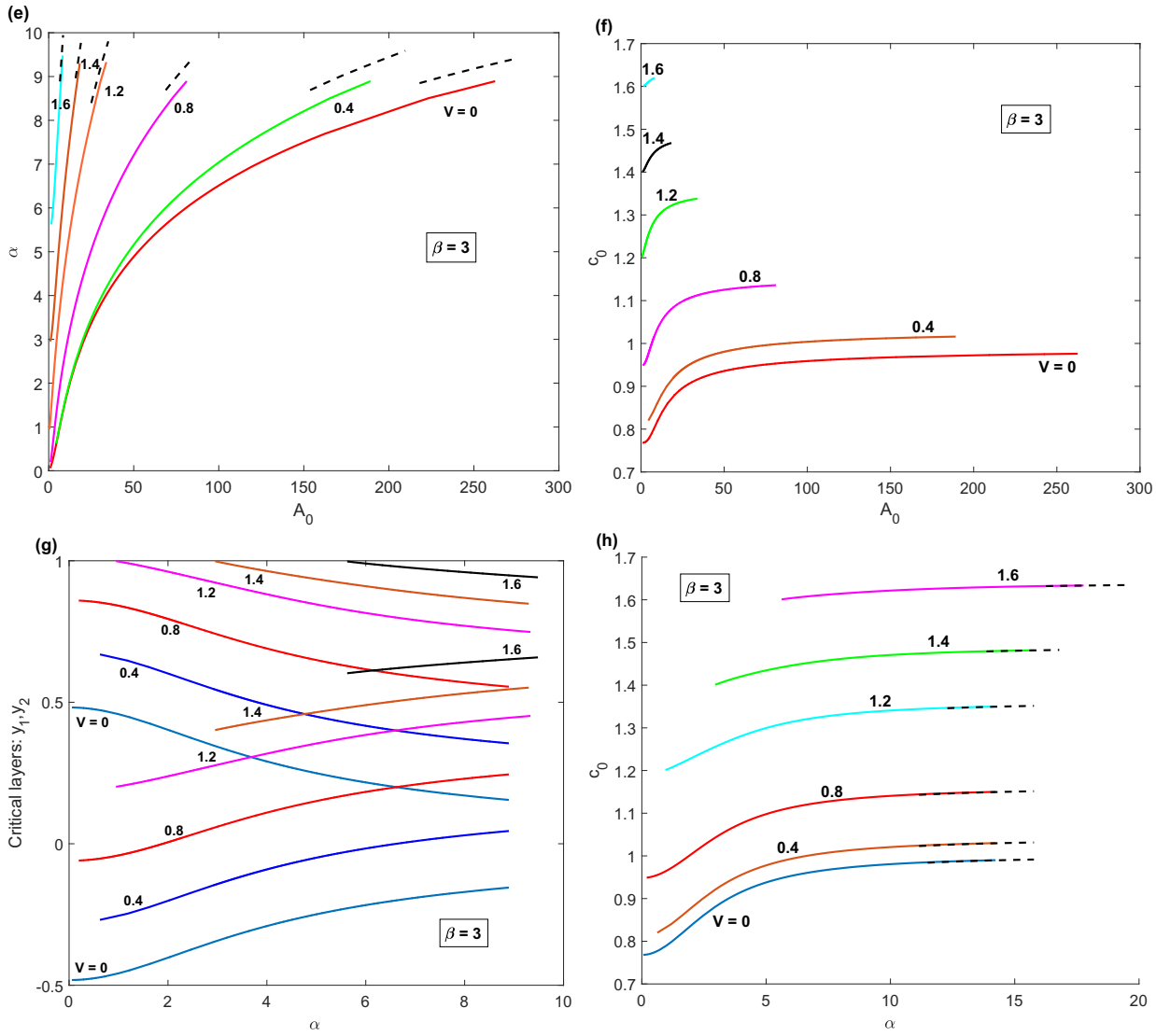

Figure 4.10: For caption see facing page.

structure considered in subsection 4.2.2 breaks down. Indeed, as V increases to around 1.8, the critical layers become sited in the vicinity of the upper wall which adds complications to the numerical matching of the RK and series solutions at the appropriate junctions. To overcome this we adopt an asymptotic approach to the Rayleigh problem in the limit $V \to 2$ which is the subject of a brief discussion in section 4.2.3(d) with this paving the way for the identification of the flow scalings and asymptotic structure in the new regime.

(c) Analysis of the nonlinear modes in the large amplitude limit

The numerical calculations just presented suggest that this limit, in which the two critical layers approach the location $y = V/2$ with $V \neq 2$, is worthy of further investigation. Examination of figures 4.8, 4.9, 4.10 suggests that as $A_0 \to \infty$ we have $\alpha \to \infty$, $y_1 \to (V/2)^+$ and $y_2 \to (V/2)^-$ with $c_0 \to 1 + V^2/4$ in view of figure 4.6(b). For $|y_1 - y_2| \ll 1$ solutions of (4.97), (4.98) are sought with α large and $O(y_1 - y_2)^{-1}$. Then the main variation of G_2 occurs when $y = V/2 + (y_1 - y_2)\hat{y}$ with $-\infty < \hat{y} < \infty$, and so the dominant scalings are

$$\alpha = (y_1 - y_2)^{-1}\hat{\alpha},\ G_2 = (y_1 - y_2)\hat{G}_2(\hat{y}),\ g_1^{(0)} = (y_1 - y_2)\hat{g}_1^{(0)},\ g_2^{(0)} = (y_1 - y_2)\hat{g}_2^{(0)}, \quad (4.168)$$

where the $O(1)$ constants $\hat{\alpha}$, $\hat{g}_1^{(0)}$ and $\hat{g}_2^{(0)}$ are to be determined, while the leading order phasespeed is given by $c_0 = 1 + V^2/4 - (y_1 - y_2)^2/4$. Taking into account the scalings (4.168), the Rayleigh equation (4.97) reduces to

$$\frac{d^2\hat{G}_2}{d\hat{y}^2} - \hat{\alpha}^2\hat{G}_2 = \left(\frac{2}{\hat{y}^2 - 1/4}\right)\hat{G}_2, \quad (4.169)$$

at leading order, while the appropriate boundary conditions (4.98), (4.103) respectively transform as

$$\hat{G}_2(-\infty) = 0, \quad \hat{G}_2(\infty) = 0, \quad \text{zero velocity jump at } \hat{y} = \pm 1/2. \quad (4.170)$$

It is easy to establish the series solutions of (4.169) about the regular singular points $\hat{y} = \pm 1/2$ with unknowns $\hat{g}_i^{(0)}$, $\hat{g}_i^{(1)}$, with $i \in \{1, 2\}$, which are determined numerically by solving (4.169), (4.170) in an infinite domain. Imposing the normalization condition $\hat{G}_2'(\infty) = 1$ we employ a numerical method very similar to that outlined in section 4.2.3(a) to obtain the neutral value $\hat{\alpha} \approx 2.90812$ independent of the value of spanwise wavenumber β. With (4.168) holding, the amplitude equation (4.167) then reduces to

$$A_0 \sim 2^{1/3}\left(-\hat{\alpha}C^{(1)}(2 - V)\right)^{2/3}\left(|\hat{g}_1^{(0)}|^{1/2} + |\hat{g}_2^{(0)}|^{1/2}\right)^{2/3}(y_1 - y_2)^{-2/3} \text{ as } y_1 - y_2 \to 0, \quad (4.171)$$

where we have used (4.108) for b_i. We can utilise (4.171) to construct large amplitude asymptotes for the wavenumber and phase speed of the disturbance and these are shown by dashed curves in figures 4.8, 4.9 and 4.10: in each case excellent agreement with the full computations can be observed.

Using the result (4.171) and the asymptotic forms (4.168) we make the following observation in the critical layer variable scaling (4.115) in this limit:

$$\underbrace{\frac{\partial}{\partial\xi}}_{O(1)} = \underbrace{\frac{\partial}{\partial\hat{\xi}}}_{O(1)} - \underbrace{\lambda_i \sin(\xi)}_{O(A_0^{-1/2})}\frac{\partial}{\partial\eta_i}, \quad \frac{\partial}{\partial Y_i} = \underbrace{\alpha b_i}_{O(1)}\left(Y_i + \frac{\tilde{b}_i}{b_i}\right)\frac{\partial}{\partial\eta_i}, \tag{4.172}$$

where we have used (4.108) for λ_i and the scaling for α in (4.168). The multi-scaling (4.172) implies that η_i must decrease to order $(y_1 - y_2)^{1/3}$, and therefore the critical-layer variable scales as $Y_i \sim O(y_1 - y_2)^{1/6}$, while the expression for the vorticity jump (4.130) yields $\tilde{b}_i/b_i \sim O(y_1 - y_2)^{-5/6}$. The nonlinear structure set out in subsection 4.2.2 breaks down when the gap $(y_1 - y_2)$ between the critical layers becomes comparable with their individual thicknesses $R^{-1/6}Y_i$. In view of the scaling for Y_i deduced above, a new regime is encountered when $y_1 - y_2 \sim R^{-1/6}(y_1 - y_2)^{1/6}$, implying that a unified critical layer is positioned at $y = V/2$ with thickness $O(R^{-1/5})$. It follows that the streamwise wavenumber increases to $O(R^{1/5})$ with this shortening in lengthscale leading to a reconsideration of the thickness of the Stokes layers III± in figure 4.6(a). Balancing the terms $\alpha(U_0 - c)$ and $R^{-1}\partial/\partial y^2$ within the wall layers we infer that these regions are now reduced in thickness to $O(R^{-3/5})$. Note that, since $A_0 \sim R^{2/15}$ from (4.171), we deduce that the appropriate disturbance amplitude for the new structure is $\Delta = R^{-1/3}A_0 \sim R^{-1/5}$. This larger amplitude five-zone regime is sketched in figure 4.12(a) and will form the focus of subsequent work.

(d) Analysis of the nonlinear modes in the limit $V \to 2$

In this limit, where the maximum of the basic flow (2.2) is attained on the upper wall, the critical layers also merge but at a location arbitrarily close to that upper boundary, rendering numerical computation difficult. For $|2 - V| \ll 1$ we seek solutions of (4.97), (4.98) with α large and of order $(2 - V)^{-1}$. Then the main alteration to G_2 arises when $y = 1 - (2 - V)\tilde{y}$ with $0 \le \tilde{y} < \infty$, and so the leading-order scalings are

$$\alpha = (2 - V)^{-1}\tilde{\alpha},\ G_2 = -(2 - V)\tilde{G}_2(\tilde{y}),\ g_1^{(0)} = -(2 - V)\tilde{g}_1^{(0)},\ g_2^{(0)} = -(2 - V)\tilde{g}_2^{(0)}, \tag{4.173}$$

where the $O(1)$ constants $\tilde{\alpha}$, $\tilde{g}_1^{(0)}$ and $\tilde{g}_2^{(0)}$ are to be evaluated. Under the scaling (4.173), the Rayleigh equation (4.97) reduces to

$$\frac{d^2\tilde{G}_2}{d\tilde{y}^2} - \tilde{\alpha}^2\tilde{G}_2 = \left(\frac{2}{\tilde{y}^2 - \tilde{y} + \tilde{c}}\right)\tilde{G}_2, \tag{4.174}$$

while the appropriate boundary conditions (4.98) and (4.103) respectively become

$$\tilde{G}_2(\infty) = 0, \quad \tilde{G}_2(0) = 0, \quad \text{zero velocity jump at } \tilde{y} = (1 \pm \sqrt{1 - 4\tilde{c}})/2. \tag{4.175}$$

Here the phase speed perturbation parameter

$$\tilde{c} = (c_0 - V)/(2 - V)^2, \tag{4.176}$$

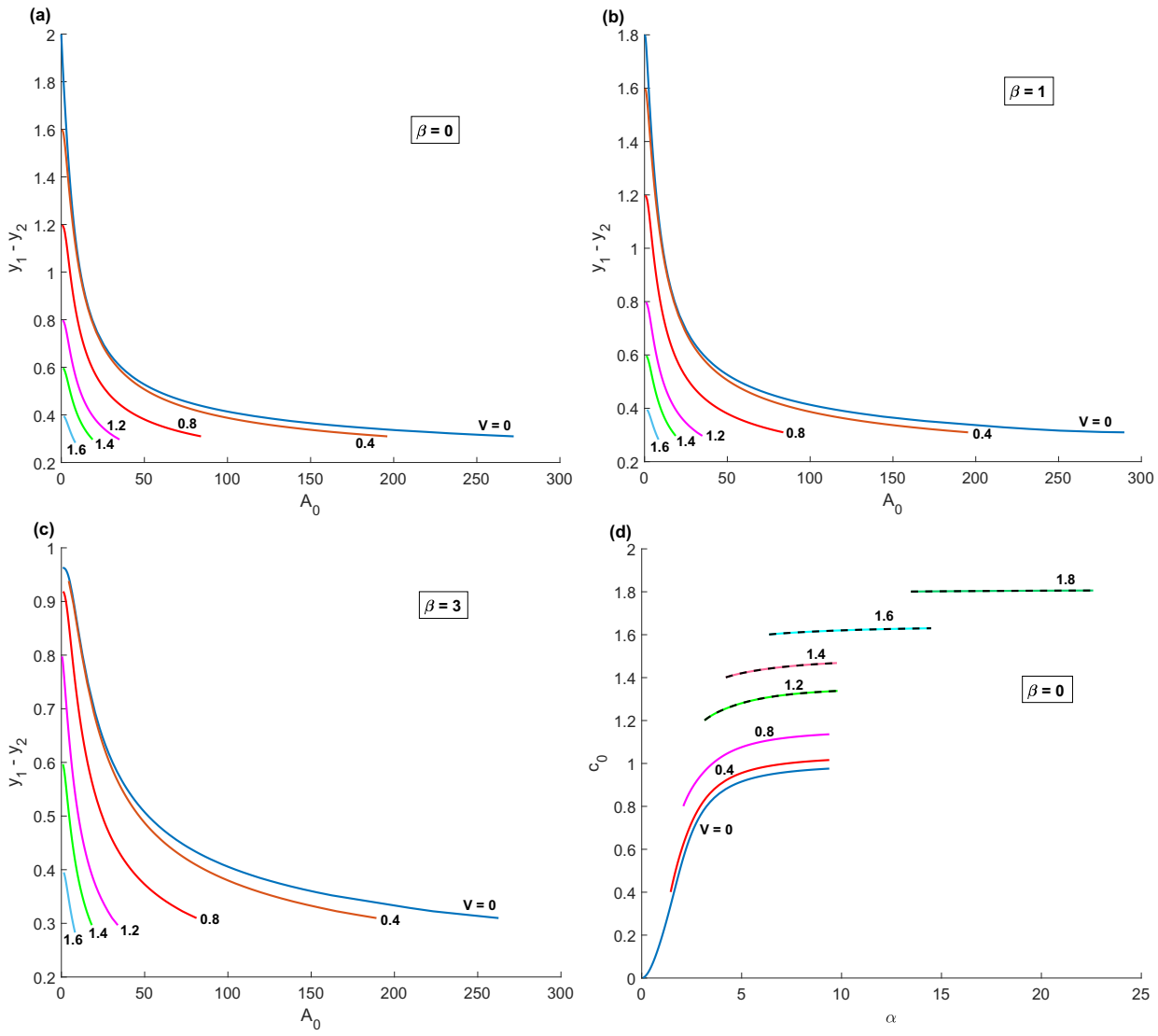

Figure 4.11: (a), (b) and (c): Difference in the critical layers location $(y_1 - y_2)$ versus amplitude A_0 for various values of β. (d) Nonlinear dispersion relation in the limit $V \to 2$. The solid curves are the full computations from the theory of section 4.2.2, while the dashed curves are the corresponding asymptotes obtained from the theory of section 4.2.3(d).

is an $O(1)$ quantity whose value lies in the interval $(0, 1/4)$, given that $V < c_0 < 1 + V^2/4$. In terms of this quantity the critical layer gap may be expressed in the form

$$y_1 - y_2 = (2 - V)\sqrt{1 - 4\tilde{c}}, \tag{4.177}$$

from (4.175) and the scaling for y just above (4.173). The numerical solution to the problem (4.174), (4.175), which again is independent of the value of β, allows us to calculate $\tilde{\alpha}$, $\tilde{g}_1^{(0)}$ and $\tilde{g}_2^{(0)}$ as functions of $\tilde{c}$. If we analyze the amplitude expression (4.167) under the scalings (4.173), (4.176), (4.177), together with the normalization condition $\tilde{G}_2'(0) = 1$ we find that

$$A_0 \to 2(-\tilde{\alpha}C^{(1)})^{2/3}\left(\left|\tilde{g}_1^{(0)}\right|^{1/2} + \left|\tilde{g}_2^{(0)}\right|^{1/2}\right)^{2/3}\left(\frac{\tilde{c}}{\sqrt{1 - 4\tilde{c}}}\right)^{1/3} \text{ as } V \to 2-, \tag{4.178}$$

implying that the size of the disturbance amplitude remains unchanged in this limit, namely $\Delta = O(R^{-1/3})$. Using this result we can calculate the nonlinear dispersion relation $c_0(\alpha)$ in the limit $V \to 2$ and this is represented for the case $\beta = 0$ by dashed curves on figure 4.11(d) alongside the full computations for various V. Similar results can be obtained for non-zero β and in all cases there is excellent agreement between the full numerics and asymptotic theory as $V \to 2$.

In this limit, since both critical layers are approaching the upper wall while the gap between them is diminishing, it follows that our nonlinear structure will break down when $V - 2$ is sufficiently close to zero. From (4.108), (4.109), (4.173) the critical layers have reduced in thickness to $O(R^{-1/6}(2 - V)^{1/2})$, while the gap between them is $O(2 - V)$ from (4.177). The critical layers therefore merge when

$$2 - V = O(R^{-1/3}). \tag{4.179}$$

However, since the critical layers are heading towards the upper wall in this limit, we also need to take into account the thickness of the upper Stokes layer which is formally $O(\alpha R(c_0 - V))^{-1/2}$ from balancing the effects of inertia and viscosity. In view of the scalings for α and $c_0 - V$ in (4.173), (4.176) the thickness of this layer increases to $O(R^{-1/2}(2 - V)^{-1/2})$. The critical layers therefore become embedded in the wall layer when $2 - V \sim O(R^{-1/2}(2 - V)^{-1/2})$ which again leads to the distinguished scaling (4.179). Thus, when V is sufficiently close to 2 that this scaling comes into play, the critical layers merge and move into an $O(R^{-1/3})$ thick upper wall layer which is now nonlinear in nature, with the streamwise scaling shortening, also to $O(R^{-1/3})$. The dynamics of the lower Stokes layer remains essentially the same as in the previous regime, although in view of the shortened lengthscale it reduces to an $O(\alpha^{-1/2}R^{-1/2}) \sim O(R^{-2/3})$ thickness. A sketch of the new asymptotic framework is shown in figure 4.12(b). Again, we plan to study this novel structure, cf. the production layer in more detail in the future.

4.2.4 Conclusions

Figure 4.13 illustrates the interconnections between the asymptotic stability theories we have considered here as a function of the disturbance size Δ superimposed on the basic PPCF

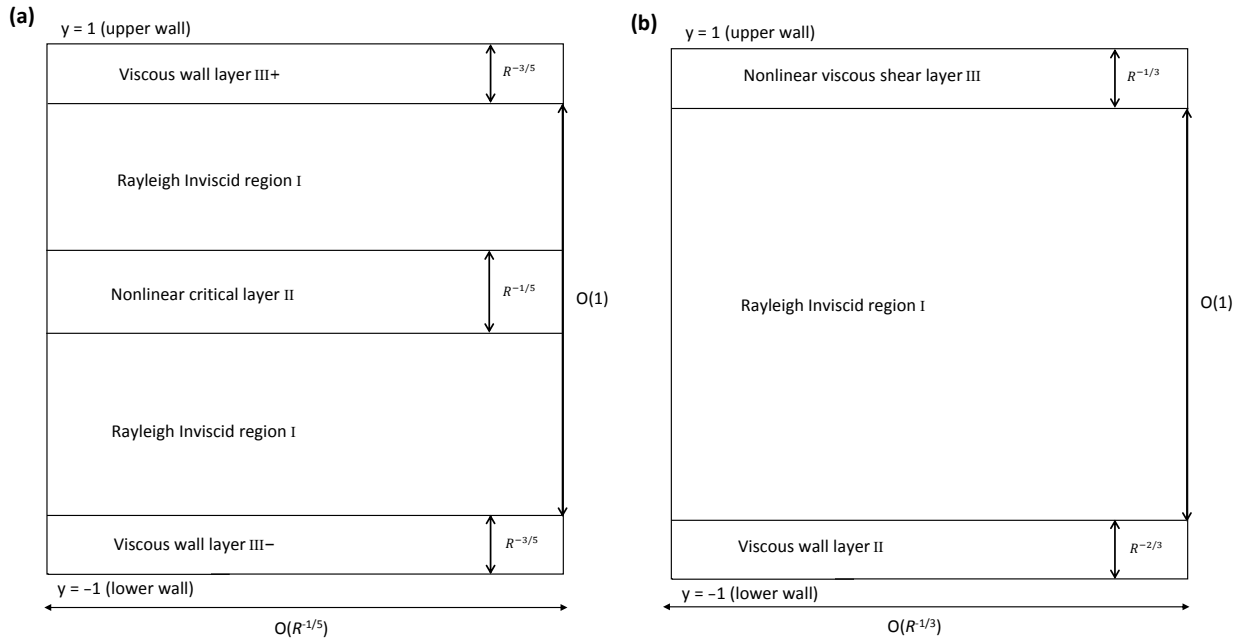

Figure 4.12: (a) The five zone single critical layer structure with a short streamwise scaling that emerges at $O(R^{-1/5})$ amplitude. (b) The short-scaled asymptotic structure that holds for $2 - V \sim O(R^{-1/3})$ in which the critical layers have merged and fused with the upper Stokes layer to form a nonlinear viscous shear layer.

state (2.2). Our main asymptotic and numerical results may be summarized as follows.

(i) An examination of the classical nine-zone asymptotic structure of the linear upper branch mode for PPCF inclusive of spanwise wavenumber leads to the establishment of the three-dimensional upper-branch eigenrelations. Investigation of the viscous critical layers sited within their respective shear layers reveals that the structure associated with this mode alters slightly when Δ increases to $O(R^{-14/33})$, with the critical layers acquiring weakly nonlinear characteristics including a reduced phase shift.

(ii) From the consideration of the weakly nonlinear structure as the disturbance amplitude is increased further we show in subsection 4.2.1 that a strongly nonlinear regime emerges at $\Delta = O(R^{-1/3})$ with this structure forming our focus in 4.2.2. The new structure involves two critical layers sited within an inviscid core region at locations which are dependent on the amplitude-dependent phase speed of the disturbance. These layers are of an equilibrium, inviscid, fully nonlinear type and possess flow structures which bear some similarities to those previously studied by Smith & Bodonyi (1982a), Walton (2002) and Walton (2003) among others. The amplitude-dependence of the neutral modes is determined by a method of balancing the phase shifts across the critical layers with those induced by the Stokes layers adjacent to the channel walls.

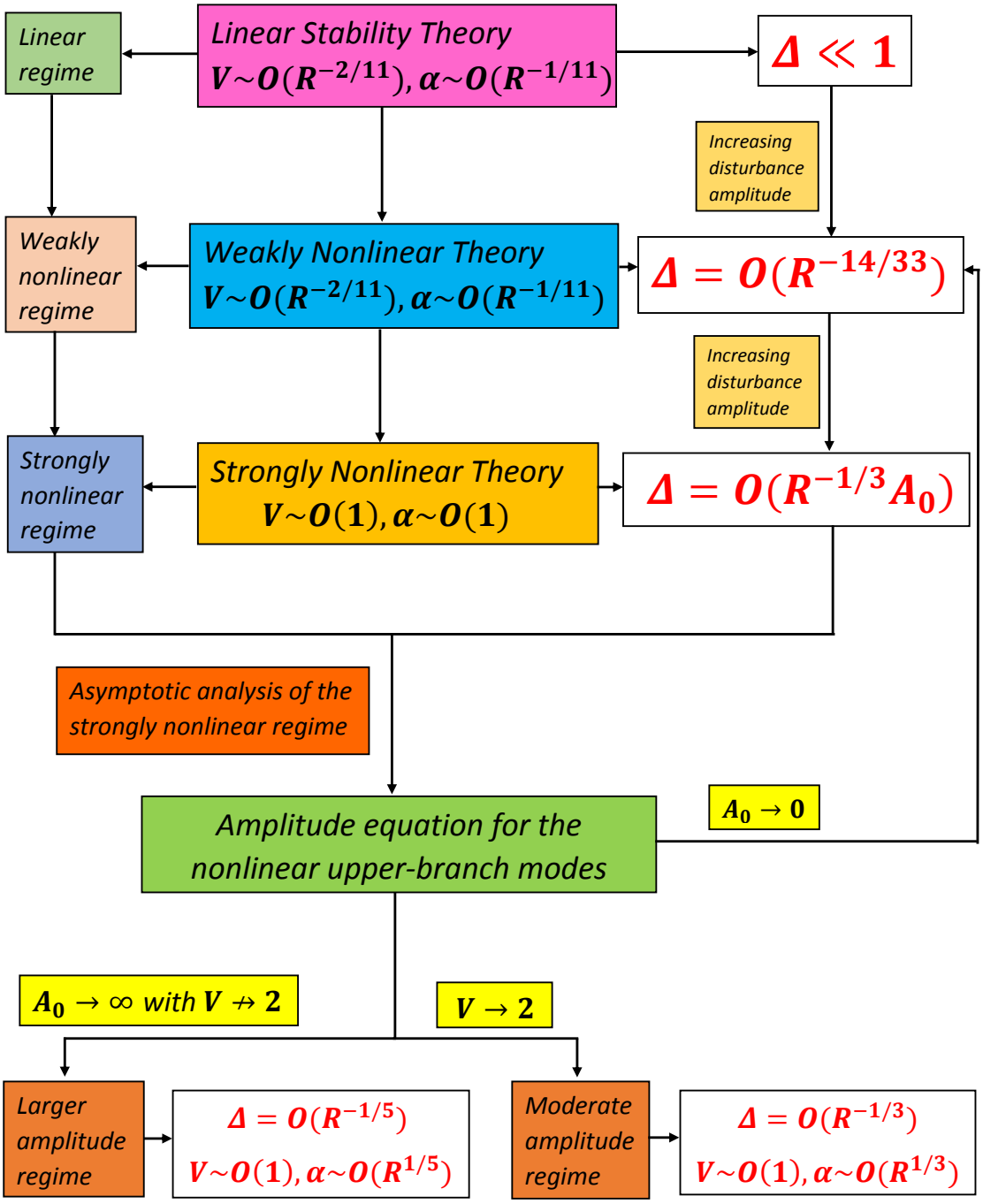

Figure 4.13: Diagram showing the dependence of various regimes on the disturbance size Δ.

(iii) The numerical results presented in subsection 4.2.3 establish the existence of such modes over a wide range of $O(1)$ wavenumbers and for sliding speeds in the range $0 \leq V < 2$ with the $O(1)$ dominant phase speed lying between the minimum and maximum of the basic PPCF. We note that these instability modes exist at sliding speeds well in excess of the linear instability cut-off. Investigation of the strongly nonlinear structure in the large amplitude limit, when the two critical layers merge, is performed in subsection 4.2.3(c), and the new short-scaled structure that emerges is discussed in some detail. The nonlinear stability structure set out in subsection 4.2.2 also breaks down in the limit $V \to 2$ when, in addition to the merging described above, the critical layers penetrate the upper Stokes layer to form a new nonlinear near-wall region. The new structure found here is identical to the boundary-region structure uncovered by Kumar & Walton (2019) for nonlinear disturbances bifurcating from the upper neutral curve in figure 2.3(c). A systematic study of the asymptotic structures corresponding to the new regimes shown in figure 4.12 will form the focus of future work.

(iv) Finally, one of the main achievements is the establishment that three-dimensional nonlinear neutral modes exist in PPCF for disturbances of $O(R^{-1/3})$ when $R \gg 1$.

We have seen that, by using high Reynolds number asymptotic analysis, it is possible to derive two distinct systems of equations which describe three-dimensional nonlinear travelling waves in PPCF. It is demonstrated that that the solutions to one of these systems, in which the phasespeed and sliding speed are almost equal, is relevant to the bifurcation from a previously undetected linear neutral curve which splits from the main curve as the sliding speed increases (see figure 2.3). In the next chapter, we will consider a computational study of PPCF for various values of V and compare the results of the asymptotic theory developed in section 4.1 with travelling wave computations of the full nonlinear two-dimensional Navier–Stokes equations.

Chapter 5

Finite Reynolds numbers numerical solutions

In this chapter, we present a computational study of plane Poiseuille–Couette flow (the exact Navier–Stokes solution arising from the constant pressure-gradient flow driven through a plane channel with sliding walls) for various values of sliding speed V. Two-dimensional nonlinear travelling wave solutions for PPCF, which bifurcates from the linear neutral curves, are found for a range of sliding speed V and disturbance amplitude A by directly solving the full Navier–Stokes equations. The equations are tackled numerically using the Chebyshev collocation method and the Newton–Raphson iteration technique. It is interesting to note that the linear eigenvalue computations in section 5.2 reveal that four neutral curves exist for PPCF at a very small value of sliding speed. In section 5.3, we describe our numerical method for calculating the nonlinear travelling waves. In section 5.4, we first start by describing the nonlinear numerical results for plane Poiseuille flow and then consider non-zero sliding speeds for solutions that bifurcate from the main neutral curve and finally, compare our results with Balakumar (1997). In the remainder of this chapter, we investigate the bifurcation from the additional neutral curves for which there are no existing results in the literature and compare the results obtained from the high-Reynolds-numbers asymptotic theory proposed in subsection 4.1.2 with our Navier–Stokes computations at finite Reynolds number. In particular, we are interested in finding answers to the following questions: (i) how large the Reynolds numbers must be before we obtain reasonable agreement between the solutions; and (ii) is it possible to detect the delicate asymptotic flow structure in the finite Reynolds numbers computations?

5.1 The governing equations in travelling wave form

The basic state of the flow is described in section 2.1 of chapter 2 (see equation (2.2)). We now seek travelling wave solutions to (1.1) of the following form

$$(u, v, p) = (U_0(y) + \hat{u}_0(y), 0, p(x) + \hat{p}_0(y)) + \sum_{n=1}^{\infty} (\hat{u}_n(y), \hat{v}_n(y), \hat{p}_n(y)) E^n + c.c., \qquad (5.1)$$

where $E = \exp(i\alpha(x - ct))$, with U_0 given in (2.2) and the streamwise wavenumber α and wavespeed c both prescribed to be real. Substitution into the Navier–Stokes equations (1.1) and retention of N terms in the sums for computational purposes yields the following equations for $n = 1, \ldots, N$:

$$in\alpha\hat{u}_n + \hat{v}_n' = 0, \tag{5.2}$$

$$\begin{aligned}(R^{-1}D_n^2 - in\alpha(U_0 + \hat{u}_0 - c))\hat{u}_n &= in\alpha\hat{p}_n + \sum_{k=1}^{n-1}(\hat{v}_k\hat{u}_{n-k}' + i(n-k)\alpha\hat{u}_{n-k}\hat{u}_k) \\ &\quad + \hat{v}_n(U_0 + \hat{u}_0)' + \sum_{k=1}^{N-n}(\hat{v}_k^*\hat{u}_{n+k}' + i(n+k)\alpha\hat{u}_{n+k}\hat{u}_k^*) \\ &\quad + \sum_{k=n+1}^{N}(\hat{v}_k\hat{u}_{k-n}^{*\prime} - i(k-n)\alpha\hat{u}_{k-n}^*\hat{u}_k),\end{aligned} \tag{5.3}$$

$$\begin{aligned}(R^{-1}D_n^2 - in\alpha(U_0 + \hat{u}_0 - c))\hat{v}_n &= \hat{p}_n' + \sum_{k=1}^{n-1}(\hat{v}_k\hat{v}_{n-k}' + i(n-k)\alpha\hat{v}_{n-k}\hat{u}_k) \\ &\quad + \sum_{k=1}^{N-n}(\hat{v}_k^*\hat{v}_{n+k}' + i(n+k)\alpha\hat{v}_{n+k}\hat{u}_k^*) \\ &\quad + \sum_{k=n+1}^{N}(\hat{v}_k\hat{v}_{k-n}^{*\prime} - i(k-n)\alpha\hat{v}_{k-n}^*\hat{u}_k).\end{aligned} \tag{5.4}$$

In addition, the governing equations for $\hat{u}_0$ and $\hat{p}_0$ uncouple at $O(E^0)$ from the streamwise and normal momentum balances respectively in (1.1). These may be expressed as

$$R^{-1}D_0^2\hat{u}_0 = \sum_{k=1}^{N}(\hat{v}_k^*\hat{u}_k' + \hat{v}_k\hat{u}_k^{*\prime}), \tag{5.5}$$

$$-\frac{d\hat{p}_0}{dy} = \sum_{k=1}^{N} in\alpha(\hat{u}_k^*\hat{v}_k - \hat{u}_k\hat{v}_k^*) + \sum_{k=1}^{N}(\hat{v}_k^*\hat{v}_k' + \hat{v}_k\hat{v}_k^{*\prime}), \tag{5.6}$$

where $D_n^2 \equiv d^2/dy^2 - n^2\alpha^2$. It is noteworthy that equation (5.6) uncouples from the other equations and so will not be considered further in the analysis. However, it provides the explicit expression for the pressure distortion $\hat{p}_0$. Equations (5.2)–(5.5) are to be solved subject to the usual no-slip boundary conditions

$$\hat{u}_0 = \hat{u}_n = \hat{v}_n = 0 \text{ on } y = \pm 1 \text{ for } n = 1, \ldots, N. \tag{5.7}$$

We begin by splitting the aforementioned equations into their real and imaginary parts, giving us a total of $(6N + 1)$ real equations for the $(6N + 3)$ unknowns $\mathrm{Re}(\hat{u}_n, \hat{v}_n, \hat{p}_n)$,

$\mathrm{Im}(\hat{u}_n, \hat{v}_n, \hat{p}_n)$, the mean flow distortion $\hat{u}_0$, the wavenumber α and wavespeed c. Hence, we need to impose two additional equations so that a unique solution can be obtained for a given Reynolds numbers R. To this end, it remains to observe that (5.2)–(5.5) and (5.7), which constitute the nonlinear eigenvalue problem for c in terms of α, R and V, are invariant under the transformation

$$(\hat{u}_n, \hat{v}_n, \hat{p}_n) \to (\tilde{u}_n, \tilde{v}_n, \tilde{p}_n) \exp(in\Theta), \tag{5.8}$$

where Θ is any real number. It is this property of the eigenvalue problem which can be used to impose a phase normalisation condition. This condition effectively fixes the quantity Θ. The second equation is concerned with the measurement of the amplitude of the travelling wave, which will be discussed in section 5.3, along with the outline of the numerical method of solution employed.

5.2 Linear computations on the hybrid neutral curves

Consideration of infinitesimal travelling wave disturbances with only the first term in the sum in (5.1) followed by elimination of the streamwise velocity and pressure yields the appropriate Orr–Sommerfeld equation given in (2.8) together with the no-slip boundary conditions (2.9). Applying the method of solution, involving Chebyshev collocation at Gauss points, described in Chapter 1, we perform further computations on the upper curve (hybrid curve) in figure 2.3. Typically, we took 100 collocation points, which proved sufficient to obtain six decimal places of accuracy.

We start by presenting in figures 5.1 and 5.2 the neutral curves labelled by **A**, **B** and **C** in the (R, α) and (R, c) planes respectively for PPCF. In figures 5.3 and 5.4, we concentrate on **A**, which closes up at approximately $R = 35500000$ and investigate what happens to the neutral curve as the sliding speed increases. When V is increased in the range $0.019 \leq V \leq 0.023$, we observe that a kink develops in the upper and lower stability boundaries, eventually slicing **A** into two curves **X** and **Y**. Interestingly enough, at around $V \simeq 0.025$, the neutral curve **X** splits further into two curves **B** and **C**, which closes up now as shown in figures 5.5 and 5.6, while it is found that the instability region within **Y** increases and becomes **D** so that there are three distinct curves as indicated schematically in figures 5.7 and 5.8. As V is increased further to 0.0254 (figures 5.9 and 5.10), we see that the curve **B** has thinned substantially and slightly beyond this value of V it disappears completely, and hence only two curves **C** and **D** persist beyond this critical value. Figures 5.11–5.14 display the corresponding neutral stability diagrams for the curve **C** and how it alters as V is increased. It can be seen that the value of the critical Reynolds number increases with an increase in the sliding speed, and the region of instability exists over a large range of Reynolds number.

In figure 5.15, we plot $alr = \alpha R$ against Reynolds number R for various values of sliding speed, and examine what happens to the neutral curve for plane Poiseuille flow ($V = 0$) as V increases. When $V = 0$, there are two values of R for which alr attains a constant

value, and we observe that as V is increased, one of these intersection points moves in such a way that $R \to \infty$. Figure 5.16 indicates that the cut-off velocity at which the main neutral curve shown in figure 2.3 disappears is $V_c \approx 0.34$. This plot is computed from solving a long-wave version of the Orr–Sommerfeld equation (2.8) with the boundary conditions (2.9) (see Cowley & Smith (1985)).

5.3 Numerical method for the nonlinear problem

It is easily seen that the nonlinear eigenvalue problem set out above in section 5.1 can be simplified further by eliminating the streamwise wave component and the pressure and introducing the quantity ϕ_n defined as

$$R^{-1}\phi_n = \hat{v}_n. \tag{5.9}$$

After performing some algebraic manipulations, the equation for ϕ_n is found to be

$$\begin{aligned}\phi_n'''' - 2n^2\alpha^2\phi_n'' + n^4\alpha^4\phi_n - (in\alpha R)\{(U_0+\hat{u}_0-c)(\phi_n''-n^2\alpha^2\phi_n) - (U_0+\hat{u}_0)''\phi_n\} \\ + \sum_{k=1}^{n-1} S_{k,n}^{(1)}(y) + \sum_{k=1}^{N-n} S_{k,n}^{(2)}(y) + \sum_{k=n+1}^{N} S_{k,n}^{(3)}(y) = 0,\end{aligned} \tag{5.10}$$

while the mean flow distortion equation acquires the form

$$D_0^2\hat{u}_0 + \sum_{k=1}^{N} \frac{1}{ik\alpha R}\left(\phi_k^*\phi_k'' - \phi_k\phi_k^{*\prime\prime}\right) = 0, \tag{5.11}$$

and the no-slip boundary conditions modify to

$$\phi_n(\pm 1) = \phi_n'(\pm 1) = \hat{u}_0(\pm 1) = 0, \tag{5.12}$$

for $n = 1, \ldots, N$. The quantities $S_{k,n}^{(i)}$ represent the nonlinear contributions arising from inertial responses and are given as follows:

$$S_{k,n}^{(1)} = -\left(\frac{n}{n-k}\right)\left(\phi_k\phi_{n-k}''' + \phi_k'\phi_{n-k}''\right) + \left(\frac{n}{k}\right)\left(\phi_k'\phi_{n-k}'' + \phi_k''\phi_{n-k}'\right) + n^2\alpha^2\left\{\phi_k\phi_{n-k}' - \left(\frac{n-k}{k}\right)\phi_k'\phi_{n-k}\right\},$$

$$S_{k,n}^{(2)} = -\left(\frac{n}{n+k}\right)\left(\phi_k^*\phi_{n+k}''' + \phi_k^{*\prime}\phi_{n+k}''\right) - \left(\frac{n}{k}\right)\left(\phi_k^{*\prime}\phi_{n+k}'' + \phi_k^{*\prime\prime}\phi_{n+k}'\right) + n^2\alpha^2\left\{\phi_k^*\phi_{n+k}' + \left(\frac{n+k}{k}\right)\phi_k^{*\prime}\phi_{n+k}\right\},$$

$$S_{k,n}^{(3)} = \left(\frac{n}{k-n}\right)\left(\phi_k'\phi_{k-n}^{*\prime\prime} + \phi_k\phi_{k-n}^{*\prime\prime\prime}\right) + \left(\frac{n}{k}\right)\left(\phi_k'\phi_{k-n}^{*\prime\prime} + \phi_k''\phi_{k-n}^{*\prime}\right) + n^2\alpha^2\left\{\phi_k\phi_{k-n}^{*\prime} + \left(\frac{k-n}{k}\right)\phi_k'\phi_{k-n}^*\right\}.$$

It is evident that (5.10) reduces to its Orr–Sommerfeld counterpart in the limit of zero amplitude owing to a negligible contribution from the mean flow distortion and the nonlinear

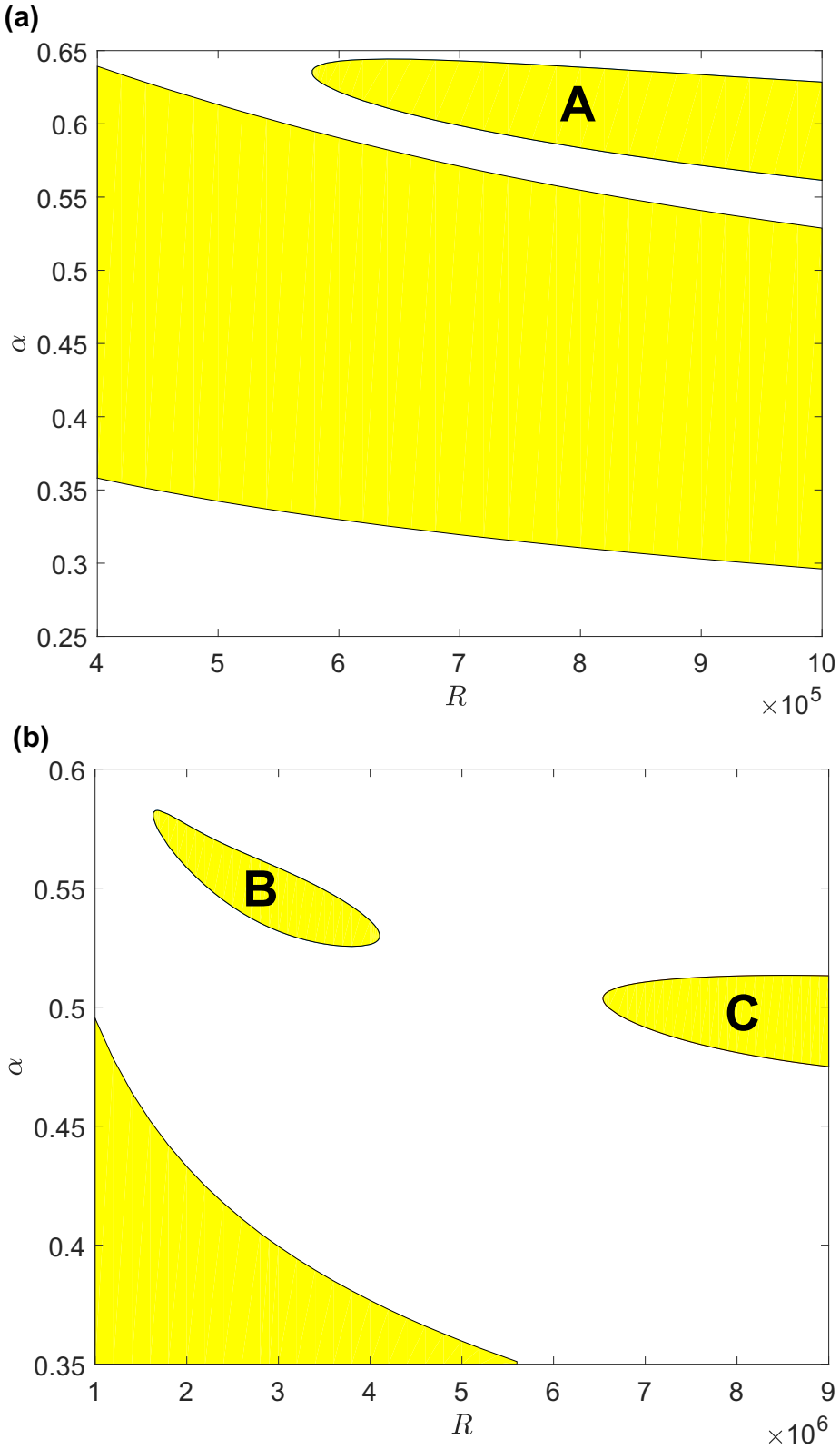

Figure 5.1: Neutral stability curves in the (R, α)-plane for (a) $V = 0.019$, (b) $V = 0.025$.

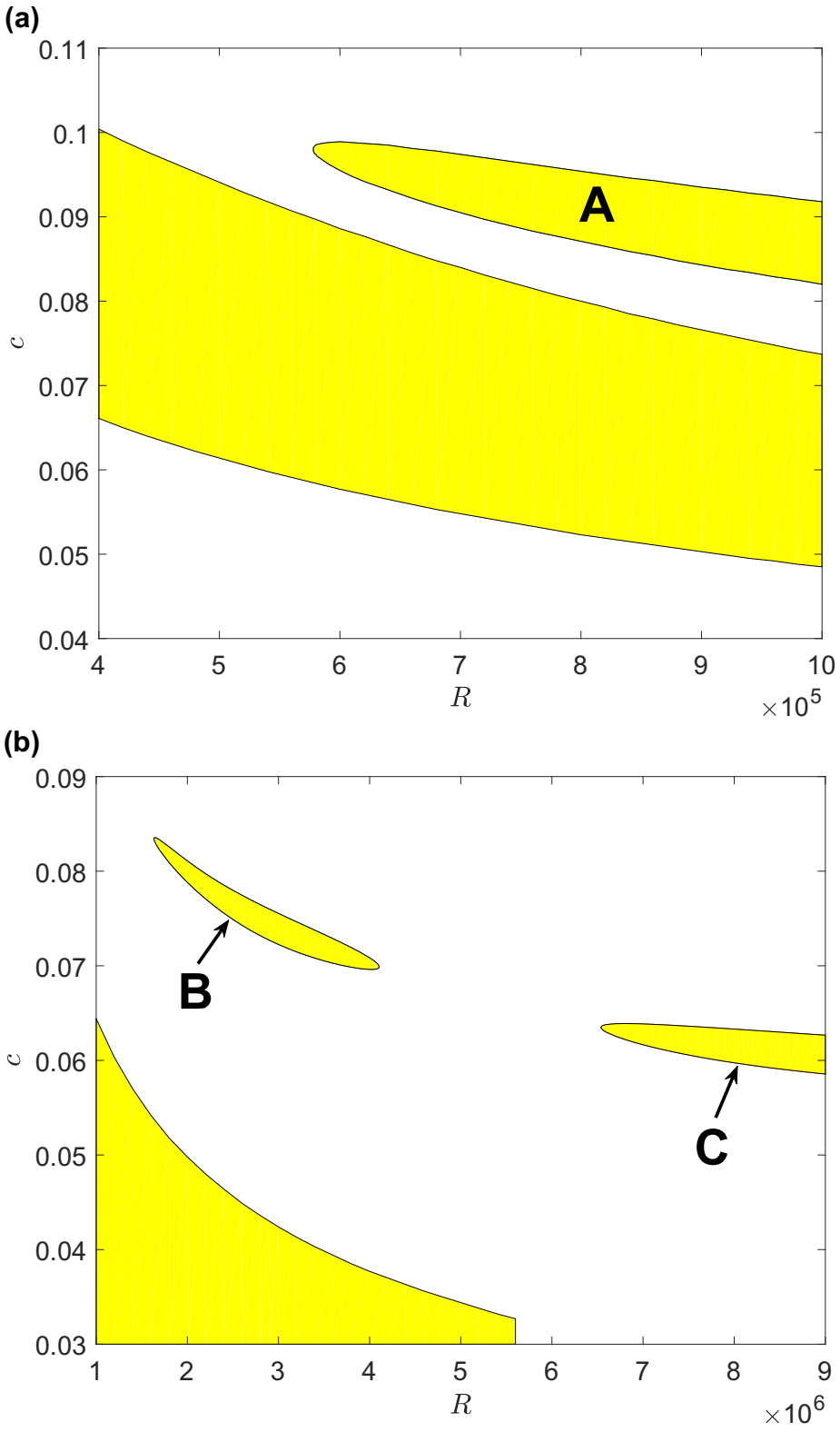

Figure 5.2: Neutral stability curves in the (R, c)-plane for (a) $V = 0.019$, (b) $V = 0.025$.

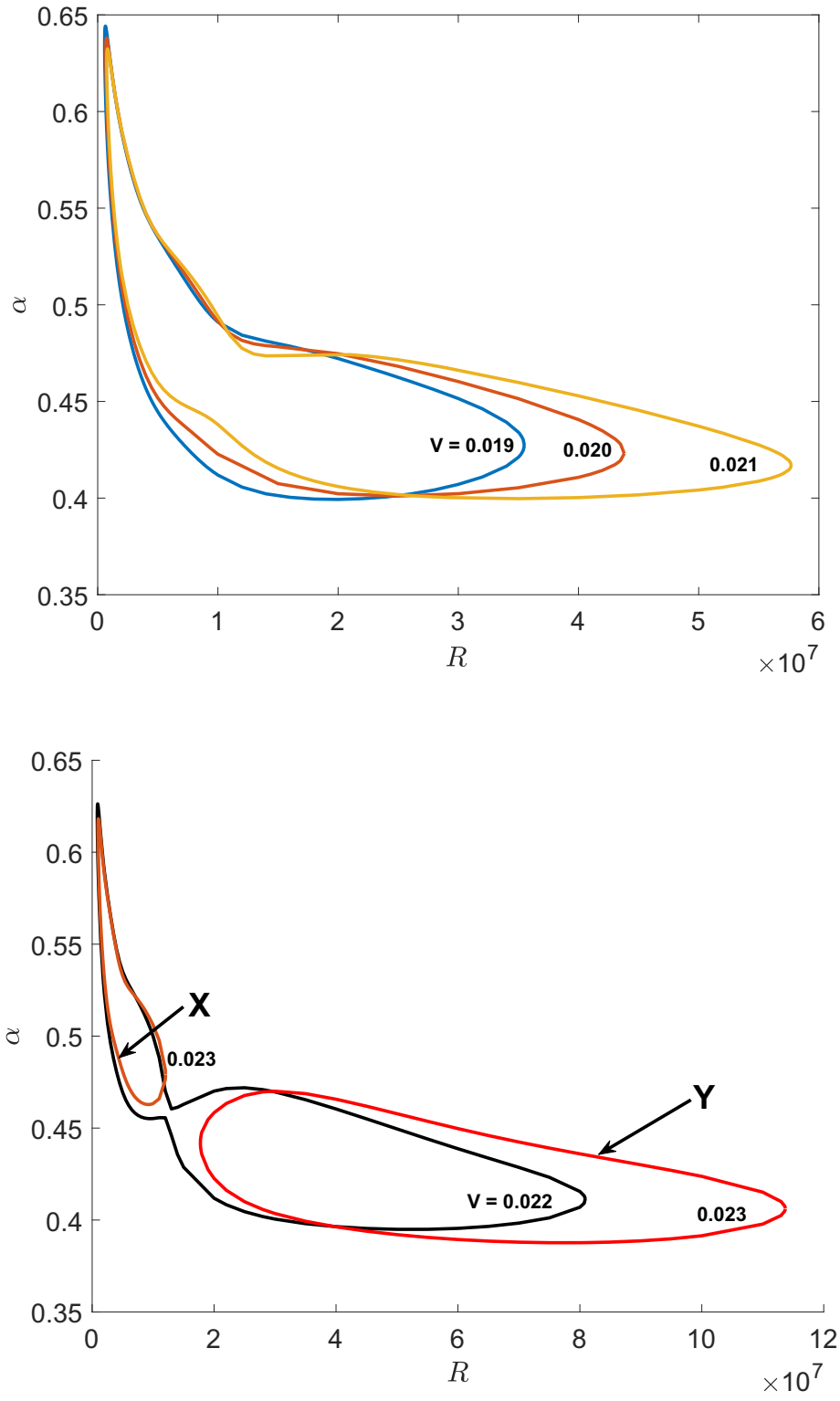

Figure 5.3: Effect of increasing the sliding speed on the curve "**A**" in the (R, α)-plane.

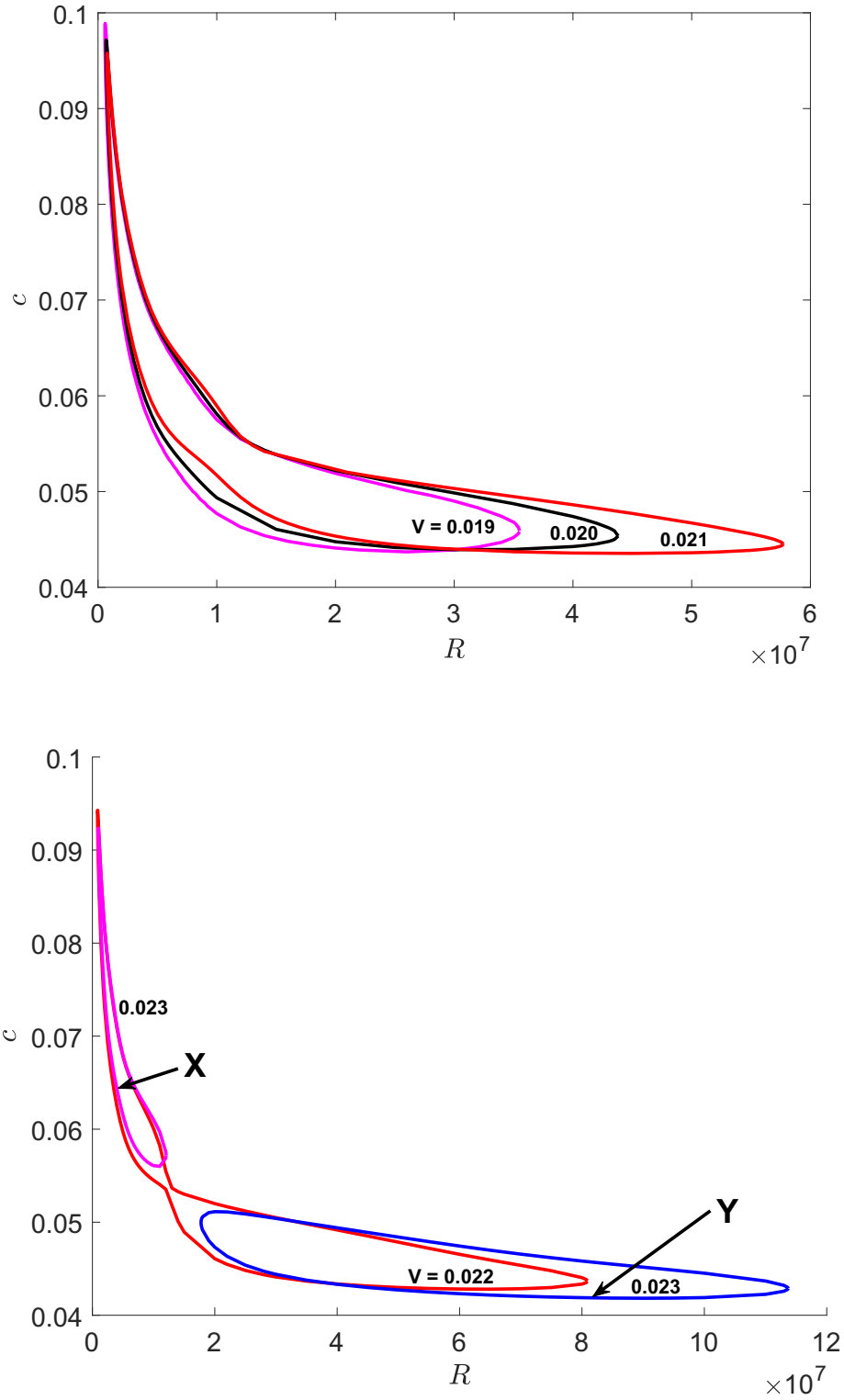

Figure 5.4: Effect of increasing the sliding speed on the curve "**A**" in the (R, c)-plane.

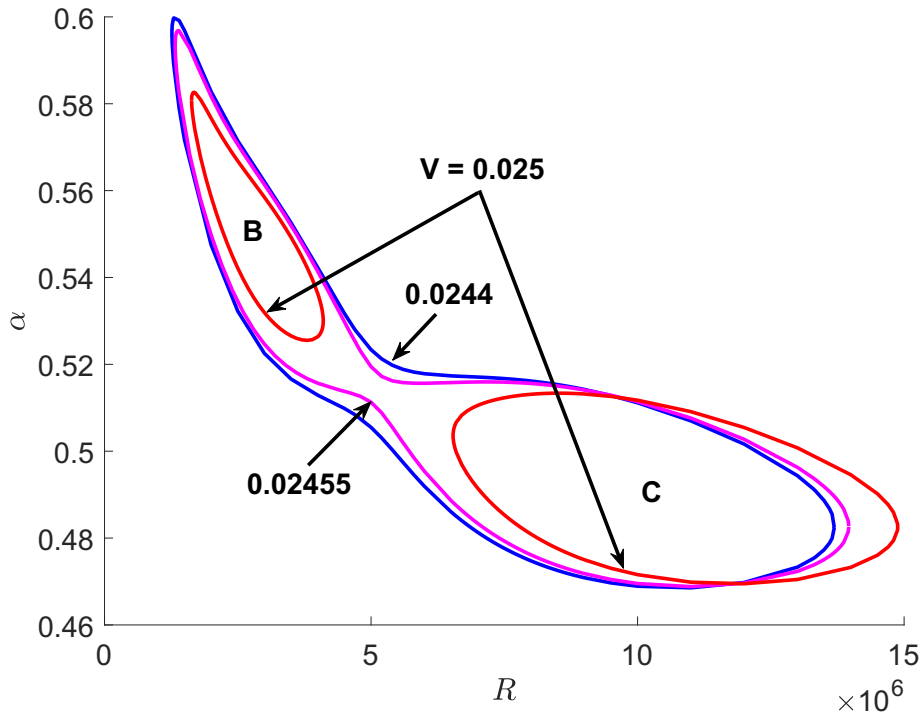

Figure 5.5: Effect of increasing the sliding speed on the curve "**X**" in the (R, α)-plane.

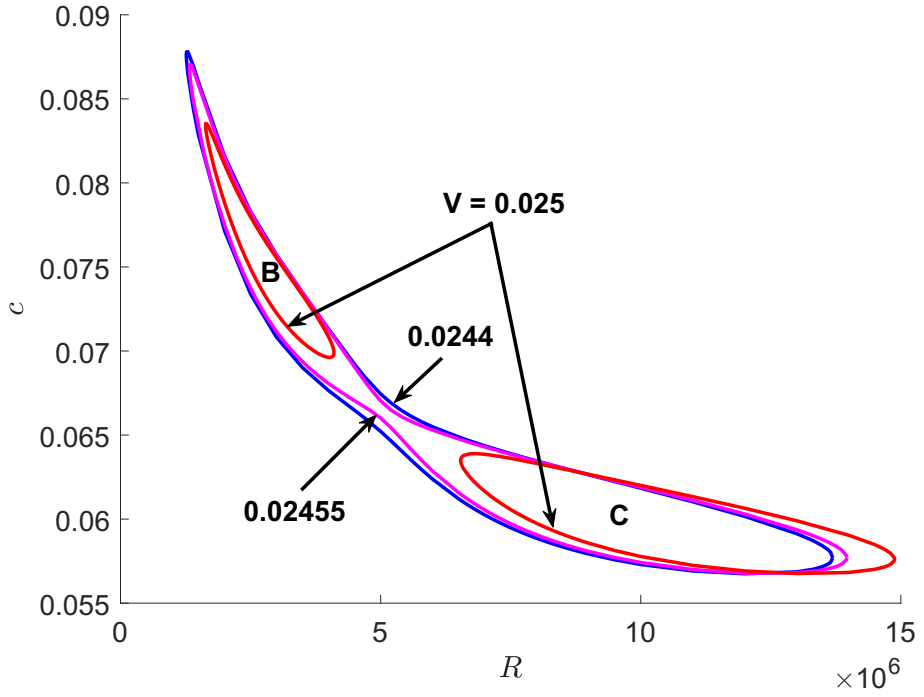

Figure 5.6: Effect of increasing the sliding speed on the curve "**X**" in the (R, c)-plane.

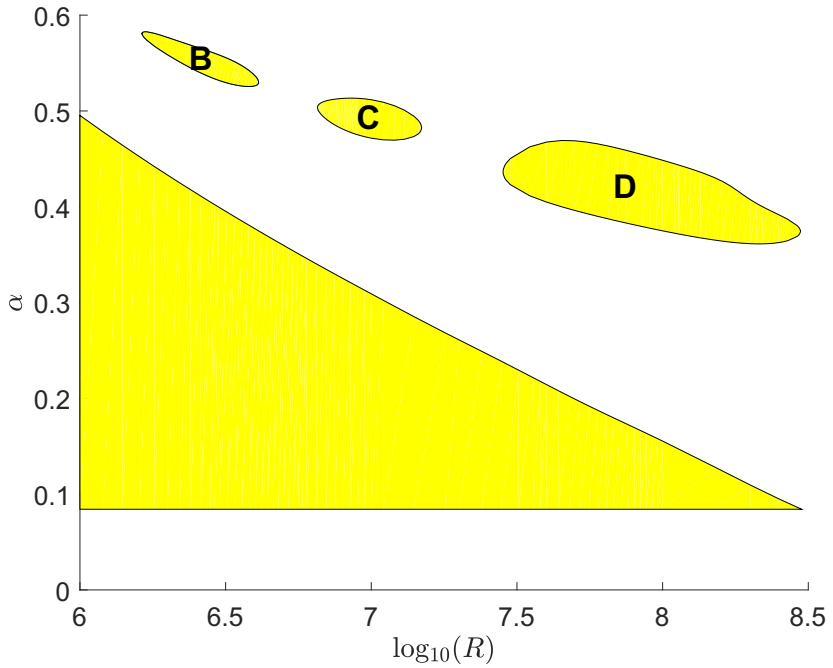

Figure 5.7: Neutral stability curves in the $(\log_{10}(R), \alpha)$-plane at $V = 0.025$.

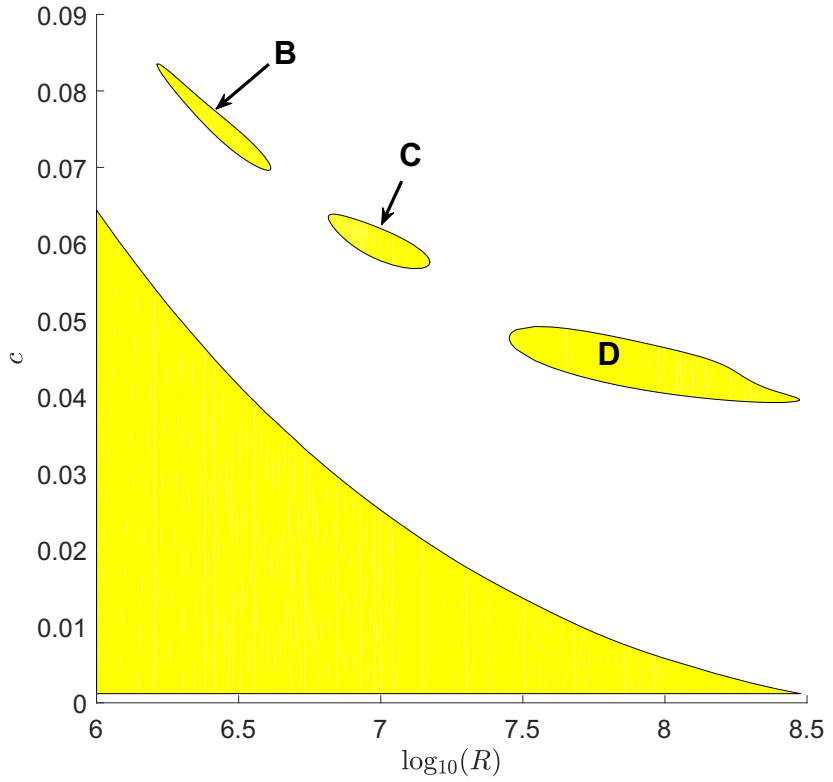

Figure 5.8: Neutral stability curves in the $(\log_{10}(R), c)$-plane at $V = 0.025$.

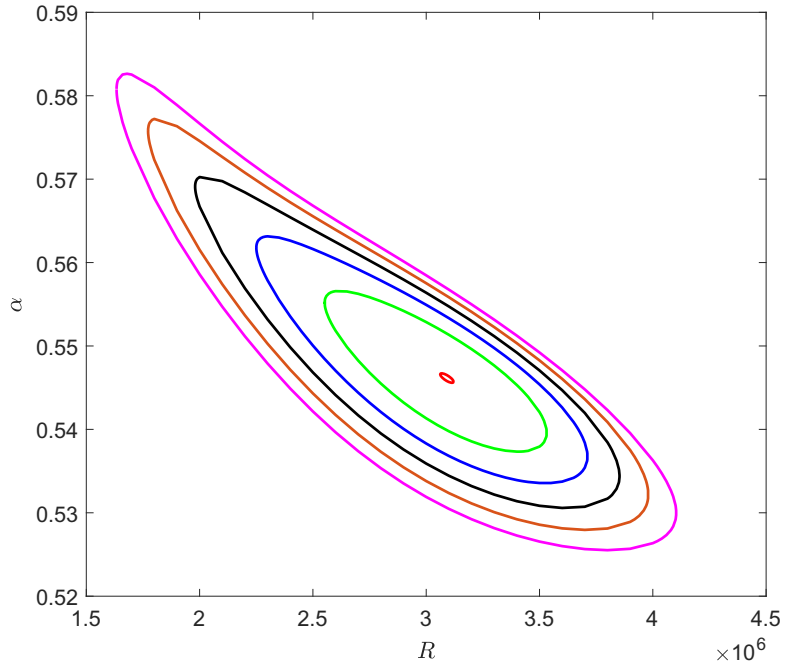

Figure 5.9: Effect of increasing the sliding speed on the curve "**B**" in the (R, α)-plane. Neutral stability curves for $V = 0.025, 0.0251, 0.0252, 0.0253, 0.0254, 0.025496$ (outer to inner).

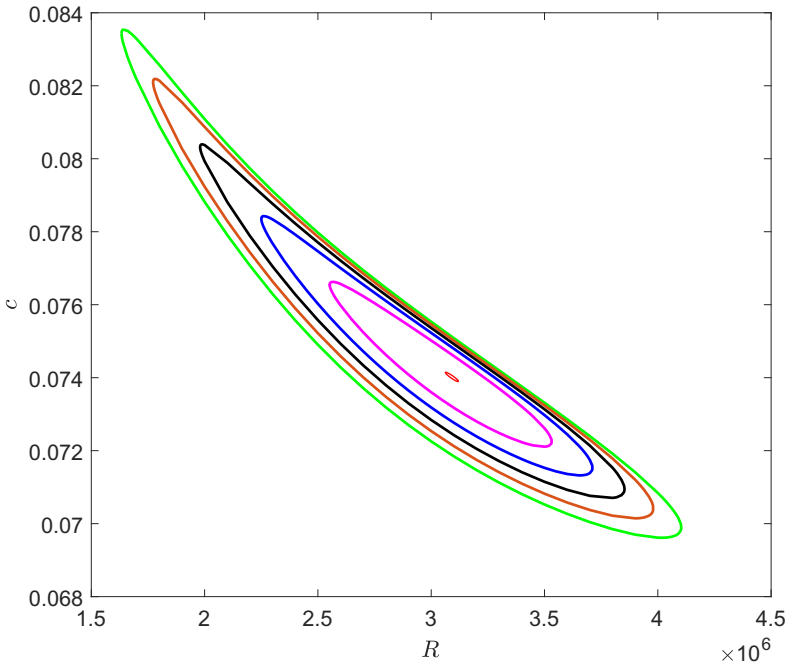

Figure 5.10: Effect of increasing the sliding speed on the curve "**B**" in the (R, c)-plane. Neutral stability curves for $V = 0.025, 0.0251, 0.0252, 0.0253, 0.0254, 0.025496$ (outer to inner).

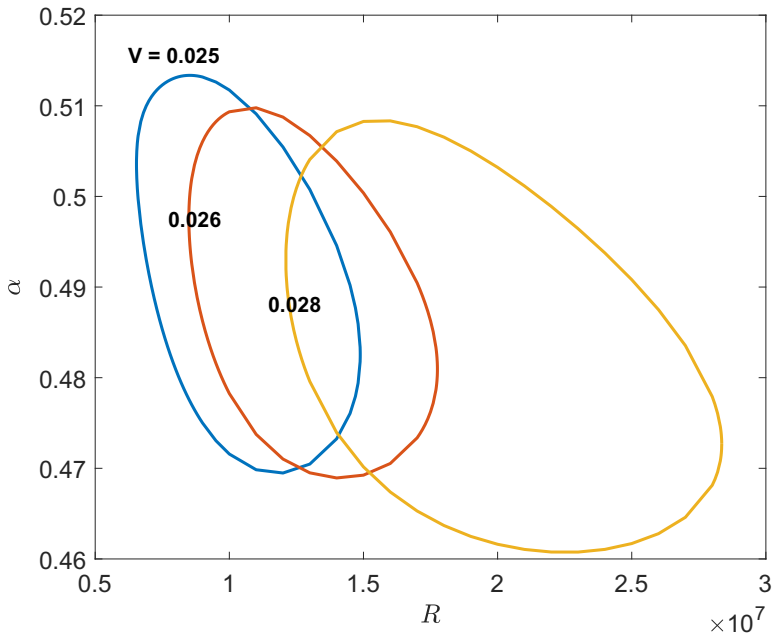

Figure 5.11: Effect of increasing the sliding speed on the curve "**C**" in the (R, α)-plane. Neutral stability curves for various values of V.

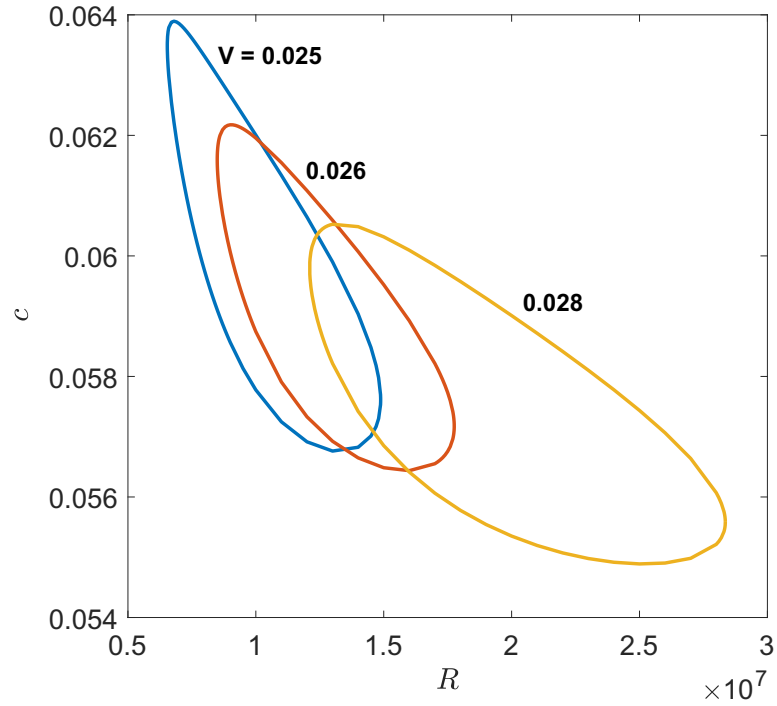

Figure 5.12: Effect of increasing the sliding speed on the curve "**C**" in the (R, c)-plane. Neutral stability curves for various values of V.

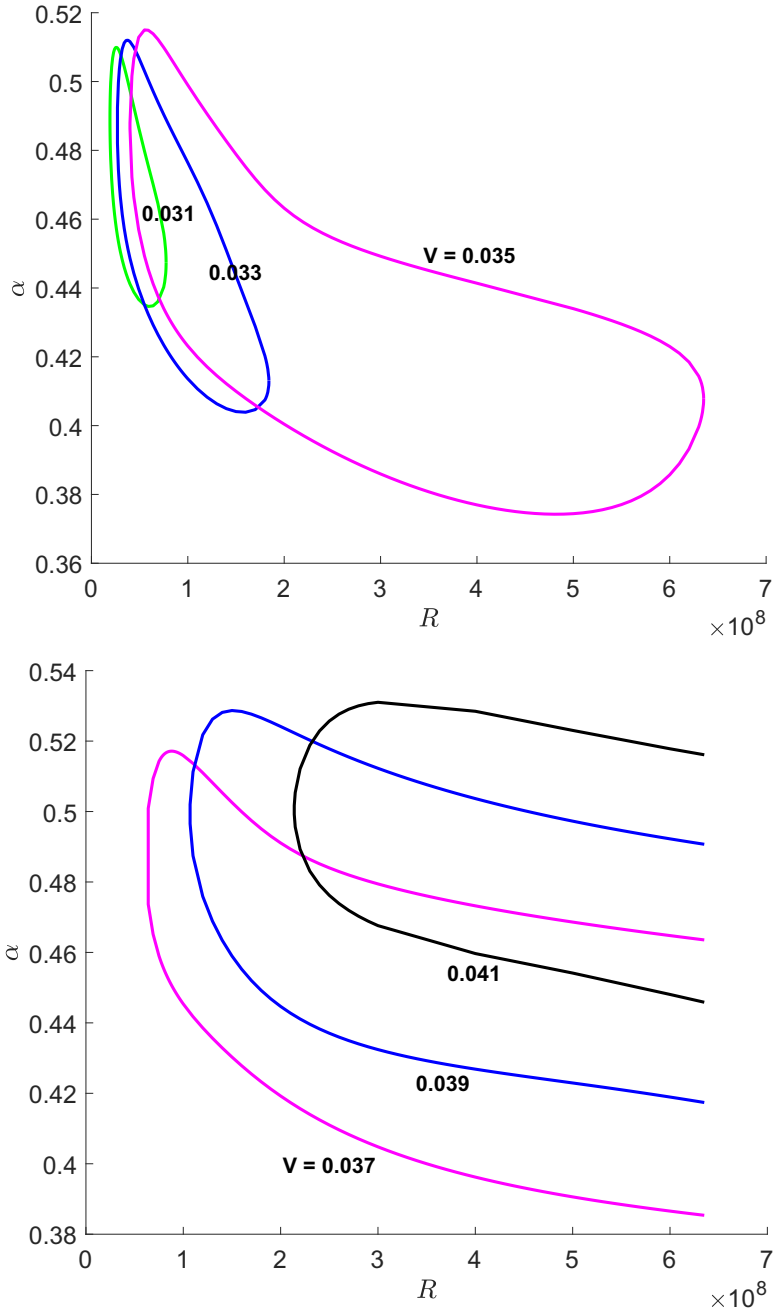

Figure 5.13: Effect of increasing the sliding speed on the curve "**C**" in the (R, α)-plane. Neutral stability curves for various values of V.

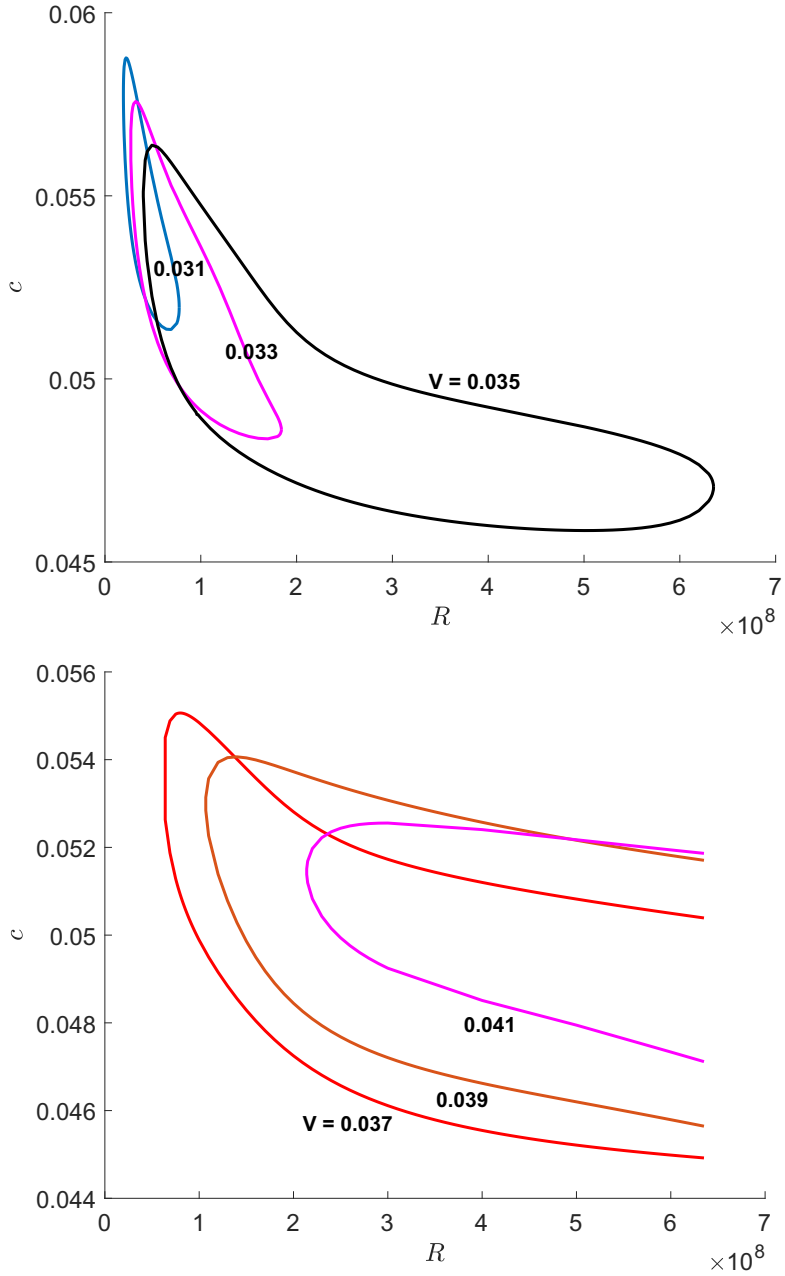

Figure 5.14: Effect of increasing the sliding speed on the curve "**C**" in the (R, c)-plane. Neutral stability curves for various values of V.

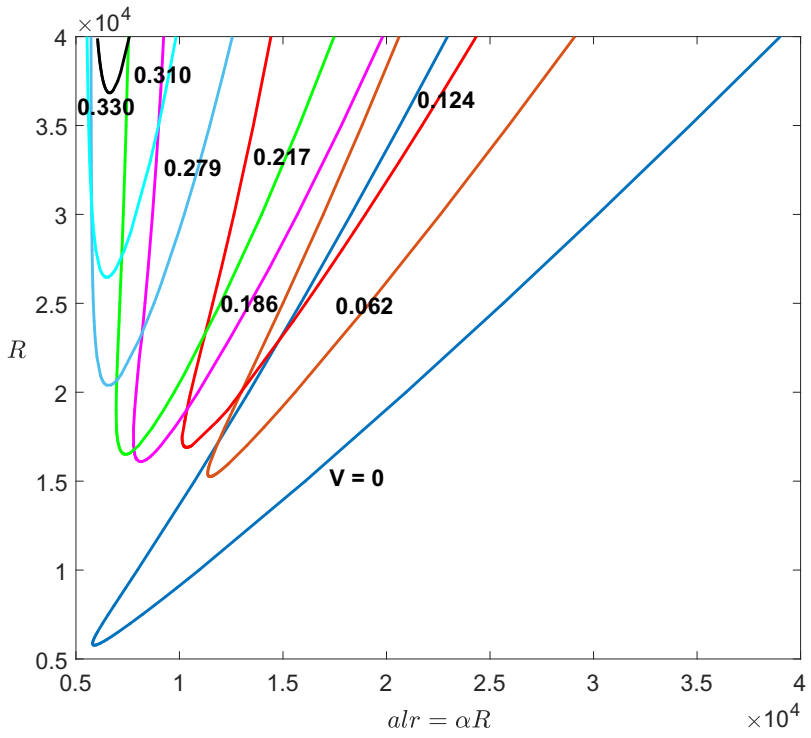

Figure 5.15: Neutral stability curves for various wall sliding speeds V.

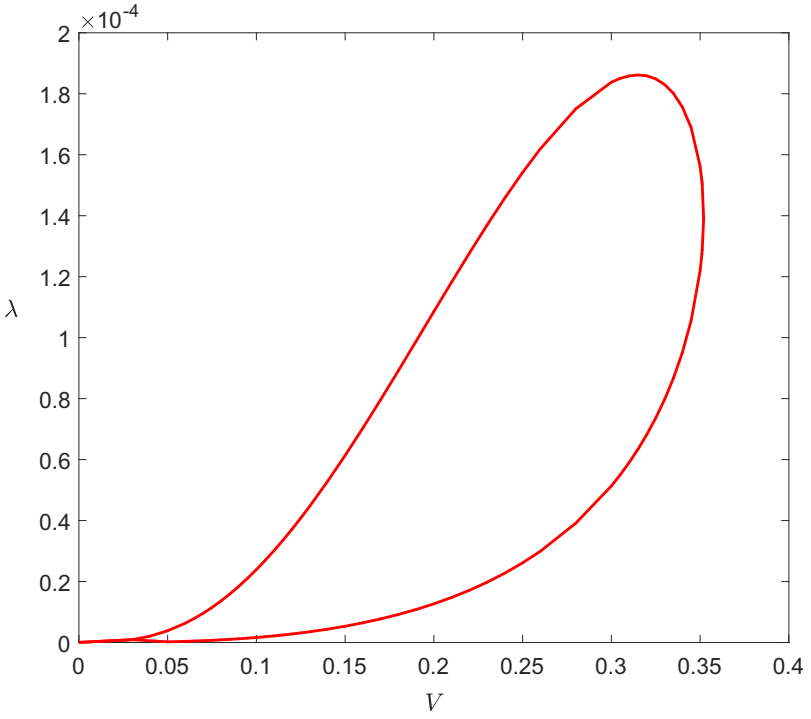

Figure 5.16: Plot of the scaled wavelength $\lambda = (\alpha R)^{-1}$ versus wall sliding speeds V.

sums in this limit. We decompose the complex problem (5.10)–(5.12) into their real and imaginary parts by writing

$$\phi_n = \Phi_n + i\Psi_n, \tag{5.13}$$

and as a result, we obtain the following set of nonlinear equations:

$$\Phi_n'''' - 2n^2\alpha^2\Phi_n'' + n^4\alpha^4\Phi_n + (n\alpha R)\{(U_0+\hat{u}_0-c)(\Psi_n''-n^2\alpha^2\Psi_n) - (U_0+\hat{u}_0)''\Psi_n\} + \mathrm{Re}\Big(\sum_{k=1}^{n-1} S_{k,n}^{(1)}(y)\Big) + \mathrm{Re}\Big(\sum_{k=1}^{N-n} S_{k,n}^{(2)}(y)\Big) + \mathrm{Re}\Big(\sum_{k=n+1}^{N} S_{k,n}^{(3)}(y)\Big) = 0, \tag{5.14a}$$

$$\Psi_n'''' - 2n^2\alpha^2\Psi_n'' + n^4\alpha^4\Psi_n - (n\alpha R)\{(U_0+\hat{u}_0-c)(\Phi_n''-n^2\alpha^2\Phi_n) - (U_0+\hat{u}_0)''\Phi_n\} + \mathrm{Im}\Big(\sum_{k=1}^{n-1} S_{k,n}^{(1)}(y)\Big) + \mathrm{Im}\Big(\sum_{k=1}^{N-n} S_{k,n}^{(2)}(y)\Big) + \mathrm{Im}\Big(\sum_{k=n+1}^{N} S_{k,n}^{(3)}(y)\Big) = 0, \tag{5.14b}$$

$$D_0^2\hat{u}_0 + \sum_{k=1}^{N}\Big(\frac{2}{k\alpha R}\Big)\Big(\Psi_k''\Phi_k - \Psi_k\Phi_k''\Big) = 0, \tag{5.14c}$$

which are to be solved with the entire set of the boundary conditions

$$\Phi_n(\pm1) = \Phi_n'(\pm1) = \Psi_n(\pm1) = \Psi_n'(\pm1) = \hat{u}_0(\pm1) = 0, \tag{5.15}$$

for $n = 1, \ldots, N$. The explicit expressions for $\mathrm{Re}(S_{k,n}^{(i)})$ and $\mathrm{Im}(S_{k,n}^{(i)})$ are presented in Appendix D. The standard approach to deal with the type of problem (5.14)–(5.15) numerically at finite Reynolds number is to apply a Chebyshev spectral collocation method, involving the idea that the functions Φ_n, Ψ_n and $\hat{u}_0$ are approximated by a series of Chebyshev polynomials T_n as

$$\Phi_n = \sum_{m=1}^{M+1} a_m^{(n)} T_{m-1}(y), \quad \Psi_n = \sum_{m=1}^{M+1} b_m^{(n)} T_{m-1}(y), \quad \hat{u}_0 = \sum_{m=1}^{M+1} \gamma_m T_{m-1}(y), \tag{5.16}$$

where y is evaluated at the Gauss points $y_j = \cos(\pi(j-1)/M)$ for $j = 1, \ldots, M+1$. As has been already mentioned at the end of section 5.1, the amplitude and phase conditions are required to close the nonlinear eigenvalue problem or equivalently the problem formulation (5.14)–(5.15). We define the amplitude A of the disturbance by

$$A^2 = \sum_{n=1}^{N}\{(\Phi_n(y_{J_1}))^2 + (\Psi_n(y_{J_1}))^2\},$$

while the phase condition is imposed through the equation

$$\Phi_1(y_{J_2}) = 0.$$

The values of J_1 and J_2 are arbitrarily chosen. In our numerical computations, the linear solution for Ψ_1 attains maximum value at the location y_{J_1}, while we choose y_{J_2} to be the

location where the zero amplitude form for Φ_1 passes through zero. There are a total of $(2N+1)(M+1)+2$ equations with the inclusion of the boundary conditions, which can be symbolically expressed via the vector equation

$$\mathbf{f}(\mathbf{m}) = \mathbf{0}, \tag{5.17}$$

with $\mathbf{m}$ consisting of the real unknowns $a_i^{(j)}, b_i^{(j)}, \gamma_i, \alpha, c$ for $i = 1, \ldots, M+1$ and $j = 1, \ldots, N$. For a prescribed amplitude A, we can apply Newton's method to solve (5.17):

$$J(\mathbf{m_k})(\mathbf{m_{k+1}} - \mathbf{m_k}) = -\mathbf{f}(\mathbf{m_k}),$$

in an iterative manner until $\mathbf{m}$ converges to some acceptable tolerance, we typically took $|\mathbf{m_{k+1}} - \mathbf{m_k}| \simeq 10^{-5}$. Provided we have a good initial guess for a small-amplitude nonlinear calculation (supplied by the point on the neutral curve known from the linear solution), the nonlinear equations (5.17) can be solved using Newton's method to obtain solutions at higher amplitudes.

The Jacobian matrix J consists of the derivatives of each equation with respect to each of the real unknowns in $\mathbf{m}$ and can be calculated explicitly for this problem. For example, if we denote the nonlinear sum in (5.11) by $\mathscr{L}_1$, we have

$$\mathscr{L}_1 = 2(\alpha R)^{-1} \sum_{k=1}^{N} \left(\frac{\Psi_k'' \Phi_k - \Psi_k \Phi_k''}{k} \right),$$

upon use of (5.13). With the aid of (5.16), we can determine the relevant contributions to the Jacobian matrix. For example,

$$\frac{\partial \mathscr{L}_1}{\partial a_i^{(j)}} = 2(\alpha R)^{-1} \left(\frac{\Psi_j'' T_{i-1} - \Psi_j T_{i-1}''}{j} \right),$$

for $i = 1, \ldots, M+1$ and $j = 1, \ldots, N$. It is straightforward to carry out similar calculations for all other linear and nonlinear terms. It turns out that $M = 100$ collocation points provide sufficient accuracy to our computations, while the required value of N is a function of the amplitude A. Typically, we took $8 \leq N \leq 15$. In the next section, we discuss the nonlinear results obtained from the application of the numerical technique described above.

5.4 Nonlinear results for plane Poiseuille–Couette flow

Figure 5.17 displays the nonlinear neutral solutions for the case when the channel walls are at rest at different values of αR with $N = 8$ taken into account. It is observed that all the neutral surfaces are similar in shape, and the surfaces gradually shrink in size with decreasing αR. The critical αR for which neutral solution exists is found to be 3780. Figures 5.18–5.20 show the variation of the Reynolds numbers R, the streamwise wavenumber α

and wavespeed c at various values of αR as a function of the amplitude A. It is seen that corresponding to each situation the following feature emerges: the gap between the upper and lower branch solutions widens and the nose of the surface (the top neutral point where these branch solutions meet) rises with the increase in the value of αR so that the region of nonlinear instability increases.

In figure 5.21, we concentrate on the case $\alpha R = 5823.66$ and investigate what happens to the neutral surface for plane Poiseuille flow as V increases. It is observed that the neutral surfaces contract, the lower and upper branch solutions leave the zero amplitude plane to form the closed loops and the nose of the surface descends as the sliding speed is increased from zero to 0.135. The largest value of V for which we obtain in neutral solution at this αR is approximately at $V = 0.137$. In figures 5.22–5.24 we plot the amplitude versus the Reynolds numbers, the streamwise wavenumber and wavespeed for various values of the sliding speed V and note that the general trends described above remain unchanged.

In figures 5.25 and 5.26, we present results for $\alpha R = 7971.60$ and examine the effect on the neutral surface for plane Poiseuille flow of increasing the sliding speed. For values of V in the range $0 \leq V \leq 0.091$, we have that a familiar pattern is emerging: the size of the neutral surfaces decreases, the lower and upper branch solutions depart from the zero amplitude plane A_c to form the closed loops, and the nose of the surface goes down as V is increased. It is intriguing that for the same value of αR with the increase in V from 0.121 to 0.177, the neutral surfaces expand with both the branch solutions retreating the zero amplitude plane, while the nose of the surface still falling. As V is increased further, we find that the upper branch solution remains in A_c, and simultaneously, the lower branch solution rises, as can be seen in figure 5.33. Beyond a value of $V \simeq 0.371$, the upper branch solutions again leave the zero amplitude plane, while the lower branch solutions continue rising, as shown in figure 5.34. In figures 5.27, 5.28, 5.35 and 5.36, we plot the amplitude A as a function of R, indicating that the nonlinear instability is supported over a large range of the Reynolds numbers. The dependence of the amplitude upon the streamwise number α and wavespeed c in figures 5.29–5.32, 5.37–5.40 is observed with the same trends as the sliding speed is increased.

Figures 5.41 and 5.42 show the neutral stability diagrams in (R, α, A) space for various combination of parameters R and V. The results obtained are in excellent agreement with previous work (see Balakumar 1997) when allowance is made for the difference in scaling of the Reynolds numbers: the sliding speed V in our case equals $(2/3)(\sigma_2/(1-\sigma_2))$ where σ_2 is the Couette velocity component in the aforementioned reference. Figures 5.43 and 5.44 show the corresponding dependence of the amplitude A on α for various values of V and R. We present in figures 5.45 and 5.46 neutral surfaces in the (c, A)-plane for the same values of V and R.

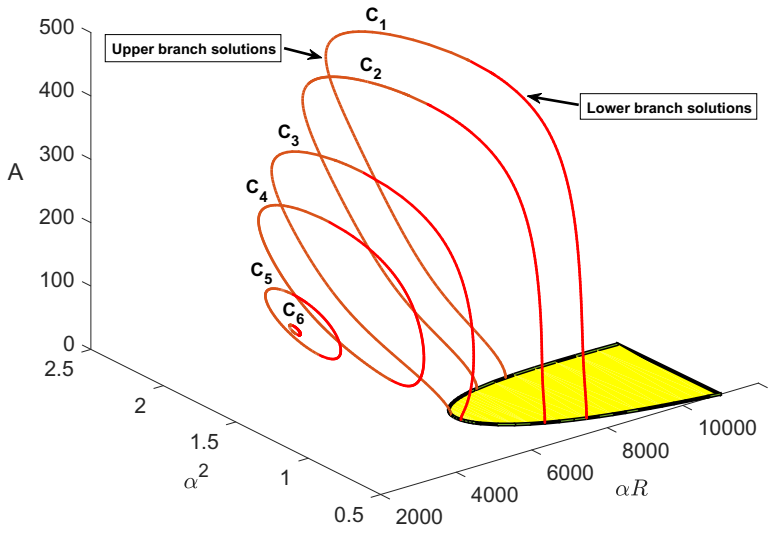

Figure 5.17: Nonlinear neutral surfaces for plane Poiseuille flow for various values of $alr = \alpha R$: $C_1 = 7971.60$; $C_2 = 7123$; $C_3 = 5823.66$; $C_4 = 5000$; $C_5 = 4000$; $C_6 = 3790$.

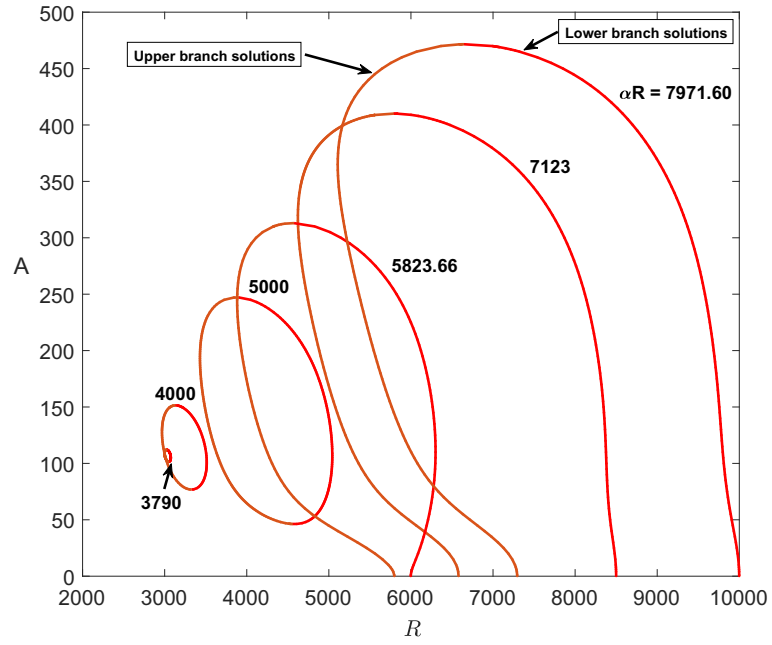

Figure 5.18: Cross-section of the nonlinear neutral surfaces for plane Poiseuille flow in the parameter space formed by the Reynolds numbers and amplitude.

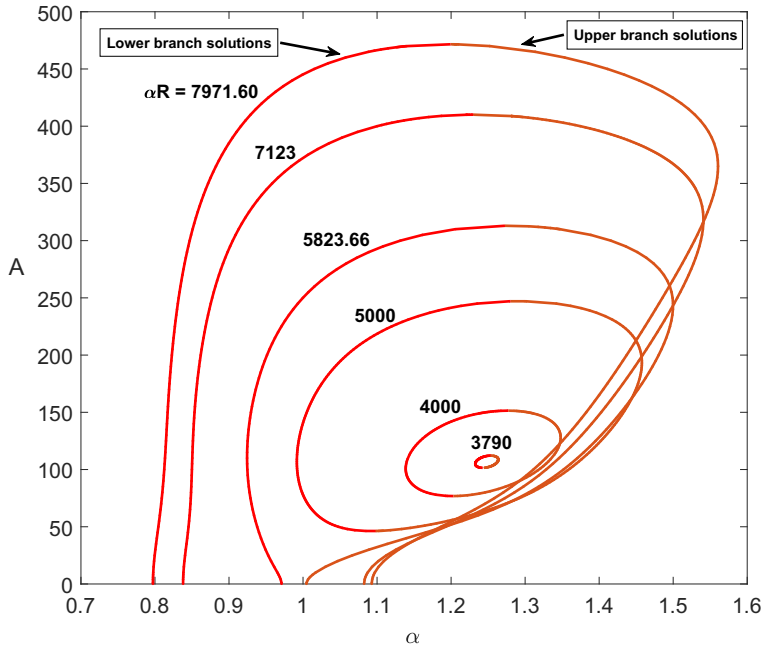

Figure 5.19: Cross-section of the nonlinear neutral surfaces for plane Poiseuille flow in the parameter space formed by the streamwise wavenumber and amplitude.

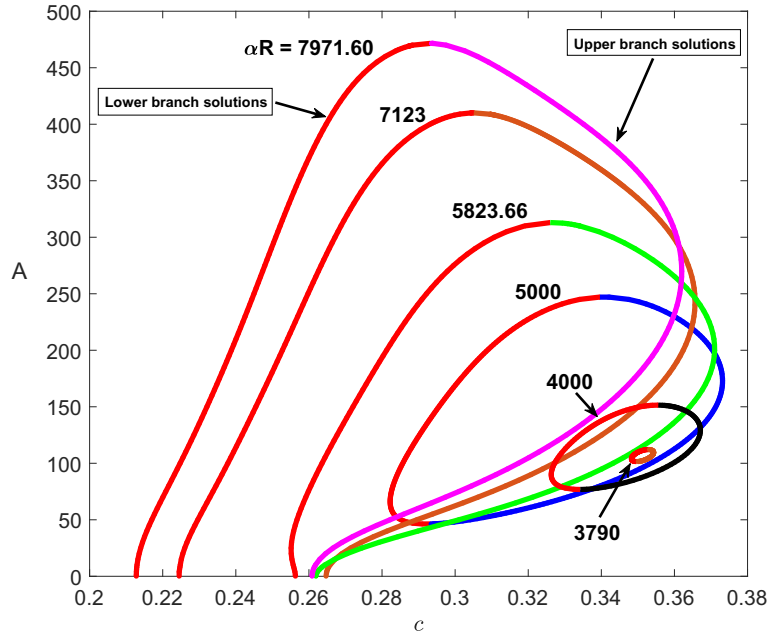

Figure 5.20: Nonlinear neutral surfaces for plane Poiseuille flow in the (c, A)-plane.

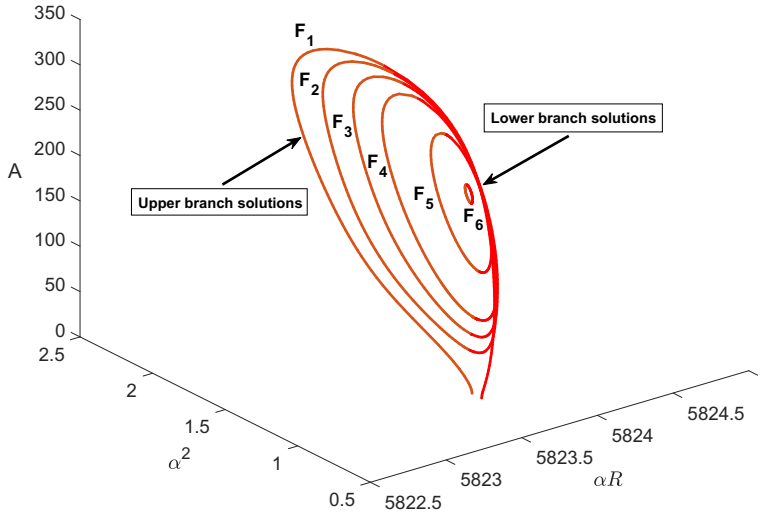

Figure 5.21: Nonlinear neutral surfaces in $(\alpha R, \alpha^2, A)$ space at $\alpha R = 5823.66$ marked by F_1, F_2, F_3, F_4, F_5, F_6 corresponding to sliding speed $V = 0, 0.031, 0.051, 0.071, 0.111, 0.135$ respectively.

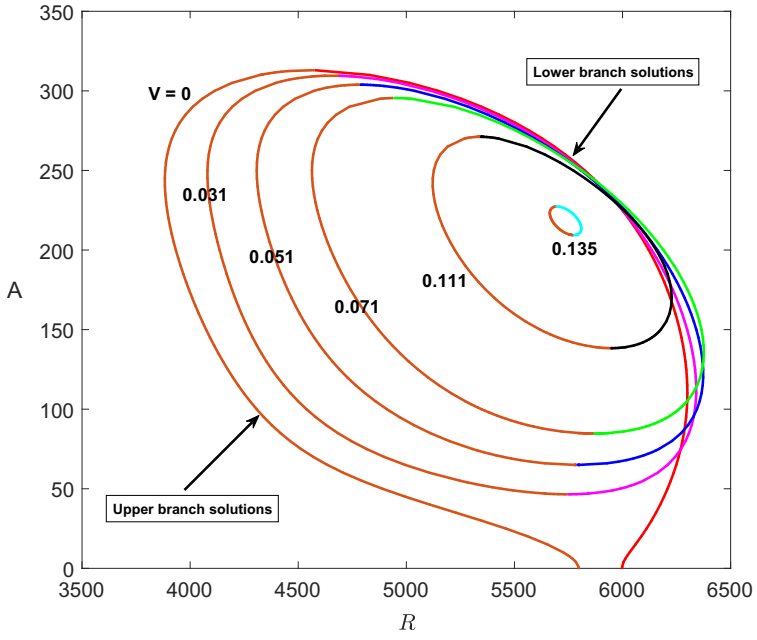

Figure 5.22: Cross-section of the nonlinear neutral surfaces for plane Poiseuille–Couette flow at $alr = 5823.66$ for various values of V in the parameter space formed by the Reynolds numbers and amplitude.

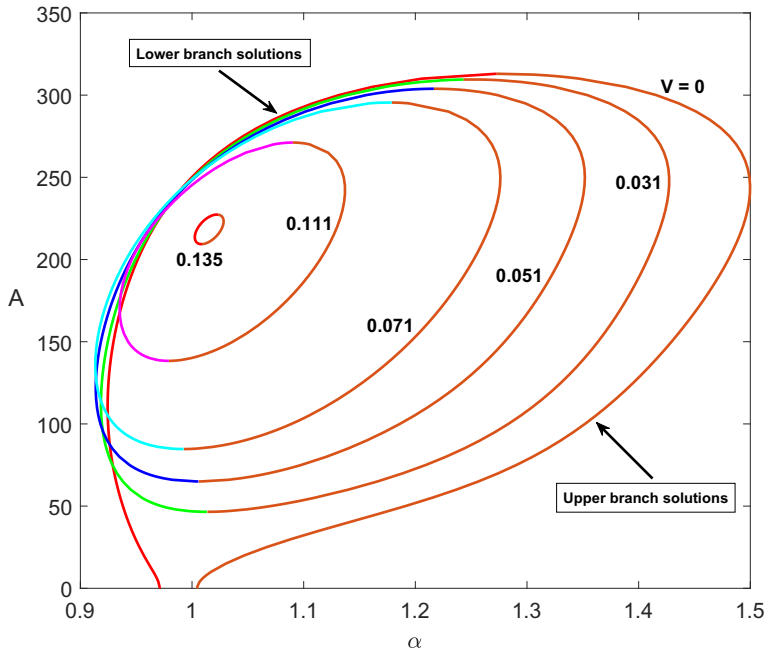

Figure 5.23: Cross-section of the nonlinear neutral surfaces for plane Poiseuille–Couette flow at $alr = 5823.66$ for various values of V in the parameter space formed by the streamwise wavenumber and amplitude.

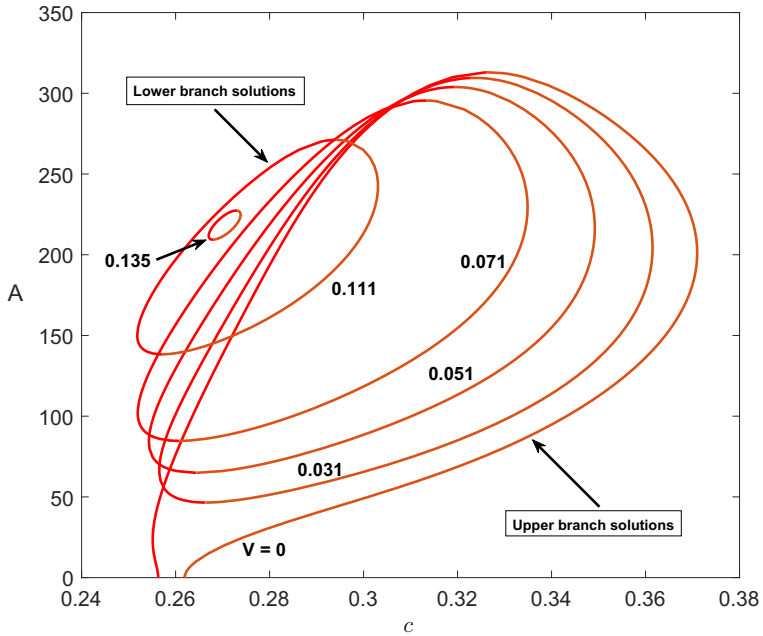

Figure 5.24: Nonlinear neutral surfaces for plane Poiseuille–Couette flow at $alr = 5823.66$ for various values of V in the (c, A)-plane.

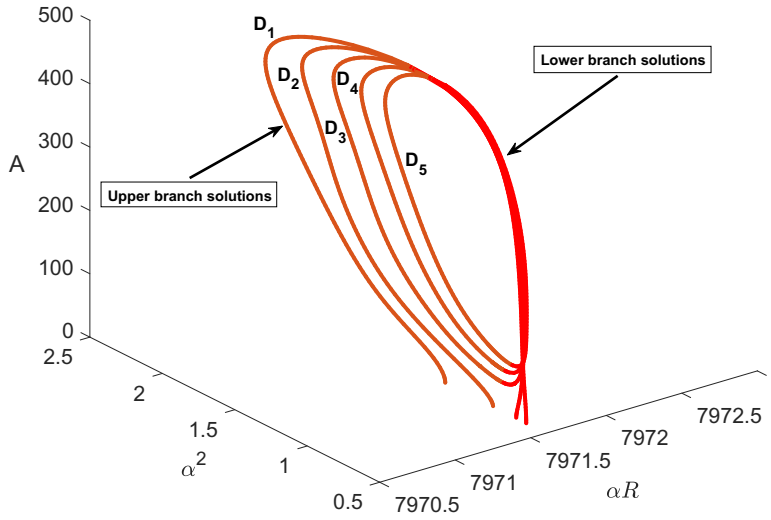

Figure 5.25: Nonlinear neutral surfaces in $(\alpha R, \alpha^2, A)$ space at $\alpha R = 7971.60$ marked by D_1, D_2, D_3, D_4, D_5 corresponding to sliding speed $V = 0, 0.031, 0.051, 0.071, 0.091$ respectively.

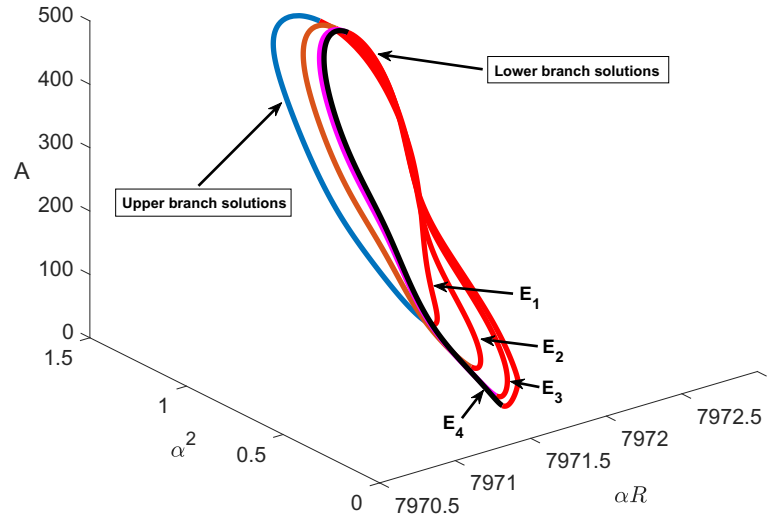

Figure 5.26: Nonlinear neutral surfaces in $(\alpha R, \alpha^2, A)$ space at $\alpha R = 7971.60$ marked by E_1, E_2, E_3, E_4 corresponding to sliding speed $V = 0.121, 0.151, 0.171, 0.177$ respectively.

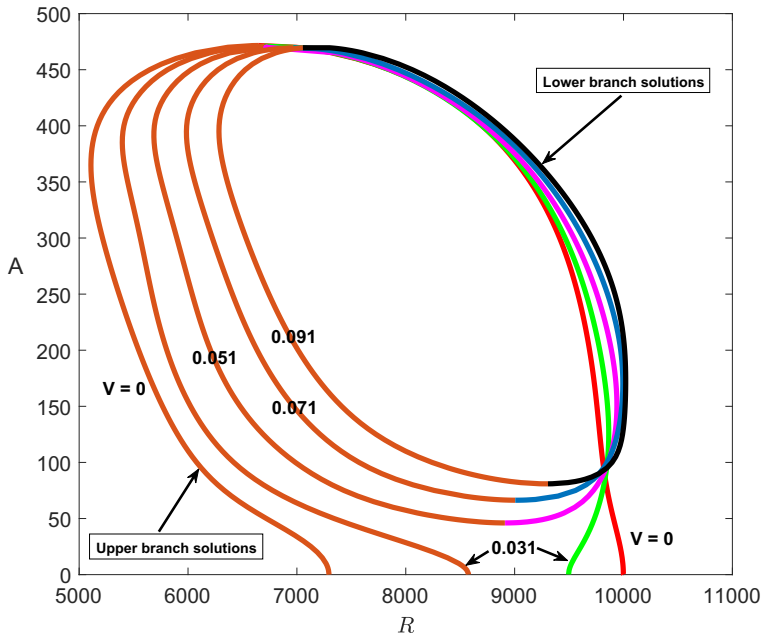

Figure 5.27: Cross-section of the nonlinear neutral surfaces for plane Poiseuille–Couette flow at $alr = 7971.60$ for various values of V in the parameter space formed by the Reynolds numbers and amplitude.

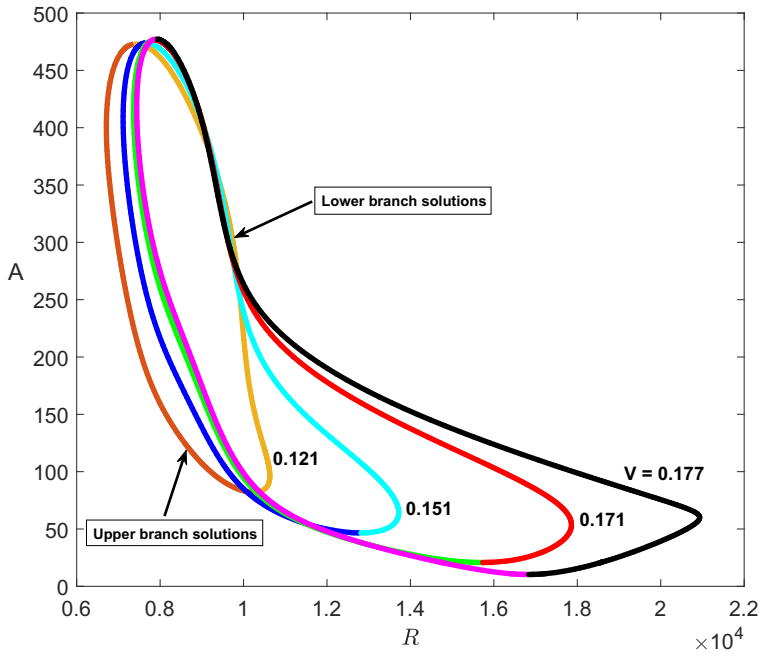

Figure 5.28: Cross-section of the nonlinear neutral surfaces for plane Poiseuille–Couette flow at $alr = 7971.60$ for various values of V in the parameter space formed by the Reynolds numbers and amplitude.

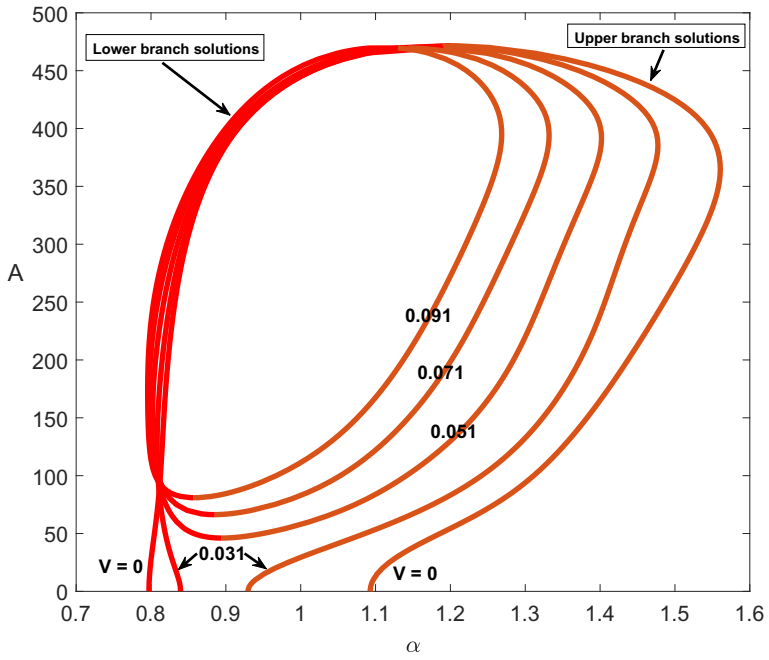

Figure 5.29: Cross-section of the nonlinear neutral surfaces for plane Poiseuille–Couette flow at $alr = 7971.60$ for various values of V in the parameter space formed by the streamwise wavenumber and amplitude.

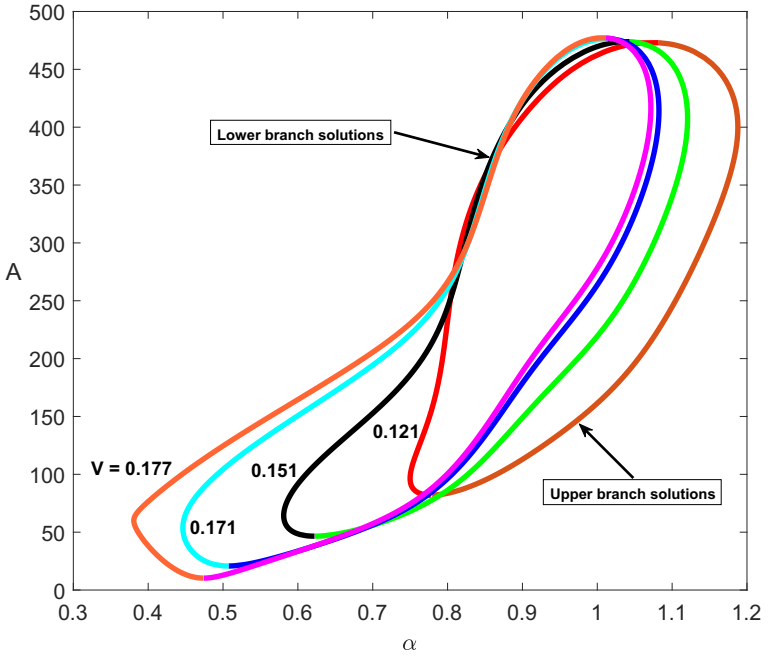

Figure 5.30: Cross-section of the nonlinear neutral surfaces for plane Poiseuille–Couette flow at $alr = 7971.60$ for various values of V in the parameter space formed by the streamwise wavenumber and amplitude.

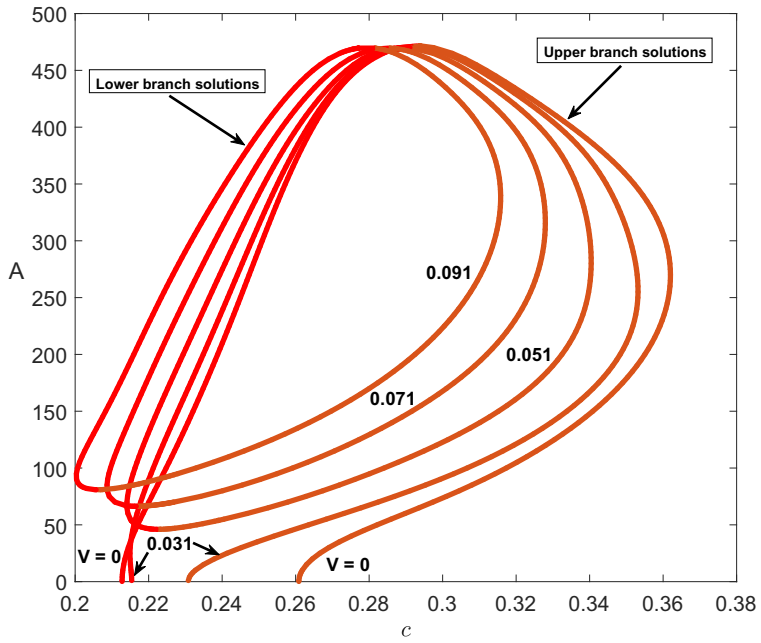

Figure 5.31: Nonlinear neutral surfaces for plane Poiseuille–Couette flow at $alr = 7971.60$ for various values of V in the (c, A)-plane.

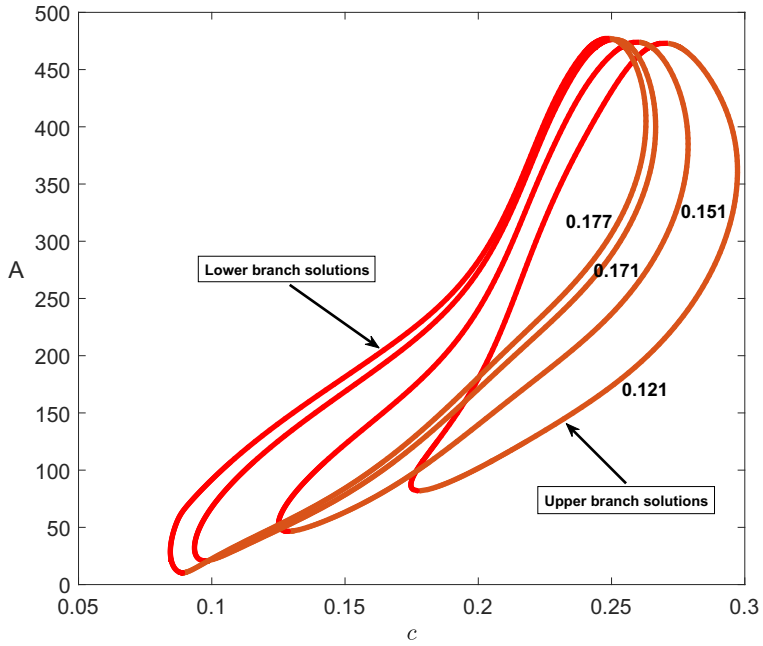

Figure 5.32: Nonlinear neutral surfaces for plane Poiseuille–Couette flow at $alr = 7971.60$ for various values of V in the (c, A)-plane.

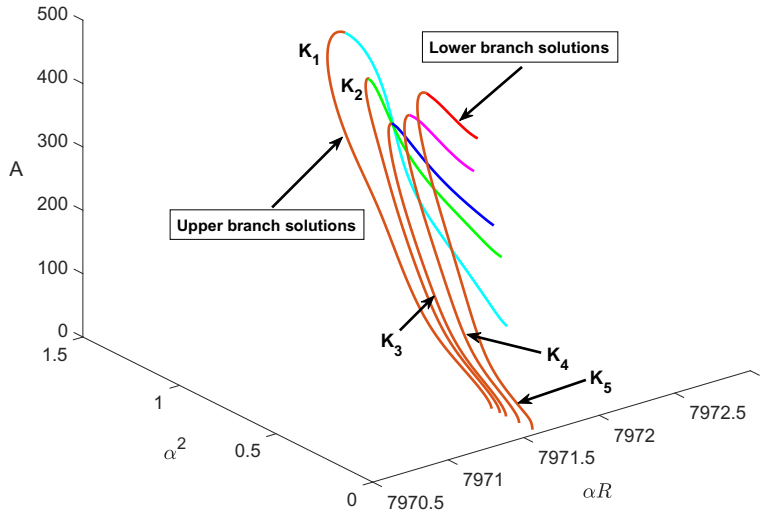

Figure 5.33: Nonlinear neutral surfaces in $(\alpha R, \alpha^2, A)$ space at $\alpha R = 7971.60$ marked by K_1, K_2, K_3, K_4, K_5 corresponding to $V = 0.191, 0.231, 0.251, 0.291, 0.331$ respectively.

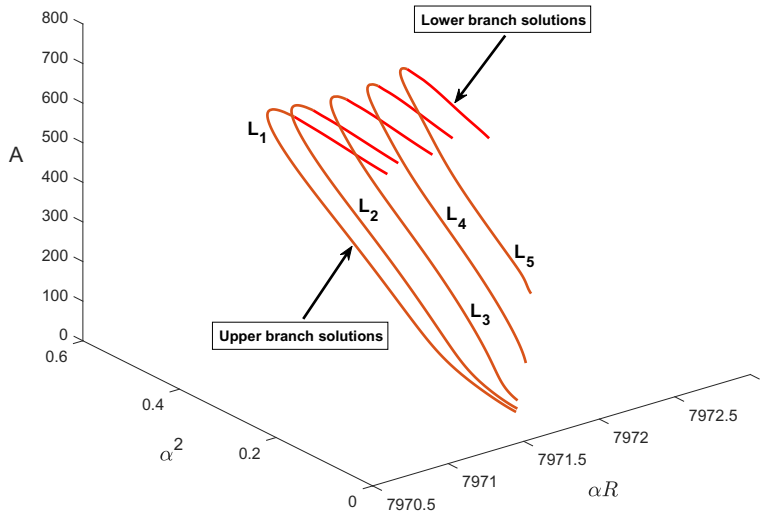

Figure 5.34: Nonlinear neutral surfaces in $(\alpha R, \alpha^2, A)$ space at $\alpha R = 7971.60$ marked by L_1, L_2, L_3, L_4, L_5 corresponding to sliding speed $V = 0.371, 0.401, 0.451, 0.501, 0.551$ respectively.

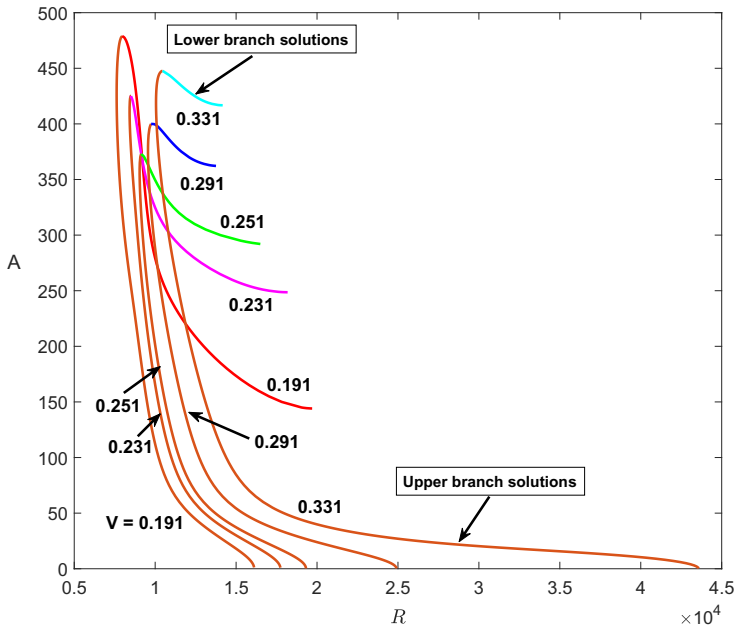

Figure 5.35: Cross-section of the nonlinear neutral surfaces for plane Poiseuille–Couette flow at $alr = 7971.60$ for various values of V in the parameter space formed by the Reynolds numbers and amplitude.

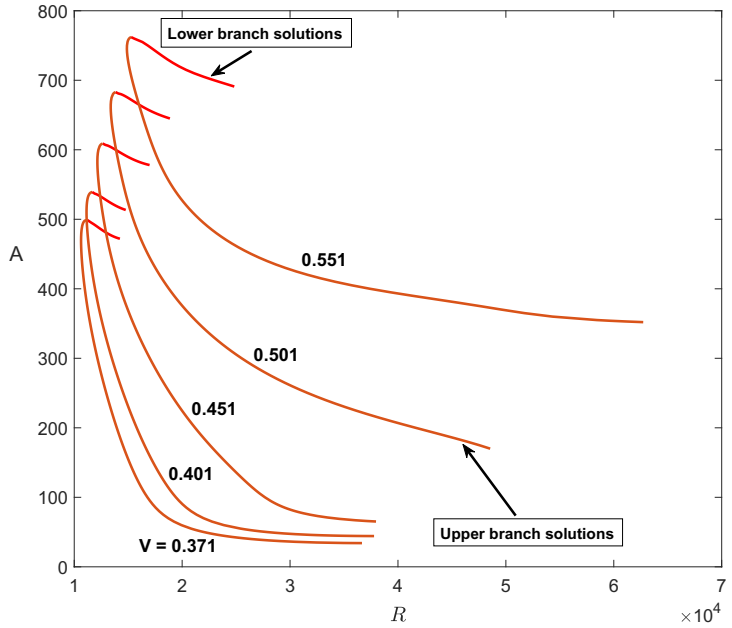

Figure 5.36: Cross-section of the nonlinear neutral surfaces for plane Poiseuille–Couette flow at $alr = 7971.60$ for various values of V in the parameter space formed by the Reynolds numbers and amplitude.

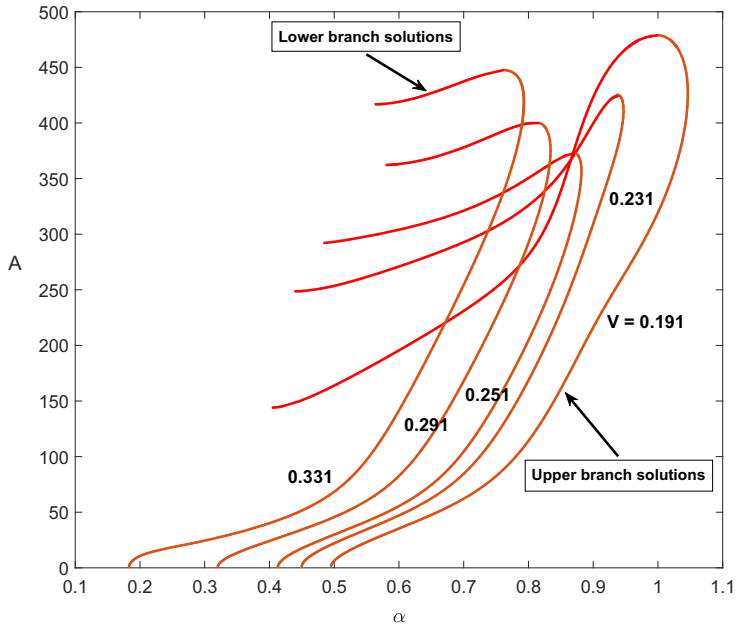

Figure 5.37: Cross-section of the nonlinear neutral surfaces for plane Poiseuille–Couette flow at $alr = 7971.60$ for various values of V in the parameter space formed by the streamwise wavenumber and amplitude.

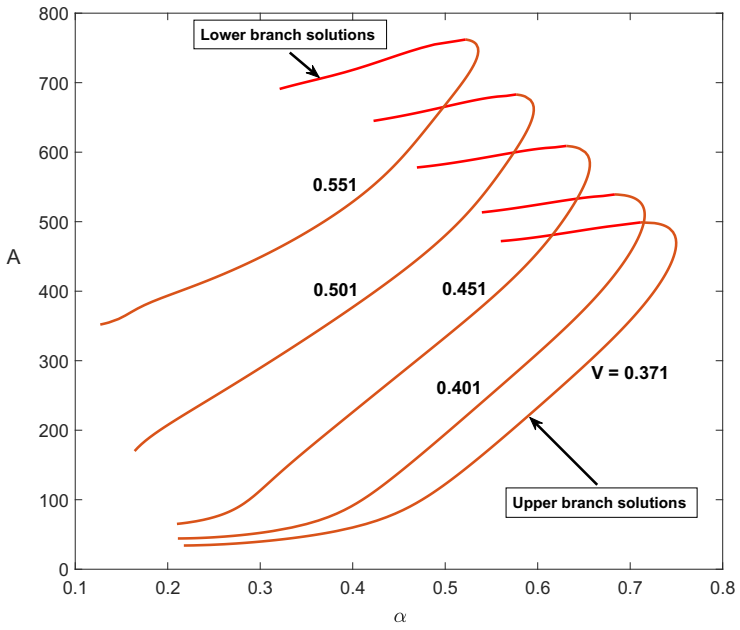

Figure 5.38: Cross-section of the nonlinear neutral surfaces for plane Poiseuille–Couette flow at $alr = 7971.60$ for various values of V in the parameter space formed by the streamwise wavenumber and amplitude.

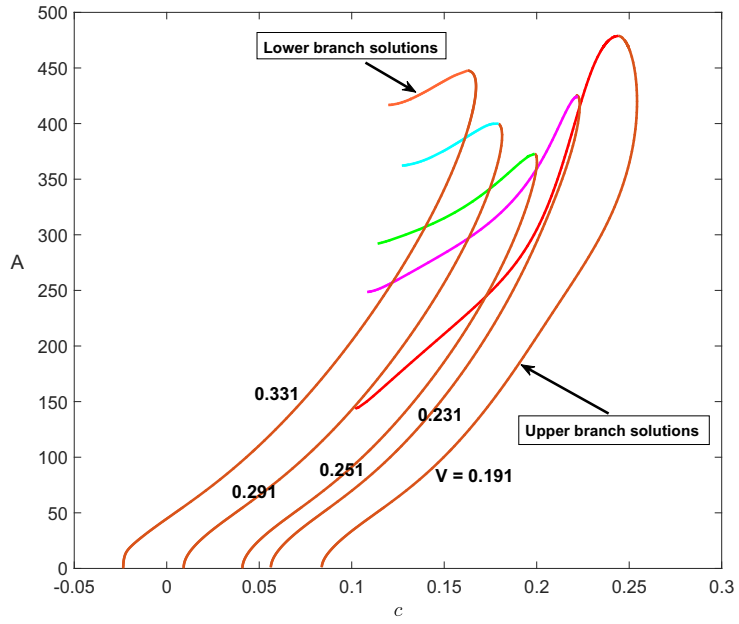

Figure 5.39: Nonlinear neutral surfaces for plane Poiseuille–Couette flow at $alr = 7971.60$ for various values of V in the (c, A)-plane.

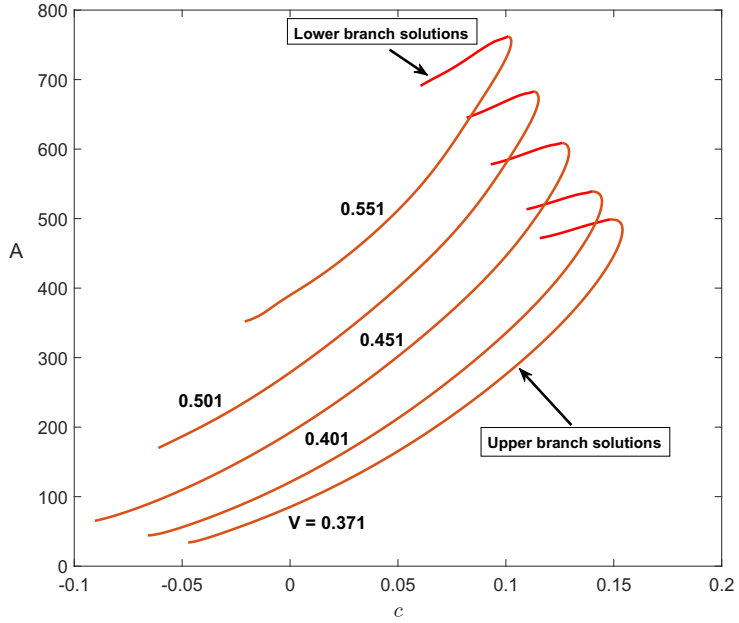

Figure 5.40: Nonlinear neutral surfaces for plane Poiseuille–Couette flow at $alr = 7971.60$ for various values of V in the (c, A)-plane.

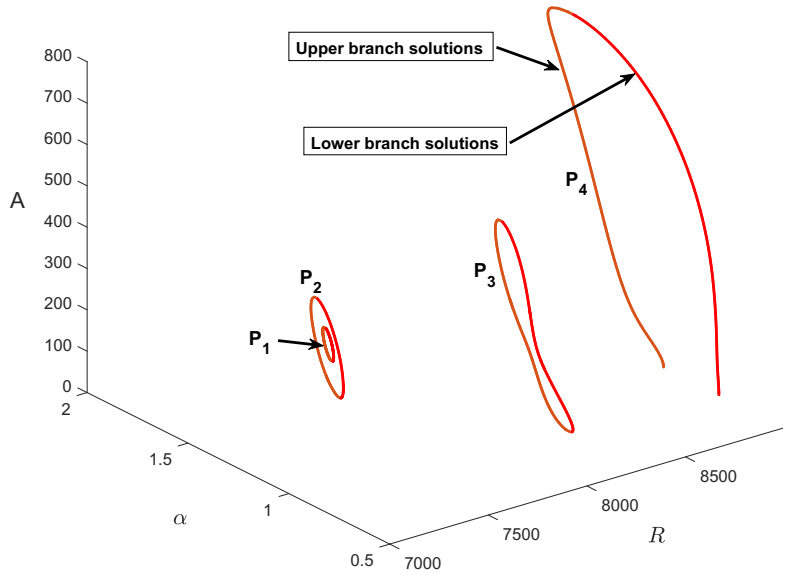

Figure 5.41: Nonlinear neutral surfaces for PPCF for various values of the wall sliding speed V and Reynolds numbers R: $P_1 = 0.1858, 7038$; $P_2 = 0.167, 7200$; $P_3 = 0.1969, 8106$; $P_4 = 0, 9000$.

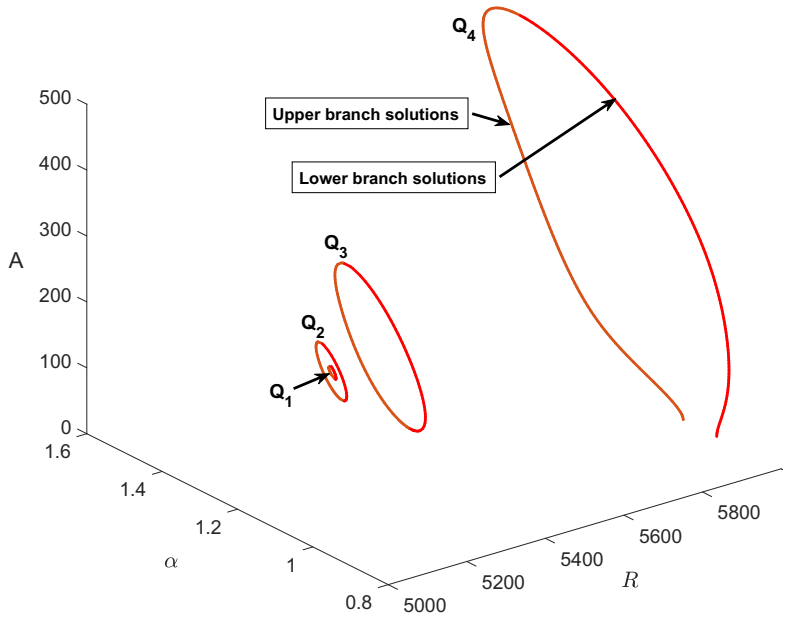

Figure 5.42: Nonlinear neutral surfaces for PPCF for various values of the wall sliding speed V and Reynolds numbers R: $Q_1 = 0.115, 5118$; $Q_2 = 0.112, 5136$; $Q_3 = 0.091, 5280$; $Q_4 = 0, 6000$.

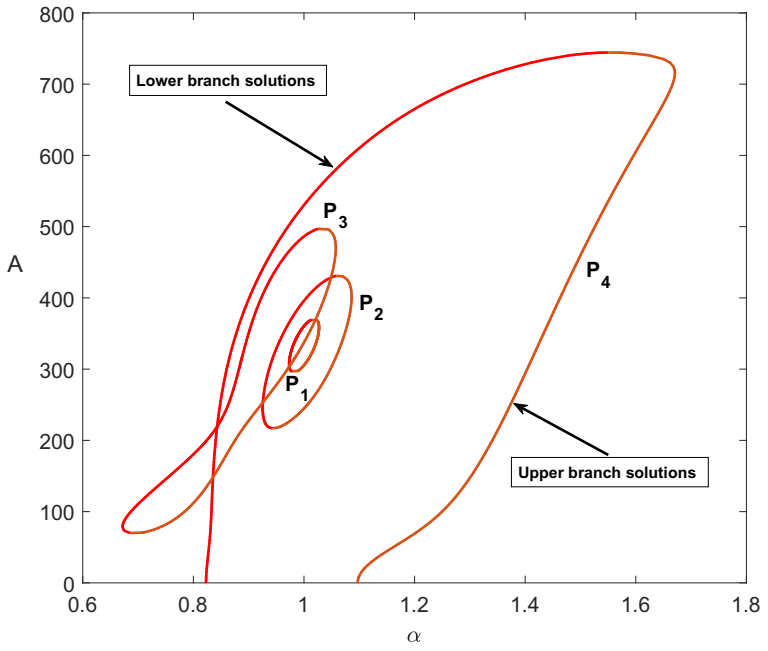

Figure 5.43: Nonlinear neutral surfaces for PPCF in the (α, A)-plane.

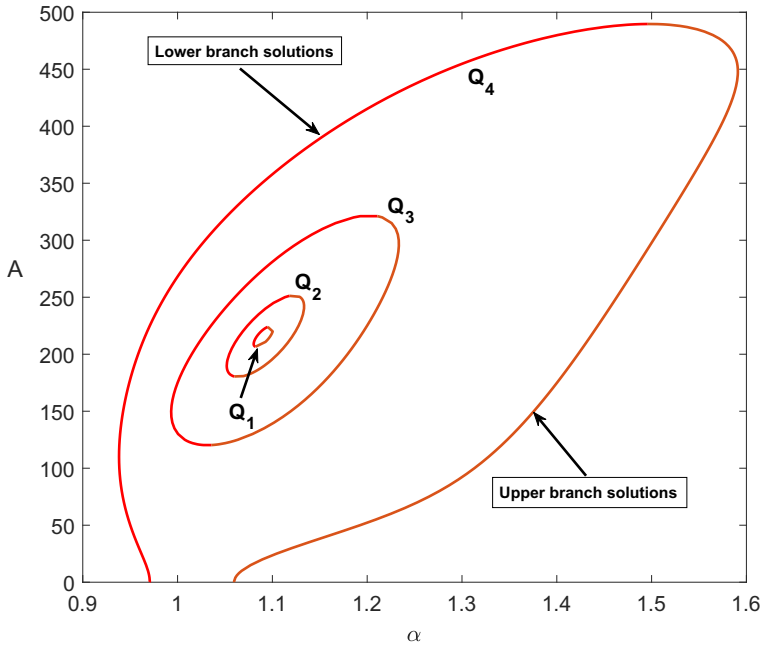

Figure 5.44: Nonlinear neutral surfaces for PPCF in the (α, A)-plane.

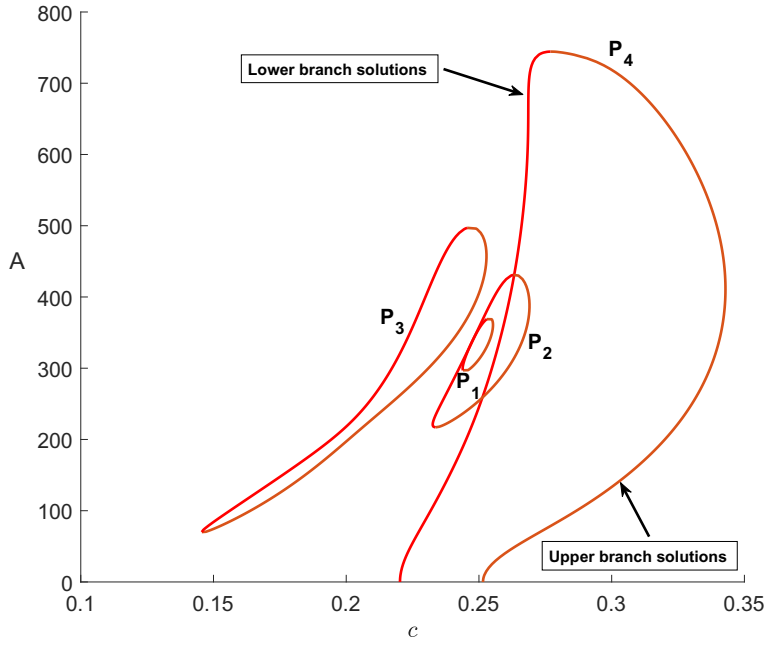

Figure 5.45: Nonlinear neutral surfaces for PPCF in the (c, A)-plane.

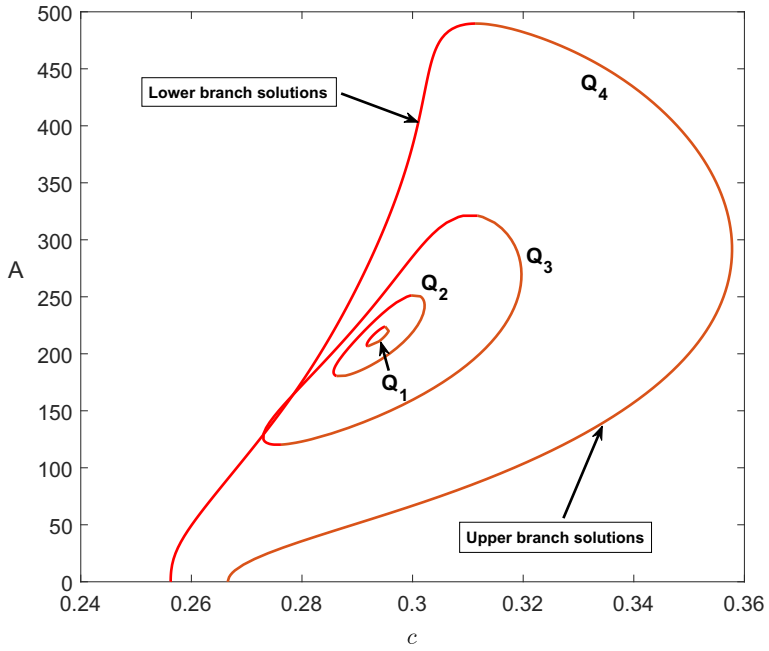

Figure 5.46: Nonlinear neutral surfaces for PPCF in the (c, A)-plane.

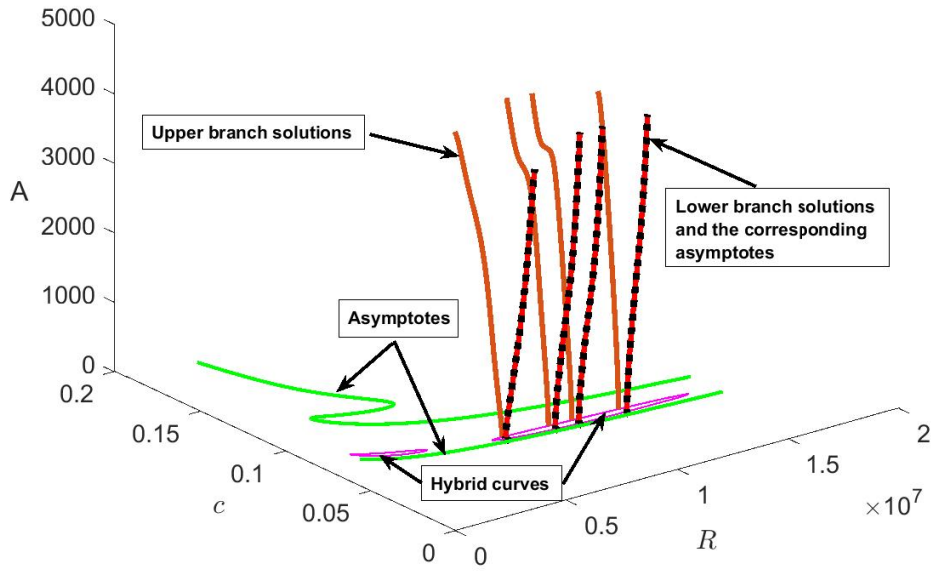

Figure 5.47: Comparison of finite Reynolds numbers computations and the corresponding solutions to the hybrid branch eigenrelation (2.148) and the amplitude equation (4.85) for $V \approx 0.025$. The solid lines are Navier–Stokes solutions at fixed Reynolds numbers that bifurcate from the upper linear neutral curve (denoted by 'hybrid curves' here). The dots are asymptotic predictions by the theory of chapter 4.

5.5 Comparison of asymptotic and numerical results

We now present some new computations of the Navier–Stokes equations and compare the results with those obtained from our asymptotic theory developed in section 4.1 of chapter 4. Previous numerical work on PPCF flow (Balakumar (1997)) concentrated on solutions which bifurcate from the main neutral curve. Here we consider solutions which at vanishingly small amplitude lie on the additional neutral curve marked 'C' in figure 5.2(b). On this curve the phasespeed of the disturbance and the sliding velocity are of similar magnitudes and the asymptotic theory developed in section 4.1 proves to be relevant in describing finite-amplitude solutions in the vicinity of this curve. In figure 5.47 we plot some Navier–Stokes solution trajectories for $V \approx 0.025$ at various large Reynolds numbers and the corresponding results from the asymptotic theory. The vertical axis represents a measure of the disturbance amplitude A. In the zero amplitude plane we plot the linear neutral curve and its asymptotic approximation. The solid paths projecting upwards out of the plane are the Navier–Stokes solutions emanating from particular positions on the linear neutral curve. For each value of R there are two Navier–Stokes solution trajectories: one bifurcating from the lower branch of the linear neutral curve and the other from the upper branch. The dots show the corresponding asymptotic predictions from the solution of the Rayleigh problem (4.16) and the amplitude equation (4.85). We see that there is excellent agreement with the Navier–Stokes solutions emanating from the lower branch. There was difficulty in achieving the convergence of the Newton–Raphson method at higher values of A so we could not obtain a comparison

with the upper branch solutions.

We have shown by comparing with finite Reynolds numbers Navier-Stokes solutions that the asymptotic theory accurately describes the nonlinear behaviour for a range of disturbance amplitudes. The comparison here was made for a value of V below the linear cut-off V_c, ensuring that a linear neutral curve exists. In future work we hope to use a continuation method to investigate nonlinear solutions for $V > V_c$ where the neutral surface is detached from the zero amplitude plane.

Chapter 6

Conclusions

The main focus of this thesis is the linear and nonlinear stability of plane Poiseuille–Couette flow numerically at finite Reynolds numbers and asymptotically at large values of the Reynolds numbers. In chapter 2, we first formulated the governing Orr–Sommerfeld equation for linear perturbations and solved it numerically in two-dimensions ($\beta = 0$) at finite Reynolds numbers to demonstrate the coexistence of multiple neutral curves for non-zero V below the linear cut-off $V_c \simeq 0.34$ as anticipated in Cowley & Smith (1985) based on an asymptotic approach. Next, we examined the linear stability equations in the limit of the large Reynolds numbers to study the asymptotic structures of the lower, upper and hybrid-branch modes and derived the eigenrelations corresponding to these modes. We presented numerical solutions to the corresponding eigenrelations for a set of non-zero values of the scaled spanwise wavenumber β_0 and investigated what happens as its value is increased. Further, we indicated a theoretical proof that the hybrid mode is the continuation of the lower-branch and upper-branch mode on the new scaling, thereby showing that these two modes form the lower and upper branches of the upper curve (see figure 2.3(c)) on the hybrid scaling, as illustrated by arrows in figure 2.16. We compared the finite Reynolds numbers computations of the two-dimensional problem and the corresponding solutions to the hybrid-branch eigenrelation for various small values of sliding velocity.

In chapter 3, we established a link between the linear and weakly nonlinear stability theory by investigating the effect of increasing the disturbance size Δ on the viscous critical layer(s) in the hybrid and upper-branch regimes (where $\varepsilon = R^{-1/13}$ and $\varepsilon = R^{-1/11}$ respectively). This suggested a pathway to find the relationship between the phase shift(s) (which is π in the linear theory) and the Reynolds numbers. It emerged that the linear asymptotic structure of the upper-branch modes alters slightly when Δ rises to $O(R^{-14/33})$, with the critical layers possessing weakly nonlinear characteristics including a reduced phase shift. We showed that the structure associated with the upper neutral curve, which is a mixture of a traditional upper and lower-branch modes, remains intact until Δ increases to $O(R^{-6/13})$. At the stage $\Delta = O(R^{-6/13})$ the main variations are found to occur only within the balances governing the properties of the viscous critical layer due to the development of weakly nonlinear effects. We concluded that in the weakly nonlinear regime the flow stability properties outside the

critical layer remain substantially unaltered. We posed the weakly nonlinear critical-layer problem, and investigated its behaviour at large scale amplitudes, indicating that the phase shift decreases as nonlinearity begins to take effect.

In chapter 4, we set up a connection between the weakly nonlinear theory and strongly nonlinear theory by increasing further the disturbance size from $O(R^{-6/13})$ to $O(R^{-4/9})$, thus leading to the scalings and recognition of the asymptotic structure for the strongly nonlinear hybrid modes. It turned out that at this stage a dominant flow feature resembling a Kelvin cat's eye containing uniform vorticity develops within the critical layer. Such cat's eye structures have recently been observed in full Navier–Stokes simulations of related flows (see Deguchi & Walton (2013)). Although the asymptotic structure bears some similarities to the structures considered by Smith & Bodonyi (1982b), Smith & Bodonyi (1982a), Walton (2002), Walton (2003) among others, there are some novel features here including a viscous shear layer near the upper wall which affects the matching condition on the core region. The numerical results for the strongly nonlinear regime revealed that nonlinear neutral solutions exist over a wide range of $O(1)$ spanwise and streamwise wavenumbers and for sliding velocities in the range $0 \leq V < 2$. Numerical computation established that the inclusion of three-dimensionality restricts nonlinear neutral solutions to the range $V_b < V < 2$, where V_b is a lower cut-off value and is a function of the spanwise wavenumber. In the limit $V \to 2$, the disturbances became more localized in the streamwise direction, and the critical layer moved ever closer to the shear layer adjacent to the upper wall. It is found that a new distinguished scaling transpires when $V - 2 \sim O(R^{-1/3})$ and simultaneously the streamwise wavenumber rises to $O(R^{1/3})$, so that this new short-scale structure possesses comparable-sized derivatives in the streamwise and wall-normal directions. In addition, it is shown that the amplitude of the travelling waves increases to $O(R^{-1/3})$ while the phasespeed stays $O(1)$. The governing balances in this new nonlinear near-wall region are the full 2D Navier–Stokes equations but with unit Reynolds number and are subject to matching conditions to the $O(1)$ Rayleigh region and a link to the Stokes region (now of thickness $O(R^{-2/3})$) near the lower wall. These equations are reminiscent of those governing the 'production layer' in Deguchi & Hall (2014). This structure will be considered further in future work.

From the consideration of the weakly nonlinear structure for the upper-branch modes as the disturbance amplitude is increased further from $O(R^{-14/33})$ we demonstrate that a strongly nonlinear regime comes into play at $\Delta = O(R^{-1/3})$. The new structure involves two critical layers sited within an inviscid core region at locations which are dependent on the amplitude-dependent phase speed of the disturbance. These layers are of an equilibrium, inviscid, fully nonlinear type and possess flow structures which bear some similarities to those previously studied by Smith & Bodonyi (1982a), Walton (2002) and Walton (2003) among others. The amplitude-dependence of the neutral modes is determined and the numerical results indicate the existence of such modes over a wide range of $O(1)$ wavenumbers and for sliding speeds in the range $0 \leq V < 2$ with the $O(1)$ dominant phase speed lying between the minimum and maximum of the basic PPCF. Investigation of the strongly nonlinear structure in the large

amplitude limit, when the two critical layers merge, is performed, and the new short-scaled structure that emerges is discussed in some detail. It is interesting to note that the nonlinear stability structure also breaks down in the limit $V \to 2$ when the critical layers penetrate the upper Stokes layer to form a new nonlinear near-wall region. The new structure found here is identical to the boundary-region structure uncovered by Kumar & Walton (2018) for nonlinear disturbances bifurcating from the upper neutral curve. A systematic study of the asymptotic structures corresponding to the new regimes will form the focus of future work.

In chapter 5, we investigated the linear and nonlinear stability properties of plane Poiseuille–Couette flow at finite Reynolds numbers for various values of sliding speed V. It is discovered in section 5.2 that there exist four neutral curves for PPCF at a very small value of sliding speed. In section 5.4, we first considered the nonlinear neutral solutions for plane Poiseuille flow at different values of αR with the number of Fourier series $N = 8$. It is found in figure 5.17 that although the neutral surfaces are similar in shape, these surfaces gradually shrink in size as αR is decreased. It is observed in figures 5.18–5.20 that corresponding to each situation the following feature emerges: the gap between the upper and lower branch solutions widens and the nose of the surface (the top neutral point where these branch solutions meet) rises with the increase in the value of αR so that the region of nonlinear instability increases. In figure 5.21, we considered the case $\alpha R = 5823.66$ and investigated the effect of increasing V on the neutral surface for plane Poiseuille flow. It is observed that the neutral surfaces contract, the lower and upper branch solutions leave the zero amplitude plane to form the closed loops and the nose of the surface descends as the sliding speed is increased from zero to 0.135. In figures 5.22–5.24, we presented the plots for the amplitude versus the Reynolds number, the streamwise wavenumber and wavespeed for various values of the sliding speed V and noted that the general trends described above remain unchanged. In figures 5.25–5.40, we presented interesting results for $\alpha R = 7971.60$ and examined the effect on the neutral surface for plane Poiseuille flow of increasing the sliding speed. In figures 5.41 and 5.42, we presented comparison of our results with Balakumar (1997). In figures 5.43 and 5.44, we showed the corresponding dependence of the amplitude A on α for various values of V and R. In figures 5.45 and 5.46, we considered the neutral surfaces in the (c, A)-plane for the same values of V and R. In section 5.5, we demonstrated the existence of the nonlinear hybrid neutral modes at finite Reynolds numbers from full two-dimensional Navier–Stokes computations. In addition, we compare the results from the high Reynolds numbers asymptotic theory developed in chapter 4 with the corresponding Navier–Stokes solutions.

Regarding future work, it would be interesting to verify the existence of multiple neutral surfaces in (α, β, R) plane at finite Reynolds numbers by tackling the full Navier–Stokes equations numerically and compare our numerical solutions with the corresponding results of the asymptotic theory developed in chapter 4.

Bibliography

Balakumar P., Finite-Amplitude Equilibrium Solutions for Plane Poiseuille–Couette flow, *Theoret. Comput. Fluid Dynamics.* **9** (1997) 103–119.

Batchelor G.K., On steady laminar flow with closed streamlines at large Reynolds number, *J. Fluid. Mech.* **1** (1956) 177–190.

Bender C.M. and Orszag S.A., Advanced mathematical methods for scientists and engineers, Springer (1999).

Benney D.J. and Bergeron R.F., A new class of nonlinear waves in parallel flows, *Stud. Appl. Math.* **48** (1969) 181–204.

Brown S.N. and Stewartson K., The evolution of the critical layer of a Rossby wave, Part II, *Geophys. Astrophys. Fluid Dyn.* **10** (1978) 1–24.

Cowley S.J. and Smith F.T., On the stability of Poiseuille–Couette flow: a bifurcation from infinity, *J. Fluid. Mech.* **156** (1985) 83–100.

Deguchi K. and Walton A.G., A swirling spiral wave solution in pipe flow, *J. Fluid. Mech.* **737** (2013) 1–12.

Deguchi K. and Walton A.G., Axisymmetric travelling waves in annular sliding Couette flow at finite and asymptotically large Reynolds number, *J. Fluid. Mech.* **720** (2013) 582–617.

Deguchi K. and Hall P., Free-stream coherent structures in parallel boundary-layer flows, *J. Fluid. Mech.* **752** (2014) 602–625.

Dempsey L.J., Nonlinear exact coherent structures in high Reynolds number shear flows, Ph.D. Thesis, Imperial College London (2016).

Dryden H.L., The international congress for applied mechanics, *Science.* **105(2720)** (1947) 167–169.

Ehrenstein U., Nagata M., and Rincon F., Two-dimensional nonlinear plane Poiseuille–Couette flow homotopy revisited, *Phys. Fluids.* **20** (2008) 064103.

Haberman R., Critical layers in parallel flows, *Stud. Appl. Maths.* **51** (1972) 139–161.

Haberman R., Nonlinear perturbations of the Orr-Sommerfeld equation - asymptotic expansion of the logarithmic phase shift across the critical layer, *SIAM J. Math. Anal.* **7** (1976) 70–81.

Hains F.D., Stability of plane Couette–Poiseuille flow, *Phys. Fluids* **10** (1967) 2079–2080.

Herbert T., Die neutrale Fläche der ebenen Poiseuille-Strömung. Habilitationsschrift, Universität Stuttgart (1977).

Kawahara G., Uhlmann M. and van Veen L., The significance of simple invariant solutions in turbulent flows, *Ann. Rev. Fluid Mech.* **44** (2012) 203–225.

Klebanoff P.S. and Tidstrom K.D., Evolution of amplified waves leading to transition in a boundary layer with zero pressure gradient. *N.A.S.A. Tech. note*, no. D–195 (1959).

Kumar R. and Walton A.G., Amplitude–dependent three–dimensional neutral modes in plane Poiseuille–Couette flow at large Reynolds number, *Quart. Appl. Math.* **72** (2018) 87–130.

Kumar R. and Walton A.G., Self-sustaining dual critical layer states in plane Poiseuille–Couette flow at large Reynolds number, *Proc. R. Soc. A* **475** (2019) 20180881.

Lin C.C., On the stability of two-dimensional parallel flows, *Quart. Appl. Math.* **3** (1945) 117–142; 218–234; 277–301.

Lin C.C., The Theory of Hydrodynamic Stability, Cambridge University Press (1955).

Maslowe S.A., Critical Layers in Shear Flows, *Ann. Rev. Fluid Mech.* **18** (1986) 405–432.

Orszag S.A., Accurate solution of the Orr–Sommerfeld stability equation, *J. Fluid.*

Mech. **50** (1971) 689–703.

Potter M.C., Stability of plane Poiseuille–Couette flow, *J. Fluid. Mech.* **24** (1966) 609-619.

Reid W.H., The stability of parallel flows, In Basic Developments in Fluid Dynamics (ed. M. Holt), vol. 1. Academic (1965).

Reynolds O., An experimental investigation of the circumstances which determine whether the motion of water shall be direct or sinuous, and of the law of resistance in parallel channels, *Phil. Trans. R. Soc. A* **174** (1883) 935–982.

Reynolds W.C. and Potter M.C., Finite-amplitude instability of parallel shear flows, *J. Fluid. Mech.* **27** (1967) 465–492.

Romanov V.A., Stability of plane-parallel Couette flow, *Funct. Anal. Applics* **7** (1973) 137–146.

Schmid P.J. and Henningson D.S., Stability and transition in shear flows, Springer (2001).

Schubauer G.B. and Skramstad H. K., Laminar boundary-layer oscillations and stability of laminar flow, *J. Aero. Sci.* **14** (1947) 68–78.

Smith F.T., Instability of flow through pipes of general cross-section, Parts I and II, *Mathematika.* **26** (1979) 187–210, 211–223.

Smith F.T. and Bodonyi R.J., Amplitude-Dependent Neutral Modes in the Hagen–Poiseuille Flow Through a Circular Pipe, *Proc. R. Soc. A* **384** (1982a) 463–489.

Smith F.T. and Bodonyi R.J., Nonlinear critical layers and their development in streaming-flow stability, *J. Fluid. Mech.* **118** (1982b) 165–185.

Stuart J.T., In Laminar Boundary Layers (ed. L. Rosenhead), chap. 9, Oxford University Press (1963).

Tollmien W., Uber die Entstehung der Turbulenz. Nachr. Ges. Wiss. Göttingen, (1929) 21–44.

Walton A.G., Stability of circular Poiseuille–Couette flow to axisymmetric disturbances, *J. Fluid. Mech.* **500** (2004) 169–210.

Walton A.G., The temporal evolution of neutral modes in the impulsively started flow through a circular pipe and their connection to the nonlinear stability of Hagen–Poiseuille flow, *J. Fluid. Mech.* **457** (2002) 339–376.

Walton A.G., The nonlinear instability of thread–annular flow at high Reynolds number, *J. Fluid. Mech.* **477** (2003) 227–257.

Walton A.G. and Patel R.A., Singularity formation in the strongly nonlinear wide-vortex/Tollmien–Schlichting-wave interaction equations, *J. Fluid. Mech.* **400** (1999) 265–293.

Wu X., Nonlinear Theories for Shear Flow Instabilities: Physical Insights and Practical Implications, *Ann. Rev. Fluid Mech.* **51** (2019) 451–85.

Zhuk V.I. and Protsenko I.G., Asymptotic model for the evolution of perturbations in the plane Couette–Poiseuille flow, *Dokl. Math.* **74** (2006) 896–900.

Appendix A

Derivation of the equation governing the function $g(s)$ and the initial conditions

The function $g(s)$ is defined by

$$g(s) = \mathrm{i}^{5/3}\frac{\mathrm{Ai}'(\xi)}{\kappa(\xi)}, \tag{A.1}$$

where Ai is the Airy function, $\kappa(\xi) = \int_{\xi}^{\infty} \mathrm{Ai}(\xi)\ \mathrm{d}\xi$ and $\xi = -\mathrm{i}^{1/3}s$. Consider the following useful properties of the Airy function

$$\mathrm{Ai}(0) = \frac{1}{3^{2/3}\Gamma(2/3)}, \tag{A.2}$$

$$\mathrm{Ai}'(0) = -\frac{1}{3^{1/3}\Gamma(1/3)}, \tag{A.3}$$

$$\kappa(0) = \int_0^{\infty} \mathrm{Ai}(\xi)\ d\xi = \frac{1}{3}, \tag{A.4}$$

$$\mathrm{Ai}''(\xi) = \xi\mathrm{Ai}(\xi). \tag{A.5}$$

Differentiating (A.1) with respect to s and applying the chain rule yields

$$\begin{aligned} g'(s) &= \mathrm{i}^{5/3}\left(\frac{\mathrm{Ai}''(\xi)\kappa(\xi) - \kappa'(\xi)\mathrm{Ai}'(\xi)}{(\kappa(\xi))^2}\right)\left(\frac{d\xi}{ds}\right), \\ &= \frac{\mathrm{Ai}(\xi)}{\kappa(\xi)}\left(\xi + \frac{\mathrm{Ai}'(\xi)}{\kappa(\xi)}\right), \quad \text{(using (A.5))} \\ &= -\mathrm{i}^{1/3}\frac{\mathrm{Ai}(\xi)}{\kappa(\xi)}(s + g(s)). \quad \text{(using (A.1) to substitute for } \mathrm{Ai}'(\xi)/\kappa(\xi)) \end{aligned} \tag{A.6}$$

Differentiating (A.6) with respect to s and making use of the chain rule we find that

$$g''(s) = \mathrm{i}^{2/3}\left\{\frac{\mathrm{Ai}'(\xi)}{\kappa(\xi)} + \left(\frac{\mathrm{Ai}(\xi)}{\kappa(\xi)}\right)^2\right\}(s + g(s)) - \mathrm{i}^{5/3}\frac{\mathrm{Ai}(\xi)}{\kappa(\xi)}(1 + g'(s)), \tag{A.7}$$

where use has been made of the property of the Airy function (A.5). Then, from substitution of the expression for $\mathrm{Ai}'(\xi)/\kappa(\xi)$, $\mathrm{Ai}(\xi)/\kappa(\xi)$ from equations (A.1) and (A.6), respectively, into (A.7), after some manipulation, we finally obtain the governing second order nonlinear equation satisfied by $g(s)$, namely

$$g''(s) = \frac{g'(s) + 2(g'(s))^2}{s + g(s)} - \mathrm{i}g(s)(s + g(s)), \tag{A.8a}$$

subject to the initial conditions

$$\begin{aligned} g(0) &= \mathrm{i}^{5/3}\frac{\mathrm{Ai}'(0)}{\kappa(0)}, \\ &= -\frac{\mathrm{i}^{5/3}3^{2/3}}{\Gamma(1/3)}, \quad \text{(using (A.3) and (A.4))} \end{aligned} \tag{A.8b}$$

and

$$\begin{aligned} g'(0) &= -\mathrm{i}^{1/3}\frac{\mathrm{Ai}(0)}{\kappa(0)}g(0), \\ &= -\frac{3}{\Gamma(1/3)\Gamma(2/3)}. \quad \text{(using (A.2), (A.4) and (A.8b))} \end{aligned} \tag{A.8c}$$

The integration method used is the classical fourth-order Runge–Kutta method to find the solution of the initial value problem (A.8a–c). In order to apply this numerical method the second order equation satisfied by $g(s)$, (A.8a), is transformed into two first-order equations. Introducing the notation

$$y_1 = g(s) \text{ and } y_2 = g'(s), \tag{A.9}$$

the equivalent first-order equations are

$$\frac{dy_1}{ds} = y_2, \tag{A.10a}$$

$$\frac{dy_2}{ds} = \frac{y_2 + 2y_2^2}{y_1 + s} - \mathrm{i}y_1(s + y_1), \tag{A.10b}$$

with the initial conditions

$$y_1(0) = -\frac{\mathrm{i}^{5/3}3^{2/3}}{\Gamma(1/3)}, \tag{A.10c}$$

$$y_2(0) = -\frac{3}{\Gamma(1/3)\Gamma(2/3)}, \tag{A.10d}$$

from (A.8b) and (A.8c). The system of equations (A.10a–b) subject to intial conditions (A.10c–d) are solved numerically using a computer algebra program "Mathematica" and plots of the imaginary and real parts of $g(s)$ are illustrated in figures 2.19 and 2.20 respectively.

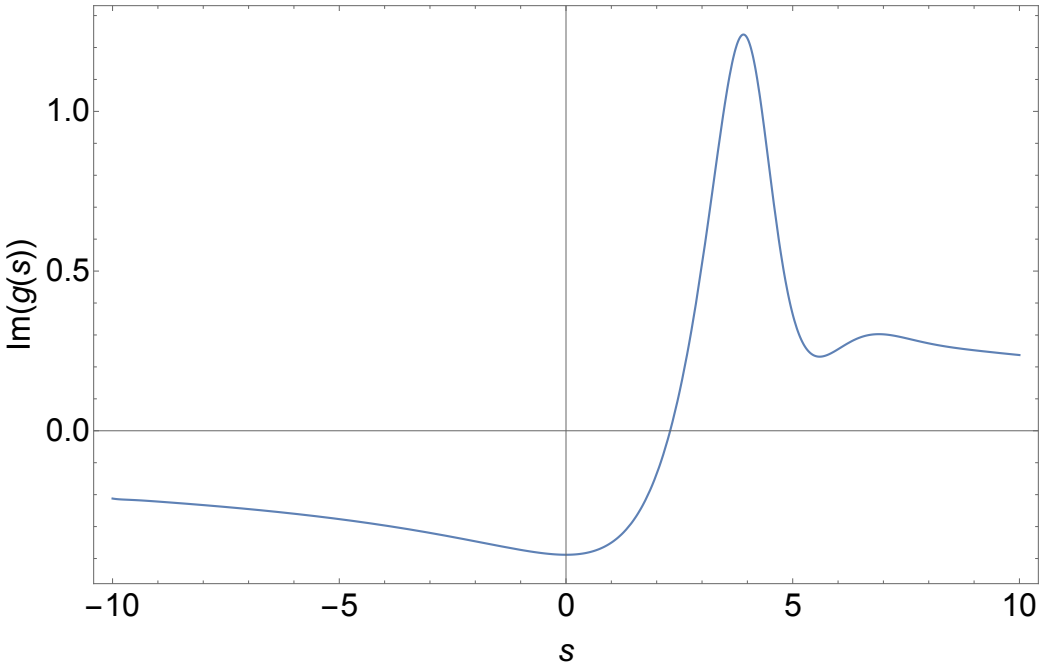

Figure 6.1: The imaginary part of the function $g(s)$.

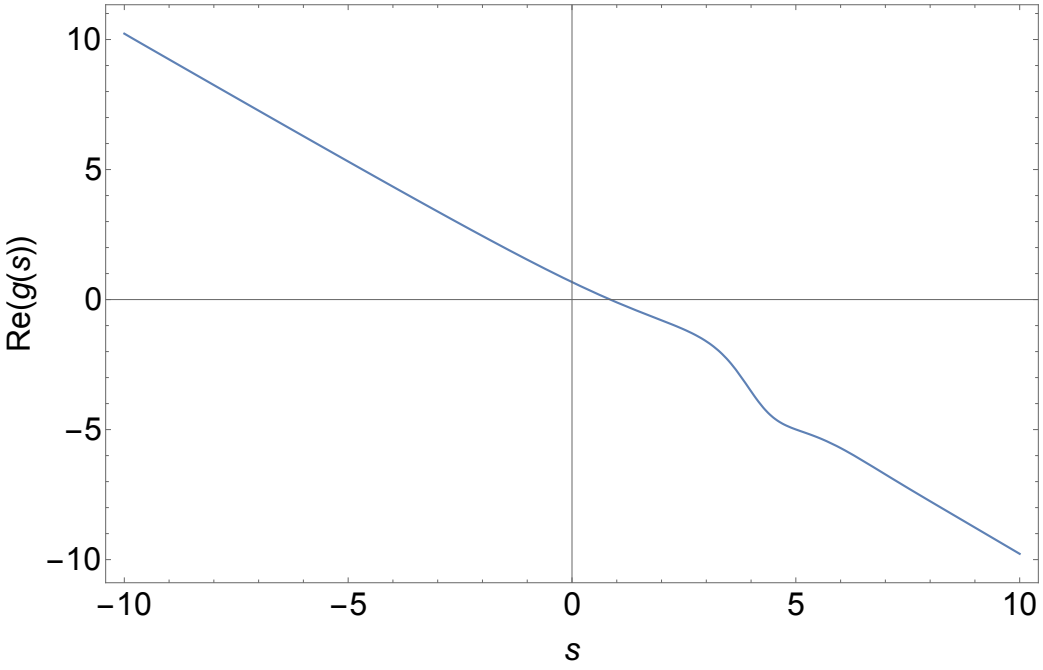

Figure 6.2: The real part of the function $g(s)$.

Appendix B

The series solution of the Rayleigh equation

For the Rayleigh equation (4.97) subject to the basic PPCF flow (2.2) it is possible to find a set of recurrence relations for the coefficients in the Frobenius solutions about the regular singular points y_1 and y_2. For $y > y_i$, $i \in \{1, 2\}$ the solution may be expressed as

$$G_2(y) = \sum_{n=0}^{\infty} g_i^{(n)} (\tilde{\varepsilon}_i)^n + \ln(\tilde{\varepsilon}_i) \sum_{n=1}^{\infty} \mathscr{G}_i^{(n)} (\tilde{\varepsilon}_i)^n \quad \text{with } \tilde{\varepsilon}_i = y - y_i > 0, \tag{B.1}$$

as given in (4.100). After considerable algebra, it is found that the coefficients can be expressed most succinctly in terms of the quantities

$$q_0^{(i)} = 2(-1)^{i+1}(y_2 - y_1)^{-1},\ q_1^{(i)} = -(\alpha^2 + \beta^2) + 2(y_1 - y_2)^{-2},\ q_n^{(i)} = (q_0^{(i)})^{n+1}/2^n\ (n \geq 2).$$

The coefficients in the first series in (B.1) can then be calculated recursively from the relations

$$g_i^{(n)} = -\frac{1}{n(n-1)} \left(\sum_{k=0}^{n-1} (q_{n-k-1}^{(i)}) g_i^{(k)} + (2n-1) \mathscr{G}_i^{(n)} \right),$$

for $n \geq 2$, with $g_i^{(0)}, g_i^{(1)}$ left arbitrary. The coefficients in the second series in (B.1) then follow in the form

$$\mathscr{G}_i^{(1)} = -q_0^{(i)} g_i^{(0)}, \quad \mathscr{G}_i^{(n)} = -\frac{1}{n(n-1)} \left(\sum_{k=0}^{n-2} (q_{n-k-2}^{(i)}) \mathscr{G}_i^{(k+1)} \right), \quad (n \geq 2).$$

This series expansion representation forms part of the numerical method described in section 4.2.3(a).

Appendix C

Derivation of the jump condition on G_5'

Substituting the core expansions (4.94) into the dimensionless Navier–Stokes equations (1.1) and collecting the $O(\varepsilon^2 R^{-1/2})$ terms we find that the continuity equation reads as

$$\alpha\frac{\partial u_5}{\partial \xi} + \frac{\partial v_5}{\partial y} + \beta\frac{\partial w_5}{\partial \xi} = 0. \tag{D.1}$$

Taking the finite part of the jump of (D.1) across the critical layers we find that

$$\left[\left[\alpha\frac{\partial u_5}{\partial \xi} + \beta\frac{\partial w_5}{\partial \xi}\right]\right]_{y_i^-}^{y_i^+} + \left[\left[\frac{\partial v_5}{\partial y}\right]\right]_{y_i^-}^{y_i^+} = 0. \tag{D.2}$$

Rewritting equation (D.2) in terms of the scaled normal variable and using the definition of the skewed velocity component (4.112) we have

$$\left[\left[\frac{\partial \overline{u}_5^{(i)}}{\partial \xi}\right]\right]_{Y_i=-\infty}^{Y_i=\infty} + \left[\left[\frac{\partial v_5}{\partial y}\right]\right]_{y_i^-}^{y_i^+} = 0. \tag{D.3}$$

Inserting the form for $\overline{u}_5^{(i)}$ from (4.131) and differentiating with respect to ξ we obtain

$$\left[\left[\frac{\partial v_5}{\partial y}\right]\right]_{y_i^-}^{y_i^+} = -\sum_{m=1}^{\infty} m(F_m^{(i)}\cos(m\xi) - \tilde{F}_m^{(i)}\sin(m\xi)). \tag{D.4}$$

Applying Leibniz rule for differentiation under integral sign it can be seen that

$$\frac{dG_5(y)}{dy} = \frac{d}{dy}\left(\frac{1}{\pi}\int_0^{2\pi} v_5(\xi, y)\,\cos(\xi)\,d\xi\right) = \frac{1}{\pi}\int_0^{2\pi}\left(\frac{\partial v_5(\xi, y)}{\partial y}\right)\cos(\xi)\,d\xi. \tag{D.5}$$

Now consider the finite part of the jump in (D.5) from y_i^- to y_i^+ and then combining it with (D.4) yields

$$\left[\left[\frac{dG_5(y)}{dy}\right]\right]_{y_1^{(i)}}^{y_1^{(i)}} = -F_1^{(i)} = -\phi^{(i)}, \tag{D.6}$$

from use of some auxiliary formulas concerning the integral properties of the trignometric functions

$$\int_0^{2\pi}\cos(k_1\xi)\,\cos(k_2\xi)\,d\xi = 0, \quad \int_0^{2\pi}\cos(k_1\xi)\,\sin(k_2\xi)\,d\xi = 0, \quad \text{and} \quad \int_0^{2\pi}\cos^2(\xi)\,d\xi = \pi,$$

for any integers k_1 and k_2 ($k_1 \neq k_2$).

Appendix D

$$
\begin{aligned}
\mathrm{Re}(S^{(1)}_{k,n}) &= -\left(\frac{n}{n-k}\right)\left(\Phi_k\Phi'''_{n-k} - \Psi_k\Psi'''_{n-k} + \Phi'_k\Phi''_{n-k} - \Psi'_k\Psi''_{n-k}\right) \\
&+ \left(\frac{n}{k}\right)\left(\Phi'_k\Phi''_{n-k} - \Psi'_k\Psi''_{n-k} + \Phi'_{n-k}\Phi''_k - \Psi'_{n-k}\Psi''_k\right) \\
&+ n^2\alpha^2\left\{\Phi_k\Phi'_{n-k} - \Psi_k\Psi'_{n-k} - \left(\frac{n-k}{k}\right)\left(\Phi'_k\Phi_{n-k} - \Psi'_k\Psi_{n-k}\right)\right\},
\end{aligned}
$$

$$
\begin{aligned}
\mathrm{Im}(S^{(1)}_{k,n}) &= -\left(\frac{n}{n-k}\right)\left(\Phi_k\Psi'''_{n-k} + \Psi_k\Phi'''_{n-k} + \Psi'_k\Phi''_{n-k} + \Phi'_k\Psi''_{n-k}\right) \\
&+ \left(\frac{n}{k}\right)\left(\Psi'_k\Phi''_{n-k} + \Phi'_k\Psi''_{n-k} + \Psi'_{n-k}\Phi''_k + \Phi'_{n-k}\Psi''_k\right) \\
&+ n^2\alpha^2\left\{\Psi_k\Phi'_{n-k} + \Phi_k\Psi'_{n-k} - \left(\frac{n-k}{k}\right)\left(\Psi'_k\Phi_{n-k} + \Phi'_k\Psi_{n-k}\right)\right\},
\end{aligned}
$$

$$
\begin{aligned}
\mathrm{Re}(S^{(2)}_{k,n}) &= -\left(\frac{n}{n+k}\right)\left(\Phi_k\Phi'''_{n+k} + \Psi_k\Psi'''_{n+k} + \Phi'_k\Phi''_{n+k} + \Psi'_k\Psi''_{n+k}\right) \\
&- \left(\frac{n}{k}\right)\left(\Phi'_k\Phi''_{n+k} + \Psi'_k\Psi''_{n+k} + \Phi'_{n+k}\Phi''_k + \Psi'_{n+k}\Psi''_k\right) \\
&+ n^2\alpha^2\left\{\Phi_k\Phi'_{n+k} + \Psi_k\Psi'_{n+k} + \left(\frac{n+k}{k}\right)\left(\Phi'_k\Phi_{n+k} + \Psi'_k\Psi_{n+k}\right)\right\},
\end{aligned}
$$

$$
\begin{aligned}
\mathrm{Im}(S^{(2)}_{k,n}) &= -\left(\frac{n}{n+k}\right)\left(\Phi_k\Psi'''_{n+k} - \Psi_k\Phi'''_{n+k} + \Phi'_k\Psi''_{n+k} - \Psi'_k\Phi''_{n+k}\right) \\
&- \left(\frac{n}{k}\right)\left(\Phi'_k\Psi''_{n+k} - \Psi'_k\Phi''_{n+k} + \Psi'_{n+k}\Phi''_k - \Phi'_{n+k}\Psi''_k\right) \\
&+ n^2\alpha^2\left\{\Phi_k\Psi'_{n+k} - \Psi_k\Phi'_{n+k} + \left(\frac{n+k}{k}\right)\left(\Phi'_k\Psi_{n+k} - \Psi'_k\Phi_{n+k}\right)\right\},
\end{aligned}
$$

$$
\begin{aligned}
\mathrm{Re}(S^{(3)}_{k,n}) &= \left(\frac{n}{k-n}\right)\left(\Phi'_k\Phi''_{k-n} + \Psi'_k\Psi''_{k-n} + \Phi_k\Phi'''_{k-n} + \Psi_k\Psi'''_{k-n}\right) \\
&+ \left(\frac{n}{k}\right)\left(\Phi'_k\Phi''_{k-n} + \Psi'_k\Psi''_{k-n} + \Phi'_{k-n}\Phi''_k + \Psi'_{k-n}\Psi''_k\right) \\
&+ n^2\alpha^2\left\{\Phi_k\Phi'_{k-n} + \Psi_k\Psi'_{k-n} + \left(\frac{k-n}{k}\right)\left(\Phi'_k\Phi_{k-n} + \Psi'_k\Psi_{k-n}\right)\right\},
\end{aligned}
$$

$$
\begin{aligned}
\mathrm{Im}(S^{(3)}_{k,n}) &= \left(\frac{n}{k-n}\right)\left(\Psi'_k\Phi''_{k-n} - \Phi'_k\Psi''_{k-n} + \Psi_k\Phi'''_{k-n} - \Phi_k\Psi'''_{k-n}\right) \\
&+ \left(\frac{n}{k}\right)\left(\Psi'_k\Phi''_{k-n} - \Phi'_k\Psi''_{k-n} + \Phi'_{k-n}\Psi''_k - \Psi'_{k-n}\Phi''_k\right) \\
&+ n^2\alpha^2\left\{\Psi_k\Phi'_{k-n} - \Phi_k\Psi'_{k-n} + \left(\frac{k-n}{k}\right)\left(\Psi'_k\Phi_{k-n} - \Phi'_k\Psi_{k-n}\right)\right\}.
\end{aligned}
$$